

Copyright

By

Kevin Chang

2020

# **Structure-Property Relationships in Polymer Membranes for Desalination Applications**

---

A Dissertation

Presented to the Faculty of the School of Engineering and Applied Science at the  
University of Virginia

---

In Partial Fulfillment of the Requirements for the Degree of  
Doctor of Philosophy in Chemical Engineering

By

Kevin Chang

December 2020

**The Dissertation Committee for Kevin Chang Certifies that this is the Approved Version of  
the Following Dissertation:**

**Structure-Property Relationships in Polymer Membranes for  
Desalination Applications**

**Committee:**

Geoffrey M. Geise, Dissertation Advisor

Rachel A. Letteri, Chairperson

David L. Green

Roseanne M. Ford

Louis A. Madsen

## **Dedication**

To my parents – Yuan-Da and Shu-Hui.

## **Acknowledgements**

The journey of earning a Ph.D. is not an easy one, and I have had the opportunity to experience a broad number of things during the past 4 years in the Department of Chemical Engineering at the University of Virginia at Charlottesville, VA, from attending the program orientation to getting ready to defend my dissertation, from learning how to design/execute experiments to understanding how to effectively interpret/analyze experimental results, from drafting the manuscript outlines to being scolded by peer-reviewers on the manuscript reviews, from studying for mid-terms/finals to getting my papers published, from someone who did not know what to expect when he joined the program to someone who was able to get his first job offers in the industry, and most importantly, from someone who did not know anyone in the area to someone who has met all the brilliant friends and people during this time. It surely has been an incredible and unforgettable journey at Charlottesville, VA, and I would like to thank all of you for your support and encouragement. I would not have been able to make it through this far without the involvement of every single one of you.

Throughout the journey, I am the most grateful to my dissertation advisor, Dr. Geoff Geise, who is not only an incredibly intelligent and creative researcher, but he is also a thoughtful and caring person. I have benefited considerably, both professionally and personally, from his mentorship and guidance over the past 4 years. Under his instructions, in the lab, I have learnt about idea construction and experimental design to test the hypotheses as well as data interpretation and analysis to turn the results into impactful manuscripts; in the office, I have learnt about important techniques to deliver oral presentations and skills to write professionally for both journals and research proposals/statements; at home, I have learnt about time management and the ability to be organized and responsible for everything I do in grad school. Dr. Geise's continuous

patience and effort in training and mentoring his students has greatly inspired me and turned me into not only a qualified researcher but also a better person, and I appreciate him for everything that he has said and done to guide me through the Ph.D. program. He is surely the best advisor that I could ever ask for. Further, I also would like to thank Dr. Geise's wife, Elise, for her hospitality during the Geise Group happy hours and social events connecting and talking to us.

I would like to also thank my committee members, Dr. Rachel Letteri, Dr. David Green, and Dr. Roseanne Ford, for their guidance and advice on my Ph.D. projects, and I would like to thank my lab mates in the Geise Group, Dr. Bill Morris, Dr. Yuanyuan Ji, Hongxi, Saring, and Patrick, for being such incredible colleagues and friends. I especially would like to thank Dr. Morris for his mentorship when I first joined the group, and I also would like to thank Hongxi for being the most collaborative and supportive lab mate/classmate. Hongxi and I have turned our hard work into 5 co-author publications, and we are definitely proud of what we have achieved together, as a team, as friends, and as brothers. I appreciate the fact that the lab members have always been there for each other through the ups and downs, and I am excited to see the next steps for each of us and hope to stay connected with you all in the future.

I am also grateful to my three collaborators, Dr. Bradley Frieberg, for traveling to the Oak Ridge National Lab with us to conduct neutron scattering experiments, Dr. Louis Madsen, for helping us measure water diffusivity using the NMR facility at Virginia Tech and collaborating on our papers, and Dr. Chris Arges, for trusting my ability to perform microwave dielectric relaxation spectroscopy on the membranes made in his lab and listing us as co-authors to his paper. I am thankful for the opportunities to collaborate with these fantastic researchers to think outside of the box and to learn some different skills and knowledge.

Working as a Ph.D. student, I also had the opportunity to mentor two undergraduate research assistants, Kevin Bahati and Sin Yan Lin, and I would like to thank them for their hard work and dedication on the research projects in our group. Because of their hard work and effort, we were able to publish three papers together where they were listed as the co-authors in these papers. I hope Kevin and Sin enjoyed working with us and we were able to have some positive influence on their career development. I recognize that there is still a lot for me to learn to become a better mentor/advisor, and I thank them for giving me the opportunities to develop my leadership and mentorship skills in grad school.

My experience working as a co-op at the Department of Downstream Process Development at Bristol Myers Squibb, Devens, MA was remarkable. I would like to thank my manager Dr. Mark Geng, Principle Scientist of our team, Dr. Deqiang Yu, Principle Scientist of Upstream Process Development Dr. Yueming Qian, and Principle Scientist of Method Development/Process Development Analytics Dr. Letha Chemmalil, for their training and the trust in my ability to quickly learn things and effectively lead projects. On top of the scientific knowledge and the experimental skills that I learnt at BMS, I was also able to develop interpersonal and communication skills to work with scientists from different functional areas as well as getting trained on the techniques to deliver professional presentations at company internal seminars/forums. The experience at BMS made me recognize how important it is to be innovative and collaborative in the industry, and I would strive to further develop these skills once I join the industry as a permanent employee in the near future.

Finally, I cannot thank my family enough, especially my parents, for their encouragement and support through the years. I will continue to work hard to make you all proud. Hopefully, we will be able to travel again and my family and I can be re-united in the near future.

## Abstract

Low cost and highly energy efficient membrane-based separation techniques are poised to address global water needs. These techniques use polymer membranes to control the rates of water and ion transport. For membranes to be effective for desalination, they must have excellent water/ion permeability selectivity, thus allowing water molecules through the polymer while blocking ions. The water and ion permeability properties of non-porous polymer membranes have been traditionally described in terms of sorption (thermodynamic) and diffusion (kinetics) factors via the solution-diffusion model, so high water/ion permeability selectivity can be achieved by preparing membranes that suppress either ion sorption or diffusion, or both, to a greater extent compared to water sorption and diffusion. Such membranes will have properties that favor desalination applications. One strategy to achieve high permeability selectivity is to prepare polymers that preferentially slow ion diffusion relative to water diffusion, which can be done by preparing polymers that have rigid and glassy backbones. Another way to enhance membrane selectivity properties is to prepare polymers that suppress ion sorption by evenly distributing the chemical functional groups throughout the polymer matrix, thus giving rise to high permeability selectivity in the polymers. Using these structure-property relationships, a promising desalination membrane material, sulfonated polysulfone, that has a combination of excellent mechanical and chemical stability and relatively good desalination performance compared to commercially available polyamide membranes, can be further modified in an attempt to control and engineer the water and salt transport and selectivity properties. Ultimately, structure-property understanding is important to guide the design of chemically and mechanically stable and highly selective future generation desalination membranes to purify water efficiently and effectively.

## Table of Contents

List of Tables .....	x
List of Figures.....	xiv
Chapter 1: Introduction .....	1
1.1. Addressing Global Water Shortages with Membrane-based Desalination .....	1
1.2. Goals and Organization of the Dissertation.....	2
1.3. References.....	5
Chapter 2: Materials and Methods.....	9
2.1. Materials .....	9
2.1.1. Hydroxyethyl Acrylate- and Methacrylate-based Polymers.....	9
2.1.2. Glycidyl and Glycerol Methacrylate-based Polymers.....	11
2.1.3. Hydroxyl Group-containing Methacrylate-based Polymers.....	14
2.1.4. Hydroquinone-containing Sulfonated Polysulfones.....	17
2.2. Methods .....	19
2.2.1. Water Uptake .....	19
2.2.2. Salt Sorption.....	21
2.2.3. Thermal Characterization .....	23
2.2.4. Microwave Dielectric Spectroscopy .....	23
2.2.5. State of Water Analysis (DSC).....	26
2.2.6. State of Water Analysis (FT-IR).....	26
2.2.7. Nuclear Magnetic Resonance (NMR) Diffusometry .....	28
2.2.8. Ionic Conductivity.....	30
2.2.9. Salt Diffusion.....	31
2.2.10. Water Permeability.....	32
2.2.11. Salt Permeability .....	33
2.3. References.....	34
Chapter 3: Increasing Salt Size Selectivity in Low Water Content Polymers via Polymer Backbone Dynamics .....	40
3.1. Introduction.....	40

3.2.	Results and Discussion .....	41
3.2.1.	Water Uptake .....	41
3.2.2.	Thermal Characterization .....	42
3.2.3.	Salt Permeability .....	45
3.2.4.	Size Selectivity .....	45
3.3.	Conclusions .....	53
3.4.	References .....	54
Chapter 4: Influence of Rubbery versus Glassy Backbone Dynamics on Multiscale Transport in Polymer Membranes .....		59
4.1.	Introduction .....	59
4.2.	Results and Discussion .....	61
4.2.1.	Material Selection .....	61
4.2.2.	Water Content .....	61
4.2.3.	Salt Sorption Properties .....	63
4.2.4.	Polymer and Water Dynamics .....	64
4.2.5.	Restricted Diffusion .....	69
4.3.	Conclusions .....	81
4.4.	References .....	81
Chapter 5: Water Content, Relative Permittivity, and Ion Sorption Properties of Polymers for Membrane Desalination .....		86
5.1.	Introduction .....	86
5.2.	Results and Discussion .....	88
5.2.1.	Water Uptake .....	88
5.2.2.	Microwave Dielectric Spectroscopy .....	89
5.2.3.	State of Water Analysis .....	92
5.2.4.	Static Permittivity .....	95
5.2.5.	Ion Sorption .....	96
5.2.6.	Free Energy of Ion Sorption .....	100
5.3.	Conclusions .....	102
5.4.	References .....	103
Chapter 6: Functional Group Configuration Influences Salt Transport in Desalination Membrane Materials .....		110

6.1.	Introduction.....	110
6.2.	Results and Discussion .....	111
6.2.1.	Water Uptake .....	111
6.2.2.	Salt Transport Properties .....	113
6.2.2.1.	Salt Sorption.....	115
6.2.2.2.	Salt Permeability and Diffusivity .....	116
6.2.3.	Microwave Dielectric Spectroscopy .....	119
6.2.4.	State of Water Analysis .....	121
6.3.	Conclusions.....	125
6.4.	References.....	125
Chapter 7: Engineering Selective Desalination Membranes via Molecular Control of Polymer Functional Groups.....		
		131
7.1.	Introduction.....	131
7.2.	Results and Discussion .....	132
7.3.	Conclusions.....	139
7.4.	References.....	139
Chapter 8: Influence of Salt Concentration on Hydrated Polymer Relative Permittivity and State of Water Properties .....		
		142
8.1.	Introduction.....	142
8.2.	Results and Discussion .....	143
8.2.1.	Water Uptake .....	144
8.2.2.	Salt Sorption Properties .....	145
8.2.3.	Relative Permittivity.....	150
8.2.4.	State of Water.....	153
8.2.5.	Static Permittivity.....	155
8.3.	Conclusions.....	157
8.4.	References.....	158
Chapter 9: Functional Group Modification Influences Relative Permittivity and Transport Properties in Sulfonated Polysulfone Desalination Materials .....		
		162
9.1.	Introduction.....	162
9.2.	Results and Discussion .....	164
9.2.1.	Water and Salt Permeability .....	164

9.2.2.	Water and Salt Sorption.....	166
9.2.3.	Donnan-Manning Counter-ion Condensation Theory.....	170
9.2.4.	Water and Salt Diffusion .....	173
9.3.	Conclusions.....	176
9.4.	References.....	177
Chapter 10: Conclusions and Recommendations .....		183
10.1.	Conclusions.....	183
10.2.	Significance.....	186
10.3.	Recommendations for Future Work.....	188
10.3.1.	The Role of Experimental Factors in Dielectric Permittivity Measurements.....	188
10.3.2.	Influence of Chemical Functional Groups on Water and Ion Transport and Selectivity Properties in Sulfonated Polysulfone .....	189
10.4.	References.....	189
Appendix A: Nomenclature.....		192
Appendix B: Supporting Information for Chapter 3.....		195
B.1.	Chemical Structures of the Components Used to Prepare the Co-polymers .....	195
B.2.	Effective Salt Diffusion Coefficients (Experimentally Determined and Calculated).....	196
B.3.	Comparison of Water Content and the Amount of Water Required to Hydrate Ions .....	196
B.4.	References.....	198
Appendix C: Supporting Information for Chapter 4.....		199
C.1.	Water Content Calculations .....	199
C.2.	Diffusion Length as a Function of Diffusion Time.....	200
C.3.	Mackie and Meares Model Calculations .....	200
C.4.	References.....	201
Appendix D: Supporting Information for Chapter 5.....		202
D.1.	Cross-linked Poly(glycidyl methacrylate) (XL-pGMA) .....	202
D.1.1.	Polymer Synthesis .....	202
D.1.2.	Membrane Casting .....	203
D.1.3.	Fourier-Transform Infrared Spectroscopy (FT-IR).....	203
D.2.	Scattering Parameters (S-parameters) .....	204

D.3. Microwave Dielectric Spectroscopy .....	205
D.3.1. Dielectric Permittivity Properties of Air and PTFE .....	205
D.3.2. Dielectric Permittivity Properties of Water .....	206
D.4. References.....	208
Appendix E: Supporting Information for Chapter 6 .....	210
E.1. Fourier-Transform Infrared Spectroscopy (FT-IR).....	210
E.2. Freezable Water Content Per Equivalent of Hydroxyl Group Functionality.....	211
E.3. References.....	212
Appendix F: Supporting Information for Chapter 7 .....	213
F.1. Additional Material Properties and Characterization.....	213
F.1.1. Chemical Structure and Composition.....	213
F.1.2. Fourier-Transform Infrared (FT-IR) Spectroscopy.....	214
F.1.3. Thermal Properties .....	215
F.2. Hydrated Polymer Dielectric Property Characterization.....	216
F.3. Microwave Dielectric Spectroscopy .....	217
F.4. Hydration of Hydroxyl Groups in HEMA and GMAOH.....	220
F.5. References.....	222
Appendix G: Supporting Information for Chapter 8.....	225
G.1. References.....	228
Appendix H: Supporting Information for Chapter 9.....	229
Vita.....	230

## List of Tables

<b>Table 3.1.</b> Water content measured at room temperature. The reported data are averages of four measurements, and the uncertainty was taken as one standard deviation from the mean. ....	42
<b>Table 3.2.</b> Glass transition temperatures calculated using the Fox equation (Equation 3.1) and the measured glass transition temperatures for the co-polymers. ....	44
<b>Table 3.3.</b> Cation and anion diffusion coefficients and average salt diffusion coefficients calculated using (Equation 3.2) for the electrolytes considered in bulk aqueous solution at infinite dilution. ....	46
<b>Table 3.4.</b> Salt sorption coefficients measured after equilibrating co-polymer samples with 0.5 mol/L aqueous LiCl, NaCl, or KCl solutions. Measurements were made at room temperature, and the uncertainty was taken as one standard deviation from the mean of four measurements. ....	47
<b>Table 3.5.</b> Effective salt diffusion coefficients for the two copolymers were determined from measured salt permeability and sorption coefficient data using Equation 3.3. The uncertainty was calculated using standard error propagation methods. <sup>42</sup> .....	50
<b>Table 3.6.</b> Ratios of the experimentally determined $D_s$ value (Table 3.5) to the value calculated using the Mackie and Meares model (Equation 3.4 and Table B.2) for each of the materials and electrolytes.....	52
<b>Table 4.1.</b> Dry polymer density and water content data (water uptake, $wu$ , and water sorption coefficient, $K_w$ , c.f. Equations 2.1 and 2.5), determined using both aqueous NaCl solution (0.5 mol/L) and pure (DI) water, for the three compositions of each co-polymer. All data were measured at room temperature, and the uncertainties are reported as one standard deviation from the mean value. ....	62
<b>Table 4.2.</b> Glass transition temperatures calculated using the Fox equation <sup>9</sup> and the measured glass transition temperatures (Figure 4.2) for the co-polymers. ....	66
<b>Table 5.1.</b> Water content and dry polymer density data measured at $22 \pm 1$ °C. Water content measurements were made on samples initially equilibrated with DI water. The volume fraction of water in the polymer, $\phi_w$ , (equivalent to the water sorption coefficient, $K_w$ ) was calculated from water uptake and dry density data using Equation 2.2. <sup>31</sup> The uncertainty was taken as the standard deviation from the mean of three measurements. Hydrolysis time, $z$ , refers to the length of time (in hours) that the XL-pGMA- $z$ samples were immersed in 0.5 mol/L $H_2SO_4$ at 45 °C. ....	89
<b>Table 5.2.</b> The distribution of freezable and non-freezable water in XL-pGMA- $z$ samples and Nafion <sup>®</sup> 117. The values for XL-pGMA- $z$ were calculated using water uptake data reported in Table 5.1. The values for Nafion <sup>®</sup> 117 were calculated using a measured water uptake of $0.320 \pm 0.005$ g(water)/g(dry polymer). This value was measured using Nafion <sup>®</sup> 117 films treated in the same manner as those films analyzed via DSC. The effect of residual water in Nafion <sup>®</sup> 117 after vacuum drying (as discussed in the literature) <sup>46, 47</sup> was estimated to potentially affect the results by	

approximately 2%. The sum of the values of  $wf$  and  $wnf$  is equivalent to the total water uptake of the material (Equation 5.2). The hydrolysis time,  $z$ , refers to the length of time (in hours) that the XL-pGMA- $z$  samples were immersed in 0.5 mol/L  $H_2SO_4$  at 45 °C.....94

**Table 5.3.** Ion sorption coefficients for XL-pGMA- $z$  and Nafion® 117 were measured after equilibrating the samples with 0.5 mol/L of NaCl. The hydrolysis time,  $z$ , refers to the length of time (in hours) that the XL-pGMA- $z$  samples were immersed in 0.5 mol/L  $H_2SO_4$  at 45 °C. Measurements were made at  $22 \pm 1$  °C, and uncertainty was taken as the standard deviation from the mean of three measurements.....97

**Table 6.1.** Water content and dry polymer density data measured at  $22 \pm 1$  °C. Water content measurements were made on samples initially equilibrated with DI water. The water sorption coefficient,  $K_w$ , was taken as equivalent to the volume fraction of water in the material, which was calculated using Equation 2.5. Co-polymer composition is reported as in Figure 2.4. The uncertainty was taken as one standard deviation from the mean of three measurements..... 113

**Table 6.2.** Salt transport property data for the series of HEMA:GMA:GMAOH materials. The salt sorption coefficient measurements were made at  $22 \pm 1$  °C using sample that initially had been equilibrated with 0.5 mol/L NaCl. Salt permeability was measured at  $25 \pm 0.2$  °C using an upstream salt concentration of 0.5 mol/L NaCl. For each experimentally determined value, the uncertainty was taken as one standard deviation from the mean of three measurements. The apparent salt diffusion coefficient was calculated from the measured salt sorption and salt permeability coefficients using Equation 3.3, and standard propagation of error<sup>19</sup> was used to estimate the uncertainty in the salt diffusion coefficient. Co-polymer composition is reported as in Figure 2.4. .... 115

**Table 6.3.** The distribution of freezable and non-freezable water in the HEMA:GMA:GMAOH materials was calculated using water uptake (Table 6.1) and DSC data. The sum of  $wf$  and  $wnf$  is equivalent to the total water uptake of the material. The co-polymer composition is reported as in Figure 2.4..... 123

**Table 9.1.** Dry polymer density data for the HQ:BP and MHQ:BP materials. All measurements were made at  $22 \pm 1$  °C. The uncertainty was taken as the standard deviation from the mean of three measurements..... 166

**Table 9.2.** Salt sorption coefficients experimentally measured at  $22 \pm 1$  °C and predicted using the Donnan-Manning model (Equation 9.1). The uncertainty was taken as one standard deviation from the mean of three measurements..... 173

**Table 9.3.** Diffusivity and conductivity data for HQ:BP and MHQ:BP. Samples were equilibrated with 1.0 mol/L NaCl solution prior to measurements. All measurements were made at  $22 \pm 1$  °C, and the uncertainty was taken as the standard deviation from the mean of three measurements. Co-ion and counter-ion diffusivity values were calculated by solving Equations 9.6 and 9.7 simultaneously. .... 175

**Table A.1.** Nomenclature..... 192

<b>Table B.1.</b> Chemical structures of the co-monomers and cross-linker used to prepare the HEMA-co-MMA and HEA-co-EA co-polymers. Pure water uptake data are included for polymers prepared from each component, and the homopolymer glass transition temperature is reported for polymers prepared from each component. ....	195
<b>Table B.2.</b> Effective salt diffusion coefficients in the HEA-co-EA and HEMA-co-MMA materials, $D_s$ , determined both experimentally and via the Mackie and Meares model. <sup>5</sup> .....	196
<b>Table B.3.</b> Hydration numbers <sup>6</sup> for the ions considered. ....	196
<b>Table B.4.</b> Values of the number of moles of water available in the polymer divided by the number of moles of water required to fully hydrate the ions sorbed in the polymer. ....	197
<b>Table B.5.</b> Free energy values for the hydration of monovalent ions at 25 °C. <sup>7</sup> The energies given on the per mole of water basis were calculated from the per mole of ion basis using the hydration numbers in Table B.3. ....	198
<b>Table C.1.</b> Equivalents of sorbed water per total equivalents of –OH and –O– in the HEA-co-EA and HEMA-co-MMA co-polymers.....	199
<b>Table C.2.</b> Local to bulk tortuosity values for the HEA-co-EA and HEMA-co-MMA materials calculated using the Mackie and Meares model (Equation 4.5 in Chapter 4) and values of $K_w$ measured using 0.5 mol/L NaCl (Table 4.1 in Chapter 4). ....	201
<b>Table E.1.</b> The freezable water content, non-freezable water content, and the number of moles of freezable water per equivalent of hydroxyl group in the hydrated HEMA:GMA:GMAOH co-polymers. ....	212
<b>Table F.1.</b> Pre-polymerization solution co-monomer and cross-linker mole fractions and the theoretical hydroxyl group content of the materials. ....	213
<b>Table F.2.</b> Relaxation time constants and dielectric strengths determined by fitting the dielectric loss spectra (Figure F.2) to a three Debye relaxation process model (Equation F.1). The uncertainty was taken as one standard deviation from the mean of three parameters regressed from three distinct dielectric loss spectra. ....	219
<b>Table G.1.</b> Water uptake, $w_u$ , water volume fraction, $\phi_w$ , and dry polymer density data measured at $22 \pm 1$ °C. Water uptake measurements were made on samples initially equilibrated with either DI water or an aqueous solution of 0.01, 0.1, or 1.0 mol/L NaCl. The uncertainty was taken as one standard deviation from the mean of three measurements. Hydrolysis time, $z$ , refers to the length of time (in hours) that the XL-pGMA- $z$ samples were immersed in 0.5 mol/L H <sub>2</sub> SO <sub>4</sub> at 40 °C. ....	225
<b>Table G.2.</b> Amounts of strongly-bound, intermediate, and bulk-like water present in XL-pGMA- $z$ when equilibrated in DI water or 0.01, 0.1, or 1.0 mol/L aqueous NaCl solutions. The results were obtained by fitting the OD stretch of each FTIR spectrum of XL-pGMA- $z$ with three Gaussian curves. Each curve represents a different water state, and the area of each Gaussian curve was divided by the total area of the OD stretch. The three values for each material and condition	

sum to the overall volume fraction of sorbed water,  $\phi_w$ . Hydrolysis time,  $z$ , refers to the length of time (in hours) that the XL-pGMA- $z$  samples were immersed in 0.5 mol/L  $H_2SO_4$  at 40 °C. ...225

**Table H.1.** Water uptake and dry polymer density data for the HQ:BP and MHQ:BP materials. The volume fraction of water in the polymer (equivalent to the water sorption coefficient) was calculated from water uptake and dry density data using Equation 2.5. All measurements were made at  $22 \pm 1$  °C. The uncertainty was taken as the standard deviation from the mean of three measurements. ....229

**Table H.2.** Properties of HQ:BP and MHQ:BP materials used to conduct the Donnan-Manning counter-ion condensation theory analysis described in Chapter 9.....229

## List of Figures

**Figure 2.1.** (A) HEA-co-EA and (B) HEMA-co-MMA random co-polymers for investigation of water and salt transport properties. The ratios of hydrophilic to hydrophobic co-monomers are represented on each structure as mass percentages (e.g., the HEA-co-EA material contained a X:Y (by mass) ratio of HEA:EA). Due to differences in the hydrophilicity of the monomer units, we expect some degree of nanophase separation of the hydroxyl (and possibly ester) groups from the backbone and alkyl sidechains. This nanophase separation may be more kinetically trapped or sharper in the more rigid HEMA-co-MMA co-polymers than in the HEA-co-EA co-polymers, where more flexible backbone dynamics may smooth out these nano-scale structural features. .11

**Figure 2.2.** Structures of non-hydrolyzed, i.e., XL-pGMA-0, (left) and partially hydrolyzed, i.e., XL-pGMA-z, (right) materials. The value of z in the sample nomenclature corresponds to the hydrolysis time (in hours) during the membrane preparation process, i.e. z is 0 for the non-hydrolyzed material, and z is 8, 10, or 12 for the partially hydrolyzed materials. All materials were prepared from a base polymer that contained 2.4% (by mole) cross-linker (i.e.,  $x = 0.024$ ), and the value of y increased as the hydrolysis time increased. ....13

**Figure 2.3.** Chemical structure of the cross-linked HEMA:GMA:GMAOH co-polymer. The co-polymers were prepared from pre-polymerization solutions that contained a x:y:z, by mass, ratio of HEMA:GMA:GMAOH co-monomers (such that  $x + y + z = 100$ ). The cross-linker was added such that the mass of cross-linker was 10% of the total mass of the co-monomers. ....14

**Figure 2.4.** The co-monomer content of the co-polymer was systematically varied (by adjusting the composition of the pre-polymerization solution used to prepare the co-polymers) to probe the influence of hydroxyl group configuration on the salt transport properties of the five HEMA:GMA:GMAOH materials considered. The nomenclature on the horizontal axis corresponds to the pre-polymerization solution mass composition. ....17

**Figure 2.5.** Synthesis of the HQ:BP-X and MHQ:BP-X sulfonated poly(arylene ether sulfone) random co-polymers. ....18

**Figure 2.6.** Measuring water diffusion with NMR diffusometry. The linearized signal attenuation plot (A) for fully hydrated HEA-co-EA 30:70 at 298 K shows the attenuation of the normalized NMR signal intensity as a function of the Stejskal-Tanner parameter,  $b$  (Equation 2.9). The slope of the data is equal to the self-diffusion coefficient of water in the polymer, which is  $5.6 \times 10^{-8}$  cm<sup>2</sup>/sec in this example. NMR diffusometry signal attenuation, from the first to the last measurement, can be seen in the 1D spectra (slices) from the experiment (B), which are from the first and last ( $g_{max} = 300$  G/cm) point in (A). ....30

**Figure 3.1.** Differential scanning calorimetry (DSC) second scan thermograms for pure water equilibrated HEA-co-EA and HEMA-co-MMA samples. The dashed line represents  $T = 20$  °C and illustrates that the HEMA-co-MMA material is glassy at room temperature (i.e.,  $T_g > 20$  °C) while the HEA-co-EA material is rubbery at room temperature (i.e.,  $T_g < 20$  °C). ....43

**Figure 3.2.** Salt permeability, at 25 °C, measured using an upstream aqueous electrolyte concentration of 0.5 mol/L of LiCl, NaCl, or KCl. The uncertainty was taken as one standard deviation from the mean of three measurements. ....45

**Figure 3.3.** Salt permeability data (measured at 25 °C using a 0.5 mol/L upstream aqueous LiCl, NaCl, or KCl solution) normalized by the KCl permeability value and plotted as a function of the average salt diffusion coefficient in aqueous solution at infinite dilution and 25 °C. The average salt diffusion coefficient in aqueous solution at infinite dilution (horizontal axis) is a measure of the effective size of the electrolyte, and the horizontal axis is inverted such that the effective electrolyte size increases from left to right as the value of average salt diffusion coefficient decreases. ....49

**Figure 3.4.** Effective salt diffusion coefficients (calculated from measured salt permeability and salt sorption coefficients using (Equation 3.3) normalized by the effective KCl diffusion coefficient and plotted as a function of the average salt diffusion coefficient in aqueous solution at infinite dilution and 25 °C. The average salt diffusion coefficient in aqueous solution at infinite dilution (horizontal axis) is a measure of the effective size of the electrolyte, and the horizontal axis is inverted such that the effective electrolyte size increases from left to right as the value of average salt diffusion coefficient decreases. ....53

**Figure 4.1.** Salt sorption coefficient,  $K_s$ , data for HEA-co-EA and HEMA-co-MMA co-polymers as a function of water uptake in 0.5 mol/L NaCl solution. Sorption data were measured after equilibrating samples in 0.5 mol/L NaCl, at room temperature. The uncertainty in the data was taken as one standard deviation from the mean of four measurements. ....63

**Figure 4.2.** Second scan DSC thermograms for hydrated poly(HEMA-co-MMA) and poly(HEA-co-EA) samples. Sealed hermetic aluminum pans were used to maintain sample hydration, and the heating rate was 10 °C/min. The thermograms are displaced vertically for clarity, and the compositions of the co-polymers are listed as the ratio of hydrophilic to hydrophobic co-monomer (by mass). ....64

**Figure 4.3.**  $^1\text{H}$  NMR spectra that illustrate water and polymer spectral components in 1D and in diffusometry experiments for HEA-co-EA 30:70 and HEMA-co-MMA 30:70 equilibrated in 0.5 mol/L NaCl solution. Plots A and B are 1D pulse-acquire NMR spectra (32 scans each), and spectra C and D were obtained from the first gradient step (smallest  $g$ ) of the NMR diffusometry experiment (16 scans each). Signal from the HEMA-co-MMA measurements was weak compared to that from HEA-co-EA, so the vertical scales of the B and D spectra have been multiplied by scaling factors to illustrate peak shapes more clearly. ....68

**Figure 4.4.** Water diffusion coefficients,  $D_w$ , decrease as diffusion time,  $\Delta$  (and diffusion length,  $ld$ ) increase in both the (A) HEA-co-EA and (B) HEMA-co-MMA co-polymers. We define  $D_0$  as the water diffusion coefficient at the shortest diffusion time measured, and  $D_\infty$  as the water diffusion coefficient at the longest diffusion time measured. ....69

**Figure 4.5.** Diffusion through a heterogeneous polymer matrix over diffusion length scales  $ld$  ranging from less than 1 nm to greater than 1  $\mu\text{m}$ . Water molecules that diffuse within nm-scale hydrophilic pathways (A) over a mean-square displacement less than the radius  $R$  of the cavity or

pathway ( $ld2 = D\Delta < R2$ ) will not show restricted diffusion behavior as the pathways are not tortuous on this length scale. This nm-scale “local” diffusion coefficient we define as  $D_{loc}$ . At larger length scale (B), we expect the pathways to be tortuous (indirect) paths. Average water diffusion on this length scale,  $D_w[ld]$  will be slower than what is observed in (A). At lengths  $\sim 1 \mu\text{m}$  and above (C), structural heterogeneities may reduce the observed water diffusivity relative to that observed at smaller length scales. As the diffusion length scale increases ( $ld2 = D\Delta \gg R2$ ), water diffusivity measured by NMR will approach the bulk diffusivity. .... 71

**Figure 4.6.** Local to bulk (Equation 4.3, patterned bars) and micron to bulk (Equation 4.4, solid bars) tortuosity values for HEA-co-EA and HEMA-co-MMA. All of the co-polymers exhibit similar micron to bulk tortuosity, but the local to bulk tortuosity value for HEMA-co-MMA is larger than that for HEA-co-EA likely due to local nanoscale differences between the two co-polymers. .... 74

**Figure 4.7.** Illustration of the arrangement of hydrophilic and hydrophobic regions of the HEA-co-EA and HEMA-co-MMA membranes. Self-organization of hydrophilic functional groups present within the co-polymers may create different geometries or dynamics of nm-scale transport pathways for the rubbery and glassy systems, due to the differing arrangements and mobilities of the hydroxyl side chains from the HEA and HEMA moieties. We expect the hydroxyl side chains to extend into the pathways to interact with sorbed water, leading to wider pathways than one might expect for the observed ratio of sorbed water to hydrophilic moieties (roughly 2 equivalents sorbed water per equivalent of  $-\text{OH}$  and  $-\text{O}-$ ). .... 76

**Figure 4.8.** Proposed model of the heterogeneous hydrophilic network inside the HEA-co-EA and HEMA-co-MMA co-polymers. Polymer domains are separated by clusters of “dead ends” where the hydrophilic network is interrupted by higher concentrations of hydrophobic chain segments. Continuous paths (green) allow water to transport through the membrane, however, dead ends along this path will restrict diffusion. .... 77

**Figure 4.9.** Water diffusivity,  $D_w$ , (A) and permeability,  $P_w$ , (B) data for poly(HEA-co-EA) ( $\blacktriangle$ ) and poly(HEMA-co-MMA) ( $\blacktriangle$ ) co-polymers and sodium chloride diffusivity,  $D_s$ , (A) and permeability,  $P_s$ , (B) data for poly(HEA-co-EA) ( $\square$ ) and poly(HEMA-co-MMA) ( $\square$ ) co-polymers as a function of water uptake. Water diffusivity data were measured via NMR. Salt diffusivity data were measured via kinetic desorption, where samples were characterized at  $25^\circ\text{C}$  following equilibration in 0.5 mol/L aqueous NaCl. Water permeability was calculated as  $P_w = D_w \times K_w$  using the measured diffusion and sorption (Table 4.1) coefficients. Salt permeability was calculated as  $P_s = D_s \times K_s$  using the measured diffusion and sorption (Figure 4.1) coefficients. The uncertainty was taken as the standard deviation from the mean of three measurements. .... 78

**Figure 4.10.** Water/salt permeability selectivity ( $P_w/P_s$ ) for poly(HEA-co-EA) ( $\blacktriangle$ ) and poly(HEMA-co-MMA) ( $\blacktriangle$ ) co-polymers and water/salt diffusion selectivity ( $D_w/D_s$ ) for poly(HEA-co-EA) ( $\square$ ) and poly(HEMA-co-MMA) ( $\square$ ) co-polymers as a function of water uptake. .... 80

**Figure 5.1.** (A, left) Relative permittivity,  $\epsilon'$ , as a function of frequency for DI water, Nafion<sup>®</sup> 117<sup>29</sup>, XL-pGMA-z, and PTFE. (B, right) Data for XL-pGMA-z are shown with the single Debye relaxation fit (dashed curves). The hydrolysis time,  $z$ , is labeled for each XL-pGMA-z sample. All

measurements were made at  $295 \pm 1$  K, and the uncertainty was taken as the standard deviation from the mean of three measurements. ....91

**Figure 5.2.** Differential scanning calorimetry (DSC) thermograms for XL-pGMA-z and Nafion<sup>®</sup> 117. The hydrolysis time, z, refers to the length of time (in hours) that the XL-pGMA-z samples were immersed in 0.5 mol/L H<sub>2</sub>SO<sub>4</sub> at 45 °C. ....93

**Figure 5.3.** Static permittivity,  $\epsilon_s$ , of XL-pGMA-z (measured at  $22 \pm 1$  °C), Nafion<sup>®</sup> 117<sup>a</sup> (measured at 25 °C)<sup>29</sup>, and Nafion<sup>®</sup> 117<sup>b</sup> (measured at 30 °C)<sup>10</sup>, plotted as a function of the volume fraction of water sorbed in the polymer. Values for the static permittivity of water and PTFE are also shown. The long dashed line represents a static permittivity (or dielectric constant) linear approximation. The short dashed line illustrates the different functional relationship between static permittivity and volume fraction of water for XL-pGMA-z compared to Nafion<sup>®</sup>. Uncertainty in the XL-pGMA-z data was taken as the standard deviation from the mean of three measurements. ....95

**Figure 5.4.** Water/ion sorption selectivity,  $K_w/K_s$  as a function of  $K_w$  for XL-pGMA-z, Nafion<sup>®</sup> 117, and previously reported uncharged polymers (circles)<sup>53</sup>. The solid line represents a sorption selectivity trade-off frontier reported for desalination membranes.<sup>2, 52</sup> .....98

**Figure 5.5.** Solvation energy barrier calculated (solid bars, experimental data) using measured sorption coefficients (Table 5.3) and Equation 5.5, and calculated (striped bars, electrostatic theory) using static permittivity values (Figure 5.3) and the Born model (Equation 5.6). ....102

**Figure 6.1.** Salt sorption coefficient data as a function of the water sorption coefficient for HEMA:GMA:GMAOH (this study, ■) and hydrogels (□).<sup>13</sup> The dashed line on this parity plot indicates the border between salt exclusion from the polymer (points below the line) and salt enrichment in the polymer (points above the line). For HEMA:GMA:GMAOH, the HEMA co-monomer composition of the pre-polymerization solution used to prepare each co-polymer is reported for each data point. ....116

**Figure 6.2.** Salt permeability (A) and apparent salt diffusion (B) coefficients as a function of inverse water sorption coefficient for HEMA:GMA:GMAOH (this study, ■) and hydrogels (□).<sup>13</sup> For HEMA:GMA:GMAOH, the HEMA co-monomer composition of the pre-polymerization solution used to prepare each co-polymer is reported for each data point. The dashed lines are drawn to guide the eye for the hydrogel data. The uncertainty in the data for the HEMA:GMA:GMAOH materials is within the size of the data points. ....117

**Figure 6.3.** Frequency-dependent relative permittivity,  $\epsilon'$ , data for the HEMA:GMA:GMAOH co-polymers. The data sets are labeled with the HEMA co-monomer composition of the pre-polymerization solution used to prepare each co-polymer. Dashed curves are a single Debye relaxation fit to the measured data. All measurements were made at  $22 \pm 1$  °C, and the uncertainty was taken as one standard deviation from the mean of three measurements. ....120

**Figure 6.4.** Differential scanning calorimetry (DSC) thermograms for the hydrated GMA:HEMA:GMAOH materials. The HEMA co-monomer composition of the pre-polymerization solution used to prepare each co-polymer is reported for each data set. ....122

**Figure 7.1.** Water/salt sorption selectivity (A) and water/salt diffusivity selectivity (B) as a function of water sorption coefficient and apparent water diffusion coefficient, respectively, for HEMA:GMA:GMAOH (■) and PEG (□)<sup>6</sup> materials. For HEMA:GMA:GMAOH, the HEMA comonomer composition of the pre-polymerization solution used to prepare the co-polymer is reported for each data point. The dashed lines represent reported empirical sorption (left) and diffusivity (right) trade-off frontiers for desalination membrane materials,<sup>7,8</sup> and the solid lines are least-squares fits to the data..... 134

**Figure 7.2.** Water/salt permeability selectivity as a function of diffusive water permeability for HEMA:GMA:GMAOH (■) and PEG (□)<sup>6</sup> materials. For HEMA:GMA:GMAOH, the HEMA comonomer composition of the pre-polymerization solution used to prepare the co-polymer is reported for each data point. The dashed line represents a reported empirical permeability trade-off frontier for desalination membrane materials,<sup>7,8</sup> and the solid lines are least-squares fits to the data..... 138

**Figure 8.1.** Volume fraction of water as a function of external NaCl concentration for XL-pGMA-z, where z represents the hydrolysis time in hours, ranging from 7 to 11 hours. The dashed lines are included to guide the eye. All measurements were made at 22 °C ± 1 °C, and the uncertainty was taken as one standard deviation from the mean of three measurements..... 144

**Figure 8.2.** Salt sorption coefficient as a function of external NaCl concentration for XL-pGMA-z. Salt sorption in XL-pGMA-7 equilibrated with 0.01 mol/L NaCl solution was too low to measure reliably. The dashed lines are included to guide the eye. All measurements were made at 22 ± 1 °C, and the uncertainty was taken as one standard deviation from the mean of three measurements..... 145

**Figure 8.3.** Experimentally measured (■) and reported<sup>1</sup> static permittivity (●) properties, as a function of the volume fraction of sorbed water, of XL-pGMA-z materials (squares) equilibrated in pure water. The dashed and dotted lines represent the prediction made using the Maxwell Garnett equation, the dashed line treats the dry polymer and the sorbed water as the continuous and the dispersed phase, respectively, for  $\phi_w < 0.45$ , whereas the dotted line treats the dry polymer and the sorbed water as the dispersed and the continuous phase, respectively, for  $\phi_w > 0.5$ .<sup>21</sup> 148

**Figure 8.4.** Salt sorption coefficient as a function of volume fraction of water for XL-pGMA-z (circles) and XL-PEGDA-w (squares)<sup>22</sup> materials. The value of w represents the percentage (by mass) of DI water added to the pre-polymerization mixture of XL-PEGDA.<sup>22</sup> The XL-pGMA-z materials were equilibrated with external salt solutions of 0.01, 0.1, and 1.0 mol/L NaCl, and the XL-PEGDA-w samples were equilibrated with external salt solutions of 0.01, 0.03, 0.1, 0.3, and 1.0 mol/L NaCl. For both materials, the value of the salt sorption coefficient increased as the external salt concentration increased (i.e., the lowest datum point for each material corresponds to the lowest external salt solution concentration (i.e. 0.01 mol/L NaCl), and the highest datum point for each material corresponds to the highest external salt solution concentration (i.e., 1.0 mol/L NaCl). The dashed line describes the variation of the salt sorption coefficient with the volume fraction of water in a situation where long-range electrostatic forces dominate ion sorption thermodynamics and the functional relationship between the static dielectric constant of the hydrated polymer and the volume fraction of water sorbed in the polymer is described by the Maxwell Garnett model..... 149

<b>Figure 8.5.</b> Frequency-dependent relative permittivity of hydrated XL-pGMA-7 (A), -9 (B), and -11 (C). Labeled on each curve is the external solution used to equilibrate the samples. Data for XL-pGMA-z are shown with the single Debye relaxation fit as dashed curves. All measurements were made at $22\text{ }^{\circ}\text{C} \pm 1\text{ }^{\circ}\text{C}$ , and the uncertainty was taken as the standard deviation from the mean of three measurements.....	151
<b>Figure 8.6.</b> Illustration of possible sodium ion-water competition in the XL-pGMA-7 material. ....	152
<b>Figure 8.7.</b> Bulk-like water content of XL-pGMA-z measured using samples that were equilibrated in DI water or 0.01, 0.1, and 1.0 mol/L aqueous NaCl solutions. The dashed curves were drawn to guide the eye. The bulk-like water content represents a percentage of the total sorbed water mass in XL-pGMA-z. ....	154
<b>Figure 8.8.</b> Static permittivity of XL-pGMA-z as a function of the volume fraction of water sorbed by the polymer. Samples were equilibrated in either pure water (■), 0.01 mol/L NaCl (▲), 0.1 mol/L NaCl (◆), or 1.0 mol/L NaCl (●). Each data set represented in the figure contains a data point for XL-pGMA-7, -9, and -11, and in all cases, the volume fraction of water increases as the z value of XL-pGMA-z increases. The dashed lines are included to guide the eye.....	156
<b>Figure 9.1.</b> Water (A) and salt (B) permeability as a function of water content for the HQ:BP and MHQ:BP materials. The dashed lines are included to guide the eye. All measurements were made at $22 \pm 1\text{ }^{\circ}\text{C}$ , and the uncertainty was taken as one standard deviation from the mean of three measurements. ....	165
<b>Figure 9.2.</b> Salt (NaCl) sorption coefficient values as a function of water content for the HQ:BP and MHQ:BP materials. The dashed lines are included to guide the eye. All measurements were made at $22\text{ }^{\circ}\text{C} \pm 1\text{ }^{\circ}\text{C}$ , and the uncertainty was taken as one standard deviation from the mean of three measurements.....	167
<b>Figure 9.3.</b> Frequency-dependent relative permittivity of the HQ:BP (A) and MHQ:BP (B) materials. All measurements were made at $22\text{ }^{\circ}\text{C} \pm 1\text{ }^{\circ}\text{C}$ , and the uncertainty was taken as one standard deviation from the mean of three measurements.....	168
<b>Figure 9.4.</b> Water (A) and salt (B) diffusivity as a function of water content for HQ:BP and MHQ:BP. The dashed lines are included to guide the eye. All measurements were made at $22\text{ }^{\circ}\text{C} \pm 1\text{ }^{\circ}\text{C}$ , and the uncertainty was taken as one standard deviation from the mean of three measurements. ....	174
<b>Figure C.1.</b> Diffusion length as a function of the experimental diffusion time. At long diffusion times, we see a plateauing of the diffusion length due to restricted diffusion effects in both series of membranes.....	200
<b>Figure D.1.</b> FT-IR spectra of pGMA and XL-pGMA-z measured using film samples and an attenuated total reflectance (ATR) cell. ....	204

**Figure D.2.** Schematic of the four S-parameters in a two-port vector network analyzer measurement (Top).<sup>4</sup> DUT stands for device under test. The calibration plane (i.e., the region between the two coaxial cable ports) and both the air and sample regions in the DUT are illustrated (Bottom). The amount of sample loaded in the transmission line is represented by the length dimension,  $d$ . .....205

**Figure D.3.** Dielectric permittivity properties for air (i.e., an empty transmission line) and PTFE. Measurements were made at  $22 \pm 1$  °C, and the uncertainty for PTFE was taken as the standard deviation from the mean of three measurements. ....206

**Figure D.4.** Dielectric permittivity properties measured for DI water. Data were fit to a single Debye relaxation process (dashed curves). Measurements were made at  $22 \pm 1$  °C using different sample lengths (values of  $d$ ) to optimize the measurement over the entire frequency range. ....207

**Figure E.1.** FT-IR spectra of hydrated HEMA:GMA:GMAOH film samples measured using an attenuated total reflectance (ATR) cell. The composition of the pre-polymerization solution used to prepare each co-polymer is listed for each spectrum. The dashed line indicates the position of the primary alcohol stretching peak (approximately  $1070\text{ cm}^{-1}$ ) for the HEMA:GMA:GMAOH 60:40:0 material to illustrate the shift that occurs as GMAOH content increases. Additionally, the shoulder on the  $1160\text{ cm}^{-1}$  peak is identified. ....210

**Figure F.1.** Fourier-transform infrared (FT-IR) spectra for dry HEMA:GMA:GMAOH co-polymers. The spectra were obtained in attenuated total reflectance mode using co-polymers that had been dried under vacuum for 24 hours after an approximately 2 month long period where the films were soaked in DI water. The figure on the right highlights the  $700$  to  $1000\text{ cm}^{-1}$  region of the spectra shown on the left. ....215

**Figure F.2.** Frequency-dependent dielectric loss spectra,  $\epsilon''$ , for the hydrated HEMA:GMA:GMAOH co-polymers. The spectra are labeled with the composition of the HEMA content of the pre-polymerization solution used to prepare the co-polymer. All measurements were made at  $22 \pm 1$  °C, and the uncertainty was taken as one standard deviation from the mean of three measurements. ....218

**Figure F.3.** Enthalpy of mixing data as a function of mole fraction of water for mixtures of water and either ethanol<sup>25</sup> or 1,2-propanediol<sup>26</sup> at  $25$  °C. Ethanol and 1,2-propanediol were chosen because of their similarity to the side chain moieties on the HEMA and GMAOH co-monomers. The enthalpy of mixing data were normalized by the equivalents of  $-\text{OH}$  moieties in the organic molecule (i.e., 1 eq( $-\text{OH}$ ) for ethanol and 2 eq( $-\text{OH}$ ) for 1,2-propanediol). ....221

**Figure G.1.** Representative FT-IR spectra for XL-pGMA-7 (top), -9 (middle), and -11 (bottom) materials that were equilibrated in  $1.0\text{ mol/L NaCl}$ . The three Gaussian peaks that represent the three water states (bulk-like water, intermediate water, and strongly-bound water) are labeled on the figures. ....226

**Figure G.2.** Static permittivity of XL-pGMA-z measured using samples that were equilibrated in DI water or  $0.01$ ,  $0.1$ , and  $1.0\text{ mol/L}$  aqueous  $\text{NaCl}$  solutions. The dashed line is included to guide the eye. ....227

**Figure G.3.** Static permittivity as a function of NaCl concentration for bulk aqueous NaCl solution.<sup>1</sup> The dashed line is included to guide the eye. ....228

# Chapter 1: Introduction

## 1.1. Addressing Global Water Shortages with Membrane-based Desalination

Polymers are widely used as membranes to efficiently desalinate saline water and to address global need for clean water.<sup>1-7</sup> While membrane-based desalination technology has been used for several decades, current state-of-the-art polyamide-based reverse osmosis (RO) and nanofiltration (NF) membranes in desalination systems are susceptible to oxidative degradation via chlorine-containing compounds used to disinfect water and prevent membrane biofouling. For this reason, advanced chlorine-tolerant desalination membrane materials are needed to address the material degradation challenge.<sup>1, 5, 8-12</sup>

While others have produced chlorine-tolerant polymers from polysulfone,<sup>11, 13-18</sup> poly(phenylene oxide),<sup>19-21</sup> polymethacrylates,<sup>22-26</sup> polybenzimidazoles,<sup>5, 27</sup> and styrenics,<sup>5</sup> a combination of chlorine tolerance and favorable selectivity properties remains elusive. The selectivity of a membrane can be defined as the ratio of the permeability (flux normalized by membrane thickness and the driving force for transport) of the desired compounds relative to that of the undesired compounds. For example, in desalination applications, selectivity typically is defined as the ratio of the water permeability to that of salt, and effective desalination membranes permeate water faster than hydrated ions.<sup>4, 5, 28, 29</sup>

Permeability is often used to describe rates of water and ion transport in desalination membrane materials and includes sorption and diffusivity properties components of transport.<sup>4, 5, 30</sup> These properties define the thermodynamic and kinetic, respectively, contributions to membrane transport properties.<sup>5, 9, 12, 31</sup> For effective desalination, polymers needs to be designed with the ability to either suppress ion sorption and/or diffusivity properties, thus increasing the selectivity

properties in these membrane materials. Currently, few structure-property relationships are available to guide the development of chemically stable polymer membranes that offer selective properties comparable to the current state-of-the-art polyamide-based membranes.<sup>4, 28, 29, 32, 33</sup>

To solve this challenge, the studies enclosed in this dissertation focus on understanding the structure-property relationships between polymer chemistry and desalination properties in polymer membranes using model polymers that have well-controlled polymer chemistry and water content. These model polymers can be subsequently used for transport and selectivity property characterization that are important for understanding structure-property relationships in the materials. Ultimately, the formation of integrated structure-property guidance is critical to help engineer advanced polymer membranes to desalinate water efficiently and effectively.

## **1.2. Goals and Organization of the Dissertation**

The primary goal of the study is to understand the structure-property relationships between polymer chemistry and desalination properties in polymer membranes, which is critical information to guide the design of advanced and highly selective desalination membranes. To achieve this goal, a few model polymers (different from polyamide-based commercial desalination membranes)<sup>5, 32</sup> were generated with specific polymer chemistry modifications, either on the polymer backbone or the polymer side chain. This chemical modification is important to study the influence of polymer chemistry on transport and selectivity properties, which includes the water and salt permeability, sorption, and diffusion properties, that are important properties for desalination applications.

This dissertation contains 10 chapters beginning with the introduction chapter as [Chapter 1](#). [Chapter 2](#) summarizes the materials used for all studies, which mainly include model polymers,

electrolytes (i.e., ions), and solvents/solution. [Chapter 2](#) also introduces the polymer characterization methods used to understand the properties of the model polymers.

[Chapters 3](#) and [4](#) focus on investigating the influence of polymer backbone rigidity on membrane transport and selectivity properties in desalination membrane materials. Two series of structurally similar low water content hydroxyethyl methacrylate- and acrylate-based polymers with different backbone rigidity were prepared. Thermal characterization techniques were used to probe backbone rigidity and homogeneity of these materials. Water and salt sorption and diffusion coefficients, and permeability values were measured, and water/salt permeability selectivity properties were determined for the two series of materials and further compared and discussed. The salt size selectivity of these two series of liquid separation membranes was also compared to that of the gas separation membranes and the result further discussed.

[Chapter 5](#) demonstrates the unique approach of using the microwave dielectric relaxation spectroscopy (DRS) to probe the dipole relaxation mechanism of water molecules, in terms of frequency-dependent relative (or dielectric) permittivity, in hydrated polymers. The functional relationship between relative permittivity (and freezable water content) and polymer water content in the glycidyl and glycerol methacrylate-based model polymer was determined and compared to that of pure water, hydrophobic PTFE, and a commercially available ion exchange membrane. The polymer ion sorption and selectivity properties also were measured and were compared to that of the commercially available ion exchange membrane. Important to understand the physics that governs the ion sorption process in these hydrated polymers, the ion sorption measured experimentally were compared to that predicted by the electrostatic exclusion theory.

Based on the findings in [Chapter 5](#), the microwave DRS technique was further used as a tool to investigate the influence of chemical functional group configuration on polymer transport

and selectivity properties in [Chapters 6](#) and [7](#). A series of water content equivalent hydroxyl group-containing methacrylate-based polymers, which have different mass fractions of 2-hydroxyethyl methacrylate (HEMA, a single hydroxyl group) and glycerol methacrylate (GMAOH, a vicinal diol, or two hydroxyl, group), were prepared. The polymer composition was varied systematically from a vicinal diol-rich (GMAOH-rich) configuration to a distributed hydroxyl group (HEMA-rich) configuration, and the relative permittivity, freezable water content, water and salt sorption, diffusion, and permeability of these model polymers were measured and discussed. Important for desalination, water/salt transport selectivity of these model polymers were compared to that of a series of polyethylene glycol (PEG)-based desalination membrane materials.

In [Chapter 8](#), glycidyl and glycerol methacrylate-based polymers (same materials that were used in [Chapter 5](#)) were further used to investigate the influence of salt concentration on relative permittivity and ion sorption properties. The effect of salt concentration on osmotic de-swelling and sorption properties was discussed. The functional relationship between salt concentration and sorption properties was also discussed and compared to that of the relationship predicted by the electrostatic exclusion theory. Relative permittivity and bulk-like water content were measured to further understand the molecular level interactions between ion, water, and the polymer backbone in these materials. Lastly, influence of salt concentration on relative permittivity in these hydrated polymers were investigated and compared to that of the situation in aqueous salt solutions.

In [Chapter 9](#), two series of water content equivalent sulfonated polysulfones were prepared to investigate the influence of functional group incorporation on polymer dry density, relative permittivity, and water and ion transport properties in charged polymers. The functional group incorporation was achieved by adding methoxy groups to the polymer backbone of these materials. Important for the field, the characterization results of the charged polymers were compared to that

of the uncharged polymers to understand the governing factors of water and ion sorption and diffusion properties in these two types of materials (i.e., charged versus uncharged polymers).

[Chapter 10](#) summarizes the main conclusions of the dissertation. In the same chapter, the significance of the studies and recommendations for future work/research directions are also included. Finally, there are 8 appendices (i.e., [Appendices A to H](#)) attached at the end of the dissertation that begins with a nomenclature ([Appendix A](#)) section followed by 7 supporting information sections for [Chapters 3 to 9](#), respectively.

### 1.3. References

1. Cohen, Y.; Semiat, R.; Rahardianto, A., A perspective on reverse osmosis water desalination: Quest for sustainability. *AIChE Journal* **2017**, *63* (6), 1771-1784.
2. Elimelech, M.; Phillip, W. A., The future of seawater desalination: Energy, technology, and the environment. *Science* **2011**, *333*, 712-717.
3. Shannon, M. A.; Bohn, P. W.; Elimelech, M.; Georgiadis, J. G.; Marinas, B. J.; Mayes, A. M., Science and technology for water purification in the coming decades. *Nature* **2008**, *452* (7185), 301-310.
4. Geise, G. M.; Paul, D. R.; Freeman, B. D., Fundamental water and salt transport properties of polymeric materials. *Progress in Polymer Science* **2014**, *39* (1), 1-42.
5. Geise, G. M.; Lee, H.-S.; Miller, D. J.; Freeman, B. D.; McGrath, J. E.; Paul, D. R., Water purification by membranes: The role of polymer science. *Journal of Polymer Science Part B: Polymer Physics* **2010**, *48* (15), 1685-1718.
6. Kamcev, J.; Freeman, B. D., Charged polymer membranes for environmental/energy applications. *Annual Review of Chemical and Biomolecular Engineering* **2016**, *7* (1), 111-133.
7. Fritzmann, C.; Löwenberg, J.; Wintgens, T.; Melin, T., State-of-the-art of reverse osmosis desalination. *Desalination* **2007**, *216* (1), 1-76.

8. Park, H. B.; Freeman, B. D.; Zhang, Z.-B.; Sankir, M.; McGrath, J. E., Highly chlorine-tolerant polymers for desalination. *Angew. Chem.* **2008**, *120*, 6108-6113.
9. Baker, R. W., *Membrane Technology and Applications*. 3rd ed.; Wiley: New York, 2012.
10. Allegrezza Jr., A. E.; Parekh, B. S.; Parise, P. L.; Swiniarski, E. J.; White, J. L., Chlorine resistant polysulfone reverse osmosis modules. *Desalination* **1987**, *64*, 285-304.
11. Parise, P. L.; Allegrezza Jr., A. E.; Parekh, B. S., Reverse osmosis: Chlorine-resistant polysulfone reverse osmosis membrane and module. *Ultrapure Water* **1987**, *4* (7), 54-65.
12. Geise, G. M.; Paul, D. R.; Freeman, B. D., Fundamental water and salt transport properties of polymeric materials. *Prog. Polym. Sci.* **2014**, *39*, 1-42.
13. Allegrezza, A. E.; Parekh, B. S.; Parise, P. L.; Swiniarski, E. J.; White, J. L., Chlorine resistant polysulfone reverse osmosis modules. *Desalination* **1987**, *64*, 285-304.
14. Park, H. B.; Freeman, B. D.; Zhang, Z.-B.; Sankir, M.; McGrath, J. E., Highly chlorine-tolerant polymers for desalination. *Angewandte Chemie International Edition* **2008**, *47* (32), 6019-6024.
15. Xie, W.; Cook, J.; Park, H. B.; Freeman, B. D.; Lee, C. H.; McGrath, J. E., Fundamental salt and water transport properties in directly copolymerized disulfonated poly(arylene ether sulfone) random copolymers. *Polymer* **2011**, *52* (9), 2032-2043.
16. Oh, H. J.; Freeman, B. D.; McGrath, J. E.; Lee, C. H.; Paul, D. R., Thermal analysis of disulfonated poly(arylene ether sulfone) plasticized with poly(ethylene glycol) for membrane formation. *Polymer* **2014**, *55* (1), 235-247.
17. Zhang, Y.; Zhao, C.; Yan, H.; Pan, G.; Guo, M.; Na, H.; Liu, Y., Highly chlorine-resistant multilayer reverse osmosis membranes based on sulfonated poly(arylene ether sulfone) and poly(vinyl alcohol). *Desalination* **2014**, *336*, 58-63.

18. Luo, H.; Aboki, J.; Ji, Y.; Guo, R.; Geise, G. M., Water and salt transport properties of triptycene-containing sulfonated polysulfone materials for desalination membrane applications. *ACS Applied Materials & Interfaces* **2018**, *10* (4), 4102-4112.
19. Kimura, S. G., Reverse osmosis performance of sulfonated poly(2,6-dimethylphenylene ether) ion exchange membranes. *Industrial & Engineering Chemistry Product Research and Development* **1971**, *10* (3), 335-339.
20. Li, N.; Yan, T.; Li, Z.; Thurn-Albrecht, T.; Binder, W. H., Comb-shaped polymers to enhance hydroxide transport in anion exchange membranes. *Energy & Environmental Science* **2012**, *5* (7), 7888-7892.
21. McCormack, P. M.; Luo, H.; Geise, G. M.; Koenig, G. M., Conductivity, permeability, and stability properties of chemically tailored poly(phenylene oxide) membranes for Li<sup>+</sup> conductive non-aqueous redox flow battery separators. *Journal of Power Sources* **2020**, *460*, 228107.
22. Chang, K.; Xue, T.; Geise, G. M., Increasing salt size selectivity in low water content polymers via polymer backbone dynamics. *Journal of Membrane Science* **2018**, *552*, 43-50.
23. Chang, K.; Korovich, A.; Xue, T.; Morris, W. A.; Madsen, L. A.; Geise, G. M., Influence of rubbery versus glassy backbone dynamics on multiscale transport in polymer membranes. *Macromolecules* **2018**, *51* (22), 9222-9233.
24. Chang, K.; Luo, H.; Geise, G. M., Water content, relative permittivity, and ion sorption properties of polymers for membrane desalination. *Journal of Membrane Science* **2019**, *574*, 24-32.
25. Luo, H.; Chang, K.; Bahati, K.; Geise, G. M., Functional group configuration influences salt transport in desalination membrane materials. *Journal of Membrane Science* **2019**, *590*, 117295.
26. Luo, H.; Chang, K.; Bahati, K.; Geise, G. M., Engineering selective desalination membranes via molecular control of polymer functional groups. *Environmental Science & Technology Letters* **2019**, *6* (8), 462-466.

27. Harrison, W. L.; Hickner, M. A.; Kim, Y. S.; McGrath, J. E., Poly(arylene ether sulfone) copolymers and related systems from disulfonated monomer building blocks: Synthesis, characterization, and performance – a topical review. *Fuel Cells* **2005**, *5* (2), 201-212.
28. Geise, G. M.; Park, H. B.; Sagle, A. C.; Freeman, B. D.; McGrath, J. E., Water permeability and water/salt selectivity tradeoff in polymers for desalination. *Journal of Membrane Science* **2011**, *369* (1), 130-138.
29. Zhang, H.; Geise, G. M., Modeling the water permeability and water/salt selectivity tradeoff in polymer membranes. *Journal of Membrane Science* **2016**, *520*, 790-800.
30. Wijmans, J. G.; Baker, R. W., The solution-diffusion model: A review. *Journal of Membrane Science* **1995**, *107* (1), 1-21.
31. Paul, D. R., Reformulation of the solution-diffusion theory of reverse osmosis. *Journal of Membrane Science* **2004**, *241* (2), 371-386.
32. Park, H. B.; Kamcev, J.; Robeson, L. M.; Elimelech, M.; Freeman, B. D., Maximizing the right stuff: The trade-off between membrane permeability and selectivity. *Science* **2017**, *356* (6343).
33. Werber, J. R.; Deshmukh, A.; Elimelech, M., The critical need for increased selectivity, not increased water permeability, for desalination membranes. *Environmental Science & Technology Letters* **2016**, *3* (4), 112-120.

## Chapter 2: Materials and Methods

### 2.1. Materials

#### 2.1.1. Hydroxyethyl Acrylate- and Methacrylate-based Polymers\*

Two series of chemically-similar co-polymers were prepared so that one series would have a flexible backbone and the other series would have a rigid backbone at room temperature. An acrylic co-polymer composed of 2-hydroxyethyl acrylate (HEA, 96%, Sigma-Aldrich) and ethyl acrylate (EA, 99%, Sigma-Aldrich) co-monomers was chosen as the flexible backbone polymer, and the rigid backbone material was chosen to be a methacrylate-based copolymer and was a composed of 2-hydroxyethyl methacrylate (HEMA, 97%, Sigma-Aldrich) and methyl methacrylate (MMA, 99%, Sigma-Aldrich) co-monomers. Poly(ethylene glycol diacrylate) (PEGDA, average  $M_n = 250 \text{ g mol}^{-1}$ , Sigma-Aldrich) was used as a cross-linker. The methacrylate backbone co-polymer was expected to be more rigid than the acrylic co-polymer because of the extra methyl group on the methacrylate backbone that increases the energy barrier for chain rotation.<sup>1</sup>

Co-polymers were prepared by mixing the co-monomers, cross-linker, and a UV photoinitiator (1-hydroxycyclohexyl phenyl ketone, HCPK, 99%, Sigma-Aldrich) to form a pre-polymerization solution. This solution was stirred for 10 minutes to form a homogeneous mixture and then sonicated for 15 minutes in an ultrasonic water bath to degas the solution. Then, the pre-polymerization solution was confined between a quartz plate and a glass plate and irradiated with  $120 \mu\text{J}/\text{cm}^2$  of 254 nm UV radiation to form clear and transparent films using free radical

---

\* This section has been adapted with permission from: Chang, K.; Korovich, A.; Xue, T.; Morris, W. A.; Madsen, L. A.; Geise, G. M., Influence of rubbery versus glassy backbone dynamics on multiscale transport in polymer membranes. *Macromolecules* **2018**, *51* (22), 9222-9233.

polymerization. Film thickness was controlled by stainless steel spacers that were used to separate the quartz and glass plates during the curing process. Typical final film thicknesses were in the range of 50 – 200  $\mu\text{m}$ .

Three compositions of each co-polymer were prepared. Sample nomenclature is based on the hydrophilic co-monomer (i.e., HEA or HEMA) and hydrophobic co-monomer (i.e., EA or MMA). Thus, the flexible co-polymer is designated HEA-co-EA X:Y, and the rigid co-polymer is designated HEMA-co-MMA X:Y. The prepared compositions (X:Y = 30:70, 35:65, or 40:60) represent the mass ratios of the hydrophilic co-monomer to hydrophobic co-monomer. All co-polymers were cross-linked using 3% (by mass relative to the total mass of the hydrophilic and hydrophobic co-monomers) PEGDA ([Figure 2.1](#)), and the HCPK initiator concentration in the pre-polymerization solution was 0.5% (by mass). The curing times were 120 seconds and 500 seconds for the HEA-co-EA and HEMA-co-MMA materials, respectively. After curing, the clear and transparent films were soaked promptly in de-ionized (DI) water (18.2 M $\Omega$  cm and 1.2 ppb total organic carbon) to hydrate the co-polymers.

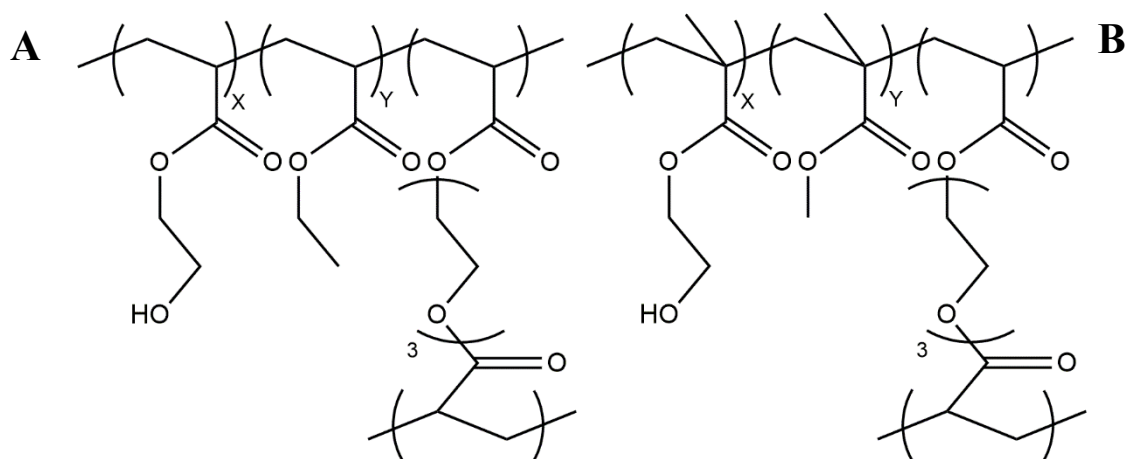


**Figure 2.1.** (A) HEA-co-EA and (B) HEMA-co-MMA random co-polymers for investigation of water and salt transport properties. The ratios of hydrophilic to hydrophobic co-monomers are represented on each structure as mass percentages (e.g., the HEA-co-EA material contained a X:Y (by mass) ratio of HEA:EA). Due to differences in the hydrophilicity of the monomer units, we expect some degree of nanophase separation of the hydroxyl (and possibly ester) groups from the backbone and alkyl sidechains. This nanophase separation may be more kinetically trapped or sharper in the more rigid HEMA-co-MMA co-polymers than in the HEA-co-EA co-polymers, where more flexible backbone dynamics may smooth out these nano-scale structural features.

### 2.1.2. Glycidyl and Glycerol Methacrylate-based Polymers<sup>†</sup>

Poly(glycidyl methacrylate), pGMA, was synthesized from glycidyl methacrylate (GMA, 97%, Sigma-Aldrich) using a reported initiators for continuous activator regeneration atom transfer radical polymerization (ICAR ATRP) technique.<sup>2</sup> The weight-average molecular weight ( $M_w$ ) and dispersity ( $\mathcal{D}$ ) of the resulting polymer were determined to be 24,000 g/mol and 1.11, respectively, via gel permeation chromatography (GPC) using tetrahydrofuran (THF) as the solvent and polystyrene as the molecular weight standard. The pGMA polymer was mixed with poly(propylene glycol) bis(2-aminopropyl ether) ( $M_n \sim 2,000$  g/mol, Sigma Aldrich) cross-linker (such that the composition of cross-linker in the mixture was 2.4% by mole) and was dissolved in a 5:1 (by volume) solution of dimethyl sulfoxide (DMSO,  $\geq 99.9\%$ , Macron Fine Chemicals) : *N*-

<sup>†</sup> This section has been adapted with permission from: Chang, K.; Luo, H.; Geise, G. M., Water content, relative permittivity, and ion sorption properties of polymers for membrane desalination. *Journal of Membrane Science* **2019**, *574*, 24-32.

methyl-2-pyrrolidone (NMP, laboratory grade, Fisher Chemical). The cross-linker content of 2.4% (by mole) balanced the need to prepare mechanically robust membranes that could be characterized via microwave dielectric spectroscopy with the goal of minimizing the amount of cross-linker to probe the influence of co-monomer functionality on the dielectric properties of the materials.

The casting solution (5.2% polymer and cross-linker in solvent, by mass) was poured into a flat poly(tetrafluoroethylene) (PTFE) mold and was heat treated to remove solvent, cross-link the polymer, and obtain a dense cross-linked pGMA membrane (XL-pGMA). Coupons of XL-pGMA were cut and subsequently immersed in 0.5 mol/L sulfuric acid ( $\text{H}_2\text{SO}_4$ , RICCA Chemical) solution at either 45 °C ([Chapter 5](#)) or 40 °C ([Chapter 8](#)) to partially hydrolyze the epoxide rings on the pGMA side chains ([Figure 2.2](#)). The nomenclature for the hydrolyzed XL-pGMA materials is XL-pGMA-z where z represents the hours of hydrolysis used to prepare the material. Additional details about ICAR ATRP synthesis, membrane casting, and FT-IR characterization are provided in [Appendix D](#). All samples were stored in DI water until use.

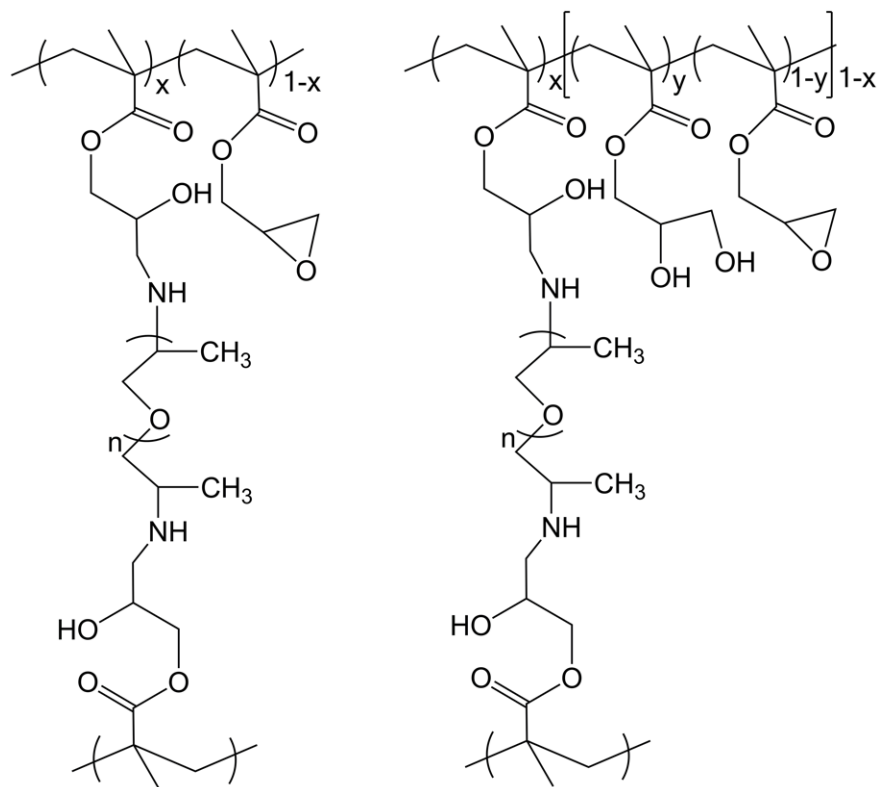


**Figure 2.2.** Structures of non-hydrolyzed, i.e., XL-pGMA-0, (left) and partially hydrolyzed, i.e., XL-pGMA-z, (right) materials. The value of  $z$  in the sample nomenclature corresponds to the hydrolysis time (in hours) during the membrane preparation process, i.e.  $z$  is 0 for the non-hydrolyzed material, and  $z$  is 8, 10, or 12 for the partially hydrolyzed materials. All materials were prepared from a base polymer that contained 2.4% (by mole) cross-linker (i.e.,  $x = 0.024$ ), and the value of  $y$  increased as the hydrolysis time increased.

In [Chapter 5](#), the XL-pGMA- $z$  materials were compared to PTFE (i.e., Teflon<sup>®</sup>) and Nafion<sup>®</sup> 117 (Catalog Number 42180, Alfa Aesar) polymers. PTFE was used as an uncharged, hydrophobic, and low dielectric loss control material,<sup>3-5</sup> and Nafion<sup>®</sup> 117 was a perfluorinated ionomer consisting of a hydrophobic PTFE backbone and side chains terminating with sulfonic acid groups. Prior to use, Nafion<sup>®</sup> samples were treated by boiling the samples in 3% hydrogen peroxide for one hour, rinsing the samples in boiling water for one hour, then boiling the samples in 0.5 mol/L H<sub>2</sub>SO<sub>4</sub> for one hour, and finally, rinsing the samples in boiling water for one hour.<sup>4-7</sup>

### 2.1.3. Hydroxyl Group-containing Methacrylate-based Polymers<sup>‡</sup>

Co-polymers (Figure 2.3) were prepared by photo-initiated cross-linking of 2-hydroxyethyl methacrylate (HEMA, 99%, Sigma-Aldrich), glycidyl methacrylate (GMA, 97%, Sigma-Aldrich), and glycerol methacrylate (GMAOH, synthesized as reported by Tan et al.<sup>8</sup>). The cross-linker was poly(ethylene glycol) dimethacrylate (PEGDMA, average  $M_n = 550$  g/mol, Sigma-Aldrich). The cross-linker content (10% of the total mass of the co-monomers) was chosen to mitigate two competing objectives: minimizing the cross-linker content to study the influence of co-monomer functionality on transport properties while incorporating enough cross-linker to yield mechanically robust materials. The initiator was 1-hydroxycyclohexyl phenyl ketone (HCPK, 99%, Sigma-Aldrich), and the amount of initiator used was 1% of the total co-monomer mass.<sup>1,9</sup>

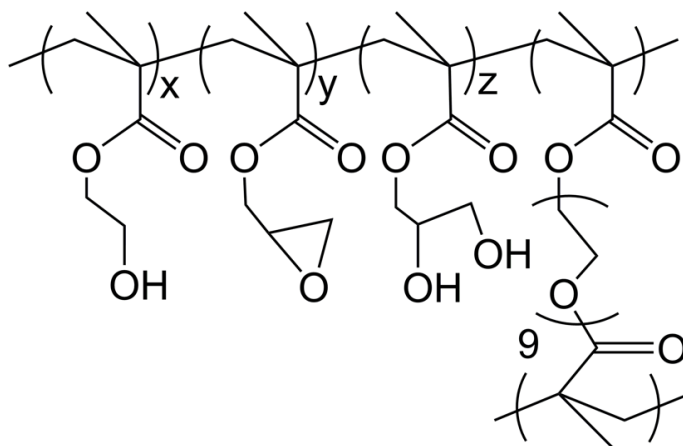


**Figure 2.3.** Chemical structure of the cross-linked HEMA:GMA:GMAOH co-polymer. The co-polymers were prepared from pre-polymerization solutions that contained a  $x:y:z$ , by mass, ratio of HEMA:GMA:GMAOH co-monomers (such that  $x + y + z = 100$ ). The cross-linker was added such that the mass of cross-linker was 10% of the total mass of the co-monomers.

In a typical preparation of the 15:55:30 HEMA:GMA:GMAOH material, 0.15 g of HEMA, 0.55 g of GMA, 0.3 g of GMAOH, 0.1 g of PEGDMA, and 10 mg of HCPK were mixed, via

<sup>‡</sup> This section has been adapted with permission from: Luo, H.; Chang, K.; Bahati, K.; Geise, G. M., Functional group configuration influences salt transport in desalination membrane materials. *Journal of Membrane Science* **2019**, *590*, 117295.

magnetic stirring, in a 20 mL glass vial. The mixture was stirred at room temperature for 30 minutes and then was degassed for 10 minutes in an ultrasonic bath (Catalog Number 97043, VWR). The result of this process was a homogeneous and bubble-free pre-polymerization solution.

This solution subsequently was deposited slowly onto a clean glass plate. Two 100  $\mu\text{m}$  thick metal spacers were placed on either side of the solution, and a quartz plate was placed on top of the spacers to create a uniformly thick film of the pre-polymerization solution. This assembly was placed on a leveled platform in a UV-crosslinking chamber (Select™ Series, Spectroline). The pre-polymerization solution was irradiated with 120  $\mu\text{J}/\text{cm}^2$  312 nm light for 5 minutes, which was sufficiently long to form mechanically robust membranes, to obtain a colorless and transparent membrane film.

The transparent nature of the films was an indicator that the materials are relatively homogeneous. Glass transition temperatures can also provide additional information about the morphology of these dense thick films.<sup>10</sup> Homogeneous co-polymers, i.e., materials where the comonomers are well-mixed at the molecular level, are expected to exhibit a single glass transition temperature.<sup>1, 10</sup> Unfortunately, the glass transition temperatures of all of the HEMA:GMA:GMAOH co-polymers appear to be obscured by vaporization of some of the water initially sorbed by the co-polymer. The Fox equation<sup>11, 12</sup>, which can be used to calculate a first approximation estimate of the co-polymer glass transition temperature based on homopolymer glass transition temperatures and co-polymer composition, provides evidence for this situation. Furthermore, the Fox equation has been used to calculate values in good agreement with experimentally measured glass transition temperatures for HEMA-containing materials.<sup>9</sup> The Fox equation estimated hydrated co-polymer glass transition temperatures increased in the order of 108 °C, 113 °C, 116 °C, 121 °C, and 126 °C as the HEMA composition of the pre-polymerization

solution increased from 0 to 60% (by mass). Importantly, we did not observe glass transition temperatures at the temperatures where a glass transition would be expected if the co-monomers were prepared as homopolymers, and this result further suggests that the co-polymers were relatively homogeneous. As such, the transparent nature of the films and the glass transition temperature data/analysis suggest that the co-polymers considered here are relatively homogeneous.

Following the cross-linking process, the membrane was removed carefully from the surface and immersed in DI water. Five materials, with different ratios of the co-monomers ([Figure 2.4](#)), were prepared using this process. The mass composition of the pre-polymerization solution used to prepare the co-polymers was used to distinguish the materials, and Fourier-transform infrared (FT-IR) spectroscopy (see [Appendix E](#)) suggests that the pre-polymerization solution composition is representative of the composition of these cross-linked networks. All materials were stored in DI water until use.

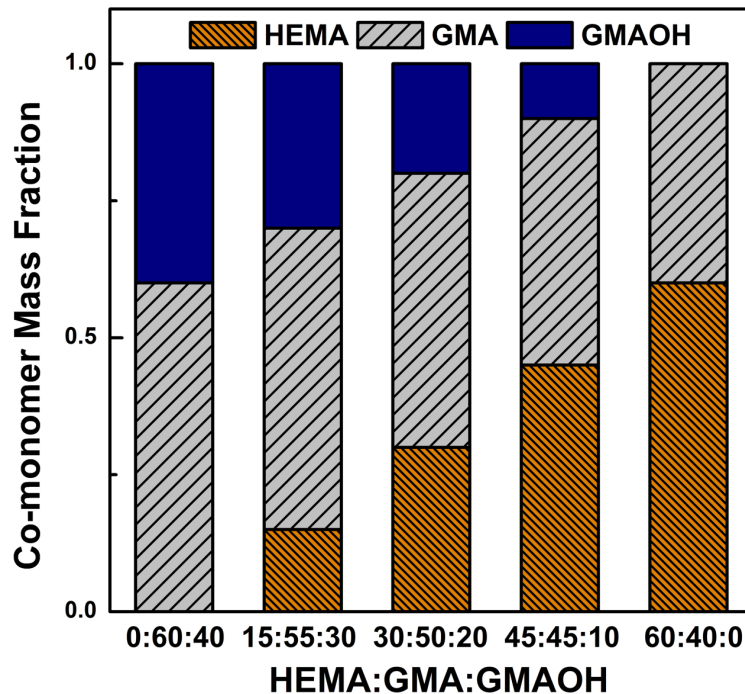


**Figure 2.4.** The co-monomer content of the co-polymer was systematically varied (by adjusting the composition of the pre-polymerization solution used to prepare the co-polymers) to probe the influence of hydroxyl group configuration on the salt transport properties of the five HEMA:GMA:GMAOH materials considered. The nomenclature on the horizontal axis corresponds to the pre-polymerization solution mass composition.

#### 2.1.4. Hydroquinone-containing Sulfonated Polysulfones

Prior to use, 4,4'-biphenol (BP, 97%, Acros Organics), 4,4'-dichlorodiphenylsulfone (DCDPS, 98%, Sigma-Aldrich), 3,3'-disulfonated-4,4'-dichlorodiphenylsulfone (SDCDPS, > 99%, Akron Polymer Systems) and anhydrous potassium carbonate ( $K_2CO_3$ ,  $\geq 99\%$ , Sigma-Aldrich) were dried under vacuum at  $110\text{ }^\circ\text{C}$  for 24 hours, and hydroquinone (HQ,  $\geq 99\%$ , Sigma-Aldrich) and 2-methoxyhydroquinone (MHQ, 98%, Sigma-Aldrich) were dried under vacuum at  $22 \pm 1\text{ }^\circ\text{C}$  (room temperature) for 24 hours. Anhydrous *N,N*-dimethylacetamide (DMAc, 99.8%, Fisher Chemical), toluene ( $\geq 99.5\%$ , Fisher Chemical), and isopropyl alcohol (IPA,  $\geq 99.5\%$ , Fisher Chemical) were used as received.

Two series of sulfonated poly(arylene ether sulfone) random co-polymers were synthesized via nucleophilic step growth polymerization to have 2:3 molar ratios of HQ:BP or MHQ:BP and degrees of di-sulfonation of 20%, 25%, or 30% (by mol) (Figure 2.5). The nomenclature used for the co-polymers is HQ:BP/MHQ:BP-X, where X is the degree of di-sulfonation in the co-polymers. For example, MHQ:BP-25 refers to a co-polymer containing 25% (by mole) of the sulfonated co-monomer (SDCDPS) and 75% (by mole) of the non-sulfonated co-monomer (DCDPS).

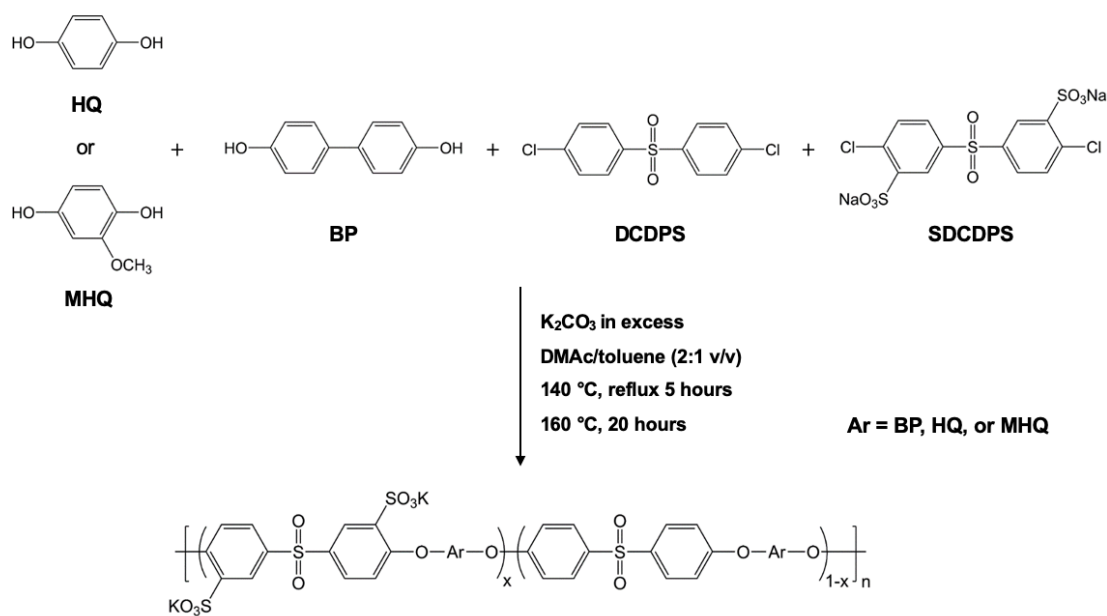


**Figure 2.5.** Synthesis of the HQ:BP-X and MHQ:BP-X sulfonated poly(arylene ether sulfone) random co-polymers.

In a typical preparation of the MHQ:BP-25 material, 2.5844 g of DCDPS (9.0 mmol), 1.4738 g of SDCDPS (3.0 mmol), 0.6727 g of MHQ (4.8 mmol), 1.3407 g of BP (7.2 mmol), and 2.7642 g  $\text{K}_2\text{CO}_3$  (20.0 mmol, in excess) were charged into a three-necked round-bottom glass flask equipped with a condenser, a Dean-Stark trap, and a purge gas inlet. Anhydrous DMAc (24 mL) and toluene (12 mL) (2:1 volume ratio of DMAc to toluene) were then added to the flask, and the reaction was heated and well-mixed using a magnetic stir bar, under a nitrogen purge, to 140 °C for 5 hours to azeotropically dehydrate the reacting solution. Afterwards, toluene was removed

from the solution by slowly increasing the temperature to 160 °C. The reaction was allowed to proceed at 160 °C for another 20 hours until a dark and viscous solution formed. The resulting polymer solution was cooled to room temperature, filtered to remove salts, and precipitated into a mixture of IPA (210 mL) and deionized (DI) water (90 mL) IPA (7:3 volume ratio of IPA to DI water). The precipitated fibrous co-polymer was washed twice with DI water, collected, and dried under vacuum at 80 °C for 24 hours.

Films were prepared via a solution casting method. The co-polymers were dissolved in DMAc (~7% w/v), and the dissolved solution was filtered through a 1 µm poly(tetrafluoroethylene) PTFE syringe filter. The filtered solution then was poured into a clean and flat-bottom PTFE mold and dried in a convection oven at 70 °C for 24 hours. Then, the films were dried subsequently under vacuum at 110 °C for 24 hours to further remove residual solvent. All films were stored in DI water until use.

## **2.2. Methods**

### **2.2.1. Water Uptake<sup>§</sup>**

Samples were cut from larger pieces of polymer film and were equilibrated in either DI water or aqueous solutions of 0.5 mol/L lithium chloride (LiCl, Sigma-Aldrich), sodium chloride (NaCl, Sigma-Aldrich), potassium chloride (KCl, Sigma-Aldrich), 0.01 or 0.1 mol/L NaCl, or 1.0 mol/L NaCl. After equilibration, the sample was removed from the DI water or salt solution, the surface was dried quickly with a laboratory wipe, and the wet mass of the sample,  $m_{wet}$ , was measured. Then, the sample was dried under vacuum at room temperature for 48 hours. After

---

<sup>§</sup> This section has been adapted with permission from: Chang, K.; Xue, T.; Geise, G. M., Increasing salt size selectivity in low water content polymers via polymer backbone dynamics. *Journal of Membrane Science* **2018**, 552, 43-50.

drying, the sample was removed from the drying oven and the dry mass of the sample,  $m_{dry}$ , was measured immediately. Water uptake,  $w_u$ , was calculated as:

$$w_u = \frac{m_{wet} - m_{dry}}{m_{dry}} \quad (2.1)$$

Using the measured water uptake, the volume fraction of water sorbed in the polymer,  $\phi_w^m$ , was calculated, assuming volume additivity,<sup>6,13</sup> as:

$$\phi_w^m = \frac{w_u}{w_u + \rho_w / \rho_P} \quad (2.2)$$

where  $\rho_w$  is the density of water ( $1.0 \text{ g cm}^{-3}$ <sup>14</sup>), and  $\rho_P$  is the density of the dry polymer. The dry polymer density was measured (after drying the samples for the water uptake measurement) via an Archimedes' principle method where sample mass measurements were made in air and in an auxiliary liquid.<sup>15</sup> The dry polymer density was calculated as:

$$\rho_P = \frac{m_{air}}{m_{air} - m_{aux}} (\rho_{aux} - \rho_{air}) + \rho_{air} \quad (2.3)$$

where  $m_{air}$  is mass of sample in air,  $m_{aux}$  is mass of sample in auxiliary liquid,  $\rho_{aux}$  is auxiliary liquid density, and  $\rho_{air}$  is air density. Cyclohexane, which is a non-polar solvent that is commonly used to determine the dry density of hydrophilic polymers, was used as the auxiliary solvent,<sup>16-18</sup> and the value of  $\rho_{aux}$  was evaluated at the measurement temperature using reported cyclohexane density data as a function of temperature.<sup>14,19</sup>

The water sorption coefficient,  $K_w$ , is defined as the ratio of water concentration in the polymer,  $C_w^m$ , to that in the bulk external solution,  $C_w$ .<sup>20,21</sup>

$$K_w = \frac{C_w^m}{C_w} \quad (2.4)$$

The units of  $K_w$  are [g(water)/cm<sup>3</sup>(hydrated polymer)]/[g(water)/cm<sup>3</sup>(solution)], and  $K_w$  is related to the volume fraction of water in the polymer,  $\phi_w^m$ , as:<sup>17</sup>

$$K_w = \frac{\phi_w^m M_w}{C_w V_w} \quad (2.5)$$

where  $M_w$  is the molecular weight of water (18 g/mol), and  $V_w$  is the partial molar volume of water in the polymer, which was taken to be equivalent to the molar volume of water at ambient conditions (18 cm<sup>3</sup>/mol<sup>22</sup>). For dilute salt solutions or DI water,  $C_w$  is approximately equivalent to the density of pure water,  $\rho_w$ , which was taken as 1 g/cm<sup>3</sup><sup>17</sup>. As a result, the water sorption coefficient is approximately equal to the volume fraction of water sorbed in the polymer (i.e.  $K_w \cong \phi_w^m$ ).

### 2.2.2. Salt Sorption\*\*

The salt sorption coefficient,  $K_s$ , is defined as the ratio of the salt concentration in the polymer relative to the salt concentration of an external solution in equilibrium with the polymer.<sup>23</sup> The value of  $K_s$  can be measured using a desorption method where the polymer is initially equilibrated with a salt solution (detailed in [Section 2.2.1](#)) of known concentration. After equilibration, the sample is immersed in a volume of pure water so that the sorbed salt in the polymer can desorb from the polymer.

---

\*\* This section has been adapted with permission from: Chang, K.; Xue, T.; Geise, G. M., Increasing salt size selectivity in low water content polymers via polymer backbone dynamics. *Journal of Membrane Science* **2018**, 552, 43-50.

The amount of time required for the sorption and desorption processes was estimated using the characteristic time of the diffusion process,  $L^2/D_s$ , where  $D_s$  is the salt diffusion coefficient and  $L$  is the path length for diffusion (i.e., half of the film thickness).<sup>24</sup> A value of  $D_s$  was estimated using the theory of Mackie and Meares, which enables estimation of diffusion coefficients based on the volume fraction of water in the polymer (i.e.,  $K_w$ ) and salt diffusivity in bulk aqueous solution.<sup>25</sup> The polymer samples were soaked in salt solution or pure water for sufficient amount of time to allow the samples to reach equilibrium. The desorption volume,  $V_d$ , was chosen to ensure that the final concentration of the desorption solution was approximately 1 mg(salt)/L. This concentration target was chosen so the concentration of the desorption solution was sufficiently low to facilitate complete desorption of salt from the polymer but high enough to be measured accurately using ion chromatography (ICS-2100, Thermo Scientific). Salt sorption coefficients were calculated as:<sup>26</sup>

$$K_s = \frac{C_s^m}{C_s^s} = \frac{C_d V_d}{C_s^s V_p} \quad (2.6)$$

where  $C_s^s$  is the salt concentration in the initial external solution (detailed in [Section 2.2.1](#)),  $C_s^m$  is the salt concentration in the membrane,  $C_d$  is the final salt concentration of desorption solution,  $V_d$  is the desorption volume, and  $V_p$  is the volume of the hydrated sample.<sup>23</sup> The units of  $K_s$  are [g(salt)/cm<sup>3</sup>(hydrated polymer)] / [g(salt)/cm<sup>3</sup>(solution)].

The volume of the hydrated copolymer,  $V_p$ , was determined by measuring the thickness and area of the sample. The thickness was measured immediately after the sample was taken out from the desorption solution, and the area was measured by taking a photograph of the sample and analyzing it using the ImageJ software package. The uncertainty in the thickness and area

measurements was less than 10%, and the uncertainty in the calculated volume was roughly 15% based on standard error propagation calculations.<sup>27</sup>

### 2.2.3. Thermal Characterization<sup>††</sup>

Differential scanning calorimetry (DSC, Q1000, TA Instruments) was used to characterize the glass transition temperature ( $T_g$ ) of the hydrated polymers. DI water equilibrated polymer samples, with masses ranging from 5–10 mg, were sealed in hermetic aluminum sample pans to keep the samples hydrated throughout the measurement. The samples were initially heated to 150 °C, quenched to –80 °C, and subsequently scanned twice between –80 °C and 150 °C at a heating rate of 10 °C/min under a nitrogen purge flow. The glass transition temperature was determined as the midpoint of the heat capacity step change during the second heating scan.

### 2.2.4. Microwave Dielectric Spectroscopy<sup>#</sup>

Dielectric permittivity properties of the samples were characterized as the frequency-dependent relative complex permittivity,  $\epsilon^*$ ,<sup>28, 29</sup> using a microwave dielectric spectroscopy technique. The technique was developed by Nicolson, Ross, and Weir (NRW).<sup>30, 31</sup> The real part of the relative complex permittivity,  $\epsilon'$ , is typically referred to as simply the relative permittivity or the dielectric constant, and the imaginary part of the relative complex permittivity,  $\epsilon''$ , is typically referred to as the dielectric loss.<sup>29</sup>

Two port scattering parameter (S-parameter) measurements were made using a Keysight N9928A vector network analyzer (VNA). The data were analyzed using the Keysight N1500A

---

<sup>††</sup> This section has been adapted with permission from: Chang, K.; Xue, T.; Geise, G. M., Increasing salt size selectivity in low water content polymers via polymer backbone dynamics. *Journal of Membrane Science* **2018**, 552, 43-50.

<sup>##</sup> This section has been adapted with permission from: Chang, K.; Luo, H.; Geise, G. M., Water content, relative permittivity, and ion sorption properties of polymers for membrane desalination. *Journal of Membrane Science* **2019**, 574, 24-32.

materials measurement software. A 10 cm long and 3.5 mm diameter coaxial transmission line (Catalog Number 8043S10, Maury Microwave) was used as the sample holder, and shielded coaxial cables (Catalog Number N9910X0-708, Keysight Technologies) were used to connect the VNA to the transmission line. A full two-port calibration was performed to define the calibration reference plane using 3.5 mm short, open, and load impedance standards (Catalog Number 8050CK, Maury Microwave) and one transmission line standard (i.e., directly connecting the two coaxial cables together).<sup>28, 32, 33</sup>

Samples were exposed to electromagnetic radiation over a frequency range of 45 MHz to 26.5 GHz or 450 MHz to 20 GHz in the transmission line (or waveguide) sample holder. This frequency range was chosen because water molecules in the hydrated polymer are sensitive to electromagnetic radiation in the microwave region of the spectrum.<sup>4, 5, 28, 32, 34, 35</sup> The amplitude and phase of the reflected and transmitted electromagnetic radiation was measured (in two directions) using the VNA and expressed as four S-parameters:  $S_{11}$ ,  $S_{12}$ ,  $S_{21}$ , and  $S_{22}$  (Figure D.2) that describe the properties of the material under test. The S-parameters are related to the relative complex permittivity,  $\epsilon^*$ , and relative complex permeability,  $\mu^*$ , properties as:<sup>30, 36-38</sup>

$$S_{21} = S_{12} = \frac{(e^{-j\frac{\omega}{c}\sqrt{\mu^*\epsilon^*}d}) \left[ 1 - \left( \frac{\sqrt{\frac{\mu^*}{\epsilon^*}} - 1}{\sqrt{\frac{\mu^*}{\epsilon^*}} + 1} \right)^2 \right]}{1 - \left[ \left( \frac{\sqrt{\frac{\mu^*}{\epsilon^*}} - 1}{\sqrt{\frac{\mu^*}{\epsilon^*}} + 1} \right)^2 (e^{-j\frac{\omega}{c}\sqrt{\mu^*\epsilon^*}d})^2 \right]} \quad (2.7)$$

$$S_{11} = S_{22} = \frac{\left( \frac{\sqrt{\frac{\mu^*}{\varepsilon^*}} - 1}{\sqrt{\frac{\mu^*}{\varepsilon^*}} + 1} \right) \left[ 1 - \left( e^{-j\frac{\omega}{c}\sqrt{\mu^*\varepsilon^*}d} \right)^2 \right]}{1 - \left[ \left( \frac{\sqrt{\frac{\mu^*}{\varepsilon^*}} - 1}{\sqrt{\frac{\mu^*}{\varepsilon^*}} + 1} \right)^2 \left( e^{-j\frac{\omega}{c}\sqrt{\mu^*\varepsilon^*}d} \right)^2 \right]} \quad (2.8)$$

where  $\omega$  is the angular frequency,  $c$  is the speed of light in vacuum, and  $d$  is the length dimension that describes how much of the transmission line is filled with sample (Figure D.2).

An algorithm, proposed by Bartley and Begley<sup>36</sup> and built into the analysis software,<sup>39</sup> was used to calculate the relative complex permittivity properties of the samples. This algorithm is suitable for non-magnetic materials, and it reduces noise and mismatch errors during data analysis.<sup>36, 39</sup> It also addresses known issues with the NWR technique such as an analysis issue where multiple  $\varepsilon^*$  and  $\mu^*$  values can be calculated from a single set of S-parameters and a measurement issue at frequencies corresponding to situations where the sample length is an integer multiple of one-half wavelength.<sup>30, 36, 38</sup>

Samples were loaded into the transmission line in a manner that minimized air gaps (i.e., the sample filled the annular space in the coaxial transmission line) as air gaps can introduce measurement artifacts. PTFE was machined to fit perfectly in the annular space of the transmission line, and hydrated polymer films were tightly wrapped around the inner conductor of the transmission line until sufficient polymer was wrapped to fill the annular space of the transmission line.<sup>5</sup> Measurements using DI water were performed by directly pipetting DI water into the vertically positioned transmission line fitted with a customized silicone dielectric plug at the bottom end to prevent leaks. The influence of the plug on the DI water measurements was taken to be negligible, which was consistent with previous studies.<sup>28, 32, 40-42</sup>

### 2.2.5. State of Water Analysis (DSC)<sup>§§</sup>

Differential scanning calorimetry (DSC, Q1000, TA Instruments) was used to characterize the states of water present in DI water equilibrated polymer samples. Each sample (masses ranged from 3-6 mg) was sealed in a hermetic aluminum pan to avoid water loss during the experiment. The samples were quenched to  $-70\text{ }^{\circ}\text{C}$ , scanned once from  $-70\text{ }^{\circ}\text{C}$  to  $90\text{ }^{\circ}\text{C}$  at a heating rate of  $10\text{ }^{\circ}\text{C}/\text{min}$  under a dry nitrogen purge.<sup>1, 43</sup>

### 2.2.6. State of Water Analysis (FT-IR)

Fourier-transform infrared spectroscopy (FT-IR) was used to characterize the state of water present in hydrated polymer samples.<sup>44, 45</sup> The sample preparation steps are summarized as follows. A 10% (by mass) semi-heavy water (i.e., HOD) probe solution was prepared by mixing 5 g of deuterated water ( $\text{D}_2\text{O}$ , 99.9 atom% D, Sigma-Aldrich) with 95 g of DI water (i.e.,  $\text{H}_2\text{O}$ ).<sup>44, 45</sup> Dry XL-pGMA-z films were cut into 1 cm diameter circular sample coupons and placed in 20 mL open glass vials, and the 20 mL vials subsequently were placed in 50 mL glass jars. A 5 g aliquot of the HOD probe solution was added to each of the 50 mL glass jars, and the glass jars were sealed to create a closed HOD saturated atmosphere. The XL-pGMA-z samples were equilibrated at  $22 \pm 1\text{ }^{\circ}\text{C}$  (i.e., room temperature) with the HOD saturated air for 14 days. This period of time is well in excess of the characteristic time of salt diffusion into the polymer and, therefore, is well in excess of the characteristic time of HOD diffusion into the polymer (HOD diffusivity is expected to be greater than that of salt as the diffusivity of water is greater than that of salt).<sup>23</sup>

---

<sup>§§</sup> This section has been adapted with permission from: Chang, K.; Luo, H.; Geise, G. M., Water content, relative permittivity, and ion sorption properties of polymers for membrane desalination. *Journal of Membrane Science* **2019**, 574, 24-32.

All measurements were taken using a FTIR Spectrometer Frontier (Perkin Elmer) with a universal attenuated total reflection (ATR) accessory, and each spectrum was obtained by collecting 8 scans with a resolution of  $4\text{ cm}^{-1}$ . Prior to the scans, the surface of the diamond internal reflection element was cleaned with isopropyl alcohol (IPA, 99.5%, Fisher Chemical) and wiped gently with a cotton ball to remove residual IPA. A background scan was performed immediately after the cleaning step, and the background signals were subtracted automatically by the Perkin Elmer Spectrum software (version 10.5.3) during analysis. After the background scan, a HOD atmosphere incubated XL-pGMA-z sample was removed from the 20 mL glass vial, wiped gently with laboratory tissue paper, and sandwiched between the calibrated force applicator and the diamond element. Then, the sample spectrum was acquired by the spectrometer. The force applied to the samples was kept constant throughout the measurements of all samples.

After the measurement, a base-line correction was performed on the spectra by setting the absorbances at  $4000\text{ cm}^{-1}$ ,  $2800\text{ cm}^{-1}$  and  $2200\text{ cm}^{-1}$  to zero. Then, the base-line corrected spectra were further normalized by the maximum absorbance peak at  $1160\text{ cm}^{-1}$ , which corresponds to the C-O stretching mode of ester group.<sup>46</sup> Both the base-line correction and normalization were performed using the Perkin Elmer Spectrum software.

The broad and non-Gaussian OD FTIR peak, representing  $\text{D}_2\text{O}$  sorbed in hydrated XL-pGMA-z, spanned from  $2400$  to  $2700\text{ cm}^{-1}$ .<sup>44, 45, 47</sup> The OD peak was deconvoluted, using OriginPro 7.5 (Origin Labs), into three Gaussian peaks that represent three water states, bulk-like water, intermediate water, and strongly-bound water.<sup>44, 45</sup> The bulk-like water peak position and full width at half maximum (fwhm) were held constant at  $2509\text{ cm}^{-1}$  and  $170\text{ cm}^{-1}$ , respectively.<sup>44, 45</sup> The intermediate and strongly-bound water peak positions were determined by fitting the OD peak of the spectrum for the sample with the lowest water content (i.e., XL-pGMA-7).<sup>44, 45</sup> The

peak positions of intermediate ( $\sim 2513\text{ cm}^{-1}$ ) and strongly-bound ( $\sim 2570\text{ cm}^{-1}$ ) water blueshift to a frequency higher than  $2509\text{ cm}^{-1}$ , which indicates that the hydrogen bond network is perturbed and that hydrogen bond strength is generally weaker in the polymer compared to the situation in bulk water.<sup>45, 48</sup> The positions of the three peaks and the fwhm of bulk-like and strongly-bound water peaks subsequently were held constant (i.e., the fwhm of the intermediate water peak was allowed to vary) to characterize the water states in XL-pGMA-z over a range of water content.<sup>44, 45</sup>

### 2.2.7. Nuclear Magnetic Resonance (NMR) Diffusometry<sup>\*\*\*</sup>

Samples were prepared for NMR by first cutting 8 to 32 circular (3 mm in diameter) pieces of polymer. For brittle polymers, rectangular pieces of polymer (approximately 3 mm x 4 mm) were used because the samples were too brittle to cut using a circular die. The final number of pieces of polymer used was chosen to ensure that the NMR signal was sufficiently strong during the measurement. These slices were stacked and wrapped with thin strips of PTFE tape to hold them together, and were equilibrated in aqueous salt solutions for at least 72 hours prior to NMR experiments. Then, stacked samples were removed from solution, quickly blotted to remove surface water, wrapped completely in PTFE tape, and placed into a sealed poly(methyl methacrylate), PMMA, sample cell. The sample cell was designed to have a very small amount of excess volume to minimize water loss during NMR data collection.<sup>49</sup>

The  $^1\text{H}_2\text{O}$  self-diffusion measurements were made using a pulsed-gradient stimulated echo (PGSTE) sequence at  $25\text{ }^\circ\text{C}$  on a Bruker Avance III 9.4T wide-bore spectrometer. A single axis diffusion probe (Bruker Diff60) was used with a 5 mm  $^1\text{H}$  radio frequency coil. The Stejskal-

---

<sup>\*\*\*</sup> This section has been adapted with permission from: Chang, K.; Korovich, A.; Xue, T.; Morris, W. A.; Madsen, L. A.; Geise, G. M., Influence of rubbery versus glassy backbone dynamics on multiscale transport in polymer membranes. *Macromolecules* **2018**, *51* (22), 9222-9233.

Tanner equation describes the signal attenuation that results from diffusion in the PGSTE experiment:

$$I = I_0 e^{-D_w \gamma^2 g^2 \delta^2 \left(\Delta - \frac{\delta}{3}\right)} = I_0 e^{-bD} \quad (2.9)$$

where  $I$  is the signal intensity at a given gradient strength,  $g$ , (maximum gradient strengths ranged from 100 – 800 G/cm),  $I_0$  is the signal intensity at  $g = 0$  G/cm,  $D_w$  is the water diffusion coefficient,  $\gamma$  is the gyromagnetic ratio of the  $^1\text{H}$  nucleus ( $267.522 \text{ rad s}^{-1} \text{ T}^{-1}$ ),  $\delta$  is the effective rectangular gradient pulse length (2 ms),  $\Delta$  is the diffusion encoding time (values ranged from 8.2 – 750 ms), and  $b$  is the Stejskal-Tanner parameter.

The water diffusion coefficient,  $D_w$ , was obtained by fitting the  $I/I_0$  data, obtained from a PGSTE experiment, as a function of  $g$ . An example signal attenuation curve for HEA-co-EA 30:70 is shown in [Figure 2.6](#). In the PGSTE experiments, a  $90^\circ$  radiofrequency pulse of  $4.8 \mu\text{s}$  was used with 16 gradient steps (8 – 128 scans per step with a repetition time of 2 – 3 s). The 16 gradient step experiment was needed to de-convolute a fast diffusion coefficient component, which was attributed to the small amount of residual surface water on the sample, and a slower diffusion coefficient component, which was attributed to water sorbed in the polymer. Transverse relaxation times,  $T_2$ , for water signals in these polymers ranged from 1 ms to approximately 50 ms, and the longitudinal relaxation times,  $T_1$ , ranged from 700 – 750 ms.

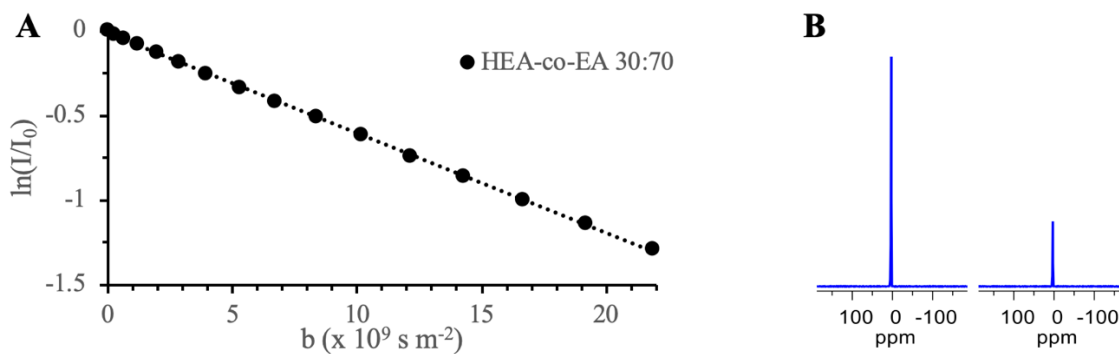


**Figure 2.6.** Measuring water diffusion with NMR diffusometry. The linearized signal attenuation plot (A) for fully hydrated HEA-co-EA 30:70 at 298 K shows the attenuation of the normalized NMR signal intensity as a function of the Stejskal-Tanner parameter,  $b$  (Equation 2.9). The slope of the data is equal to the self-diffusion coefficient of water in the polymer, which is  $5.6 \times 10^{-8} \text{ cm}^2/\text{sec}$  in this example. NMR diffusometry signal attenuation, from the first to the last measurement, can be seen in the 1D spectra (slices) from the experiment (B), which are from the first and last ( $g_{max} = 300 \text{ G/cm}$ ) point in (A).

### 2.2.8. Ionic Conductivity

Ionic conductivity was measured using a two-chamber apparatus where the membrane separated chambers each containing 1 mol/L aqueous NaCl solution.<sup>50-52</sup> Direct current (DC) measurements were performed using a potentiostat (SP-150, Biologic) and the associated automation and analysis software (EC-Lab Software, Biologic). Constant current was applied across two platinum electrodes positioned in each chamber at the end opposite to the membrane, and the applied current densities were:  $0.017 \text{ mA/cm}^2$ ,  $0.077 \text{ mA/cm}^2$ ,  $0.140 \text{ mA/cm}^2$ , and  $0.170 \text{ mA/cm}^2$ . Each current was maintained until steady state was reached, and the voltage was measured, at each current density, across two double junction silver/silver chloride (Ag/AgCl) electrodes (RREF 0024, Pine Instrument Corporation). The reference electrodes were positioned on either side of the membrane of interest at a distance approximately equal to the thickness of the membrane. The area resistance of the combined solution and membrane,  $R_{m+s}$ , was determined as the slope of the voltage plotted as a function of current density. This approach is analogous to using Ohm's Law:

$$R_{m+s} = \frac{V_c}{I_c} \quad (2.10)$$

where  $V_c$  is the voltage and  $I_c$  is the current density.

The area resistance of the solution was determined by repeating the measurement, described above, without the membrane in the cell. This solution area resistance was then subtracted from  $R_{m+s}$  to obtain the area resistance of the membrane,  $R_m$ , according to a resistances in series model. Membrane area resistance values were normalized by the swollen membrane thickness,  $L$ , to determine the membrane conductivity,  $\sigma_m$ , as:

$$\sigma_m = \frac{L}{R_m} \quad (2.11)$$

Each sample was measured three times using fresh solution each time. The reported conductivity values are the mean of the results of those three measurements, and the uncertainty was taken as one standard deviation from the mean.

### 2.2.9. Salt Diffusion<sup>†††</sup>

The effective salt diffusion coefficient,  $D_s$ , was determined by measuring the initial salt desorption from a salt solution-equilibrated polymer as a function of time. Fickian diffusion analysis provides a relationship between the mass of desorbed salt,  $M_t$ , as a function of time,  $t$ , that can be simplified for the case where the ratio of  $M_t$  to  $M_\infty$ , which is the mass of salt desorbed from the polymer at infinite time, is less than 0.6:<sup>53</sup>

---

<sup>†††</sup> This section has been adapted with permission from: Chang, K.; Korovich, A.; Xue, T.; Morris, W. A.; Madsen, L. A.; Geise, G. M., Influence of rubbery versus glassy backbone dynamics on multiscale transport in polymer membranes. *Macromolecules* **2018**, *51* (22), 9222-9233.

$$\left. \frac{M_t}{M_\infty} \right|_{\frac{M_t}{M_\infty} < 0.6} = \left( \frac{16D_s}{\pi L^2} \right)^{1/2} t^{1/2} \quad (2.12)$$

where  $L$  is the sample thickness, which was determined using the measured sample area and thickness.

Samples were initially equilibrated in aqueous salt solution (per the procedure described earlier in [Section 2.2.3](#)). The sample surface was carefully dried with a laboratory wipe prior to the desorption to remove any residual salt solution from the surface. The desorption solution (DI water) was atmospherically equilibrated so that solution conductivity changes, due to absorption of atmospheric carbon dioxide, would not influence the measurement.<sup>17</sup> The desorption solution was maintained at 25 °C using a temperature-controlled water circulator and was kept well mixed using a magnetic stir-bar.<sup>17, 54</sup> The conductivity of the desorption solution was measured as a function of time using a conductivity meter (Cond 7310, WTW) and converted to salt mass,  $M_t$ , using a calibration curve and the desorption solution volume.

### 2.2.10. Water Permeability<sup>\*\*\*</sup>

Hydraulic water permeability of samples were measured using a dead-end cell apparatus.<sup>55</sup> DI water was pressurized on the upstream side of the hydrogel (i.e., XL-pGMA-z and HEMA:GMA:GMAOH) samples at 200 psi (13.8 bar) and the sulfonated polyfulsone sample at 400 psi (27.6 bar), and permeate was collected over time to determine the steady state water flux, which was converted to hydraulic water permeability by normalizing the water flux by film thickness and the applied pressure difference.<sup>26</sup> The hydraulic permeability was converted into the

---

<sup>\*\*\*</sup> This section has been adapted with permission from: Luo, H.; Chang, K.; Bahati, K.; Geise, G. M., Engineering selective desalination membranes via molecular control of polymer functional groups. *Environmental Science & Technology Letters* **2019**, 6 (8), 462-466.

diffusive water permeability,  $P_w$ , using the convective frame of reference correction factor and assuming that mixing of polymer and water was thermodynamically ideal.<sup>26, 55</sup>

### 2.2.11. Salt Permeability<sup>§§§</sup>

Salt permeability was measured using a custom-built diffusion cell apparatus consisting of two jacketed chambers (i.e., donor and receiver) that were separated by the sample. The donor cell chamber was filled with 100 mL of aqueous salt solution while the receiver chamber was filled with 100 mL of DI water. Silicone rubber gaskets were used to seal the sample into the cell, and the solution in each chamber was mechanically stirred using overhead stirrers at a rate of 354 rpm. The conductivity of the receiver chamber solution was recorded as a function of time using a conductivity meter (Cond 7310, WTW), and conductivity was converted to salt concentration via a calibration curve. Temperature was maintained at 25 °C by circulating water through the chamber jackets using a water circulator with a temperature controller.<sup>54</sup> Salt transport was modeled as one-dimensional Fickian diffusion, and the salt permeability,  $P_s$ , was taken as the slope of a linear regression of:<sup>56</sup>

$$-\frac{VL}{2A} \ln \left( 1 - 2 \frac{C_R(t)}{C_D(0)} \right) = P_s t \quad (2.13)$$

where  $V$  is the volume of liquid in the donor and receiver chambers (i.e., 100 mL),  $A$  is the area available for transport,  $t$  is time,  $C_R(t)$  is the salt concentration in receiver chamber at time  $t$ , and  $C_D(0)$  is the initial salt concentration in donor chamber (at  $t = 0$ ).

---

<sup>§§§</sup> This section has been adapted with permission from: Chang, K.; Xue, T.; Geise, G. M., Increasing salt size selectivity in low water content polymers via polymer backbone dynamics. *Journal of Membrane Science* **2018**, 552, 43-50.

### 2.3. References

1. Chang, K.; Xue, T.; Geise, G. M., Increasing salt size selectivity in low water content polymers via polymer backbone dynamics. *Journal of Membrane Science* **2018**, *552*, 43-50.
2. Tsarevsky, N. V.; Jakubowski, W., Atom transfer radical polymerization of functional monomers employing Cu-based catalysts at low concentration: Polymerization of glycidyl methacrylate. *Journal of Polymer Science Part A: Polymer Chemistry* **2011**, *49* (4), 918-925.
3. Geyer, R. G.; Krupka, J., Microwave dielectric properties of anisotropic materials at cryogenic temperatures. *IEEE Transactions on Instrumentation and Measurement* **1995**, *44* (2), 329-331.
4. Paddison, S. J.; Reagor, D. W.; Zawodzinski Jr, T. A., High frequency dielectric studies of hydrated Nafion®. *Journal of Electroanalytical Chemistry* **1998**, *459* (1), 91-97.
5. Lu, Z.; Polizos, G.; Macdonald, D. D.; Manias, E., State of water in perfluorosulfonic ionomer (Nafion® 117) proton exchange membranes. *Journal of The Electrochemical Society* **2008**, *155* (2), B163-B171.
6. Zawodzinski, T. A.; Springer, T. E.; Davey, J.; Jestel, R.; Lopez, C.; Valerio, J.; Gottesfeld, S., A comparative study of water uptake by and transport through ionomeric fuel cell membranes. *Journal of The Electrochemical Society* **1993**, *140* (7), 1981-1985.
7. Zawodzinski, T. A.; Neeman, M.; Sillerud, L. O.; Gottesfeld, S., Determination of water diffusion coefficients in perfluorosulfonate ionomeric membranes. *The Journal of Physical Chemistry* **1991**, *95* (15), 6040-6044.
8. Tan, J.; Liu, D.; Bai, Y.; Huang, C.; Li, X.; He, J.; Xu, Q.; Zhang, X.; Zhang, L., An insight into aqueous photoinitiated polymerization-induced self-assembly (photo-PISA) for the preparation of diblock copolymer nano-objects. *Polymer Chemistry* **2017**, *8* (8), 1315-1327.
9. Chang, K.; Korovich, A.; Xue, T.; Morris, W. A.; Madsen, L. A.; Geise, G. M., Influence of rubbery versus glassy backbone dynamics on multiscale transport in polymer membranes. *Macromolecules* **2018**, *51* (22), 9222-9233.

10. Brostow, W.; Chiu, R.; Kalogeras, I. M.; Vassilikou-Dova, A., Prediction of glass transition temperatures: Binary blends and copolymers. *Materials Letters* **2008**, *62* (17), 3152-3155.
11. Fox, T. G. J.; Flory, P. J., Second-order transition temperatures and related properties of polystyrene. I. Influence of molecular weight. *Journal of Applied Physics* **1950**, *21* (6), 581-591.
12. Hiemenz, P. C.; Lodge, T. P., *Polymer Chemistry*. 2nd ed.; CRC Press LLC: Boca Raton, Florida, 2007.
13. Geise, G. M.; Freeman, B. D.; Paul, D. R., Sodium chloride diffusion in sulfonated polymers for membrane applications. *Journal of Membrane Science* **2013**, *427*, 186-196.
14. Rumble, J. R., *CRC Handbook of Chemistry and Physics*. 98th ed.; CRC Press LLC: 2017.
15. Halliday, D.; Resnick, R.; Walker, J., *Fundamentals of Physics, Chapters 33-37*. John Wiley & Sons: 2010.
16. Xie, W.; Ju, H.; Geise, G. M.; Freeman, B. D.; Mardel, J. I.; Hill, A. J.; McGrath, J. E., Effect of free volume on water and salt transport properties in directly copolymerized disulfonated poly(arylene ether sulfone) random copolymers. *Macromolecules* **2011**, *44* (11), 4428-4438.
17. Xie, W.; Cook, J.; Park, H. B.; Freeman, B. D.; Lee, C. H.; McGrath, J. E., Fundamental salt and water transport properties in directly copolymerized disulfonated poly(arylene ether sulfone) random copolymers. *Polymer* **2011**, *52* (9), 2032-2043.
18. Luo, H.; Aboki, J.; Ji, Y.; Guo, R.; Geise, G. M., Water and salt transport properties of triptycene-containing sulfonated polysulfone materials for desalination membrane applications. *ACS Applied Materials & Interfaces* **2018**.
19. Yaws, C. L.; Pike, R. W., Chapter 3 - Density of liquid—Organic compounds. In *Thermophysical Properties of Chemicals and Hydrocarbons*, William Andrew Publishing: Norwich, NY, 2009; pp 106-197.

20. Wijmans, J. G.; Baker, R. W., The solution-diffusion model: A review. *Journal of Membrane Science* **1995**, *107* (1), 1-21.
21. Merten, U., *Desalination by reverse osmosis*. M.I.T. Press: 1966.
22. Atkins, P.; de Paula, J., *Physical chemistry*. 7th ed.; W. H. Freeman and Company: New York, 2002.
23. Geise, G. M.; Falcon, L. P.; Freeman, B. D.; Paul, D. R., Sodium chloride sorption in sulfonated polymers for membrane applications. *Journal of Membrane Science* **2012**, *423*, 195-208.
24. Cussler, E. L., *Diffusion: Mass Transfer in Fluid Systems*. Cambridge University Press: 2009.
25. Mackie, J. S.; Meares, P., The diffusion of electrolytes in a cation-exchange resin membrane I. Theoretical. *Proceedings of the Royal Society of London. Series A. Mathematical and Physical Sciences* **1955**, *232* (1191), 498-509.
26. Geise, G. M.; Paul, D. R.; Freeman, B. D., Fundamental water and salt transport properties of polymeric materials. *Progress in Polymer Science* **2014**, *39* (1), 1-42.
27. Bevington, P. R.; Robinson, D. K., Chapter 4: Propagation of Errors. In *Data reduction and error analysis for the physical sciences*, McGraw Hill: New York, 2003; pp 56-65.
28. Lu, Z.; Lanagan, M.; Manias, E.; Macdonald, D. D., Two-port transmission line technique for dielectric property characterization of polymer electrolyte membranes. *The Journal of Physical Chemistry B* **2009**, *113* (41), 13551-13559.
29. Chen, L. F., *Microwave Electronics: Measurement and Materials Characterization*. Wiley: Hoboken, New Jersey, 2004.
30. Nicolson, A. M.; Ross, G. F., Measurement of the intrinsic properties of materials by time-domain techniques. *IEEE Transactions on Instrumentation and Measurement* **1970**, *19* (4), 377-382.

31. Weir, W. B., Automatic measurement of complex dielectric constant and permeability at microwave frequencies. *Proceedings of the IEEE* **1974**, 62 (1), 33-36.
32. Lu, Z.; Manias, E.; Macdonald, D. D.; Lanagan, M., Dielectric relaxation in dimethyl sulfoxide/water mixtures studied by microwave dielectric relaxation spectroscopy. *The Journal of Physical Chemistry A* **2009**, 113 (44), 12207-12214.
33. Keysight Technologies, How to Perform a Waveguide Calibration with Opt.001, [http://na.support.keysight.com/materials/help/WebHelp/Opt.001\\_How\\_to\\_Perform\\_a\\_Waveguide\\_Calibration.htm](http://na.support.keysight.com/materials/help/WebHelp/Opt.001_How_to_Perform_a_Waveguide_Calibration.htm), (accessed June 13th, 2018).
34. Paddison, S.; Bender, G.; Zawodzinski Jr, T. A., The microwave region of the dielectric spectrum of hydrated Nafion® and other sulfonated membranes. *Journal of New Materials for Electrochemical Systems* **2000**, 3, 293-302.
35. Smith, G.; Duffy, A. P.; Shen, J.; Olliff, C. J., Dielectric relaxation spectroscopy and some applications in the pharmaceutical sciences. *Journal of Pharmaceutical Sciences* **1995**, 84 (9), 1029-1044.
36. Bartley, P. G.; Begley, S. B., A new technique for the determination of the complex permittivity and permeability of materials. *2010 IEEE Instrumentation & Measurement Technology Conference Proceedings* **2010**, 54-57.
37. Kerns, D. M.; Beatty, R. W., *Basic Theory of Waveguide Junctions and Introductory Microwave Network Analysis*. 1st ed.; Pergamon Press: Oxford, New York, 1967.
38. Baker-Jarvis, J.; Vanzura, E. J.; Kissick, W. A., Improved technique for determining complex permittivity with the transmission/reflection method. *IEEE Transactions on Microwave Theory and Techniques* **1990**, 38 (8), 1096-1103.
39. Keysight Technologies, N1500A Materials Measurement Suite, <http://literature.cdn.keysight.com/litweb/pdf/5992-0263EN.pdf>, (accessed June 13th, 2018).

40. Somlo, P. I., A convenient self-checking method for the automated microwave measurement of mu and epsilon. *IEEE Transactions on Instrumentation and Measurement* **1993**, *42* (2), 213-216.
41. Qaddoumi, N.; Ganchev, S.; Zoughi, R., Microwave diagnosis of low-density fiberglass composites with resin binder. *Research in Nondestructive Evaluation* **1996**, *8* (3), 177-188.
42. Bois, K. J.; Handjojo, L. F.; Benally, A. D.; Mubarak, K.; Zoughi, R., Dielectric plug-loaded two-port transmission line measurement technique for dielectric property characterization of granular and liquid materials. *IEEE Transactions on Instrumentation and Measurement* **1999**, *48* (6), 1141-1148.
43. TA Instruments, Purge Gas Recommendations for use in Modulated DSC®, <http://www.tainstruments.com/pdf/literature/TN44.pdf>, (accessed June 13th, 2018).
44. Black, S. B.; Chang, Y.; Bae, C.; Hickner, M. A., FTIR characterization of water-polymer interactions in superacid polymers. *The Journal of Physical Chemistry B* **2013**, *117* (50), 16266-16274.
45. Smedley, S. B.; Chang, Y.; Bae, C.; Hickner, M. A., Measuring water hydrogen bonding distributions in proton exchange membranes using linear Fourier Transform Infrared Spectroscopy. *Solid State Ionics* **2015**, *275*, 66-70.
46. Socrates, G., *Infrared and raman characteristic group frequencies: Tables and charts*. 3rd ed.; John Wiley & Sons: West Sussex, England, 2004.
47. Moilanen, D. E.; Piletic, I. R.; Fayer, M. D., Tracking water's response to structural changes in Nafion membranes. *The Journal of Physical Chemistry A* **2006**, *110* (29), 9084-9088.
48. Falk, M., An infrared study of water in perfluorosulfonate (Nafion) membranes. *Canadian Journal of Chemistry* **1980**, *58* (14), 1495-1501.
49. Hou, J.; Li, J.; Madsen, L. A., Anisotropy and transport in poly(arylene ether sulfone) hydrophilic-hydrophobic block copolymers. *Macromolecules* **2010**, *43* (1), 347-353.

50. Geise, G. M.; Hickner, M. A.; Logan, B. E., Ionic resistance and permselectivity tradeoffs in anion exchange membranes. *ACS Applied Materials & Interfaces* **2013**, *5* (20), 10294-10301.
51. Geise, G. M.; Hickner, M. A.; Logan, B. E., Ammonium bicarbonate transport in anion exchange membranes for salinity gradient energy. *ACS Macro Letters* **2013**, *2* (9), 814-817.
52. Geise, G. M.; Curtis, A. J.; Hatzell, M. C.; Hickner, M. A.; Logan, B. E., Salt concentration differences alter membrane resistance in reverse electrodialysis stacks. *Environmental Science & Technology Letters* **2014**, *1* (1), 36-39.
53. Crank, J., *The Mathematics of Diffusion*. 2nd ed.; Clarendon Press: Oxford, New York, 1975.
54. Geise, G. M.; Freeman, B. D.; Paul, D. R., Characterization of a sulfonated pentablock copolymer for desalination applications. *Polymer* **2010**, *51* (24), 5815-5822.
55. Luo, H.; Aboki, J.; Ji, Y.; Guo, R.; Geise, G. M., Water and salt transport properties of triptycene-containing sulfonated polysulfone materials for desalination membrane applications. *ACS Applied Materials & Interfaces* **2018**, *10* (4), 4102-4112.
56. Yasuda, H.; Lamaze, C. E.; Ikenberry, L. D., Permeability of solutes through hydrated polymer membranes. Part I. Diffusion of sodium chloride. *Die Makromolekulare Chemie* **1968**, *118* (1), 19-35.

## Chapter 3: Increasing Salt Size Selectivity in Low Water Content Polymers via Polymer Backbone Dynamics\*\*\*\*

### 3.1. Introduction

Water and ion transport in desalination membrane materials is often discussed in terms of sorption and diffusivity properties that define the thermodynamic and kinetic, respectively, contributions to membrane transport properties.<sup>1-4</sup> Several studies have probed the thermodynamic influences of water and ion sorption on permeability properties.<sup>1, 5-8</sup> Fewer studies, however, have considered structure-property relationships for enhancing the size selectivity, via a diffusion-based mechanism, of membranes for desalination applications.

Commercially successful desalination membranes generally have been based on either polyamide or cellulose acetate chemistry,<sup>3</sup> and membrane polymers that offer high salt rejection often sorb relatively little water compared to more highly hydrated ion exchange materials and hydrogels.<sup>9-11</sup> As a result, ions diffusing through a low water content polymer matrix may be more likely to interact with the polymer backbone compared to a more highly hydrated polymer. This situation suggests that polymer backbone rigidity in low water content polymers may influence the size selectivity of salt transport by analogy to reports of increased size selectivity in rigid compared to flexible backbone gas separation membrane polymers.<sup>12</sup> The influence of polymer backbone segmental dynamics on the size selectivity properties of low water content polymers is not generally understood.

---

\*\*\*\*This section has been adapted with permission from: Chang, K.; Xue, T.; Geise, G. M., Increasing salt size selectivity in low water content polymers via polymer backbone dynamics. *Journal of Membrane Science* **2018**, 552, 43-50.

Water molecule dynamics are often considered to govern ion transport properties in more highly hydrated materials, such as Nafion<sup>®</sup> (a perfluorosulfonic acid polymer that absorbs around 30% water by volume)<sup>13</sup> and other fuel cell and ion exchange membrane materials.<sup>1, 2, 14-18</sup> Transport is often considered to be facilitated by free or bulk water in these highly hydrated polymers.<sup>14-16, 19</sup> In low water content polymers, however, little if any ‘free’ or ‘bulk’ water exists in stark contrast to many ion exchange membranes.<sup>14, 20-22</sup> This situation suggests that polymer segmental dynamics may influence transport to a greater extent when the polymer water content is low.

To investigate this question, we studied the salt size selectivity of a flexible, acrylate-based copolymer and a rigid, methacrylate-based co-polymer. The co-polymers were compared at equivalent water content, as the extent of water sorption can influence strongly the transport properties of hydrated polymers.<sup>23</sup> The chemical structures of the two co-polymers considered are very similar, and this choice was made in an effort to keep the thermodynamic interactions between salt and the polymer as similar as possible. The salt permeability, sorption, and diffusivity properties of the co-polymers were characterized using salts that were effectively different sizes, as quantified by the salt diffusivity at infinite dilution in aqueous solution. The rigid, low water content co-polymer ultimately was more size selective compared to the flexible, low water content co-polymer suggesting that polymer segmental dynamics may be important for achieving size selectivity in low water content polymers.

## **3.2. Results and Discussion**

### **3.2.1. Water Uptake**

Polymer water content has a strong influence on the salt transport properties of hydrated polymers,<sup>1, 2, 4, 14-16, 23</sup> so the co-polymer compositions ([Figure 2.1](#)) were chosen to ensure that the

water content of the HEA-co-EA (i.e., X = 30 and Y = 70) and HEMA-co-MMA (i.e., X = 25 and Y = 75) materials was statistically indistinguishable (Table 3.1). The dry polymer density was used to calculate the water sorption coefficient using Equations 2.2 and 2.5, and the dry polymer densities of the HEA-co-EA and HEMA-co-MMA materials were  $1.22 \pm 0.02 \text{ g/cm}^3$  and  $1.20 \pm 0.04 \text{ g/cm}^3$ , respectively. Water content values measured using salt solutions were less than those values measured using pure water (Table 3.1) due to osmotic de-swelling.<sup>1, 24</sup> The statistically indistinguishable water sorption coefficient values for the two co-polymers suggest that the transport data measured for the materials can be compared at equivalent water content.

**Table 3.1.** Water content measured at room temperature. The reported data are averages of four measurements, and the uncertainty was taken as one standard deviation from the mean.

Material	Water Uptake [g(water)/g(dry polymer)]	Water Sorption Coefficient, $K_w$			
		Pure Water	0.5 mol/L LiCl	0.5 mol/L NaCl	0.5 mol/L KCl
HEA-co-EA	$0.081 \pm 0.006$	$0.089 \pm 0.007$	$0.080 \pm 0.002$	$0.081 \pm 0.006$	$0.077 \pm 0.006$
HEMA-co-MMA	$0.080 \pm 0.027$	$0.088 \pm 0.030$	$0.078 \pm 0.017$	$0.088 \pm 0.009$	$0.087 \pm 0.014$

### 3.2.2. Thermal Characterization

Polymer segmental dynamics in the HEA-co-EA and HEMA-co-MMA co-polymers were characterized using the glass transition temperature,  $T_g$ , of the hydrated co-polymers (Figure 3.1). The glass transition temperature can be related to segmental dynamics in polymers, and higher  $T_g$  polymers are generally considered to have more rigid backbones compared to lower  $T_g$  polymers.<sup>25</sup> <sup>26</sup> The higher glass transition temperature of the HEMA-co-MMA material ( $T_g = 98 \text{ }^\circ\text{C}$ ) suggests that the HEMA-co-MMA polymer is more rigid compared to the HEA-co-EA material ( $T_g = -21 \text{ }^\circ\text{C}$ ) that has a lower glass transition temperature. This result is reasonable given that the additional methyl group on the methacrylate backbone is expected to slow segmental dynamics as a result of

additional steric hindrance compared to the HEA-co-EA acrylic backbone that does not contain the additional methyl group.

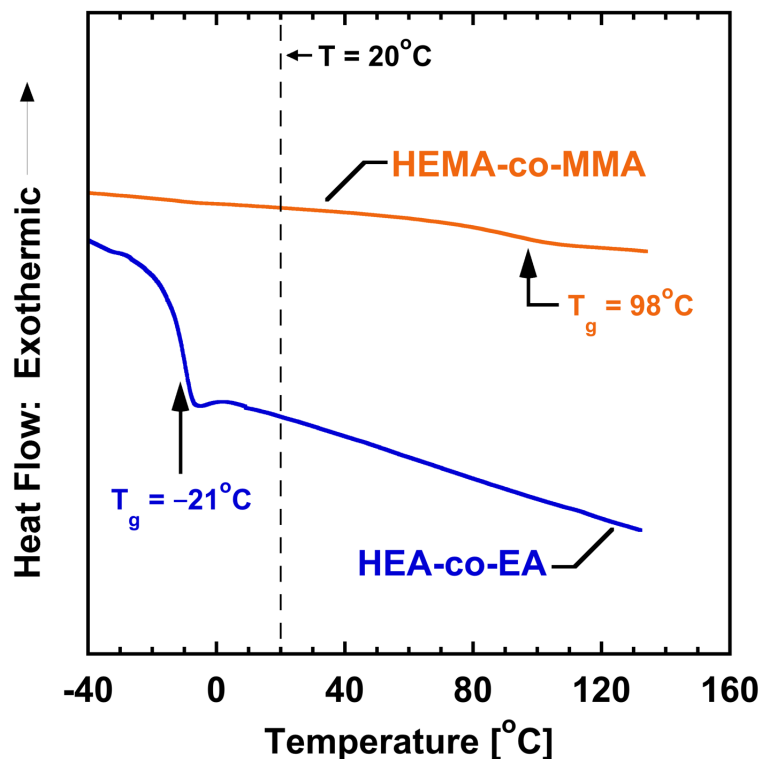


**Figure 3.1.** Differential scanning calorimetry (DSC) second scan thermograms for pure water equilibrated HEA-co-EA and HEMA-co-MMA samples. The dashed line represents  $T = 20^\circ\text{C}$  and illustrates that the HEMA-co-MMA material is glassy at room temperature (i.e.,  $T_g > 20^\circ\text{C}$ ) while the HEA-co-EA material is rubbery at room temperature (i.e.,  $T_g < 20^\circ\text{C}$ ).

A homogeneous co-polymer, where the co-monomers are well mixed, is expected to have a single  $T_g$  value.<sup>27</sup> The HEA-co-EA and HEMA-co-MMA co-polymers exhibited single glass transition temperatures (Figure 3.1). This result suggests that the co-polymers are relatively homogeneous, in contrast to other co-polymers (not reported in this study) that had hydrophilic to hydrophobic co-monomer compositions closer to 50/50 and exhibited two distinct glass transitions.

The Fox equation provides an estimate of the co-polymer glass transition temperature,  $T_{g,copolymer}$ , based on a mass fraction-weighted average of the homopolymer glass transition temperatures for each component in the co-polymer:

$$\frac{1}{T_{g,copolymer}} = \frac{\omega_1}{T_{g1}} + \frac{\omega_2}{T_{g2}} + \frac{\omega_w}{T_{gw}} + \frac{\omega_{PEG}}{T_{gPEG}} \quad (3.1)$$

where  $\omega_i$  and  $T_{gi}$  are the mass fraction and glass transition temperature, respectively, of component  $i$ .<sup>28,29</sup> The components,  $i$ , were labeled as 1: HEA or HEMA, 2: EA or MMA,  $w$ : water, and PEG: poly(ethylene oxide) diacrylate. The value of  $T_{gw}$  was taken as  $-137$  °C,<sup>30</sup> and values for  $T_{g1}$ ,  $T_{g2}$ , and  $T_{gPEG}$  are reported in [Table B.1](#). ([Equation 3.1](#) was used to estimate the glass transition temperatures of the co-polymers, and reasonable agreement was observed between the Fox equation estimates and the measured  $T_g$  values ([Table 3.2](#)). This result further suggests that the co-polymers were relatively homogeneous materials.

**Table 3.2.** Glass transition temperatures calculated using the Fox equation ([Equation 3.1](#)) and the measured glass transition temperatures for the co-polymers.

Co-polymer	Fox Equation $T_g$ [°C]	Measured $T_g$ [°C]
HEA-co-EA	-22	-21
HEMA-co-MMA	103	98

While the DSC results and Fox Equation results discussed above suggest that the HEA-co-EA and HEMA-co-MMA materials are relatively homogeneous, differences in the reactivity of the co-monomers and cross-linker do exist (particularly for PEGDA compared to the methacrylate-based co-monomers).<sup>31</sup> These differences in reactivity could result in a situation where the co-monomers and cross-linker are not distributed in a statistically random manner throughout the materials. The DSC results and Fox Equation analysis, however, suggest that the selected co-

polymer compositions did not exhibit evidence of significant phase separation even with the recognized differences in co-monomer and cross-linker reactivity.

### 3.2.3. Salt Permeability

For all salts considered and at equivalent water uptake, the more flexible backbone HEA-co-EA material exhibited greater salt permeability compared to the more rigid backbone HEMA-co-MMA material (Figure 3.2). This result is consistent with the idea that polymer chain dynamics may influence salt permeability in low water content polymers. More rigid polymers appear to slow transport dynamics while more flexible polymers permit faster transport.

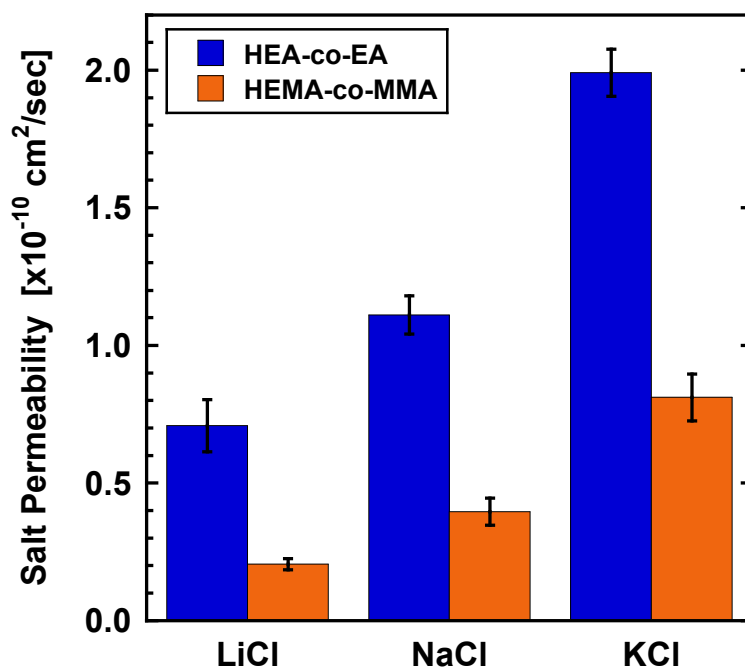


**Figure 3.2.** Salt permeability, at 25°C, measured using an upstream aqueous electrolyte concentration of 0.5 mol/L of LiCl, NaCl, or KCl. The uncertainty was taken as one standard deviation from the mean of three measurements.

### 3.2.4. Size Selectivity

To determine whether the more rigid HEMA-co-MMA co-polymer was more size selective compared to the more flexible HEA-co-EA co-polymer, the salt permeability and diffusivity

properties of the co-polymers were measured using salts of increasing effective hydrated size. In the gas separation membrane field, similar analysis has been accomplished by comparing gas diffusion coefficients in glassy versus rubbery polymers as a function of the kinetic diameter or van der Waals volume of the gas.<sup>32-34</sup> To consider salt transport size selectivity in hydrated polymers, we took the average salt diffusivity in aqueous solution,  $D_s^s$ , at infinite dilution as a measure of the effective size of a hydrated salt. The value of  $D_s^s$  can be calculated as:

$$D_s^s = \frac{(z_+ + |z_-|)D_+D_-}{z_+D_+ + |z_-|D_-} \quad (3.2)$$

where  $D_+$  and  $D_-$  are the cation and anion diffusion coefficients, respectively, at infinite dilution in aqueous solution, and the charge numbers,  $z_+$  and  $|z_-|$  are unity for sodium, potassium and lithium chloride.<sup>35</sup> The values of  $D_s^s$ ,  $D_+$ , and  $D_-$  are reported in [Table 3.3](#). As  $D_s^s$  increases, the effective salt size decreases because smaller hydrated ions diffuse more rapidly compared to larger hydrated ions.

**Table 3.3.** Cation and anion diffusion coefficients and average salt diffusion coefficients calculated using ([Equation 3.2](#)) for the electrolytes considered in bulk aqueous solution at infinite dilution.

Salt	$D_+$ [ $\times 10^{-5}$ cm <sup>2</sup> /s] <sup>36</sup>	$D_-$ [ $\times 10^{-5}$ cm <sup>2</sup> /s] <sup>36</sup>	$D_s^s$ [ $\times 10^{-5}$ cm <sup>2</sup> /s]
KCl	1.957	2.032	1.99
NaCl	1.334	2.032	1.61
LiCl	1.029	2.032	1.37

Salt sorption coefficients,  $K_s$ , were measured using 0.5 mol/L lithium, sodium, and potassium chloride ([Table 3.4](#)). The salt sorption coefficients for a given salt were relatively similar between the two co-polymers. Some evidence of ion specific sorption was observed as lithium chloride was most highly sorbed and potassium chloride was least highly sorbed by the co-polymers. The co-polymers were crosslinked with poly(ethylene oxide) diacrylate, so some of the

specific ion sorption effects observed may be related to ion-polymer interactions with the ethylene oxide repeat units in the cross-linker. For example, lithium cations interact favorably with ethylene oxide repeat units,<sup>37, 38</sup> so the observation the co-polymers sorb more lithium chloride compared to the other salts may be related to interactions between lithium ions and the ethylene oxide repeat units.

**Table 3.4.** Salt sorption coefficients measured after equilibrating co-polymer samples with 0.5 mol/L aqueous LiCl, NaCl, or KCl solutions. Measurements were made at room temperature, and the uncertainty was taken as one standard deviation from the mean of four measurements.

Material	Salt Sorption Coefficient, $K_s$		
	0.5 mol/L LiCl	0.5 mol/L NaCl	0.5 mol/L KCl
HEA-co-EA	$0.022 \pm 0.005$	$0.016 \pm 0.005$	$0.011 \pm 0.002$
HEMA-co-MMA	$0.027 \pm 0.004$	$0.015 \pm 0.004$	$0.010 \pm 0.001$

The HEA-co-EA and HEMA-co-MMA materials are relatively low water content polymers, so the question exists as to whether sufficient water is sorbed by the polymers to hydrate the ions that sorb into the materials. This question is important because the effective size of the electrolytes in the polymer was approximated using the salt diffusion coefficient of the electrolyte in dilute aqueous solution (as described earlier in this section). The salt sorption coefficient data (Table 3.4) can be combined with the water content data (Table 3.1) and ion hydration numbers to evaluate the ratio of moles of water available in the polymer to moles of water needed to hydrate the sorbed ions (Table B.4). These calculations, detailed in the Appendix B, suggest that greater than one order of magnitude (and in some cases two orders of magnitude) more sorbed water is available compared to that needed to hydrate the sorbed ions. This result suggests that sufficient water exists in the HEA-co-EA and HEMA-co-MMA polymers to hydrate the sorbed ions.

The result is further supported considering that the hydration energies for the ions (Table B.5) are generally more negative (favorable) compared to the energies of the hydrogen bonds that likely form within the hydrated polymer (i.e., ion hydration may be favored over polymer hydration in these materials).<sup>39</sup> Therefore, the use of the average salt diffusion coefficient in bulk aqueous solution at infinite dilution may be an effective proxy for hydrated ion size in the HEA-co-EA and HEMA-co-MMA materials.

To analyze size selectivity further, the salt permeability data for the three electrolytes were normalized by the KCl permeability data (Figure 3.3). Plotting the data in this manner facilitates comparison of the two co-polymers, which have comparable water sorption properties (Table 3.1). The normalized salt permeability data for the more rigid HEMA-co-MMA co-polymer decreased to a greater extent compared to that for the more flexible HEA-co-EA co-polymer over the range of electrolytes considered. While the data points for NaCl are statistically indistinguishable, the LiCl data show a statistically significant difference in the normalized salt permeability of the two co-polymers. This result suggests that the more rigid HEMA-co-MMA co-polymer is more size selective compared to the more flexible HEA-co-EA co-polymer, as the HEMA-co-MMA salt permeability decreases with increasing salt size more strongly than the HEA-co-EA salt permeability.

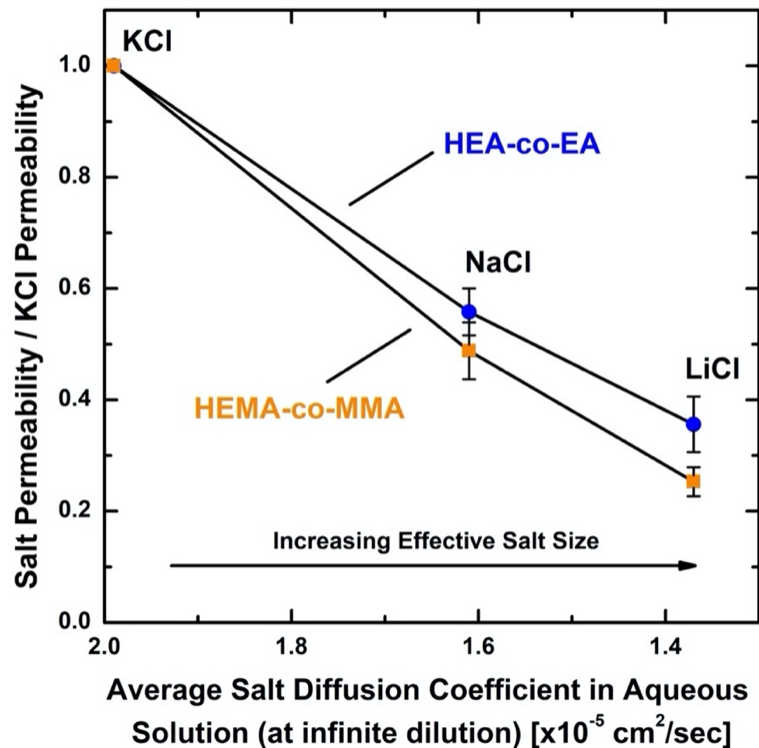


**Figure 3.3.** Salt permeability data (measured at 25 °C using a 0.5 mol/L upstream aqueous LiCl, NaCl, or KCl solution) normalized by the KCl permeability value and plotted as a function of the average salt diffusion coefficient in aqueous solution at infinite dilution and 25 °C. The average salt diffusion coefficient in aqueous solution at infinite dilution (horizontal axis) is a measure of the effective size of the electrolyte, and the horizontal axis is inverted such that the effective electrolyte size increases from left to right as the value of average salt diffusion coefficient decreases.

The difference in the normalized permeability properties of HEMA-co-MMA and HEA-co-EA (Figure 3.3) is not dramatic due to the small size range of salts considered; the hydrated radii of  $\text{Li}^+$ ,  $\text{Na}^+$  and  $\text{K}^+$  are 3.82, 3.58 and 3.31 Å, respectively.<sup>40</sup> The range of effective electrolyte size considered is much smaller compared to size selectivity studies conducted on membranes for gas separation applications where molecular size can be varied from helium to hydrocarbons, such as *n*-hexane.<sup>33, 34</sup> The restricted effective electrolyte size range was due to our desire to limit our analysis to monovalent chloride electrolytes. This choice was made to avoid additional complications related to the use of multi-valent ions.

To further analyze the permeability properties reported in [Figure 3.3](#), the measured salt permeability and sorption coefficients were used to calculate the effective salt diffusion coefficients in the materials. Fickian salt transport analysis provides a solution-diffusion relationship between the salt permeability, diffusivity, and sorption coefficients:

$$P_s = K_s \times D_s \quad (3.3)$$

where  $P_s$  is the salt permeability,  $K_s$  is the salt sorption coefficient, and  $D_s$  is the effective salt diffusion coefficient.<sup>1, 2, 4, 41</sup> The effective salt diffusion coefficients for the copolymers, which were calculated using [Equation 3.3](#) and the measured salt permeability ([Figure 3.2](#)) and sorption coefficient ([Table 3.4](#)) data, are reported in [Table 3.5](#).

**Table 3.5.** Effective salt diffusion coefficients for the two copolymers were determined from measured salt permeability and sorption coefficient data using [Equation 3.3](#). The uncertainty was calculated using standard error propagation methods.<sup>42</sup>

	Effective Salt Diffusion Coefficient in the Polymer, $D_s$ [ $\times 10^{-9}$ cm <sup>2</sup> /s]		
	0.5 mol/L LiCl	0.5 mol/L NaCl	0.5 mol/L KCl
HEA-co-EA	3.3 ± 0.9	6.9 ± 2.2	18.6 ± 3.6
HEMA-co-MMA	0.8 ± 0.1	2.7 ± 0.8	8.1 ± 1.2

To analyze further the salt diffusivity in the HEA-co-EA and HEMA-co-MMA materials, the experimentally determined effective salt diffusion coefficients were compared to salt diffusion coefficients calculated using the Mackie and Meares model.<sup>43</sup> The Mackie and Meares model describes hindered diffusion in hydrated polymers using a lattice model approach whereby small molecule diffusion is hindered by the presence of the polymer chains in the hydrated material.<sup>43</sup> The model depends only on the volume fraction of water sorbed in the polymer and the salt diffusion coefficient in bulk solution,  $D_s^s$ :<sup>43</sup>

$$\frac{D_s}{D_s^s} = \left( \frac{K_w}{2 - K_w} \right)^2 \quad (3.4)$$

As discussed with regard to [Equation 2.5](#), the water sorption coefficient,  $K_w$ , is effectively equivalent to the volume fraction of water sorbed in the polymer,  $\phi_w^m$ .

Values of  $D_s$  were calculated for the two co-polymers using  $D_s^s$  data reported in [Table 3.5](#) and  $K_w$  values reported in [Table 3.1](#). The Mackie and Meares model  $D_s$  values were greater than the experimentally measured  $D_s$  values for all of the materials and electrolytes considered ([Table B.2](#)). This observation suggests that diffusion in the HEA-co-EA and HEMA-co-MMA materials is hindered to a greater extent than predicted using a simple lattice model and that additional interactions involving the ions and the polymer influence salt diffusion properties in these materials.

Normalizing the experimentally determined  $D_s$  values by those values calculated using the Mackie and Meares model reveals that the HEMA-co-MMA diffusion coefficients are more suppressed (compared to the Mackie and Meares model  $D_s$  values) than the HEA-co-EA diffusion coefficients ([Table 3.6](#)). Additionally, the effectively larger LiCl electrolyte experienced a greater reduction in  $D_s$  compared to the Mackie and Meares model calculation compared to the effectively smaller electrolytes. These results are consistent with the physical picture that slower chain dynamics in the HEMA-co-MMA material may restrict diffusion to a greater extent and be more diffusion size selective than the more flexible HEA-co-EA material.

**Table 3.6.** Ratios of the experimentally determined  $D_s$  value (Table 3.5) to the value calculated using the Mackie and Meares model (Equation 3.4 and Table B.2) for each of the materials and electrolytes.

	Experimentally Determined $D_s$ / Mackie and Meares Model Calculated $D_s$		
	LiCl	NaCl	KCl
HEA-co-EA	0.14	0.24	0.58
HEMA-co-MMA	0.03	0.08	0.20

The effective salt diffusion coefficients for the co-polymers (Table 3.5) were normalized by the KCl diffusion coefficient and plotted as a function of increasing effective salt size (Figure 3.4). Similar to the permeability data (Figure 3.3), the normalized diffusivity properties of the more rigid HEMA-co-MMA co-polymer decrease to a greater extent compared to the more flexible HEA-co-EA copolymer over the range of electrolyte sizes considered. Since the two co-polymers have comparable water sorption properties (Table 3.1), this result also suggests that polymer segmental dynamics play a role in the diffusivity selectivity properties of these low water content polymers. The more rigid co-polymer (HEMA-co-MMA) was found to be more diffusion or size selective compared to the more flexible co-polymer (HEA-co-EA).

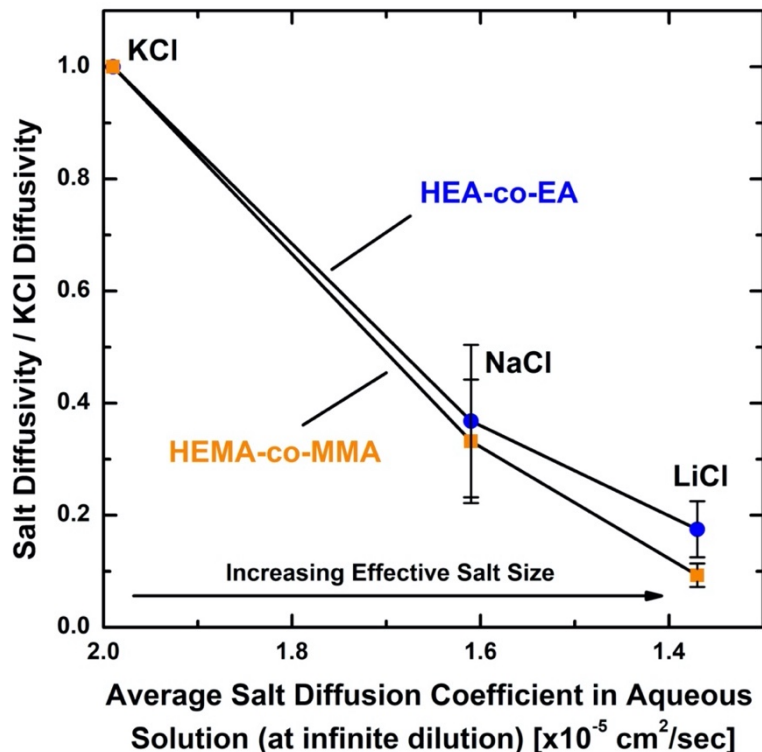


**Figure 3.4.** Effective salt diffusion coefficients (calculated from measured salt permeability and salt sorption coefficients using (Equation 3.3) normalized by the effective KCl diffusion coefficient and plotted as a function of the average salt diffusion coefficient in aqueous solution at infinite dilution and 25 °C. The average salt diffusion coefficient in aqueous solution at infinite dilution (horizontal axis) is a measure of the effective size of the electrolyte, and the horizontal axis is inverted such that the effective electrolyte size increases from left to right as the value of average salt diffusion coefficient decreases.

### 3.3. Conclusions

For the low water content polymers considered in this study, polymer segmental dynamics appear to influence salt transport size selectivity properties. A more rigid backbone HEMA-co-MMA co-polymer was more salt permeability and diffusion selective compared to a more flexible HEA-co-EA co-polymer. These results suggest that rigid polymer segments may increase the size selectivity of low water content polymers in a manner similar to that observed in gas separation membranes. These results, for low water content polymers, suggest that the influence of polymer segmental dynamics may be more important in polymers that contain very little water compared to the situation for polymers that sorb much more water and contain appreciable amounts of bulk

water. Size selectivity was characterized using monovalent chloride salts, to avoid complications of higher valence electrolytes, so the range of probed molecular size was relatively small compared to comparable studies in gas separation membranes. As a result, the increase in size selectivity for the more rigid polymer compared to the more flexible polymer is modest, but the results do suggest that incorporating rigid backbone polymers in low water content materials may be a strategy for enhancing salt transport size selectivity in polymer membrane materials.

### 3.4. References

1. Geise, G. M.; Paul, D. R.; Freeman, B. D., Fundamental water and salt transport properties of polymeric materials. *Prog. Polym. Sci.* **2014**, *39*, 1-42.
2. Geise, G. M.; Lee, H.-S.; Miller, D. J.; Freeman, B. D.; McGrath, J. E.; Paul, D. R., Water purification by membranes: The role of polymer science. *Journal of Polymer Science Part B: Polymer Physics* **2010**, *48* (15), 1685-1718.
3. Baker, R. W., *Membrane Technology and Applications*. 3rd ed.; Wiley: New York, 2012.
4. Paul, D. R., Reformulation of the solution-diffusion theory of reverse osmosis. *Journal of Membrane Science* **2004**, *241* (2), 371-386.
5. Kamcev, J.; Paul, D. R.; Manning, G. S.; Freeman, B. D., Predicting salt permeability coefficients in highly swollen, highly charged ion exchange membranes. *ACS Applied Materials & Interfaces* **2017**, *9* (4), 4044-4056.
6. Kamcev, J.; Galizia, M.; Benedetti, F. M.; Jang, E.-S.; Paul, D. R.; Freeman, B. D.; Manning, G. S., Partitioning of mobile ions between ion exchange polymers and aqueous salt solutions: Importance of counter-ion condensation. *Physical Chemistry Chemical Physics* **2016**, *18* (8), 6021-6031.
7. Kamcev, J.; Paul, D. R.; Freeman, B. D., Ion activity coefficients in ion exchange polymers: Applicability of Manning's counterion condensation theory. *Macromolecules* **2015**, *48* (21), 8011-8024.

8. Geise, G. M.; Falcon, L. P.; Freeman, B. D.; Paul, D. R., Sodium chloride sorption in sulfonated polymers for membrane applications. *Journal of Membrane Science* **2012**, *423*, 195-208.
9. Freger, V., Swelling and morphology of the skin layer of polyamide composite membranes: An atomic force microscopy study. *Environ. Sci. Technol.* **2004**, *38*, 3168-3175.
10. Chan, E. P.; Young, A. P.; Lee, J.-H.; Chung, J. Y.; Stafford, C. M., Swelling of ultrathin crosslinked polyamide water desalination membranes. *Journal of Polymer Science Part B: Polymer Physics* **2013**, *51* (6), 385-391.
11. Lonsdale, H. K.; Merten, U.; Riley, R. L., Transport properties of cellulose acetate osmotic membranes. *J. Appl. Polym. Sci.* **1965**, *9*, 1341-1362.
12. Baker, R. W.; Wijmans, J. G., Membrane separation of organic vapors from gas streams. In *Polymeric gas separation membranes*, Paul, D. R.; Yampolskii, Y. P., Eds. CRC Press: Boca Raton, 1994; pp 353-397.
13. Paddison, S. J.; Reagor, D. W.; Zawodzinski, T. A., High frequency dielectric studies of hydrated Nafion<sup>®</sup>. *J. Electroanal. Chem.* **1998**, *459*, 91-97.
14. Hickner, M. A., Ion-containing polymers: New energy & clean water. *Materials Today* **2010**, *13* (5), 34-41.
15. Hickner, M. A., Water-mediated transport in ion-containing polymers. *Journal of Polymer Science Part B: Polymer Physics* **2012**, *50* (1), 9-20.
16. Kreuer, K. D., On the development of proton conducting polymer membranes for hydrogen and methanol fuel cells. *Journal of Membrane Science* **2001**, *185* (1), 29-39.
17. Hickner, M. A.; Herring, A. M.; Coughlin, E. B., Anion exchange membranes: Current status and moving forward. *Journal of Polymer Science Part B: Polymer Physics* **2013**, *51* (24), 1727-1735.

18. Strathmann, H.; Grabowski, A.; Eigenberger, G., Ion-exchange membranes in the chemical process industry. *Industrial & Engineering Chemistry Research* **2013**, *52* (31), 10364-10379.
19. Tandon, R.; Pintauro, P. N., Solvent effects during multicomponent ion uptake into a Nafion cation-exchange membrane. *J. Membr. Sci.* **2009**, *341* (1-2), 21-29.
20. Black, S. B.; Chang, Y.; Bae, C.; Hickner, M. A., FTIR characterization of water-polymer interactions in superacid polymers. *The Journal of Physical Chemistry B* **2013**, *117* (50), 16266-16274.
21. Toprak, C.; Agar, J. N.; Falk, M., State of water in cellulose acetate membranes. *J. Chem. Soc., Faraday Trans. 1* **1979**, *75*, 803-815.
22. Taniguchi, Y.; Horigome, S., The states of water in cellulose acetate membranes. *Journal of Applied Polymer Science* **1975**, *19* (10), 2743-2748.
23. Yasuda, H.; Lamaze, C. E.; Ikenberry, L. D., Permeability of solutes through hydrated polymer membranes. Part I. Diffusion of sodium chloride. *Die Makromolekulare Chemie* **1968**, *118* (1), 19-35.
24. Khare, A. R.; Peppas, N., Swelling/deswelling of anionic copolymer gels. *Biomaterials* **1995**, *16*, 559-567.
25. van Krevelen, D. W.; Nijenhuis, K., *Properties of Polymers: Their Correlation with Chemical Structure; their Numerical Estimation and Prediction from Additive Group Contributions*. Elsevier Science: 2009.
26. Hodge, I. M., Physical aging in polymer glasses. *Science* **1995**, 1945-1947.
27. Brostow, W.; Chiu, R.; Kalogeras, I. M.; Vassilikou-Dova, A., Prediction of glass transition temperatures: binary blends and copolymers. *Materials Letters* **2008**, *62* (17), 3152-3155.

28. Fox, T. G.; Flory, P. J., Second order transition temperatures and related properties of polystyrene. I. Influence of molecular weight. *J. Appl. Phys.* **1950**, *21*, 581-591.
29. Hiemenz, P. C.; Lodge, T. P., *Polymer chemistry*. 2nd ed.; CRC Press: New York, 2007.
30. Velikov, V.; Borick, S.; Angell, C. A., The glass transition of water, based on hyperquenching experiments. *Science* **2001**, *294* (5550), 2335-2338.
31. Takács, E.; Wojnárovits, L., Comparison of the reactivity of acrylate and methacrylate monomers. *Radiation Physics and Chemistry* **1995**, *46* (4, Part 2), 1007-1010.
32. Baker, R. W., *Membrane Technology and Applications*. Wiley: 2004.
33. Paul, D. R.; Yampol'skii, Y. P., *Polymeric gas separation membranes*. CRC Press: Boca Raton, 1994.
34. Yampol'skii, Y.; Pinnau, I.; Freeman, B. D., *Materials science of membranes for gas and vapor separation*. Wiley: London, 2006; p 445.
35. Robinson, R. A.; Stokes, R. H., *Electrolyte solutions*. 2nd ed.; Dover: Mineola, NY, 2002.
36. Rumble, J. R., *CRC Handbook of Chemistry and Physics*. 98th ed.; CRC Press LLC: 2017.
37. Agrawal, R. C.; Pandey, G. P., Solid polymer electrolytes: materials designing and all-solid-state battery applications: an overview. *Journal of Physics D: Applied Physics* **2008**, *41* (22), 223001.
38. Meyer, W. H., Polymer Electrolytes for Lithium-Ion Batteries. *Adv. Mater.* **1998**, *10* (6), 439-448.
39. Desiraju, G. R.; Steiner, T., *The Weak Hydrogen Bond in Structural Chemistry and Biology*. Oxford University Press: Oxford, New York, 1999.

40. Nightingale, E. R., Phenomenological Theory of Ion Solvation. Effective Radii of Hydrated Ions. *The Journal of Physical Chemistry* **1959**, 63 (9), 1381-1387.
41. Wijmans, J. G.; Baker, R. W., The solution-diffusion model: A review. *Journal of Membrane Science* **1995**, 107 (1), 1-21.
42. Bevington, P. R.; Robinson, D. K., Chapter 4: Propagation of Errors. In *Data reduction and error analysis for the physical sciences*, McGraw Hill: New York, 2003; pp 56-65.
43. Mackie, J. S.; Meares, P., The diffusion of electrolytes in a cation-exchange resin membrane I. Theoretical. *Proceedings of the Royal Society of London. Series A. Mathematical and Physical Sciences* **1955**, 232 (1191), 498-509.

## Chapter 4: Influence of Rubbery versus Glassy Backbone Dynamics on Multiscale Transport in Polymer Membranes<sup>††††</sup>

### 4.1. Introduction

Polyamide-based commercial desalination membranes sorb only around 10% water by mass,<sup>1,2</sup> in contrast to commercial ion exchange materials, such as Nafion<sup>®</sup>, that can sorb up to about 30% water.<sup>3</sup> In high water content materials such as Nafion<sup>®</sup>, water molecule dynamics play a key role in governing water and salt transport properties.<sup>4-8</sup> In lower water content polymers, interactions between water molecules and the polymer backbone are more significant compared to that in highly hydrated materials, so backbone structure and dynamics will tend to influence transport properties to a greater extent in low water content polymers. We have previously reported glassy polymers that show greater salt permeability and diffusion selectivity than comparable rubbery polymers at equivalent water content.<sup>9</sup> Questions still remain about the influence of water dynamics, backbone dynamics, and polymer structure of on water and salt transport properties, which are critical for water purification applications, of glassy versus rubbery low water content polymers at equivalent water content.

To address these questions, two series of chemically similar low water content co-polymers were studied at room temperature; a glassy methacrylate-based co-polymer (HEMA-co-MMA) and a rubbery acrylate-based co-polymer (HEA-co-EA).<sup>9</sup> The glassy methacrylate polymer was expected to have slower segmental dynamics compared to the acrylate polymer that was rubbery

---

<sup>††††</sup> This section has been adapted with permission from: This section has been adapted with permission from: Chang, K.; Korovich, A.; Xue, T.; Morris, W. A.; Madsen, L. A.; Geise, G. M., Influence of rubbery versus glassy backbone dynamics on multiscale transport in polymer membranes. *Macromolecules* **2018**, *51* (22), 9222-9233.

at room temperature. Bulk transport properties of these co-polymers were compared at equivalent water content since water and salt transport properties are highly sensitive to water sorption.<sup>10-13</sup>

Pulsed-field-gradient NMR diffusometry offers detailed insight into water transport dynamics inside polymer systems. By varying the experimental diffusion time, we find that, in both series of co-polymer membranes, the diffusion coefficient of water decreases as the diffusion time increases, signifying the presence of structural heterogeneity on the micron length scale probed by the NMR diffusometry experiment. This phenomenon is also known as restricted diffusion,<sup>14</sup> which has been previously used to understand heterogeneity and transport in porous media<sup>15</sup> including polymeric systems.<sup>16</sup> Furthermore, we extract two separate tortuosity values, from these measurements, that correspond to averaging over different length scales (from the nanometer-to-bulk and micron-to-bulk) of transport resistance. We use these tortuosity parameters to better understand differences in water diffusion due to multi-scale polymer morphology. We find that the micron-to-bulk tortuosity is similar between both series of co-polymers, while the nanometer-to-bulk tortuosity is 5 times larger in the glassy compared to the rubbery co-polymers, suggesting that the rigid backbone of the methacrylate copolymer results in a more tortuous hydrophilic network that slows the overall water transport through the co-polymer.

Upon combining NMR diffusometry results with bulk salt sorption and transport measurements, we found that the methacrylate-based polymers were more water/salt selective than the acrylate-based polymers due to salt diffusivity properties that are suppressed to a greater extent than the water diffusivity properties in the methacrylate polymers. Therefore, the formation of more rigid and tortuous transport pathways in the glassy methacrylate polymers likely hinders transport of larger hydrated ions to a greater extent than the smaller water molecules and increases water/salt selectivity compared to the rubbery acrylate polymers. In low water content polymers,

the use of rigid backbone segments to generate selective nanoscale polymer features may be a viable strategy for increasing the water/salt selectivity of polymers for water purification applications.

## **4.2. Results and Discussion**

### **4.2.1. Material Selection**

A critical component of this study was the preparation of low water content polymers with different segmental dynamics and similar chemistry. To accomplish this task, co-polymers were prepared using chemically similar HEA, HEMA, EA, and MMA co-monomers.<sup>9</sup> In order for the membranes to have comparable water uptake to commercial desalination membranes (10% by mass), we used hydrophobic co-monomers (EA and MMA) to balance the highly hydrophilic HEA and HEMA monomers.<sup>1</sup>

### **4.2.2. Water Content**

We controlled co-polymer water content using the ratio of hydrophilic co-monomer (i.e., HEA or HEMA) to hydrophobic co-monomer. The water uptake ( $w_u$ ) and water sorption coefficient ( $K_w$ ) values for both co-polymers increased as the hydrophilic co-monomer composition increased from 30 % to 40 % (by mass) (Table 4.1). To enable accurate comparison of transport properties between the co-polymers, we controlled the co-polymer hydrophilicity such that the water uptake of the two co-polymer series overlapped. Comparing materials at equivalent water content is critical, as water and salt transport in polymers is strongly influenced by water content.<sup>13</sup> Additionally, the water content of samples initially equilibrated in 0.5 mol/L NaCl was lower than that of materials equilibrated in DI water (Table 4.1) because of osmotic de-swelling due to the lower thermodynamic activity of water in the salt solution.<sup>10, 17</sup>

**Table 4.1.** Dry polymer density and water content data (water uptake,  $w_u$ , and water sorption coefficient,  $K_w$ , c.f. Equations 2.1 and 2.5), determined using both aqueous NaCl solution (0.5 mol/L) and pure (DI) water, for the three compositions of each co-polymer. All data were measured at room temperature, and the uncertainties are reported as one standard deviation from the mean value.

Co-polymer	Composition <sup>a</sup>	Dry Polymer Density [g/cm <sup>3</sup> ]	Measured using 0.5 mol/L NaCl		Measured using DI water	
			$w_u$ <sup>b</sup>	$K_w$	$w_u$ <sup>b</sup>	$K_w$
HEA-co-EA	30:70	1.20±0.01	0.074±0.006	0.081±0.006	0.081±0.006	0.089±0.007
	35:65	1.20±0.01	0.082±0.004	0.090±0.004	0.091±0.005	0.098±0.005
	40:60	1.22±0.01	0.102±0.008	0.109±0.009	0.171±0.007	0.170±0.007
HEMA-co-MMA	30:70	1.22±0.01	0.086±0.004	0.095±0.004	0.091±0.005	0.100±0.006
	35:65	1.23±0.01	0.091±0.005	0.100±0.006	0.098±0.003	0.107±0.003
	40:60	1.25±0.02	0.115±0.003	0.126±0.003	0.192±0.008	0.190±0.008

<sup>a</sup>Co-polymer compositions are reported as hydrophilic (e.g., HEA or HEMA) : hydrophobic (e.g., EA or MMA) co-monomer content (by mass).

<sup>b</sup>Water uptake units: g(water)/g(dry polymer).

The polymer water content was analyzed in terms of the amount of water available to hydrate the hydrophilic moieties within the polymer to provide insight into the hydrogen bonding environment within the polymer. We combined measured water uptake data with polymer composition information to calculate the molar ratio (equivalents) of water sorbed in the polymer to both –OH and –O– functional groups in the copolymers. These calculations (results in Appendix C) indicate that the polymer with the highest water uptake, HEMA-co-MMA 40:60, sorbs 2 equivalents of water per total equivalents of –OH and –O–, and the polymer with the lowest water uptake, HEA-co-EA 30:70, sorbs 1.5 equivalents of water per total equivalents of –OH and –O–. These calculations suggest that the majority of the sorbed water in these co-polymers interacts with the polymer backbone to some extent.

### 4.2.3. Salt Sorption Properties

The HEA-co-EA and HEMA-co-MMA salt sorption coefficients appear to overlap as a function of water uptake (Figure 4.1). Salt sorption in uncharged polymers is expected to be primarily dependent on water uptake and the chemical structure of the polymer,<sup>18</sup> so it is reasonable that co-polymers with similar chemistry and water content exhibit similar salt sorption properties. The results shown in Figure 4.1 suggest that the chemical environment of both co-polymers is similar to the point where salt sorption properties appear to be unaffected by subtle differences in chemical structure. The practical implication of this result is that differences in transport properties between the two co-polymers, compared at equivalent water content, can be attributed to kinetic or diffusion-related phenomena as opposed to thermodynamic or sorption phenomena.

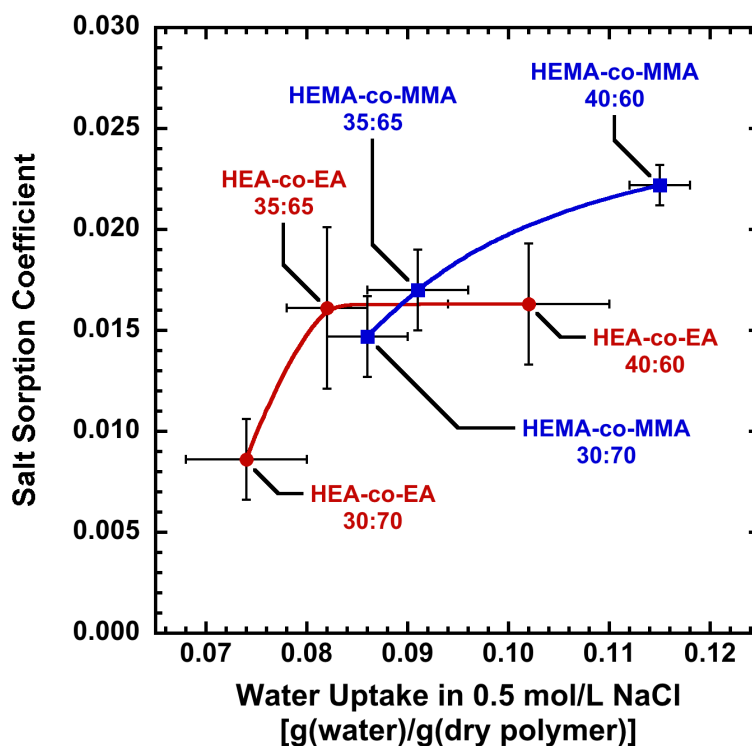


**Figure 4.1.** Salt sorption coefficient,  $K_s$ , data for HEA-co-EA and HEMA-co-MMA co-polymers as a function of water uptake in 0.5 mol/L NaCl solution. Sorption data were measured after equilibrating samples in 0.5 mol/L NaCl, at room temperature. The uncertainty in the data was taken as one standard deviation from the mean of four measurements.

#### 4.2.4. Polymer and Water Dynamics

The hydrated HEMA-co-MMA co-polymers had glass transition temperature,  $T_g$ , values that were above room temperature, and the hydrated HEA-co-EA co-polymers had  $T_g$  values that were below room temperature (Figure 4.2). This result suggests that the segmental dynamics in the HEMA-co-MMA co-polymers were slower compared to the HEA-co-EA co-polymers, as the glass transition temperature can be interpreted as the temperature at which sufficient thermal energy has been provided to the polymer to facilitate segmental motion. Below  $T_g$ , polymer chains are kinetically trapped, but above  $T_g$ , the polymer chains can relax.<sup>19</sup>

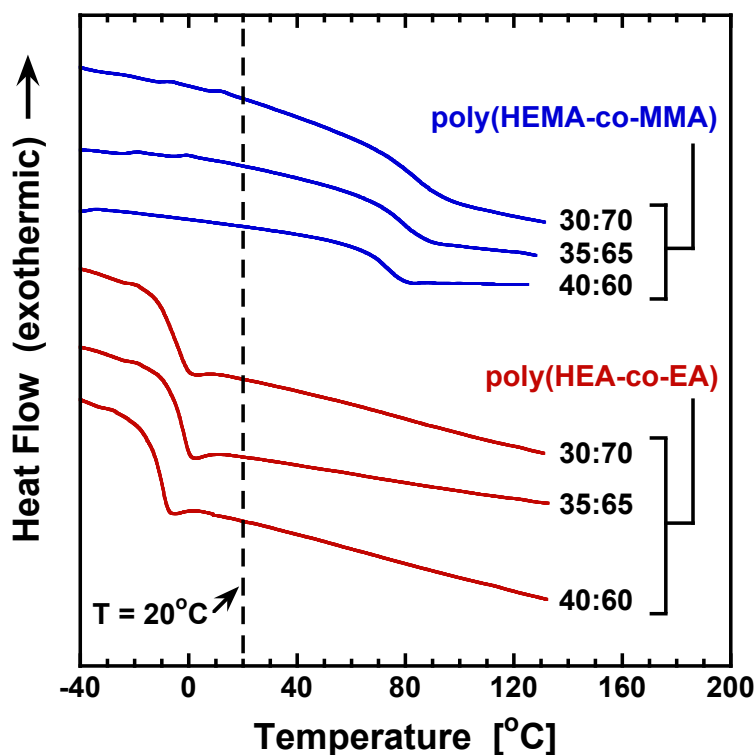


**Figure 4.2.** Second scan DSC thermograms for hydrated poly(HEMA-co-MMA) and poly(HEA-co-EA) samples. Sealed hermetic aluminum pans were used to maintain sample hydration, and the heating rate was 10 °C/min. The thermograms are displaced vertically for clarity, and the compositions of the co-polymers are listed as the ratio of hydrophilic to hydrophobic co-monomer (by mass).

This result is likely due to steric hindrance of the methyl groups on the methacrylate backbone that increase the energy barrier for segmental motion compared to acrylate backbones.<sup>20</sup> This connection between  $T_g$  and segmental dynamics is significant because, at room temperature, segmental dynamics in the glassy HEMA-co-MMA co-polymer are expected to be slower compared to the rubbery HEA-co-EA co-polymers.<sup>21</sup> In other words, at room temperature, the HEMA-co-MMA backbone is expected to be rigid compared to the more flexible HEA-co-EA backbone.

We prepared both series of co-polymers using PEGDA as the cross-linker, and due to the differing reactivity of the methacrylate co-monomers and the PEGDA acrylate groups compared to the situation for the acrylate co-monomers, co-polymers may not be statistically random. Thermal analysis, however, does suggest a high degree of molecular mixing because a single  $T_g$  is observed for all of the co-polymers, and this result contrasts other co-polymer compositions that were closer to 50:50 and exhibited two distinct glass transitions (data not reported here). Furthermore, we compared  $T_g$  values calculated from the Fox equation (based on  $T_g$ s of the co-polymer components) to the measured  $T_g$  values (Table 4.2).<sup>9, 22, 23</sup> We report details of this calculation elsewhere,<sup>9</sup> where we observed relatively good agreement between measured and calculated  $T_g$  values. These results suggest absence of significant phase separation and good incorporation of the cross-linker, but differences in reactivity and the hydrophilicity of the co-monomers may still lead to heterogeneity over sufficiently small length scales.

**Table 4.2.** Glass transition temperatures calculated using the Fox equation<sup>9</sup> and the measured glass transition temperatures (Figure 4.2) for the co-polymers.

Co-polymer	Composition	Fox Equation $T_g$ [°C]	Measured $T_g$ [°C]
HEA-co-EA	30:70	-22	-20
	35:65	-21	-19
	40:60	-22	-22
HEMA-co-MMA	30:70	100	90
	35:65	97	88
	40:60	105	80

The DSC thermograms (Figure 4.2) do not show strong evidence of free or bulk water (i.e., melting transitions at 0 °C). This point on the HEA-co-EA thermograms is obscured by the glass transition, but the absence of a strong melting transition at 0 °C for the HEMA-co-MMA co-polymers suggests that these materials do not contain appreciable amounts of free or bulk water. This observation is also consistent with the calculations discussed above, indicating that these polymers sorb 2 or less equivalents of water per total equivalents of -OH and -O-.

We further used NMR diffusometry to investigate water molecule dynamics in the co-polymers. In general, a one-dimensional (1D) <sup>1</sup>H NMR spectrum shows narrow spectral lines for species that experience fast molecular tumbling (dynamics), e.g., small molecules in liquid or solution. Broad spectral lines, however, correspond to species that experience slower molecular tumbling, e.g., proteins, polymer chains, solids, or small molecules confined inside another medium. Broad spectral lines correspond to much shorter NMR  $T_2$  relaxation times, which represent the NMR signal decay lifetimes for these slow tumbling species. In NMR diffusometry

experiments, these broad signals are partly or fully “weighted out” of the spectrum, as the signal decay lifetimes approach the length of certain delay times used in the diffusion pulse sequences.

Figure 4.3 shows a set of 1D NMR spectra for 0.5 mol/L NaCl hydrated HEA-co-EA 30:70 and HEMA-co-MMA 30:70. Figures 4.3A and 4.3B show data from pulse-acquire NMR experiments. Each spectrum shows two distinct  $^1\text{H}$  NMR signals arising from polymer chains (broader signal = less mobile) and water molecules (narrow signal = more mobile). The 1D pulse-acquire spectrum of HEMA-co-MMA 30:70 (Figure 4.3B) was broader than that of HEA-co-EA 30:70 (Figure 4.3A) due to the slower segmental dynamics of the glassy HEMA-co-MMA copolymer compared to the rubbery HEA-co-EA copolymer.

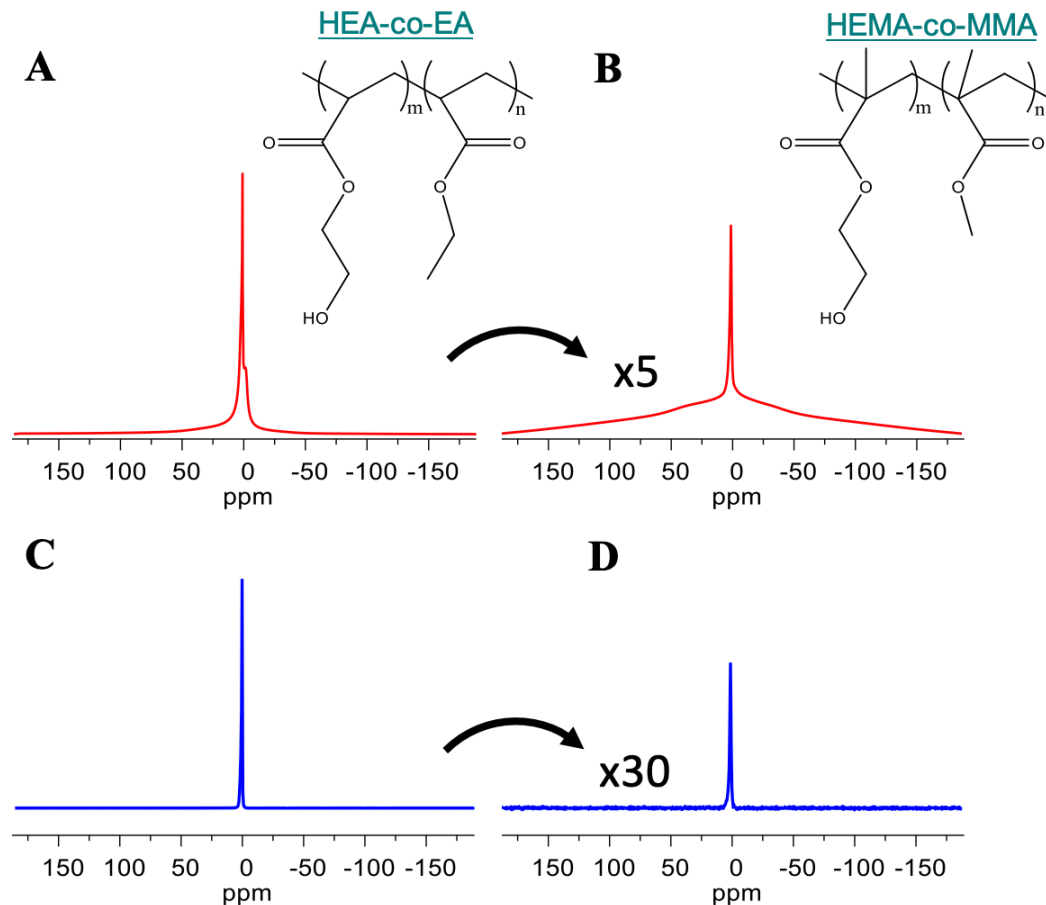


**Figure 4.3.**  $^1\text{H}$  NMR spectra that illustrate water and polymer spectral components in 1D and in diffusometry experiments for HEA-co-EA 30:70 and HEMA-co-MMA 30:70 equilibrated in 0.5 mol/L NaCl solution. Plots A and B are 1D pulse-acquire NMR spectra (32 scans each), and spectra C and D were obtained from the first gradient step (smallest  $g$ ) of the NMR diffusometry experiment (16 scans each). Signal from the HEMA-co-MMA measurements was weak compared to that from HEA-co-EA, so the vertical scales of the B and D spectra have been multiplied by scaling factors to illustrate peak shapes more clearly.

Figures 4.3C and 4.3D are 1D slices from the NMR diffusometry experiment. The broad signals from the polymers are completely attenuated (signal intensity greatly decreased) by the NMR pulse sequence due to their slow molecular motions and correspondingly short NMR relaxation time  $T_2$ . Furthermore, sorbed water motions in HEMA-co-MMA (Figure 4.3D) are substantially restricted (i.e., the  $T_2$  relaxation time is shorter) relative to HEA-co-EA. This restriction of water molecule dynamics causes substantially stronger signal attenuation (and lower signal-to-noise ratio) in the diffusometry experiment compared that for HEA-co-EA.

#### 4.2.5. Restricted Diffusion

We used NMR diffusometry to directly probe the restricted water molecule motions in the co-polymers identified in the previous section. The water diffusion coefficient in the co-polymers is length scale dependent, and NMR measurements of the water diffusion coefficient,  $D_w$ , as a function of diffusion time,  $\Delta$ , show that water diffusivity decreases as the diffusion time increases (Figure 4.4). At longer length scales, the water diffusion coefficient appears to plateau to a value,  $D_\infty$ , that we will consider to be equivalent to the water diffusion coefficient that could be measured via bulk transport property measurements.

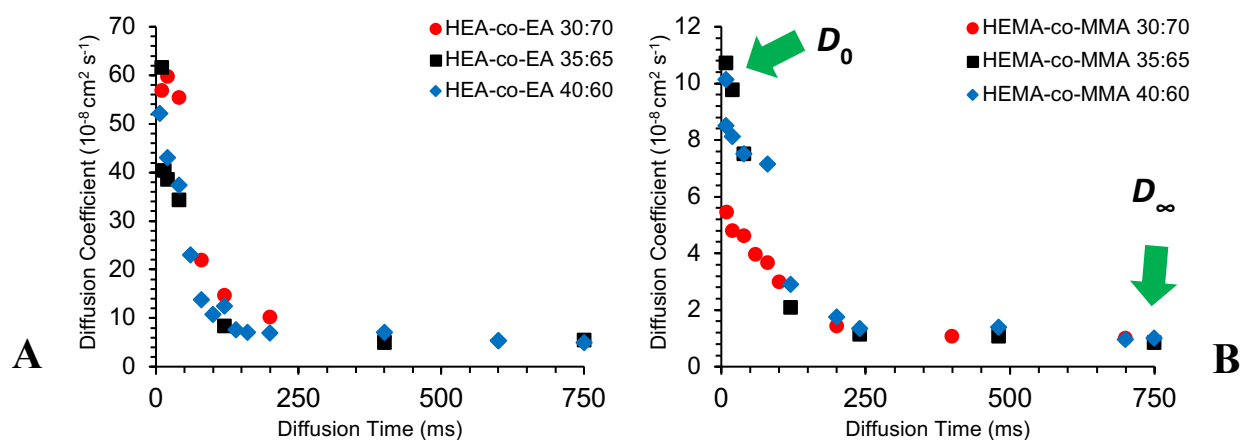


**Figure 4.4.** Water diffusion coefficients,  $D_w$ , decrease as diffusion time,  $\Delta$  (and diffusion length,  $l_d$ ) increase in both the (A) HEA-co-EA and (B) HEMA-co-MMA co-polymers. We define  $D_0$  as the water diffusion coefficient at the shortest diffusion time measured, and  $D_\infty$  as the water diffusion coefficient at the longest diffusion time measured.

The diffusion time,  $\Delta$ , is related to the diffusion length,  $l_d$ , via the diffusion coefficient:

$$l_d = \langle r^2 \rangle^{1/2} = \sqrt{2D_w\Delta} \quad (4.1)$$

where  $\langle r^2 \rangle^{1/2}$  is the root-mean-square distance that molecules travel during the NMR diffusometry experiment.  $D_w$  measurements for HEA-co-EA show that over short length scales ( $l_d$

$\approx 1 \mu\text{m}$ ) diffusion behaviors are essentially equivalent for all of the HEA-co-EA co-polymers ( $5 \times 10^{-8} \text{ cm}^2 \text{ s}^{-1}$ ). As  $l_d$  increases to  $\approx 2.7 \mu\text{m}$ ,  $D_w$  for all of the HEA-co-EA co-polymers decrease by an order of magnitude (to  $5 \times 10^{-9} \text{ cm}^2 \text{ s}^{-1}$ ). A similar order of magnitude decrease in  $D_w$  is observed for HEMA-co-MMA co-polymers when  $l_d$  increases from  $\approx 0.5 \mu\text{m}$  to  $1.2 \mu\text{m}$ .

These results show that the polymer environment imposes increased restrictions on water molecule diffusion as the diffusion length scale increases, and that micrometer scale features within the polymer are at least partially driving this length-scale-dependent diffusion behavior.<sup>16</sup> Given that the water content of these polymers is relatively low, it is reasonable to assume that diffusing water molecules must navigate a local nm-scale path, which is highly tortuous, among the hydrophilic segments of the polymer and other sorbed water molecules. Some of these pathways may lead to dead ends formed by clusters of hydrophobic polymer segments. The relevant length scales are illustrated in [Figure 4.5](#). The subsequent discussion presents an interpretation and simple model of the experimental data framed in the context of molecular tortuosity.

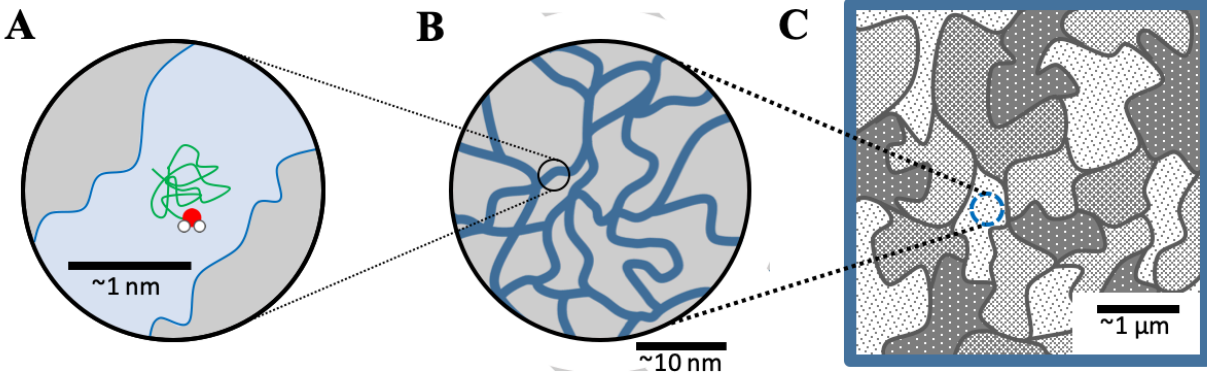


**Figure 4.5.** Diffusion through a heterogeneous polymer matrix over diffusion length scales  $l_d$  ranging from less than 1 nm to greater than 1  $\mu\text{m}$ . Water molecules that diffuse within nm-scale hydrophilic pathways (A) over a mean-square displacement less than the radius  $R$  of the cavity or pathway ( $l_d^2 = D\Delta < R^2$ ) will not show restricted diffusion behavior as the pathways are not tortuous on this length scale. This nm-scale “local” diffusion coefficient we define as  $D_{loc}$ . At larger length scale (B), we expect the pathways to be tortuous (indirect) paths. Average water diffusion on this length scale,  $D_w[l_d]$  will be slower than what is observed in (A). At lengths  $\sim 1 \mu\text{m}$  and above (C), structural heterogeneities may reduce the observed water diffusivity relative to that observed at smaller length scales. As the diffusion length scale increases ( $l_d^2 = D\Delta \gg R^2$ ), water diffusivity measured by NMR will approach the bulk diffusivity.

#### 4.2.6. Tortuosity

Tortuosity,  $\mathfrak{S}$ , can be defined as the ratio of the water diffusion coefficient (at a specific diffusion length scale) to the long diffusion time (effectively bulk) water diffusion coefficient:

$$\mathfrak{S} [l_d] = \frac{D_w[l_d]}{D_\infty} \quad (4.2)$$

where  $D_w[l_d]$  is the water diffusion coefficient at a specific length scale,  $l_d$ , which is based on the experimental diffusion time.  $D_\infty$  is the water diffusion coefficient at infinite diffusion time (or length), and can be considered equivalent to what can be measured by bulk measurements across the membrane. In the context of the co-polymers considered here, a value of  $\mathfrak{S} [l_d] = 1$  corresponds to a physical situation where the diffusivity at the specific length scale is equivalent to free diffusion with no restrictions (e.g., a free liquid). Since the water diffusion coefficient of the materials considered in this study tends to decrease as diffusion length increases (until reaching

the plateau at long diffusion time), values of  $\mathfrak{S} [l_d] > 1$  are expected at relatively short diffusion lengths.

For the purpose of analyzing the diffusivity data for the co-polymers, it is useful to define a “local-to-bulk” tortuosity,  $\mathfrak{S}_{L-B}$ , and a “micron-to-bulk” tortuosity,  $\mathfrak{S}_{\mu-B}$ :

$$\mathfrak{S}_{L-B} = \frac{D_{loc}}{D_{\infty}} \quad (4.3)$$

$$\mathfrak{S}_{\mu-B} = \frac{D_0}{D_{\infty}} \quad (4.4)$$

Both tortuosity values are defined relative to the measured water diffusion coefficient at long diffusion time/length,  $D_{\infty}$  ( $\Delta = 750$  ms or  $l_d = 2.5 - 3.0$   $\mu\text{m}$ ). The measured water diffusion coefficient plateaued at  $l_d \approx 2.7$   $\mu\text{m}$  in HEA-co-EA and  $\approx 1.1$   $\mu\text{m}$  in HEMA-co-MMA (Figure C.1).

Comparing these two definitions of the tortuosity provides insight into the length scale that most influences the differences in diffusion coefficients between the two co-polymers. The local-to-bulk tortuosity  $\mathfrak{S}_{L-B}$  (Equation 4.3) is the ratio of the water self-diffusion coefficient in bulk pure water,  $D_{loc}$ , and the water diffusion coefficient in the membrane at infinite diffusion time (or length),  $D_{\infty}$ . Therefore, this definition of the tortuosity provides information about how polymer structure affects diffusivity over nanoscale to bulk length scales. The above  $\mathfrak{S}_{L-B}$  definition is analogous to the Mackie and Meares model (Equation 3.4) for hindered diffusion where the local to bulk tortuosity can be related to the volume fraction of water in the polymer, i.e.,  $K_w$ , as:<sup>24</sup>

$$\mathfrak{S}_{L-B} = \frac{D_{loc}}{D_{\infty}} = \frac{(2 - K_w)^2}{K_w^2} \quad (4.5)$$

Furthermore, the  $\mathfrak{S}_{\mu-B}$  (Equation 4.4) is defined to describe the influence of micrometer scale features of the polymer up to the bulk length scale. The definition of  $D_0$  is established by a

fixed time (for all samples) near the minimum measurable time ( $\Delta = 20$  ms). The diffusion length scale at this diffusion time is between  $0.5 \mu\text{m}$  and  $1 \mu\text{m}$  for the materials considered in this study. Therefore, the values of the water diffusion coefficient measured by NMR diffusometry and reported in [Figure 4.4](#), represent  $\mu\text{m}$ -scale average water diffusion coefficients that are effectively averaged over a large path length relative to the molecular length scale. Note that the polymer chains will be separated by  $\leq 1$  nm given the ratio of water molecules to hydrophilic oxygen moieties in the material.

The value of  $D_{loc}$ , taken to be the water self-diffusion coefficient in bulk pure water, represents a limiting case of the largest water diffusion coefficient that could be observed in the co-polymers. While the nanophase separation of the co-polymers forms connected pathways for water to travel along, these pathways are also occupied by hydroxyl groups from the polymer chains. Given that the water content of the co-polymers is low ( $\sim 2$  equivalents of water per total equivalents of  $-\text{OH}$  and  $-\text{O}-$ , as discussed previously), the local diffusion behavior may be affected by local molecular and nanoconfinement effects.<sup>25-27</sup> This means that although the pathways are large enough for water to percolate through the entire thickness of the membrane, the local intermolecular interactions with the dipoles of the hydroxyls and esters of the polymer chains will affect the local diffusion behavior of water in these pathways. Future studies will consider more specifically the molecular interactions and nanoconfinement effects on water diffusion by measuring the activation energies of water diffusion in the co-polymers.<sup>25</sup>

#### 4.2.7. Morphology Models Related to Tortuosity Measurements

Comparing the  $\mathfrak{S}_{\mu-B}$  values for the co-polymers shows that the HEA-co-EA and HEMA-co-MMA materials exhibit very similar diffusion coefficient behavior when considering micron-to-bulk scale structural effects (Figure 4.6). Over length scales ranging from the local (or nano) scale to the bulk scale, however, HEMA-co-MMA exhibits a factor of five greater tortuosity. This analysis suggests that transport property differences between the two co-polymers arise due to differences in the materials that are present at sub- $\mu\text{m}$  scale. This result is reasonable given that the chemistry of the two co-polymers is very similar and no substantial evidence of phase separation was observed in the DSC thermograms. The critical sub- $\mu\text{m}$  features that have a strong influence on water diffusivity are likely the result of nanometer scale structures that differ between the two co-polymers as a result of the different segmental dynamics of the backbones.

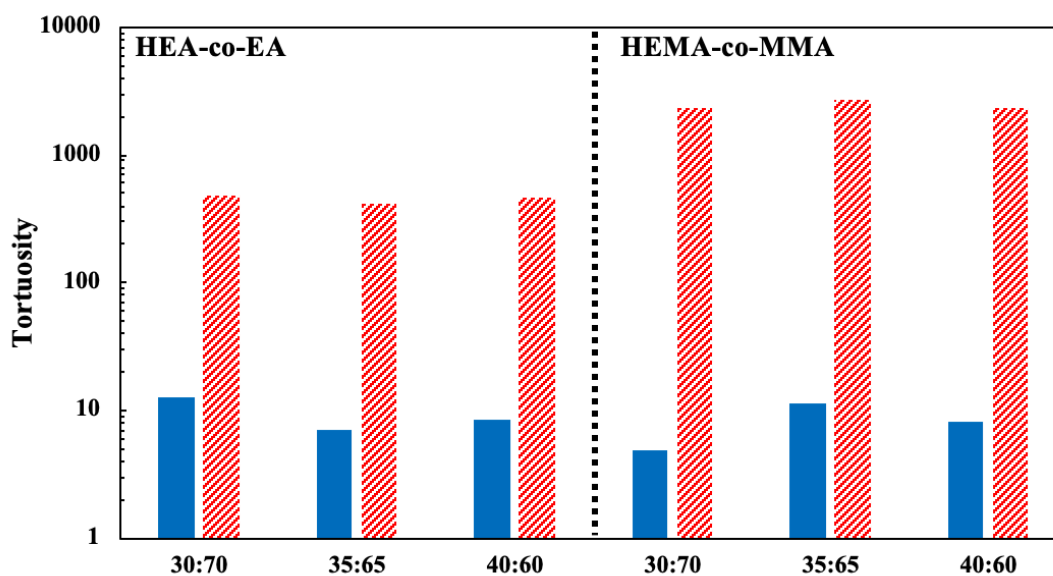


**Figure 4.6.** Local to bulk (Equation 4.3, patterned bars) and micron to bulk (Equation 4.4, solid bars) tortuosity values for HEA-co-EA and HEMA-co-MMA. All of the co-polymers exhibit similar micron to bulk tortuosity, but the local to bulk tortuosity value for HEMA-co-MMA is larger than that for HEA-co-EA likely due to local nanoscale differences between the two co-polymers.

The Mackie and Meares model can be used to calculate the  $\mathfrak{S}_{L-B}$  value based solely on the water content of the polymer (Equation 4.5). The Mackie and Meares model describes diffusion of molecules through obstacles, such as a network of polymer chains. In the context of the co-polymers considered here, decreased water content (increased volume fraction of polymer in the hydrated material) causes a reduction in the diffusion coefficient relative to the value in bulk solution.<sup>24</sup> Equation 4.5 and the 0.5 mol/L  $K_w$  data from Table 4.1 can be used to calculate values for the local to bulk tortuosity. The Mackie and Meares model yields  $\mathfrak{S}_{L-B}$  tortuosity values (reported in Appendix C) ranging from 118 to 292. These values are roughly a factor of 2 or 3 less than the measured local-to-bulk tortuosity for HEA-co-EA, but they are an order of magnitude lower than that for HEMA-co-MMA. The Mackie and Meares model is a lattice-based model that describes how transport is hindered when polymer chains take up space.<sup>24</sup> The observation that the measured local-to-bulk tortuosity is greater than that calculated by the Mackie and Meares model could suggest structural features, more significant in HEMA-co-MMA compared to HEA-co-EA, that preferentially restrict diffusion. For example, water transport in HEMA-co-MMA may be more restricted compared to HEA-co-EA if the structure of the tortuous transport pathways is more heterogeneous in the glassy co-polymer.

Figure 4.7 illustrates a proposed model for the nanometer scale features that drive the water diffusivity differences between HEA-co-EA and HEMA-co-MMA. This model is similar to a model proposed by Kreuer for charged polymer systems used in fuel cell membranes.<sup>6</sup> The length scale between polymer chains may be smaller in the co-polymers considered in the present study compared to the charged polymers considered by Kreuer due to the low water content of the co-polymers and the absence of charged groups.

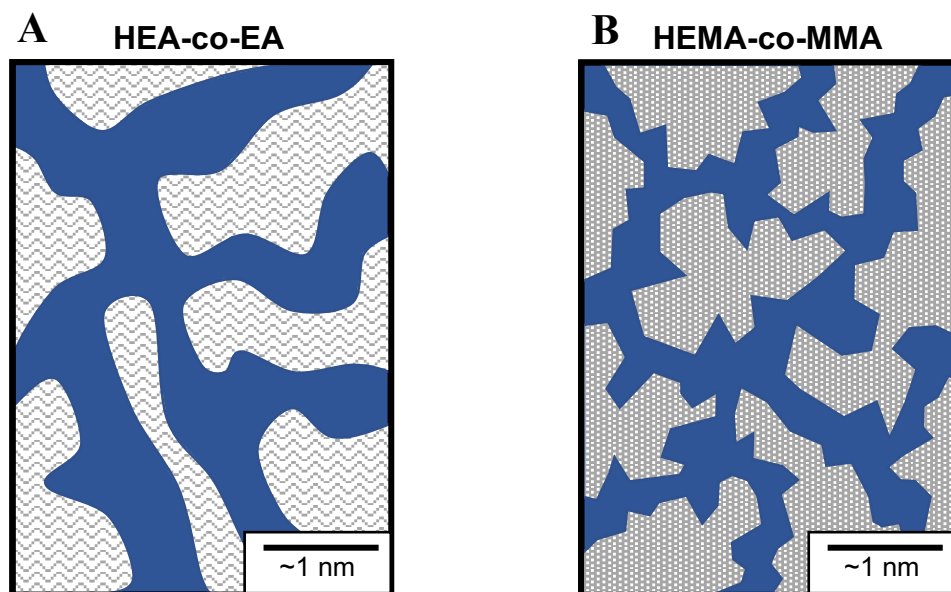


**Figure 4.7.** Illustration of the arrangement of hydrophilic and hydrophobic regions of the HEA-co-EA and HEMA-co-MMA membranes. Self-organization of hydrophilic functional groups present within the co-polymers may create different geometries or dynamics of nm-scale transport pathways for the rubbery and glassy systems, due to the differing arrangements and mobilities of the hydroxyl side chains from the HEA and HEMA moieties. We expect the hydroxyl side chains to extend into the pathways to interact with sorbed water, leading to wider pathways than one might expect for the observed ratio of sorbed water to hydrophilic moieties (roughly 2 equivalents sorbed water per equivalent of  $-OH$  and  $-O-$ ).

In the co-polymers, the hydrophilic side chains and ether groups (of the cross-linker) may self-organize into hydrophilic aggregates that define the critical nanoscale features discussed above. Faster HEA-co-EA backbone dynamics may allow polymer chains (and thus hydrophilic aggregates) to establish smoother and better connected transport pathways compared to the more rigid HEMA-co-MMA material. This physical picture agrees with the local to bulk tortuosity data in [Figure 4.6](#) as more confined (and possibly more disconnected) pathways would be expected to exhibit smaller local diffusion coefficients and larger local to bulk tortuosity.

The hydrophobic polymer chain segments may form aggregates as well. These aggregates, which would tend to exclude water, could form “dead ends” and restrict transport pathways at

larger length scales than the local effects described above. These restrictions would have the net effect of decreasing the average water diffusion coefficient at longer length scales (relative to the micrometer length scales) and explain the micro-to-bulk tortuosity values that are greater than unity. If these “dead ends” cluster together, micron-scale boundaries of limited transport pathway connectivity could form and separate regions of highly interconnected nm-scale hydrophilic pathways. These features are depicted in [Figure 4.8](#). This larger length scale of transport pathway connectivity appears to be similar between the two co-polymers, as the micron to bulk tortuosity is similar across all of the co-polymers. This similarity likely results from the similar chemical structure and polymerization process used to prepare the co-polymers.

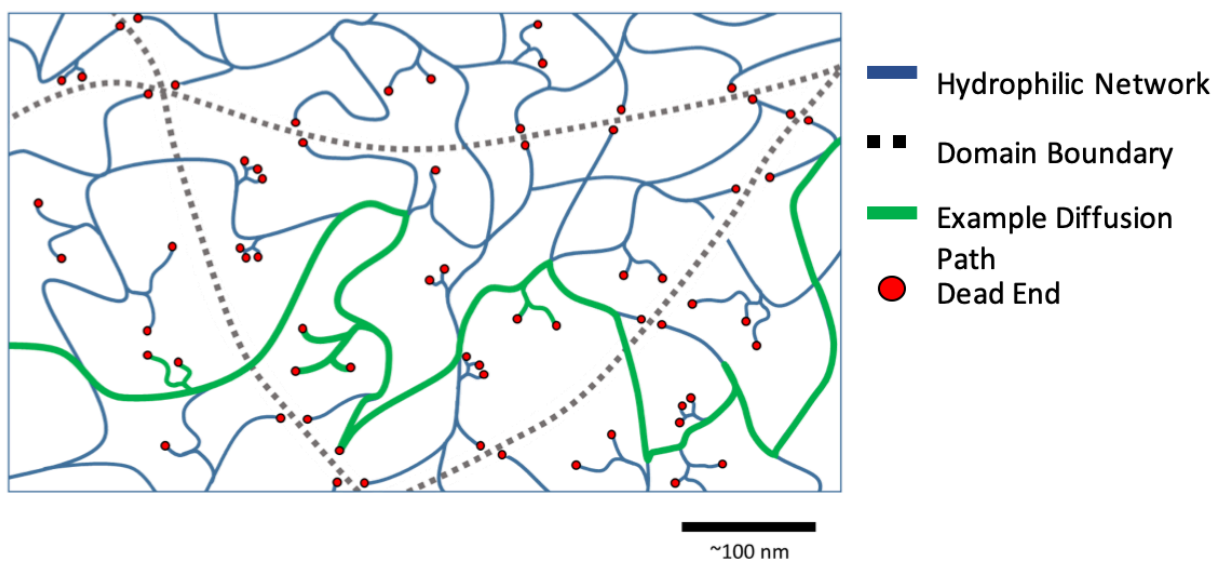


**Figure 4.8.** Proposed model of the heterogeneous hydrophilic network inside the HEA-co-EA and HEMA-co-MMA co-polymers. Polymer domains are separated by clusters of “dead ends” where the hydrophilic network is interrupted by higher concentrations of hydrophobic chain segments. Continuous paths (green) allow water to transport through the membrane, however, dead ends along this path will restrict diffusion.

#### 4.2.8. Water/Salt Diffusion Properties

Salt diffusion is faster in the HEA-co-EA materials compared to the HEMA-co-MMA materials at comparable water content ([Figure 4.9A](#)). Slower diffusion in the more rigid HEMA-

co-MMA material compared to the more flexible HEA-co-EA material is consistent with the idea that more rigid backbone polymers transport small molecules at a slower rate compared to more flexible backbone polymers,<sup>21</sup> as a result of the more tortuous pathways in HEMA-co-MMA (Figure 4.7).

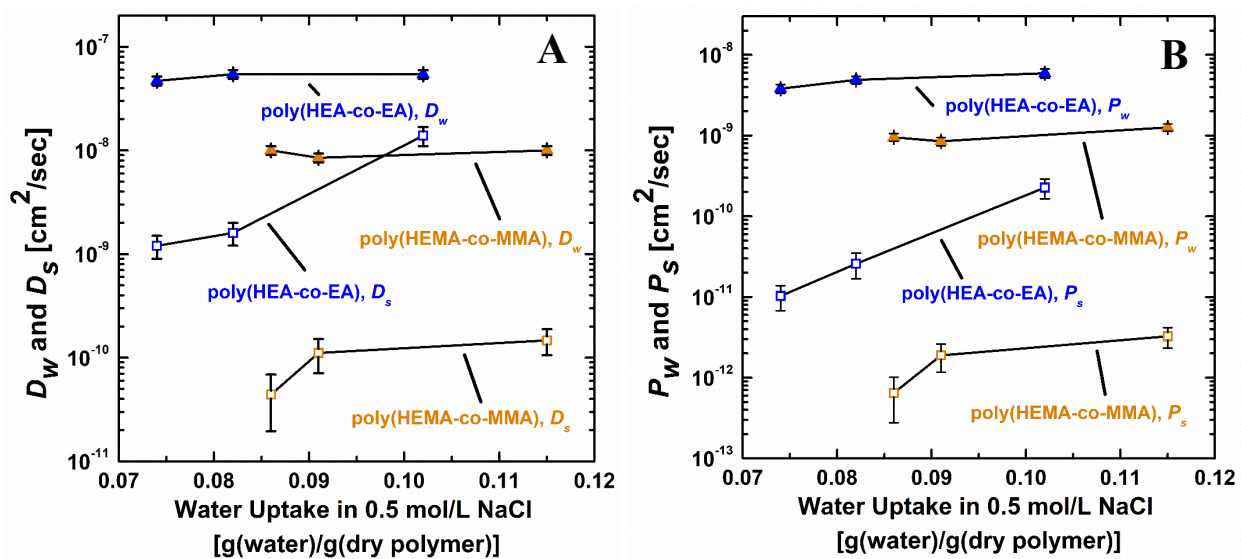


**Figure 4.9.** Water diffusivity,  $D_w$ , (A) and permeability,  $P_w$ , (B) data for poly(HEA-co-EA) ( $\blacktriangle$ ) and poly(HEMA-co-MMA) ( $\blacktriangle$ ) co-polymers and sodium chloride diffusivity,  $D_s$ , (A) and permeability,  $P_s$ , (B) data for poly(HEA-co-EA) ( $\square$ ) and poly(HEMA-co-MMA) ( $\square$ ) co-polymers as a function of water uptake. Water diffusivity data were measured via NMR. Salt diffusivity data were measured via kinetic desorption, where samples were characterized at 25°C following equilibration in 0.5 mol/L aqueous NaCl. Water permeability was calculated as  $P_w = D_w \times K_w$  using the measured diffusion and sorption (Table 4.1) coefficients. Salt permeability was calculated as  $P_s = D_s \times K_s$  using the measured diffusion and sorption (Figure 4.1) coefficients. The uncertainty was taken as the standard deviation from the mean of three measurements.

#### 4.2.9. Water/Salt Permeation Properties

Measured salt diffusivity and sorption coefficients were used to calculate salt permeability using the solution-diffusion model (Equation 3.3).<sup>10, 11, 28, 29</sup> While the salt sorption properties of the two co-polymers were similar as a function of water content, the permeability properties were not similar as a function of water content. The more flexible HEA-co-EA materials have greater water and salt permeability values compared to the more rigid HEMA-co-MMA materials at

equivalent water content (Figure 4.9B), and this observation is likely linked to the increased ability of water and salt to move through hydrophilic transport pathways in flexible, rubbery materials compared to rigid, glassy materials. These results are consistent with the idea that more flexible polymers have higher permeability properties compared to polymers with more rigid backbones,<sup>21</sup> and they are also consistent with the diffusivity data for the co-polymers (Figure 4.9A).

Additionally, the water and salt permeability values, for both sets of co-polymers, increase as co-polymer water content increases. This observation is expected for hydrated polymers and underscores the need, in this study, to compare materials at comparable water content. Theoretical models including the Yasuda free volume model and the Mackie and Meares model predict this general behavior.<sup>13, 30</sup>

#### 4.2.10. Water/Salt Permeation and Diffusion Selectivity

The water permeability values can be divided by the salt permeability values (Figure 4.9) to calculate the ideal water/salt permeability selectivity. This ideal selectivity represents the rate of water permeation relative to salt permeation in situations where the permeability values are measured separately, and high selectivity values are desirable for desalination applications.<sup>31, 32</sup> The more rigid HEMA-co-MMA materials exhibit greater permeability selectivity,  $P_w/P_s$ , compared to the more flexible HEA-co-EA materials at equivalent water content (Figure 4.10), so the water/salt diffusion selectivity ( $D_w/D_s$ ) of the rigid HEMA-co-MMA is greater than that of the flexible HEA-co-EA (Figure 4.10) in a manner similar to the permeability selectivity properties. Consistent with a free volume description of the transport process, the water/salt diffusion and permeability selectivity values decrease as polymer water content increases.<sup>18, 33</sup> The results are consistent with established gas separation membrane structure-property relationships where rigid

backbone polymers are generally more diffusion (or size) selective than flexible backbone polymers.<sup>21, 34</sup>

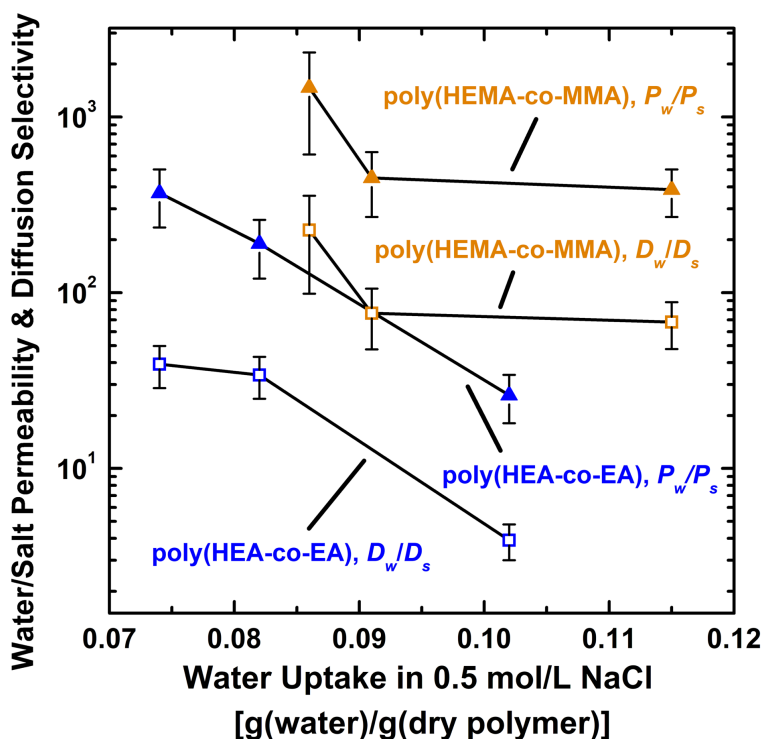


**Figure 4.10.** Water/salt permeability selectivity ( $P_w/P_s$ ) for poly(HEA-co-EA) ( $\blacktriangle$ ) and poly(HEMA-co-MMA) ( $\blacktriangle$ ) co-polymers and water/salt diffusion selectivity ( $D_w/D_s$ ) for poly(HEA-co-EA) ( $\square$ ) and poly(HEMA-co-MMA) ( $\square$ ) co-polymers as a function of water uptake.

Increased water/salt diffusivity and permeability selectivity in the glassy compared to rubbery co-polymers may be due to greater tortuosity in HEMA-co-MMA compared to HEA-co-EA. Additionally, similar results (i.e., glassy polymers having greater selectivity and lower diffusivity compared to rubbery polymers) in gas separation membranes have been ascribed to the kinetics of the opening and closing of transient free volume elements, which facilitate transport, within the polymer.<sup>21, 35</sup> While the relative contributions of these two factors are currently unknown for these materials, the data in [Figure 4.10](#) suggest that glassy materials can offer greater water/salt diffusion selectivity (and, thus, water/salt permeability selectivity) compared to chemically similar rubbery materials.

### 4.3. Conclusions

We have investigated the influence of polymer backbone structure and dynamics on water and salt transport properties in two series of chemically similar, low water content, acrylate and methacrylate random co-polymers. Micron-scale heterogeneities in both series of materials leads to water diffusivity, measured by NMR diffusometry, which decreases as the average diffusion length increases. We propose a model wherein nanometer-scale “dead ends” form micron-scale arrangements leading to this length-scale-dependent diffusion behavior in these materials. Additional morphological differences between the two co-polymers on sub-micron length scales lead to increased water/salt selectivity properties, important for desalination applications, in the glassy versus rubbery materials (at equivalent water content). The results suggest that segmental dynamics influence water and salt transport properties at the nanoscale in low water content polymers where the majority of the water molecules are likely interacting with the polymer backbone. As such, glassy low water content polymers are expected to be more water/salt selective compared to rubbery materials at equivalent water content.

### 4.4. References

1. Freger, V., Swelling and morphology of the skin layer of polyamide composite membranes: An atomic force microscopy study. *Environmental Science & Technology* **2004**, *38*, 3168-3175.
2. Zhang, X.; Cahill, D. G.; Coronell, O.; Mariñas, B. J., Absorption of water in the active layer of reverse osmosis membranes. *Journal of Membrane Science* **2009**, *331* (1), 143-151.
3. Paddison, S. J.; Reagor, D. W.; Zawodzinski Jr, T. A., High frequency dielectric studies of hydrated Nafion®. *Journal of Electroanalytical Chemistry* **1998**, *459* (1), 91-97.
4. Hickner, M. A., Ion-containing polymers: New energy & clean water. *Materials Today* **2010**, *13* (5), 34-41.

5. Hickner, M. A., Water-mediated transport in ion-containing polymers. *Journal of Polymer Science Part B: Polymer Physics* **2012**, *50* (1), 9-20.
6. Kreuer, K. D., On the development of proton conducting polymer membranes for hydrogen and methanol fuel cells. *Journal of Membrane Science* **2001**, *185* (1), 29-39.
7. Hickner, M. A.; Herring, A. M.; Coughlin, E. B., Anion exchange membranes: Current status and moving forward. *Journal of Polymer Science Part B: Polymer Physics* **2013**, *51* (24), 1727-1735.
8. Strathmann, H.; Grabowski, A.; Eigenberger, G., Ion-exchange membranes in the chemical process industry. *Industrial & Engineering Chemistry Research* **2013**, *52* (31), 10364-10379.
9. Chang, K.; Xue, T.; Geise, G. M., Increasing salt size selectivity in low water content polymers via polymer backbone dynamics. *Journal of Membrane Science* **2018**, *552*, 43-50.
10. Geise, G. M.; Paul, D. R.; Freeman, B. D., Fundamental water and salt transport properties of polymeric materials. *Progress in Polymer Science* **2014**, *39* (1), 1-42.
11. Geise, G. M.; Lee, H.-S.; Miller, D. J.; Freeman, B. D.; McGrath, J. E.; Paul, D. R., Water purification by membranes: The role of polymer science. *Journal of Polymer Science Part B: Polymer Physics* **2010**, *48* (15), 1685-1718.
12. Kamcev, J.; Freeman, B. D., Charged polymer membranes for environmental/energy applications. *Annual Review of Chemical and Biomolecular Engineering* **2016**, *7* (1), 111-133.
13. Yasuda, H.; Lamaze, C. E.; Ikenberry, L. D., Permeability of solutes through hydrated polymer membranes Part I. Diffusion of sodium chloride. *Die Makromolekulare Chemie* **1968**, *118*, 19-35.
14. Callaghan, P. T., *Translational Dynamics and Magnetic Resonance: Principles of Pulsed Gradient Spin Echo NMR*. Oxford University Press: Oxford, New York, 2011.

15. Mitra, P. P.; Sen, P. N.; Schwartz, L. M., Short-time behavior of the diffusion coefficient as a geometrical probe of porous media. *Physical Review B* **1993**, *47* (14), 8565-8574.
16. Hou, J.; Li, J.; Mountz, D.; Hull, M.; Madsen, L. A., Correlating morphology, proton conductivity, and water transport in polyelectrolyte-fluoropolymer blend membranes. *Journal Membrane Science* **2013**, *448*, 292-299.
17. Khare, A. R.; Peppas, N., Swelling/deswelling of anionic copolymer gels. *Biomaterials* **1995**, *16*, 559-567.
18. Yasuda, H.; Ikenberry, L.; Lamaze, C., Permeability of solutes through hydrated polymer membranes. Part II. Permeability of water soluble organic solutes. *Die Makromolekulare Chemie* **1969**, *125* (1), 108-118.
19. Hodge, I. M., Physical aging in polymer glasses. *Science* **1995**, *267* (5206), 1945-1947.
20. Lutz, T. R.; He, Y.; Ediger, M. D.; Cao, H.; Lin, G.; Jones, A. A., Rapid poly(ethylene oxide) segmental dynamics in blends with poly(methyl methacrylate). *Macromolecules* **2003**, *36* (5), 1724-1730.
21. Baker, R. W., *Membrane Technology and Applications*. 3rd ed.; Wiley: New York, 2012.
22. Fox, T. G. J.; Flory, P. J., Second-order transition temperatures and related properties of polystyrene. I. Influence of molecular weight. *Journal of Applied Physics* **1950**, *21* (6), 581-591.
23. Hiemenz, P. C.; Lodge, T. P., *Polymer Chemistry*. 2nd ed.; CRC Press LLC: Boca Raton, Florida, 2007.
24. Mackie, J. S.; Meares, P., The diffusion of electrolytes in a cation-exchange resin membrane I. Theoretical. *Proceedings of the Royal Society of London. Series A. Mathematical and Physical Sciences* **1955**, *232* (1191), 498-509.
25. Lingwood, M. D.; Zhang, Z. Y.; Kidd, B. E.; McCreary, K. B.; Hou, J. B.; Madsen, L. A., Unraveling the local energetics of transport in a polymer ion conductor. *Chemical Communications* **2013**, *49* (39), 4283-4285.

26. Kidd, B. E.; Forbey, S. J.; Steuber, F. W.; Moore, R. B.; Madsen, L. A., Multiscale lithium and counterion transport in an electrospun polymer-gel electrolyte. *Macromolecules* **2015**, *48* (13), 4481-4490.
27. Kidd, B. E.; Lingwood, M. D.; Lee, M.; Gibson, H. W.; Madsen, L. A., Cation and anion transport in a dicationic imidazolium-based plastic crystal ion conductor. *The Journal of Physical Chemistry B* **2014**, *118* (8), 2176-2185.
28. Paul, D. R., Reformulation of the solution-diffusion theory of reverse osmosis. *Journal of Membrane Science* **2004**, *241* (2), 371-386.
29. Wijmans, J. G.; Baker, R. W., The solution-diffusion model: A review. *Journal of Membrane Science* **1995**, *107* (1), 1-21.
30. Paul, D. R., Relation between hydraulic permeability and diffusion in homogeneous swollen membranes. *Journal of Polymer Science: Polymer Physics Edition* **1973**, *11* (2), 289-296.
31. Park, H. B.; Kamcev, J.; Robeson, L. M.; Elimelech, M.; Freeman, B. D., Maximizing the right stuff: The trade-off between membrane permeability and selectivity. *Science* **2017**, *356* (6343).
32. Werber, J. R.; Deshmukh, A.; Elimelech, M., The critical need for increased selectivity, not increased water permeability, for desalination membranes. *Environmental Science & Technology Letters* **2016**, *3* (4), 112-120.
33. Geise, G. M.; Park, H. B.; Sagle, A. C.; Freeman, B. D.; McGrath, J. E., Water permeability and water/salt selectivity tradeoff in polymers for desalination. *Journal of Membrane Science* **2011**, *369* (1), 130-138.
34. Yampol'skii, Y. P.; Pinnau, I.; Freeman, B. D., *Materials Science of Membranes for Gas and Vapor Separation*. John Wiley: Hoboken, NJ, 2006.

35. Hofmann, D.; Fritz, L.; Ulbrich, J.; Schepers, C.; Böhning, M., Detailed-atomistic molecular modeling of small molecule diffusion and solution processes in polymeric membrane materials. *Macromolecular Theory and Simulations* **2000**, 9 (6), 293-327.

## Chapter 5: Water Content, Relative Permittivity, and Ion Sorption Properties of Polymers for Membrane Desalination<sup>\*\*\*\*</sup>

### 5.1. Introduction

Many theories that relate ion sorption properties to polymer properties seek to describe the free energy change associated with moving an ion from solution into the membrane phase and require knowledge of the relative permittivity (or static dielectric constant)<sup>1</sup> of the hydrated polymer.<sup>2-9</sup> One challenge facing the use of these theories is that few investigators have reported relative permittivity data for hydrated polymers of interest for desalination membrane applications. Relative permittivity data have been reported for Nafion<sup>®</sup> 117,<sup>10-13</sup> sulfonated polysulfone,<sup>13</sup> uncharged hydrogels,<sup>14, 15</sup> cellulose acetate,<sup>16</sup> polyamide,<sup>17</sup> and other polymers.<sup>18, 19</sup> Only a few studies, however, investigated polymers over a range of water content and/or in the microwave frequency range, which is particularly relevant for hydrated polymers.

While the relative permittivity of a hydrated polymer is expected to increase with increasing polymer water content,<sup>10, 11, 20, 21</sup> the functional nature of this increase and its dependence on polymer chemistry is not well understood. Recent studies have estimated the relative permittivity (i.e., static dielectric constant) of hydrated polymers using Nafion<sup>®</sup> 117 data.<sup>2, 8, 9, 22</sup> This estimation assumes that the relative permittivity varies linearly between the relative permittivity values for poly(tetrafluoroethane) (PTFE) and bulk water.<sup>2, 23</sup> This approximation is supported by data for Nafion<sup>®</sup><sup>2</sup> and liquid mixtures of water and dimethyl sulfoxide,<sup>24</sup> but data for

---

<sup>\*\*\*\*</sup> This section has been adapted with permission from: Chang, K.; Luo, H.; Geise, G. M., Water content, relative permittivity, and ion sorption properties of polymers for membrane desalination. *Journal of Membrane Science* **2019**, 574, 24-32.

other liquid mixtures<sup>25-27</sup> suggest that a linear relationship between relative permittivity and water content may not be universally applicable to hydrated polymers.

Here we report an investigation of the relationship between hydrated polymer relative permittivity properties and water content in a series of polymers based on poly(glycidyl methacrylate) (pGMA) that was cross-linked using poly(propylene glycol) bis(2-aminopropyl ether). We increased the water content of these polymers by hydrolyzing the epoxide ring on the pGMA side chain to increasing extents. Results were compared to Nafion<sup>®</sup> 117, which is a perfluorosulfonic acid polymer widely considered for fuel cell applications<sup>28</sup> to investigate the influence of polymer chemistry on relative permittivity properties. While Nafion<sup>®</sup> 117 and the materials considered in this study are chemically different (Nafion<sup>®</sup> contains highly charged sulfonic acid groups and is not cross-linked), the comparison made in this study is important as very little microwave frequency dielectric permittivity data have been reported for hydrated polymers. Furthermore, the Nafion<sup>®</sup> data used for comparison in this study has been used to describe the dielectric permittivity properties of other hydrated polymers, so it is important to understand how chemical differences between polymers influence hydrated polymer dielectric permittivity properties.

Relative permittivity increased as the pGMA side chains were increasingly hydrolyzed and polymer water content increased. The functional form of the increase in the relative permittivity of the cross-linked hydrolyzed pGMA-based polymers considered in this study with increasing water content was different from that reported for Nafion<sup>®</sup> 117. These results suggest that polymer chemistry and/or structure, not water content alone, may play a significant role in determining the relative permittivity properties of hydrated polymers.

Furthermore, we measured and analyzed the ion sorption properties of the materials to evaluate the effectiveness of using relative permittivity measurements to understand the ion sorption properties of hydrated polymers. The free energy barrier for ion sorption in the hydrated polymer was calculated using measured relative permittivity values and electrostatic theory. These calculated values were qualitatively consistent with the measured data and suggest that measured relative permittivity data for hydrated polymers may provide qualitative insight into ion sorption properties. Therefore, controlling polymer relative permittivity via the chemical functionality of the polymer could be a viable strategy to prepare polymer membrane materials that effectively suppress ion sorption, and relative permittivity measurements made on hydrated polymers may provide insight into the design of future desalination membranes.

## **5.2. Results and Discussion**

### **5.2.1. Water Uptake**

We controlled the water content of XL-pGMA by partially hydrolyzing the epoxide ring to determine the influence of polymer water content on the relative permittivity of the hydrated polymer. The water content of XL-pGMA- $z$  increased as the hydrolysis time ( $z$  in units of hours) increased (i.e., as the hydroxyl group content of the polymer, or value of  $y$  in [Figure 2.2](#), increased) ([Table 5.1](#)). The hydrolysis process did not affect significantly the dry density of the polymer. The water sorption coefficient for Nafion<sup>®</sup> 117 was calculated using reported water uptake and dry density data.<sup>29, 30</sup>

**Table 5.1.** Water content and dry polymer density data measured at  $22 \pm 1$  °C. Water content measurements were made on samples initially equilibrated with DI water. The volume fraction of water in the polymer,  $\phi_w$ , (equivalent to the water sorption coefficient,  $K_w$ ) was calculated from water uptake and dry density data using Equation 2.2.<sup>31</sup> The uncertainty was taken as the standard deviation from the mean of three measurements. Hydrolysis time,  $z$ , refers to the length of time (in hours) that the XL-pGMA- $z$  samples were immersed in 0.5 mol/L H<sub>2</sub>SO<sub>4</sub> at 45 °C.

Polymer	Hydrolysis Time, $z$ (hr)	Water Uptake [g(water)/g(dry polymer)]	Dry Density (g/cm <sup>3</sup> )	$\phi_w$
XL-pGMA- $z$	0	$0.036 \pm 0.002$	$1.22 \pm 0.02$	$0.042 \pm 0.003$
	8	$0.163 \pm 0.008$	$1.23 \pm 0.01$	$0.167 \pm 0.008$
	10	$0.238 \pm 0.011$	$1.25 \pm 0.01$	$0.229 \pm 0.016$
	12	$0.308 \pm 0.007$	$1.25 \pm 0.01$	$0.278 \pm 0.012$
Nafion® 117	-	$0.197$ <sup>29</sup>	$1.98$ <sup>30</sup>	0.280

### 5.2.2. Microwave Dielectric Spectroscopy

Following each calibration, we measured the dielectric properties of air in the empty transmission line to verify the calibration. The measured relative permittivity (i.e., static dielectric constant) of air was essentially constant, over the frequency range considered, at a value of 1.0014 (Figure D.3). This value is consistent with the reported value of 1.0006.<sup>32</sup>

The relative permittivity of PTFE was also measured to be essentially constant over the range of frequencies considered. The measured relative permittivity of 1.898 and dielectric loss of 0.008 at 9.95 GHz, are very similar to reported values (2.048 and 0.001, respectively, at 9.95 GHz).<sup>11,33</sup> The lower experimental value compared to the reported value may result from small air gaps between the sample and the wall of the transmission line (perhaps due to imperfections in the machined PTFE sample).<sup>29,32</sup> Such small air gaps would tend to reduce the relative permittivity.

The observation that the dielectric permittivity values for air and PTFE do not change significantly as a function of frequency (Figure D.3) is due to the absence of significant dipole relaxation mechanisms in air and PTFE.<sup>34</sup> Alternatively, dipole relaxations do occur in water. We

measured the dielectric permittivity properties of DI water using different sample lengths (i.e., different values of  $d$  achieved by loading different volumes of water into the transmission line) to optimize the measurement (Figure D.2).<sup>35</sup> DI water relative permittivity and dielectric loss data were well represented by a single Debye relaxation process (Figure D.4) in agreement with the literature.<sup>21, 36, 37</sup>

Using the single Debye relaxation process model, the static permittivity,  $\epsilon_s$ , and the relaxation peak position in the dielectric loss data for DI water were regressed to be  $77.98 \pm 0.09$  and  $20.6 \pm 0.1$  GHz, respectively.<sup>10, 38</sup> These values are similar to reported values (80.18 and 18 GHz, respectively).<sup>38</sup> The measured static permittivity (i.e., the relative permittivity value measured at the lowest frequency) was 79.15 at 45 MHz, which agrees better with the reported value compared to that determined using the single Debye relaxation model. The lower values obtained in our measurement/regression could result from the presence of small air bubbles in the DI water in the transmission line. Due to the metallic nature of the transmission line, it was difficult to determine whether bubbles were present.

The Debye relaxation process observed for water is different from the dielectric permittivity versus frequency behavior observed for air and PTFE. At sufficiently low frequencies, the alternating electric field is slow enough that the water dipoles are able to remain in phase with the field, and energy can be stored in the aligned dipoles.<sup>34</sup> As the frequency increases, energy begins to dissipate as the electric field oscillations become faster and exceed the rate at which water dipoles can align.<sup>34</sup> In this situation orientation polarization disappears, and water dipoles are no longer able to remain in phase with the external electric field.<sup>34</sup> Therefore, we observe a drop in relative permittivity and a relaxation peak in the dielectric loss data (Figure D.4).<sup>34</sup>

We expect the dielectric permittivity data for hydrated XL-pGMA-z to have features similar to that of both PTFE and water because the water content of XL-pGMA-z is between that of PTFE and water. The relative permittivity data for XL-pGMA-0 is similar to that of PTFE but higher in absolute value (Figure 5.1A). This result is consistent with the low water content of XL-pGMA-0. As the water content of XL-pGMA-z increased (i.e., as z increases), we observed an increase in the magnitude of the relative permittivity, and the shape of the relative permittivity versus frequency data began to assume a shape more characteristic of water compared to PTFE. This result is reasonable given that increased water content means that more dipolar relaxations are possible in the polymer.

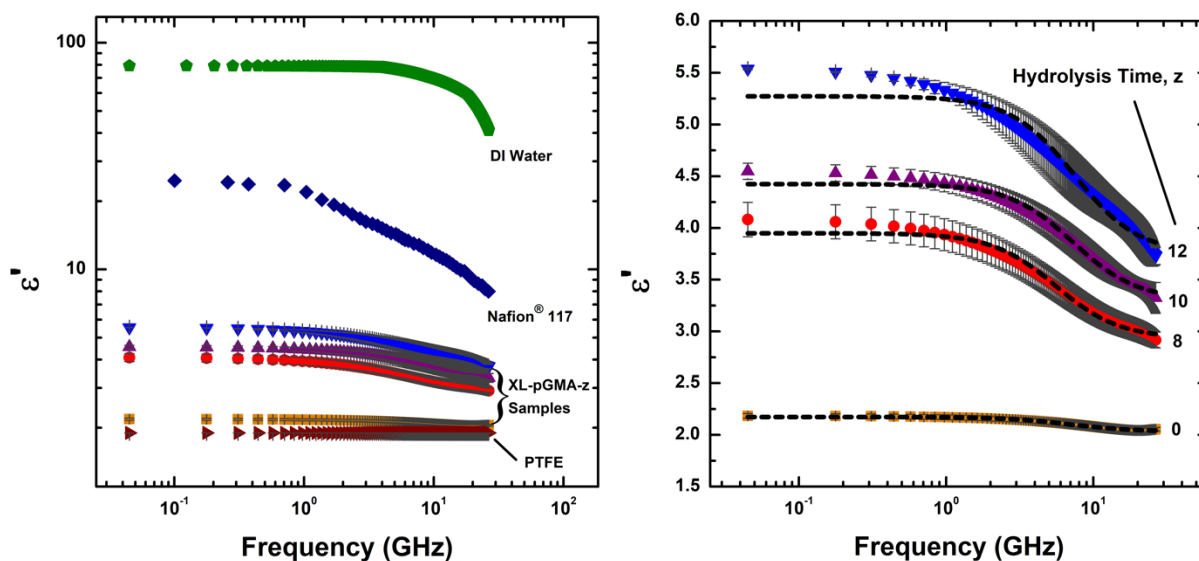


**Figure 5.1.** (A, left) Relative permittivity,  $\epsilon'$ , as a function of frequency for DI water, Nafion® 117<sup>29</sup>, XL-pGMA-z, and PTFE. (B, right) Data for XL-pGMA-z are shown with the single Debye relaxation fit (dashed curves). The hydrolysis time, z, is labeled for each XL-pGMA-z sample. All measurements were made at  $295 \pm 1$  K, and the uncertainty was taken as the standard deviation from the mean of three measurements.

We compared the dielectric relative permittivity properties of XL-pGMA-z to that of Nafion® 117. The XL-pGMA-12 material has similar water content to Nafion® 117. The relative

permittivity of XL-pGMA-12, however, is considerably lower (by approximately a factor of 5) compared to that for Nafion<sup>®</sup> 117 (Figure 5.1A).

Similar to the DI water data, XL-pGMA-z data were fit to a single Debye relaxation process model to determine the static permittivity (i.e., static dielectric constant) of the hydrated polymer (Figure 5.1B). The XL-pGMA-z static permittivity values increased as polymer water content increased, with values of 2.2, 3.9, 4.4, and 5.3 for XL-pGMA-0, -8, -10, and -12 samples, respectively. The data for XL-pGMA-0, -8, and -10 were described reasonably well by a single Debye relaxation. However, the XL-pGMA-12 data deviated more from the single Debye relaxation description compared to the other materials. This observation may indicate the existence of more than one relaxation mechanism in this material.

### 5.2.3. State of Water Analysis

We observed differences between the XL-pGMA-12 relative permittivity data and that for Nafion<sup>®</sup> 117. These materials have similar volume fractions of water, so chemical differences between the two materials appear to influence the relative permittivity properties. This difference may be linked to water dynamics, so we performed DSC measurements on hydrated XL-pGMA-z and Nafion<sup>®</sup> 117 to quantify the relative amounts of freezable (i.e., bulk, or weakly bound water) and non-freezable water (i.e., strongly bound water) in the polymers.<sup>20, 28, 39-45</sup> Both freezable,  $w_f$ , and non-freezable,  $w_{nf}$ , water content were calculated for XL-pGMA-z and Nafion<sup>®</sup> 117 as:<sup>41</sup>

$$w_f(\%) = \frac{m_f}{m_{dry}} \times 100\% = \left[ \frac{\Delta H_{polymer}}{\Delta H_{m,H_2O}^\circ} \times (w_u + 1) \right] \times 100\% \quad (5.1)$$

$$w_{nf}(\%) = (w_u \times 100\%) - w_f(\%) \quad (5.2)$$

where  $m_f$  is the mass of freezable water in the polymer,  $\Delta H_{polymer}$  is the enthalpy of melting (determined from the DSC thermogram) in the polymer, and  $\Delta H_{m,H_2O}^\circ$  is the enthalpy of melting for water (333.5 J/g).<sup>41</sup>

We did not observe evidence of a melting transition at 0 °C for the XL-pGMA-0 material (Figure 5.2). This result is reasonable given that very little water is absorbed by that polymer. As water content increased, we observed an increase in the intensity and breadth of the melting transitions observed at 0 °C, suggesting the presence of more freezable water in the partially hydrolyzed materials. The amounts of both freezable and non-freezable water increased as XL-pGMA-z hydrolysis time, z, increased (Table 5.2).

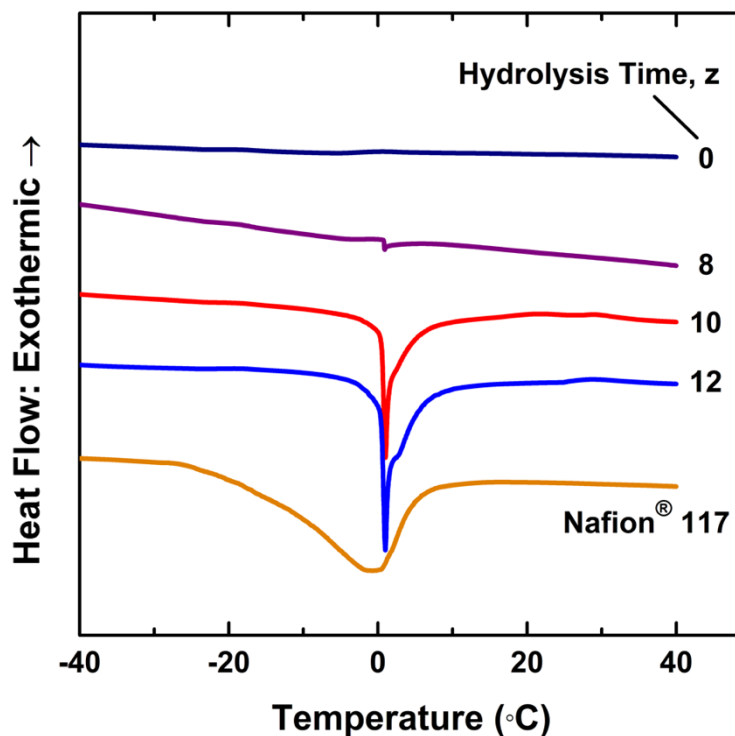


**Figure 5.2.** Differential scanning calorimetry (DSC) thermograms for XL-pGMA-z and Nafion® 117. The hydrolysis time, z, refers to the length of time (in hours) that the XL-pGMA-z samples were immersed in 0.5 mol/L H<sub>2</sub>SO<sub>4</sub> at 45 °C.

**Table 5.2.** The distribution of freezable and non-freezable water in XL-pGMA-z samples and Nafion<sup>®</sup> 117. The values for XL-pGMA-z were calculated using water uptake data reported in Table 5.1. The values for Nafion<sup>®</sup> 117 were calculated using a measured water uptake of  $0.320 \pm 0.005$  g(water)/g(dry polymer). This value was measured using Nafion<sup>®</sup> 117 films treated in the same manner as those films analyzed via DSC. The effect of residual water in Nafion<sup>®</sup> 117 after vacuum drying (as discussed in the literature)<sup>46, 47</sup> was estimated to potentially affect the results by approximately 2%. The sum of the values of  $w_f$  and  $w_{nf}$  is equivalent to the total water uptake of the material (Equation 5.2). The hydrolysis time,  $z$ , refers to the length of time (in hours) that the XL-pGMA-z samples were immersed in 0.5 mol/L H<sub>2</sub>SO<sub>4</sub> at 45 °C.

Polymer	Hydrolysis Time, $z$ (hr)	$w_f$ (%)	$w_{nf}$ (%)
XL-pGMA-z	0	0.05	3.5
	8	0.3	16.1
	10	2.6	21.2
	12	4.1	26.8
Nafion <sup>®</sup> 117	-	9.7	22.4

We observed a much broader melting transition for Nafion<sup>®</sup> 117 compared to XL-pGMA-12 (Figure 5.2, both materials have comparable water content). The melting peak for Nafion<sup>®</sup> 117 suggests the presence of more freezable (i.e., bulk or weakly bound) water<sup>21, 48-51</sup> compared to XL-pGMA-12. The XL-pGMA-12 material contained less freezable water than Nafion<sup>®</sup> 117 (4.1% compared to 9.7%) and more non-freezable water (26.8 % compared to 22.4 %) compared to Nafion<sup>®</sup> 117 (Table 5.2). Since the total water content of the two materials is similar, this result suggests that sorbed water in XL-pGMA-12 interacts with the polymer backbone (via hydrogen bonding interactions) to a greater extent compared to Nafion<sup>®</sup> 117. The higher relative permittivity of Nafion<sup>®</sup> 117 compared to XL-pGMA-12 (Figure 5.1) likely results from the presence of more freezable water in Nafion<sup>®</sup> 117 compared to XL-pGMA-12.

#### 5.2.4. Static Permittivity

The static permittivity values for XL-pGMA-z are compared to results for Nafion<sup>®</sup> 117 in Figure 5.3. We chose to use the static permittivity values obtained via regression using the single Debye relaxation model (see the Appendix D for more details) for consistency. Comparing Figures 5.1B and 5.3, however, reveals that the differences between the static permittivity values regressed using the model and the experimental data at the lowest frequency considered are relatively small with regard to the Nafion<sup>®</sup> 117 comparison. At similar water content, the XL-pGMA-z materials have a lower static permittivity compared that of Nafion<sup>®</sup> 117 membranes (where water content was adjusted by equilibrated Nafion<sup>®</sup> samples with different relative humidity environments).<sup>10, 29</sup>

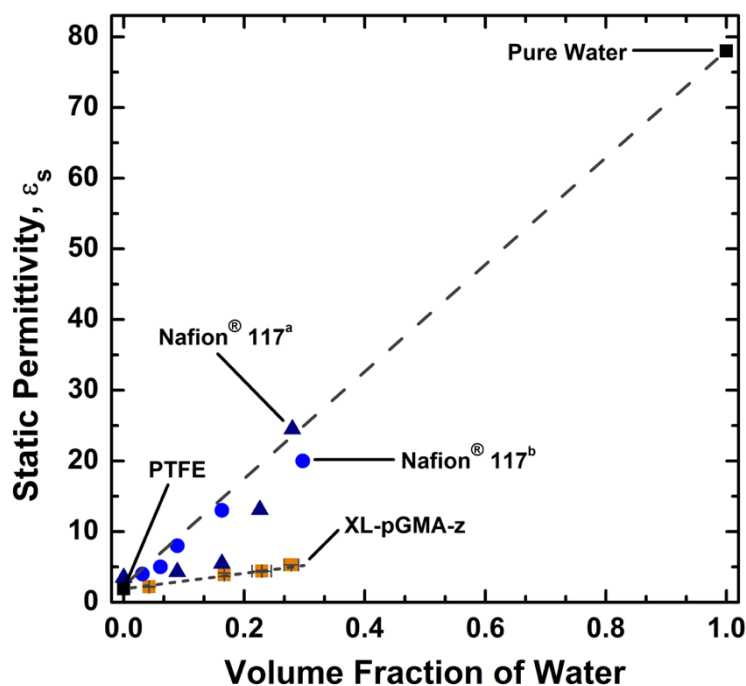


**Figure 5.3.** Static permittivity,  $\epsilon_s$ , of XL-pGMA-z (measured at  $22 \pm 1$  °C), Nafion<sup>®</sup> 117<sup>a</sup> (measured at 25 °C)<sup>29</sup>, and Nafion<sup>®</sup> 117<sup>b</sup> (measured at 30 °C)<sup>10</sup>, plotted as a function of the volume fraction of water sorbed in the polymer. Values for the static permittivity of water and PTFE are also shown. The long dashed line represents a static permittivity (or dielectric constant) linear approximation. The short dashed line illustrates the different functional relationship between static permittivity and volume fraction of water for XL-pGMA-z compared to Nafion<sup>®</sup>. Uncertainty in the XL-pGMA-z data was taken as the standard deviation from the mean of three measurements.

The long dashed line in [Figure 5.3](#) connects the static permittivity of PTFE with that for bulk pure water. The data for Nafion<sup>®</sup> samples are generally consistent with this trend. This observation has been used to approximate the static permittivity of other hydrated polymers based on knowledge of water content alone.<sup>2, 8, 9, 22</sup>

The short dashed line illustrates the increase in static permittivity for XL-pGMA-z with increasing water volume fraction. The XL-pGMA-z materials have lower static permittivity than Nafion<sup>®</sup> 117 and the linear approximation between PTFE and bulk pure water. This difference becomes more apparent as the water volume fraction increases. The data in [Figure 5.3](#) suggest that the functional relationship between hydrated polymer relative permittivity and water volume fraction may be affected by specific polymer chemistry, and relative permittivity property measurements may be needed to understand the behavior of different hydrated polymers.

The observed difference between the XL-pGMA-z and Nafion<sup>®</sup> 117 data, particularly at higher water volume fractions, is consistent with more non-freezable water in XL-pGMA-z compared to Nafion<sup>®</sup> 117 ([Figure 5.2](#)). This situation could result in slower water dynamics in XL-pGMA-z compared to Nafion<sup>®</sup> 117. The phase-separated morphology of Nafion<sup>®</sup> 117 is reported to lead to water clustering around the sulfonate groups in that polymer,<sup>28</sup> and those clusters can harbor freezable bulk or weakly bound water with faster dipole relaxations compared to the non-freezable water in XL-pGMA-z.

### 5.2.5. Ion Sorption

We measured ion sorption coefficients,  $K_s$ , and observed an increase in ion sorption as XL-pGMA-z water content increased ([Table 5.3](#)), which is consistent with results for many other hydrated polymers.<sup>31</sup> We compared the XL-pGMA-z ion sorption data to that for Nafion<sup>®</sup> 117. The water content of XL-pGMA-12 is similar to that for Nafion<sup>®</sup> 117, so it is reasonable to

compare the ion sorption coefficients for these materials because  $K_s$  is highly sensitive to water content. We observed that ions were excluded from Nafion<sup>®</sup> 117 to a greater extent than XL-pGMA-12.

**Table 5.3.** Ion sorption coefficients for XL-pGMA-z and Nafion<sup>®</sup> 117 were measured after equilibrating the samples with 0.5 mol/L of NaCl. The hydrolysis time, z, refers to the length of time (in hours) that the XL-pGMA-z samples were immersed in 0.5 mol/L H<sub>2</sub>SO<sub>4</sub> at 45 °C. Measurements were made at 22 ± 1 °C, and uncertainty was taken as the standard deviation from the mean of three measurements.

Polymer	Hydrolysis Time, z (hr)	$K_s$	$\gamma_+^m \gamma_-^m$
XL-pGMA-z	0	0.012 ± 0.001	3025
	8	0.072 ± 0.006	84
	10	0.118 ± 0.007	31
	12	0.147 ± 0.001	20
Nafion <sup>®</sup> 117	-	0.073 ± 0.003	1.1

We combined the ion and water sorption data to analyze the sorption selectivity properties of the materials. The ion sorption coefficients for these materials are representative of the mobile salt sorption coefficient (i.e., the ions that can pass through the polymer as electrically neutral salts). Plotting the water/ion (or water/salt) sorption selectivity (i.e.,  $K_w/K_s$ ) versus the water sorption coefficient,  $K_w$ , provides insight into the ability of the polymer to exclude salt from sorbing into the polymer (an important metric for desalination membrane performance) at a given water content.<sup>2, 52</sup> The sorption selectivity plays an important role in the desalination performance of a material, but details about rates of water and ion transport through the polymer, not discussed here, also influence the desalination performance of membrane materials.<sup>2, 52</sup> In general, water/ion sorption selectivity decreased as the XL-pGMA-z water content increased (Figure 5.4), which is consistent with observations for other materials.<sup>2, 31, 52</sup>

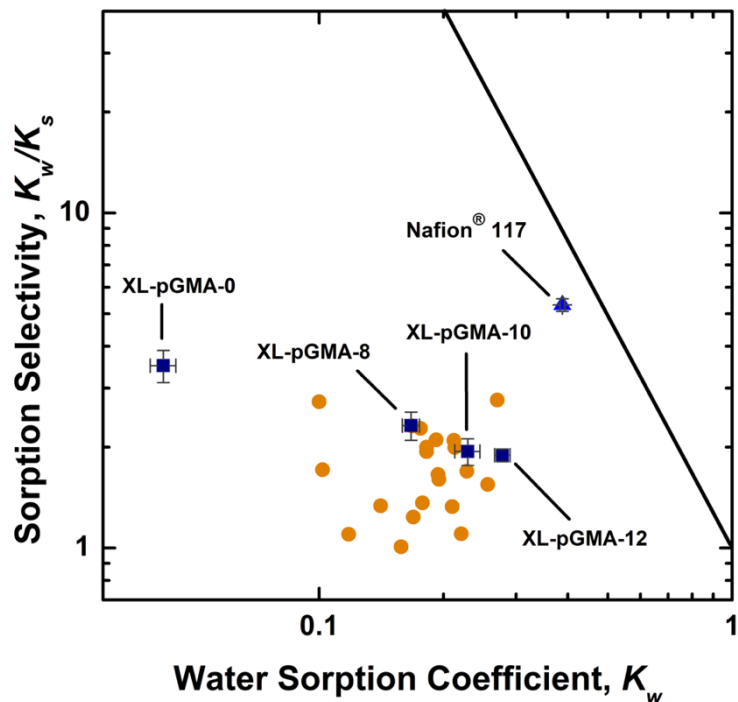


**Figure 5.4.** Water/ion sorption selectivity,  $K_w/K_s$  as a function of  $K_w$  for XL-pGMA-z, Nafion® 117, and previously reported uncharged polymers (circles)<sup>53</sup>. The solid line represents a sorption selectivity trade-off frontier reported for desalination membranes.<sup>2, 52</sup>

Nafion® 117 is more sorption selective compared to the XL-pGMA-z materials (Figure 5.4). The presence of fixed charges on the Nafion® backbone contribute to ion exclusion via the Donnan exclusion mechanism.<sup>54</sup> As such, the higher water/ion sorption selectivity of charged Nafion® 117 compared to uncharged XL-pGMA-z is not surprising.

This influence of Donnan exclusion on ion sorption can be quantified using the measured ion sorption data to calculate the activity coefficients of ions sorbed in the membrane. In uncharged polymers studied using monovalent electrolytes, the mean ionic activity coefficient in the membrane phase,  $\gamma_{\pm}^m$ , can be related to the concentration of salt in the membrane,  $C_s^m$ , when the membrane is in equilibrium with an external salt solution of concentration  $C_s^s$ , and the mean ionic activity coefficient of the external solution,  $\gamma_{\pm}^s$ , as:<sup>55, 56</sup>

$$(\gamma_{\pm}^m)^2 = \gamma_+^m \gamma_-^m = \frac{(\gamma_{\pm}^s)^2 (C_s^s)^2}{(C_s^m)^2} = \left( \frac{\gamma_{\pm}^s}{K_s} \right)^2 \quad (5.3)$$

where  $\gamma_+^m$  and  $\gamma_-^m$  are the cation and anion activity coefficients in the membrane phase, respectively. The presence of negatively charged fixed charge groups in a cation exchange material, such as Nafion<sup>®</sup> 117, results in a similar relationship for the monovalent electrolyte ionic activity coefficients in the membrane phase:<sup>8</sup>

$$\gamma_+^m \gamma_-^m = \frac{(\gamma_{\pm}^s)^2 (C_s^s)^2}{C_+^m C_-^m} = \frac{(\gamma_{\pm}^s)^2 C_s^s}{C_+^m K_s} \quad (5.4)$$

where  $C_-^m$  is the co-ion concentration in the membrane and  $C_+^m$  is the counter-ion concentration in the membrane.

In cation exchange materials, the concentration of co-ions is representative of the mobile salt concentration in the membrane phase, so  $K_s \equiv C_-^m / C_s^s$ , and  $C_+^m = C_A^m + C_-^m$ , where  $C_A^m$  is the concentration of fixed charges in the polymer.<sup>31, 57</sup> The value of  $C_A^m$  for Nafion<sup>®</sup> 117 was determined to be 2.84 meq/cm<sup>3</sup> using the ion exchange capacity of Nafion<sup>®</sup> 117<sup>30</sup> and water uptake data<sup>8</sup>. For 0.5 mol/L NaCl, the mean ionic activity coefficient in the solution phase,  $\gamma_{\pm}^s$ , was calculated to be 0.660 using the Pitzer model.<sup>58</sup>

The ionic activity coefficients, calculated from the ion sorption data, suggest that Nafion<sup>®</sup> 117 is more thermodynamically ideal (i.e., the mean ionic activity coefficients are closer to unity) than XL-pGMA-z (Table 5.3). Additionally, XL-pGMA-z becomes more thermodynamically ideal as the water content of the polymer increases. These activity coefficients are consistent with the DSC data that suggest more freezable water exists in Nafion<sup>®</sup> 117 compared to XL-pGMA-z.

The activity coefficients can provide insight into the higher water/ion sorption selectivity of Nafion<sup>®</sup> 117 compared to XL-pGMA-z. The XL-pGMA-z polymers exclude salt via a dielectric mechanism that is described by Equation 5.3.<sup>5</sup> Unfavorable interactions between ions and the membrane phase result in exclusion of salt from the polymer, and this extent of exclusion increases as the ionic activity coefficients in the membrane phase increase and the water content of the polymer decreases.

The influence of dielectric exclusion on the overall ion sorption properties of Nafion<sup>®</sup> 117 is weak, in part, because the activity coefficients for Nafion<sup>®</sup> 117 are close to unity. As such, ion exclusion in Nafion<sup>®</sup> 117 is primarily driven by Donnan exclusion.<sup>6, 54</sup> Therefore, it is reasonable that Nafion<sup>®</sup> 117 would have higher water/ion selectivity compared to XL-pGMA-z even though the relative permittivity of Nafion<sup>®</sup> 117 was greater than that of XL-pGMA-z at comparable water content.

### 5.2.6. Free Energy of Ion Sorption

The ion sorption coefficient can be related to the free energy change associated with moving ions from the solution phase into the membrane phase,  $\Delta W_s$ :<sup>2</sup>

$$K_s \equiv \frac{C_s^m}{C_s^s} = \exp \left[ -\frac{\Delta W_s}{k_B T} \right] \quad (5.5)$$

where  $k_B$  is Boltzmann's constant, and  $T$  is absolute temperature.<sup>59</sup> In the simplest case,  $\Delta W_s$  can be taken as the solvation energy barrier, which can be calculated using the electrostatic continuum-based approach proposed by Born:<sup>2, 56, 60, 61</sup>

$$\Delta W_s = \frac{z_s^2 e^2}{8\pi\epsilon_0 a_s} \left( \frac{1}{\epsilon_m} - \frac{1}{\epsilon_{sol}} \right) \quad (5.6)$$

where  $z_s$  is the ion charge number,  $e$  is the elementary charge,  $\epsilon_0$  is the permittivity of free space,  $a_s$  is the bare ion radius,  $\epsilon_m$  is the relative permittivity of the membrane, and  $\epsilon_{sol}$  is the dielectric constant of the external solution. The model assumes that both the solution and membrane can be treated as dielectric continua and that the ions are non-polarizable charged spheres.<sup>56, 62, 63</sup>

Combining [Equations 5.5](#) and [5.6](#) provides a means to estimate the significance of the difference between the static permittivity data for XL-pGMA-z and that calculated from the linear approximation discussed in regard to [Figure 5.3](#). For example, if the linear approximation was used to estimate the static permittivity of XL-pGMA-12, a value of 12.3 would be calculated based on the  $0.278 \pm 0.012$  volume fraction of water in XL-pGMA-12 ([Figure 5.3](#)). [Equations 5.5](#) and [5.6](#) suggest that this value of the static permittivity would result in a value of  $K_s$  that is eight orders of magnitude larger than that calculated using the static permittivity of 5.3 measured for XL-pGMA-12.

The electrostatic theory-based Born model overestimates the solvation energy barrier for XL-pGMA-z likely as a result of the dielectric continuum assumptions for the polymer. The predicted values (calculated using [Equation 5.6](#)), however, are qualitatively consistent with experimental data (calculated using [Equation 5.5](#)), suggesting a decrease in the free energy barrier for ion sorption as polymer water content increases ([Figure 5.5](#)). This qualitative agreement suggests that the static relative permittivity measurements captured part of the physics involved in the ion sorption process.

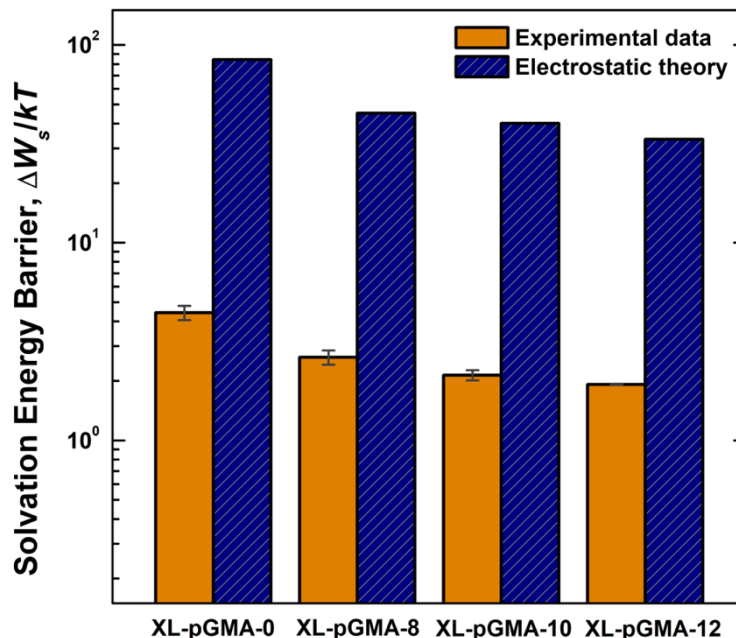


**Figure 5.5.** Solvation energy barrier calculated (solid bars, experimental data) using measured sorption coefficients (Table 5.3) and Equation 5.5, and calculated (striped bars, electrostatic theory) using static permittivity values (Figure 5.3) and the Born model (Equation 5.6).

### 5.3. Conclusions

The relative permittivity of XL-pGMA-z increases with water content in a manner that is different from Nafion<sup>®</sup> 117. The relative permittivity values for XL-pGMA-z are also lower than that of Nafion<sup>®</sup> 117 at equivalent water content. This result may be due to the presence of more extensive water-polymer hydrogen bonding in XL-pGMA-z that restricts water dipole dynamics to a greater extent than in Nafion<sup>®</sup> 117. As such, chemical details, not solely water content, appear to influence the relative permittivity properties of some hydrated polymers. These results suggest an opportunity to engineer membranes with low relative permittivity to minimize ion sorption in desalination-relevant materials. Measuring relative permittivity may provide insight into water dynamics and ion exclusion in a range of hydrated polymers.

Relative permittivity data for XL-pGMA-z was used to calculate the free energy barrier for ion sorption using the Born model. These values were compared to those values calculated using experimentally measured data. We observed qualitative agreement suggesting a decrease in the energy barrier as polymer water content increases, which is consistent with experimentally observed results. These results suggest that the static relative permittivity measurements captured part of the physics that describes the ion sorption process and may provide insight into structure-property relationships between ion sorption and polymer chemistry. This understanding could inform future efforts to engineer highly water/ion sorption selective polymers for desalination membrane applications.

#### 5.4. References

1. Chen, L. F., *Microwave Electronics: Measurement and Materials Characterization*. Wiley: Hoboken, New Jersey, 2004.
2. Zhang, H.; Geise, G. M., Modeling the water permeability and water/salt selectivity tradeoff in polymer membranes. *Journal of Membrane Science* **2016**, *520*, 790-800.
3. Glueckauf, E., On the mechanism of osmotic desalting with porous membranes. *Proceedings of the First International Symposium on Water Desalination* **1967**, 143-150.
4. Anderson, J. E.; Pusch, W., The membrane/water partition coefficients of ions: Electrostatic calculations of dielectric heterogeneity. *Berichte der Bunsengesellschaft für physikalische Chemie* **1976**, *80* (9), 846-849.
5. Yaroshchuk, A. E., Dielectric exclusion of ions from membranes. *Advances in Colloid and Interface Science* **2000**, *85* (2), 193-230.
6. Yaroshchuk, A. E., Non-steric mechanisms of nanofiltration: Superposition of Donnan and dielectric exclusion. *Separation and Purification Technology* **2001**, *22-23*, 143-158.

7. Freger, V.; Bason, S., Characterization of ion transport in thin films using electrochemical impedance spectroscopy: I. Principles and theory. *Journal of Membrane Science* **2007**, *302* (1), 1-9.
8. Kamcev, J.; Galizia, M.; Benedetti, F. M.; Jang, E.-S.; Paul, D. R.; Freeman, B. D.; Manning, G. S., Partitioning of mobile ions between ion exchange polymers and aqueous salt solutions: Importance of counter-ion condensation. *Physical Chemistry Chemical Physics* **2016**, *18* (8), 6021-6031.
9. Kamcev, J.; Paul, D. R.; Manning, G. S.; Freeman, B. D., Predicting salt permeability coefficients in highly swollen, highly charged ion exchange membranes. *ACS Applied Materials & Interfaces* **2017**, *9* (4), 4044-4056.
10. Paddison, S. J.; Reagor, D. W.; Zawodzinski Jr, T. A., High frequency dielectric studies of hydrated Nafion®. *Journal of Electroanalytical Chemistry* **1998**, *459* (1), 91-97.
11. Lu, Z.; Lanagan, M.; Manias, E.; Macdonald, D. D., Two-port transmission line technique for dielectric property characterization of polymer electrolyte membranes. *The Journal of Physical Chemistry B* **2009**, *113* (41), 13551-13559.
12. Page, K. A.; Rowe, B. W.; Masser, K. A.; Faraone, A., The effect of water content on chain dynamics in nafion membranes measured by neutron spin echo and dielectric spectroscopy. *Journal of Polymer Science Part B: Polymer Physics* **2014**, *52* (9), 624-632.
13. Paddison, S.; Bender, G.; Zawodzinski Jr, T. A., The microwave region of the dielectric spectrum of hydrated Nafion® and other sulfonated membranes. *Journal of New Materials for Electrochemical Systems* **2000**, *3*, 293-302.
14. Xu, H.; Vij, J. K.; McBrierty, V. J., Wide-band dielectric spectroscopy of hydrated poly(hydroxyethyl methacrylate). *Polymer* **1994**, *35* (2), 227-234.
15. Kyritsis, A.; Pissis, P.; Grammatikakis, J., Dielectric relaxation spectroscopy in poly(hydroxyethyl acrylates)/water hydrogels. *Journal of Polymer Science Part B: Polymer Physics* **1995**, *33* (12), 1737-1750.

16. McBrierty, V. J.; Keely, C. M.; Coyle, F. M.; Xu, H.; Vij, J. K., Hydration and plasticization effects in cellulose acetate: Molecular motion and relaxation. *Faraday Discussions* **1996**, *103*, 255-268.
17. Efligenir, A.; Fievet, P.; Déon, S.; Salut, R., Characterization of the isolated active layer of a NF membrane by electrochemical impedance spectroscopy. *Journal of Membrane Science* **2015**, *477*, 172-182.
18. Johnson, G. E.; Bair, H. E.; Matsuoka, S.; Anderson, E. W.; Scott, J. E., *Water in Polymers*. American Chemical Society: Washington, DC, 1980; Vol. 127, p 451-468.
19. De La Rosa, A.; Heux, L.; Cavaillé, J. Y., Secondary relaxations in poly(allyl alcohol), PAA, and poly(vinyl alcohol), PVA. II. Dielectric relaxations compared with dielectric behaviour of amorphous dried and hydrated cellulose and dextran. *Polymer* **2001**, *42* (12), 5371-5379.
20. Paddison, S. J., Proton conduction mechanisms at low degrees of hydration in sulfonic acid-based polymer electrolyte membranes. *Annual Review of Materials Research* **2003**, *33* (1), 289-319.
21. Lu, Z.; Polizos, G.; Macdonald, D. D.; Manias, E., State of water in perfluorosulfonic ionomer (Nafion® 117) proton exchange membranes. *Journal of The Electrochemical Society* **2008**, *155* (2), B163-B171.
22. Kamcev, J.; Paul, D. R.; Freeman, B. D., Ion activity coefficients in ion exchange polymers: Applicability of Manning's counterion condensation theory. *Macromolecules* **2015**, *48* (21), 8011-8024.
23. Müller-Plathe, F., Diffusion of water in swollen poly(vinyl alcohol) membranes studied by molecular dynamics simulation. *Journal of Membrane Science* **1998**, *141* (2), 147-154.
24. Lu, Z.; Manias, E.; Macdonald, D. D.; Lanagan, M., Dielectric relaxation in dimethyl sulfoxide/water mixtures studied by microwave dielectric relaxation spectroscopy. *The Journal of Physical Chemistry A* **2009**, *113* (44), 12207-12214.

25. Lou, J.; Hatton, T. A.; Laibinis, P. E., Effective dielectric properties of solvent mixtures at microwave frequencies. *The Journal of Physical Chemistry A* **1997**, *101* (29), 5262-5268.
26. Undre, P. B.; Khirade, P. W.; Rajenimbalkar, V. S.; Helambe, S. N.; Mehrotra, S. C., Dielectric relaxation in ethylene glycol - dimethyl sulfoxide mixtures as a function of composition and temperature. *Journal of the Korean Chemical Society* **2012**, *56* (4), 416-423.
27. Khirade, P. W.; Chaudhari, A.; Shinde, J. B.; Helambe, S. N.; Mehrotra, S. C., Static dielectric constant and relaxation time measurements on binary mixtures of dimethyl sulfoxide with ethanol, 2-ethoxyethanol, and propan-1-ol at 293, 303, 313, and 323 K. *Journal of Chemical & Engineering Data* **1999**, *44* (5), 879-881.
28. Mauritz, K. A.; Moore, R. B., State of understanding of Nafion®. *Chemical Reviews* **2004**, *104* (10), 4535-4586.
29. Lu, Z., State of water in perfluorosulfonic acid membranes studied by microwave dielectric relaxation spectroscopy. **2006**, *Ph.D. Thesis, Department of Materials Science and Engineering, The Pennsylvania State University, University Park, Pennsylvania.*
30. Alfa Aesar by Thermo Fisher Scientific, Nafion® N-117 membrane, 0.180 mm thick,  $\geq$  0.90 meq/g exchange capacity, <https://www.alfa.com/en/catalog/042180/>, (accessed June 13th, 2018).
31. Geise, G. M.; Paul, D. R.; Freeman, B. D., Fundamental water and salt transport properties of polymeric materials. *Progress in Polymer Science* **2014**, *39* (1), 1-42.
32. Keysight Technologies, Sample and Sample Holder Considerations (Opt.001), [http://na.support.keysight.com/materials/help/WebHelp/Opt.001\\_Sample\\_and\\_Sample\\_Holder\\_Considerations.htm#efd32146](http://na.support.keysight.com/materials/help/WebHelp/Opt.001_Sample_and_Sample_Holder_Considerations.htm#efd32146), (accessed June 12th, 2018).
33. Geyer, R. G.; Krupka, J., Microwave dielectric properties of anisotropic materials at cryogenic temperatures. *IEEE Transactions on Instrumentation and Measurement* **1995**, *44* (2), 329-331.

34. Keysight Technologies, Basics of Measuring the Dielectric Properties of Materials, <https://literature.cdn.keysight.com/litweb/pdf/5989-2589EN.pdf?id=670519>, (accessed June 12th, 2018).
35. Keysight Technologies, Opt.001 Sample Thickness Calculator, [http://na.support.keysight.com/materials/help/WebHelp/Opt.001\\_Sample\\_Thickness\\_Calculator.htm](http://na.support.keysight.com/materials/help/WebHelp/Opt.001_Sample_Thickness_Calculator.htm), (accessed June 12th, 2018).
36. Debye, P., *Polar Molecules*. Dover: New York, 1929.
37. Smith, G.; Duffy, A. P.; Shen, J.; Olliff, C. J., Dielectric relaxation spectroscopy and some applications in the pharmaceutical sciences. *Journal of Pharmaceutical Sciences* **1995**, *84* (9), 1029-1044.
38. Ellison, W. J.; Lamkaouchi, K.; Moreau, J. M., Water: A dielectric reference. *Journal of Molecular Liquids* **1996**, *68* (2), 171-279.
39. Kreuer, K.-D.; Paddison, S. J.; Spohr, E.; Schuster, M., Transport in proton conductors for fuel-cell applications: Simulations, elementary reactions, and phenomenology. *Chemical Reviews* **2004**, *104* (10), 4637-4678.
40. Elliott, J. A.; Paddison, S. J., Modelling of morphology and proton transport in PFSA membranes. *Physical Chemistry Chemical Physics* **2007**, *9* (21), 2602-2618.
41. TA Instruments, Thermal Analysis to Determine Various Forms of Water Present in Hydrogels, <http://www.tainstruments.com/pdf/literature/TA384.pdf>, (accessed June 12th, 2018).
42. Quinn, F. X.; Kampff, E.; Smyth, G.; McBrierty, V. J., Water in hydrogels. 1. A study of water in poly(N-vinyl-2-pyrrolidone/methyl methacrylate) copolymer. *Macromolecules* **1988**, *21* (11), 3191-3198.
43. Hodge, R. M.; Bastow, T. J.; Edward, G. H.; Simon, G. P.; Hill, A. J., Free volume and the mechanism of plasticization in water-swollen poly(vinyl alcohol). *Macromolecules* **1996**, *29* (25), 8137-8143.

44. Yoshida, H.; Miura, Y., Behavior of water in perfluorinated ionomer membranes containing various monovalent cations. *Journal of Membrane Science* **1992**, *68* (1), 1-10.
45. Shinyashiki, N.; Shimomura, M.; Ushiyama, T.; Miyagawa, T.; Yagihara, S., Dynamics of water in partially crystallized polymer/water mixtures studied by dielectric spectroscopy. *The Journal of Physical Chemistry B* **2007**, *111* (34), 10079-10087.
46. Shimoaka, T.; Wakai, C.; Sakabe, T.; Yamazaki, S.; Hasegawa, T., Hydration structure of strongly bound water on the sulfonic acid group in a Nafion membrane studied by infrared spectroscopy and quantum chemical calculation. *Physical Chemistry Chemical Physics* **2015**, *17* (14), 8843-8849.
47. Bunce, N. J.; Sondheimer, S. J.; Fyfe, C. A., Proton NMR method for the quantitative determination of the water content of the polymeric fluorosulfonic acid Nafion-H. *Macromolecules* **1986**, *19* (2), 333-339.
48. Kim, Y. S.; Dong, L.; Hickner, M. A.; Glass, T. E.; Webb, V.; McGrath, J. E., State of water in disulfonated poly(arylene ether sulfone) copolymers and a perfluorosulfonic acid copolymer (Nafion) and its effect on physical and electrochemical properties. *Macromolecules* **2003**, *36* (17), 6281-6285.
49. Boakye, E. E.; Yeager, H. L., Water sorption and ionic diffusion in short side chain perfluorosulfonate ionomer membranes. *Journal of Membrane Science* **1992**, *69* (1), 155-167.
50. Luck, W. A. P., *The Influence of Ions on Water Structure and on Aqueous Systems*. Springer: Boston, MA, 1985.
51. Kreuer, K. D., On the development of proton conducting polymer membranes for hydrogen and methanol fuel cells. *Journal of Membrane Science* **2001**, *185* (1), 29-39.
52. Geise, G. M.; Park, H. B.; Sagle, A. C.; Freeman, B. D.; McGrath, J. E., Water permeability and water/salt selectivity tradeoff in polymers for desalination. *Journal of Membrane Science* **2011**, *369* (1), 130-138.

53. Yasuda, H.; Lamaze, C. E.; Ikenberry, L. D., Permeability of solutes through hydrated polymer membranes. Part I. Diffusion of sodium chloride. *Die Makromolekulare Chemie* **1968**, *118* (1), 19-35.
54. Helfferich, F. G., *Ion Exchange*. Dover Publications, McGraw-Hill: New York, 1995.
55. Wijmans, J. G.; Baker, R. W., The solution-diffusion model: A review. *Journal of Membrane Science* **1995**, *107* (1), 1-21.
56. Ji, Y.; Luo, H.; Geise, G. M., Specific co-ion sorption and diffusion properties influence membrane permselectivity. *Journal of Membrane Science* **2018**, *563*, 492-504.
57. Geise, G. M.; Falcon, L. P.; Freeman, B. D.; Paul, D. R., Sodium chloride sorption in sulfonated polymers for membrane applications. *Journal of Membrane Science* **2012**, *423*, 195-208.
58. Pitzer, K. S.; Peiper, J. C.; Busey, R. H., Thermodynamic properties of aqueous sodium chloride solutions. *Journal of Physical and Chemical Reference Data* **1984**, *13* (1), 1-102.
59. Prausnitz, J. M.; Lichtenthaler, R. N.; Azevedo, E. G. d., *Molecular Thermodynamics of Fluid-Phase Equilibria*. 2nd ed.; Prentice-Hall: Englewood Cliffs, New Jersey, 1986.
60. Bowen, W. R.; Welfoot, J. S.; Williams, P. M., Linearized transport model for nanofiltration: Development and assessment. *AIChE Journal* **2002**, *48* (4), 760-773.
61. Born, M., Volumen und hydrationswärme der ionen. *Zeitschrift für Physik* **1920**, *1* (1), 45-48.
62. Parsegian, A., Energy of an ion crossing a low dielectric membrane: Solutions to four relevant electrostatic problems. *Nature* **1969**, *221*, 844.
63. Bontha, J. R.; Pintauro, P. N., Prediction of ion solvation free energies in a polarizable dielectric continuum. *The Journal of Physical Chemistry* **1992**, *96* (19), 7778-7782.

## Chapter 6: Functional Group Configuration Influences Salt Transport in Desalination Membrane Materials<sup>§§§§</sup>

### 6.1. Introduction

In relatively simple uncharged hydrated polymers, salt sorption properties are linked to the relative permittivity (or dielectric constant) of the material,<sup>1-4</sup> and polymer chemistry can be used to engineer relative permittivity to influence the thermodynamics of salt sorption.<sup>1</sup> Additionally, preparing membranes (with low water content – similar to desalination membranes) with rigid polymer backbones and/or bulky side groups can result in favorable water/salt transport selectivity.<sup>5-7</sup> These findings inform opportunities to engineer polymers to achieve the necessary combination of properties to purify water effectively.

One challenge in many fundamental studies of membrane transport properties is that modification of the polymer often changes the hydrophilicity of the material.<sup>8-11</sup> In other words, a change in water content often accompanies systematic variations in polymer chemistry. Water content can have a profound impact on the water and salt transport properties of polymers,<sup>4, 9, 12-14</sup> and it can be difficult to decouple the influences of changing water content and polymer chemistry on transport properties. Doing so, however, is critical to understanding how molecular engineering can be used to design advanced membrane materials.

Here we prepared five methacrylate-based co-polymers that have statistically equivalent water content but different ratios of two co-monomers that have different numbers of hydroxyl groups: 2-hydroxyethyl methacrylate (HEMA) and glycerol methacrylate (GMAOH). Selecting

---

<sup>§§§§</sup> This section has been adapted with permission from: Luo, H.; Chang, K.; Bahati, K.; Geise, G. M., Functional group configuration influences salt transport in desalination membrane materials. *Journal of Membrane Science* **2019**, 590, 117295.

these co-monomers enabled a systematic variation of the position and number density of hydroxyl groups in the co-polymers without changing the water content of the material. The chemical composition of the co-polymer was systematically varied from a vicinal diol-rich configuration (GMAOH-rich co-polymer) to a HEMA-rich material with single hydroxyl groups on the side chains. Shifting the co-polymer composition from a GMAOH-rich configuration to a HEMA-rich configuration suppressed both salt sorption and salt diffusion properties, and these results were supported by dielectric permittivity property measurements and state of water analysis. The results suggest, without complication from changing water content, that a more distributed hydrophilic functional group configuration may suppress salt transport to a greater extent than a more vicinal functional group-rich configuration within the co-polymer. As such, this study provides information about how specific chemical functional groups influence salt transport properties in a unique manner that is decoupled from polymer water content.

## **6.2. Results and Discussion**

### **6.2.1. Water Uptake**

The primary goal of this study was to determine the influence of hydroxyl group configuration on salt transport properties. To accomplish this goal, five HEMA:GMA:GMAOH materials were prepared with different ratios of HEMA and GMAOH (Figure 2.4), which have different numbers of hydroxyl groups (Figure 2.3). As polymer water content critically affects the salt transport properties of hydrated polymers,<sup>9,13</sup> it was important to prepare the materials used in this study such that the water content of all of the materials was statistically equivalent. By doing so, transport property differences between the materials can be ascribed to changes in the functional group configuration of the polymer without needing to consider the effect of changing water content.

Over the range of co-monomer compositions considered, a series of materials were prepared such that the water uptake and water sorption coefficient properties were statistically indistinguishable (Table 6.1). As the HEMA content of the co-polymer increased (and the GMAOH content of the co-polymer decreased), the overall hydroxyl group content in the co-polymer decreased by approximately 8%. We also observed similar dry density values for all co-polymers (Table 6.1), suggesting that the changing of functional group orientation does not significantly affect chain packing in the materials. As the HEMA content of the co-polymer increases, the cross-link density likely decreases to a small extent (estimated to be approximately 7% using the molar composition of the polymer<sup>15</sup>) to offset the small decrease in hydroxyl group content and yield a series of materials that have statistically indistinguishable water content (Table 6.1). It is also possible, however, that differences in the intrinsic hydrophilicity of the HEMA and GMAOH co-monomers may contribute to this balance. The water uptake of HEMA is reported to be 0.60 g(water)/g(dry polymer), and GMAOH is reported to be water soluble.<sup>5, 16</sup> Additionally, molar enthalpy of mixing data for mixtures of water and either ethanol<sup>17</sup> or 1,2-propanediol,<sup>18</sup> which are representative of the HEMA and GMAOH side chains, respectively, suggest that mixing of water and 1,2-propanediol is more thermodynamically favored compared to the situation for water and ethanol. If ethanol and 1,2-propanediol are taken to be representative of the side chains of HEMA and GMAOH, respectively, these results suggest that mixing of water and GMAOH may be more thermodynamically favored compared to that of water and HEMA.<sup>15</sup> Both analyses suggest that the GMAOH side chain is more hydrophilic compared to the HEMA side chain. Subsequent transport property data will be discussed within the framework of the co-monomer composition and hydroxyl group content of the co-polymer.

**Table 6.1.** Water content and dry polymer density data measured at  $22 \pm 1$  °C. Water content measurements were made on samples initially equilibrated with DI water. The water sorption coefficient,  $K_w$ , was taken as equivalent to the volume fraction of water in the material, which was calculated using Equation 2.5. Co-polymer composition is reported as in Figure 2.4. The uncertainty was taken as one standard deviation from the mean of three measurements.

HEMA:GMA:GMAOH Composition (by mass)	Water Uptake [g(water)/g(dry polymer)]	Dry Density (g/cm <sup>3</sup> )	$K_w$	Hydroxyl Group Content [meq(-OH)/g(dry polymer)]
<b>0:60:40</b>	$0.24 \pm 0.02$	$1.29 \pm 0.02$	$0.23 \pm 0.01$	5.0
<b>15:55:30</b>	$0.24 \pm 0.01$	$1.30 \pm 0.03$	$0.24 \pm 0.01$	4.9
<b>30:50:20</b>	$0.24 \pm 0.01$	$1.27 \pm 0.01$	$0.23 \pm 0.01$	4.8
<b>45:45:10</b>	$0.23 \pm 0.01$	$1.27 \pm 0.01$	$0.23 \pm 0.01$	4.7
<b>60:40:0</b>	$0.23 \pm 0.01$	$1.26 \pm 0.02$	$0.23 \pm 0.01$	4.6

### 6.2.2. Salt Transport Properties

As the HEMA content of the polymer increases and the GMAOH content of the polymer decreases, the configuration of hydroxyl groups on the polymer side chains shifts from a vicinal diol-rich material (when the GMAOH content is high compared to HEMA) to a material where most side chains contain a single hydroxyl group (when the HEMA content is high compared to GMAOH). Therefore, we were able to use the HEMA:GMA:GMAOH materials to study the influence of hydroxyl group distribution on salt transport properties without concern for changing water content (as the water content of the HEMA:GMA:GMAOH series of materials was equivalent, Table 6.1). Salt transport properties can be engineered by controlling the molecular distribution of hydroxyl groups within the polymer, and this observation may have implications for molecular design of desalination membrane materials.

The co-monomer content of the materials was varied by adjusting the mass composition of the co-monomers in the pre-polymerization solution used to prepare the co-polymers. While Fourier-transform infrared (FT-IR) spectroscopy (see Appendix E) indicates that the co-polymer composition reflects the pre-polymerization solution composition, the similar chemistry and cross-

linked network architecture of the co-polymers impedes quantitative measurement of the co-polymer composition. The hydroxyl group content, reported in [Table 6.1](#), was calculated from the pre-polymerization solution composition under the assumption that the pre-polymerization solution composition translates directly into the co-polymer composition.

While the hydroxyl group content of the co-polymers may vary slightly over the compositional range considered (as suggested in [Table 6.1](#)), we expect this change to be small in light of the expected changes in co-monomer composition. The pre-polymerization solution composition is given by mass, but the molar composition is more representative of the distribution of hydroxyl groups. For example, in the HEMA:GMA:GMAOH 60:40:0 sample, 62% (by mole) of the side chains have a single hydroxyl group. By comparison, the HEMA:GMA:GMAOH 0:40:60 sample has 37% (by mole) side chains that contain two hydroxyl groups. As such, the hydroxyl groups are highly localized in the HEMA:GMA:GMAOH 0:40:60 sample compared to the HEMA:GMA:GMAOH 60:40:0 sample. While we recognize the possibility for small variations in cross-link density and/or hydroxyl group content of the co-polymers, we believe that the configuration of the hydroxyl groups in the co-polymers primarily influences the resulting material properties, and the subsequent discussion is focused accordingly.

### 6.2.2.1. Salt Sorption

Increasing the HEMA content, while simultaneously reducing the GMAOH content of HEMA:GMA:GMAOH, drives a reduction in the salt sorption coefficient or an increase in the ability of the polymer to exclude salt (Table 6.2). In many hydrated polymers, salt sorption coefficients tend to vary proportionally with the water content of the polymer (i.e.,  $K_s$  typically increases as  $K_w$  increases).<sup>4,9,13</sup> The cross-linked hydrogel data in Figure 6.1 illustrate this type of relationship. Engineering the molecular position of the functional groups in the HEMA:GMA:GMAOH materials, however, allows access to different salt sorption properties without changing the water content of the polymer (Figure 6.1).

**Table 6.2.** Salt transport property data for the series of HEMA:GMA:GMAOH materials. The salt sorption coefficient measurements were made at  $22 \pm 1$  °C using sample that initially had been equilibrated with 0.5 mol/L NaCl. Salt permeability was measured at  $25 \pm 0.2$  °C using an upstream salt concentration of 0.5 mol/L NaCl. For each experimentally determined value, the uncertainty was taken as one standard deviation from the mean of three measurements. The apparent salt diffusion coefficient was calculated from the measured salt sorption and salt permeability coefficients using Equation 3.3, and standard propagation of error<sup>19</sup> was used to estimate the uncertainty in the salt diffusion coefficient. Co-polymer composition is reported as in Figure 2.4.

HEMA:GMA:GMAOH Composition (by mass)	$K_s$	$P_s$ (x $10^{-9}$ cm <sup>2</sup> /s)	$D_s$ (x $10^{-8}$ cm <sup>2</sup> /s)
<b>0:60:40</b>	0.118 ± 0.004	16.2 ± 0.6	13.7 ± 0.1
<b>15:55:30</b>	0.104 ± 0.004	11.6 ± 0.4	11.2 ± 0.1
<b>30:50:20</b>	0.097 ± 0.001	8.7 ± 0.1	9.0 ± 0.1
<b>45:45:10</b>	0.090 ± 0.002	7.0 ± 0.1	7.8 ± 0.1
<b>60:40:0</b>	0.080 ± 0.002	6.0 ± 0.1	7.5 ± 0.1

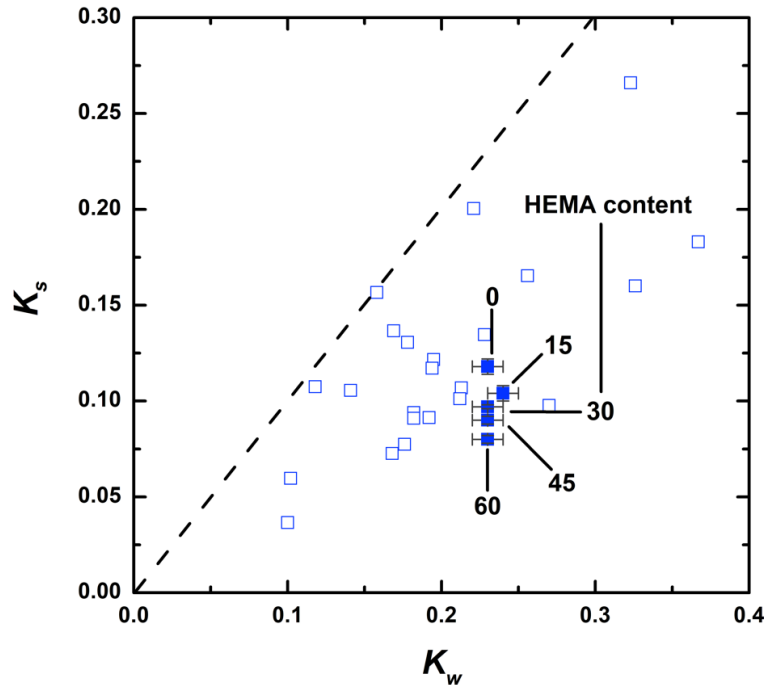


**Figure 6.1.** Salt sorption coefficient data as a function of the water sorption coefficient for HEMA:GMA:GMAOH (this study, ■) and hydrogels (□).<sup>13</sup> The dashed line on this parity plot indicates the border between salt exclusion from the polymer (points below the line) and salt enrichment in the polymer (points above the line). For HEMA:GMA:GMAOH, the HEMA co-monomer composition of the pre-polymerization solution used to prepare each co-polymer is reported for each data point.

This result may suggest that adjusting the distribution of a given functional group within a polymer can have a pronounced influence on salt sorption properties. The observed change in the salt sorption coefficient without a corresponding change in water content suggests that the change in functional group configuration affects the thermodynamic environment of the hydrated polymer. As discussed subsequently, we believe that the observed salt sorption properties are highly related to changes in the hydrogen bonding environment within the co-polymer, which can be probed via DSC and microwave dielectric spectroscopy measurements.

#### 6.2.2.2. Salt Permeability and Diffusivity

To further explore the influence of hydroxyl functional group configuration on salt transport, we characterized the salt permeability of the HEMA:GMA:GMAOH materials. Similar

to the salt sorption coefficient observations (Figure 6.1), the salt permeability decreased as the HEMA content of the co-polymer increased (Figure 6.2A). This decrease in salt permeability,  $P_s$ , is related to the observed decrease in the salt sorption coefficient,  $K_s$ , by the solution-diffusion model where  $P_s = K_s \times D_s$  (i.e., Equation 3.3).<sup>20</sup>

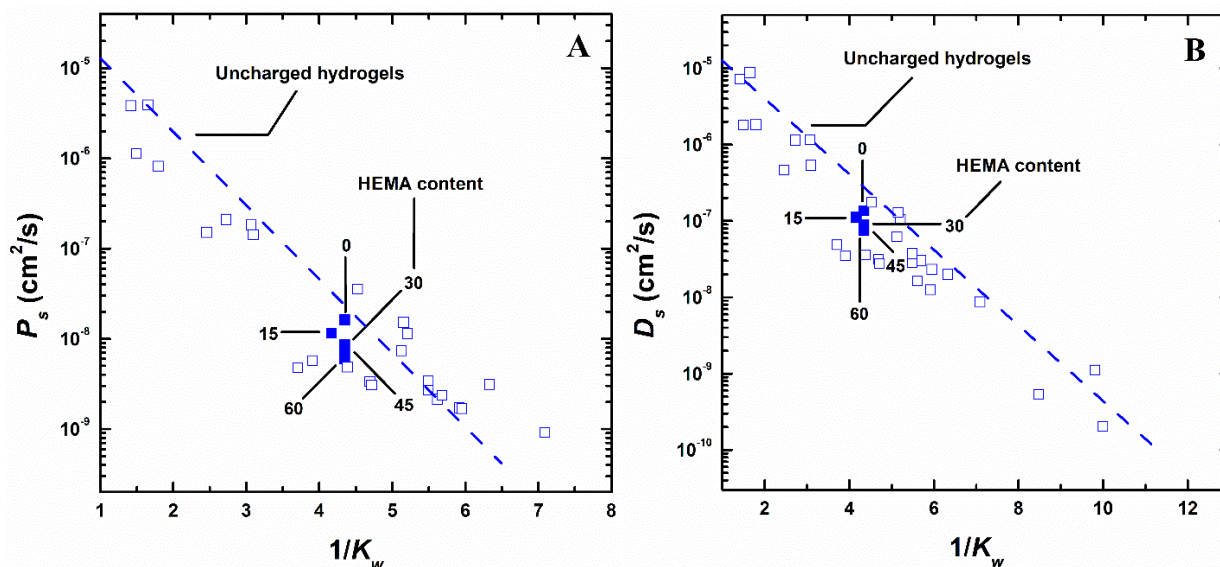


**Figure 6.2.** Salt permeability (A) and apparent salt diffusion (B) coefficients as a function of inverse water sorption coefficient for HEMA:GMA:GMAOH (this study, ■) and hydrogels (□).<sup>13</sup> For HEMA:GMA:GMAOH, the HEMA co-monomer composition of the pre-polymerization solution used to prepare each co-polymer is reported for each data point. The dashed lines are drawn to guide the eye for the hydrogel data. The uncertainty in the data for the HEMA:GMA:GMAOH materials is within the size of the data points.

Unique to this study is the fact that the observed changes in salt sorption and permeability occur at a fixed water content. Several studies have established that water content has a significant impact on salt sorption and permeability properties (e.g., the open symbols in Figures 6.1 and 6.2).<sup>8, 9, 13</sup> Our results, however, suggest that the functional group configuration of a polymer (not simply water content alone) can be used to control salt sorption and permeability properties, and this observation suggests new opportunities for membrane science.

Free volume theory provides a framework to explain the dashed line relationships shown in [Figure 6.2](#).<sup>9, 13, 21</sup> Yasuda proposed a free volume-based model where the water content of the polymer was taken to be proportional to the polymer free volume.<sup>13</sup> This model suggests that the natural logarithms of both the permeability and diffusion coefficients should scale with inverse water content provided that water content is a proxy for free volume and that transport can be described by the free volume model.<sup>13</sup> As such, the natural logarithm of salt permeability and diffusion coefficients tend to decrease linearly with the inverse water sorption coefficient (i.e.,  $1/K_w$ ). An example of this relationship is illustrated in [Figure 6.2A](#) where the salt permeability of several uncharged hydrogels decrease with  $1/K_w$ . One implication of this model is that movement along the dashed line in [Figure 6.2A](#) indicates that salt permeability is changing in response to changes in free volume brought about by water content changes in the polymer, i.e., other polymer compositional effects are secondary.

In the HEMA:GMA:GMAOH materials considered in this study, the water content of all 5 samples is statistically indistinguishable, so the observed decrease in salt permeability as HEMA content increases is due to factors other than water content. As such, the HEMA:GMA:GMAOH data points in [Figure 6.2A](#) move vertically downward as HEMA content increases and not along the dashed line, as would be expected if water content was driving the changes in permeability. This unique behavior is a result of changing the functional group configuration within the polymer.

A similar trend is observed when the salt sorption and permeability coefficients are used to calculate apparent salt diffusion coefficients that can also be plotted versus  $1/K_w$  ([Figure 6.2B](#)). We observed a decrease in the apparent salt diffusion coefficient as HEMA content increased at equivalent water content ([Table 6.1](#), [Figure 6.2B](#)), and the decrease was 1.5 times less than the decrease in salt permeability for these HEMA:GMA:GMAOH materials. This result is expected

because the decrease in both salt sorption and diffusion coefficients contribute to the overall decrease in salt permeability, according to the solution-diffusion model (Equation 3.3).

Additionally, we compared the apparent salt diffusion coefficients of HEMA:GMA:GMAOH to those values for other cross-linked hydrogels.<sup>13</sup> At similar water content values (i.e., similar values of  $1/K_w$ ), the magnitudes of the salt diffusivity are similar among these chemically similar materials (Figure 6.2B). This observation suggests that molecular motions are similarly facilitated by comparable amounts of sorbed water in these materials.

The hydroxyl group configuration in the HEMA:GMA:GMAOH materials influences salt sorption, diffusivity, and permeability. Investigating this effect using materials of comparable water content reveals unique structure property relationships. Distributing the hydroxyl groups more evenly throughout the polymer (i.e., on the HEMA side chain versus the vicinal diol of the GMAOH side chain) appears to suppress salt sorption and diffusion coefficients. This result may suggest more broadly that distributed hydrophilic functionality may be advantageous for desalination membrane materials.

### 6.2.3. Microwave Dielectric Spectroscopy

To further explore the underpinnings of the salt transport property results discussed in the previous section, we characterized the dielectric properties of the hydrated HEMA:GMA:GMAOH co-polymers. We performed the analysis in the microwave frequency range where dipolar relaxation motions of water molecules can be probed.<sup>22-27</sup> The relative permittivity properties of these materials provide insight into the thermodynamic environment of the polymer and, thus, salt sorption properties.<sup>2-4, 28-32</sup>

We fit the HEMA:GMA:GMAOH relative permittivity data (Figure 6.3) to a single Debye relaxation process to determine the static permittivity (i.e., static dielectric constant) of the

material.<sup>1, 33</sup> Though the single Debye relaxation model is likely an oversimplified description of dipolar relaxations in these hydrated polymers (i.e., agreement between the data and the single Debye relaxation is not perfect), this approach provides a uniform method to approximate the static permittivity properties (i.e., the value of the  $\epsilon'$  plateau at low frequency) of the materials.<sup>1</sup> The static permittivity is useful for quantifying the extent of water dipole relaxation and for modeling ion sorption thermodynamics in hydrated polymers.<sup>1, 2, 4</sup>

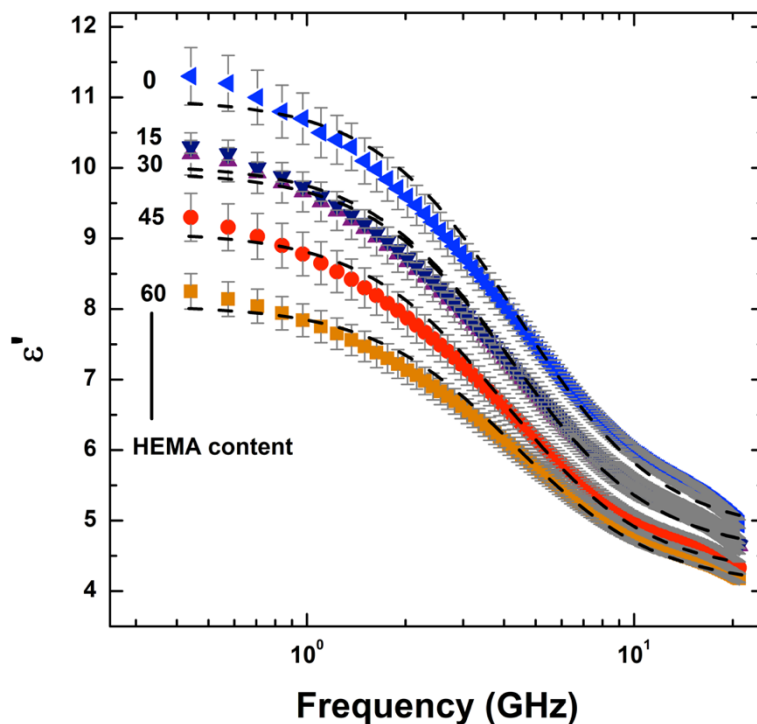


**Figure 6.3.** Frequency-dependent relative permittivity,  $\epsilon'$ , data for the HEMA:GMA:GMAOH co-polymers. The data sets are labeled with the HEMA co-monomer composition of the pre-polymerization solution used to prepare each copolymer. Dashed curves are a single Debye relaxation fit to the measured data. All measurements were made at  $22 \pm 1$  °C, and the uncertainty was taken as one standard deviation from the mean of three measurements.

The single Debye relaxation fitting process revealed that the static permittivity values of the HEMA:GMA:GMAOH materials decreased from 11.0, 10.0, 9.9, 9.1, to 8.1 as HEMA content increased from 0, 15, 30, 45, to 60%. It is important to note, again, that the water content of all of the co-polymers was statistically indistinguishable. This result is consistent with previous work

suggesting that polymer chemistry (and not water content alone) plays an important role in determining the dielectric properties of hydrated polymers.<sup>1</sup>

The observed decrease in the magnitude of the relative permittivity and the regressed static permittivity properties as the HEMA content of the co-polymer increased could be interpreted as a reduction in the dielectric constant of the co-polymer as HEMA content increases. Consistent with electrostatic theory, lower dielectric constant materials often exclude salt to a greater extent than higher dielectric constant materials.<sup>1,4</sup> As such, the relative permittivity data shown in [Figure 6.3](#) are qualitatively consistent with the salt sorption data reported in [Table 6.2](#) as the relative permittivity and salt sorption coefficient decreased as the HEMA content of HEMA:GMA:GMAOH increased.

Another molecular interpretation of the data in [Figure 6.3](#) is that dipolar relaxation processes are weaker, or less energy is dissipated during the dipolar relaxations, in materials that contain more HEMA co-monomer. We believe this result may suggest that transitioning from a vicinal diol-based co-polymer to a system where hydroxyl groups are more distributed throughout the polymer matrix may have the effect of slowing water molecule motions within the hydrated co-polymer. This result is also consistent with the observed reduction in salt diffusion coefficient values as the HEMA content of the co-polymer increases ([Figure 6.2B](#)).

#### **6.2.4. State of Water Analysis**

The dielectric permittivity data discussed in the previous section suggest that different states of water may exist within the co-polymers and mobility of sorbed water in each sample may be affected by the configuration of hydroxyl groups in the polymer. Several studies have investigated the state of water in hydrated polymers.<sup>1, 25, 34-42</sup> Many of these studies use differential

scanning calorimetry (DSC) to quantify the state of water in hydrated polymers, and we applied that approach to the HEMA:GMA:GMAOH materials.

All of the thermograms for the HEMA:GMA:GMAOH co-polymers (Figure 6.4) indicated the presence of freezable sorbed water (i.e., we observed a melting transition at 0 °C for each material). We calculated the amount of freezable and non-freezable water sorbed in the co-polymers, and freezable water content decreased from 2.3 to 0.9% as HEMA content increased (Table 6.3). Non-freezable water content remained similar among all of the co-polymers (Table 6.3) presumably because the concentration of hydroxyl groups only decreased slightly as HEMA content increased (Table 6.1).

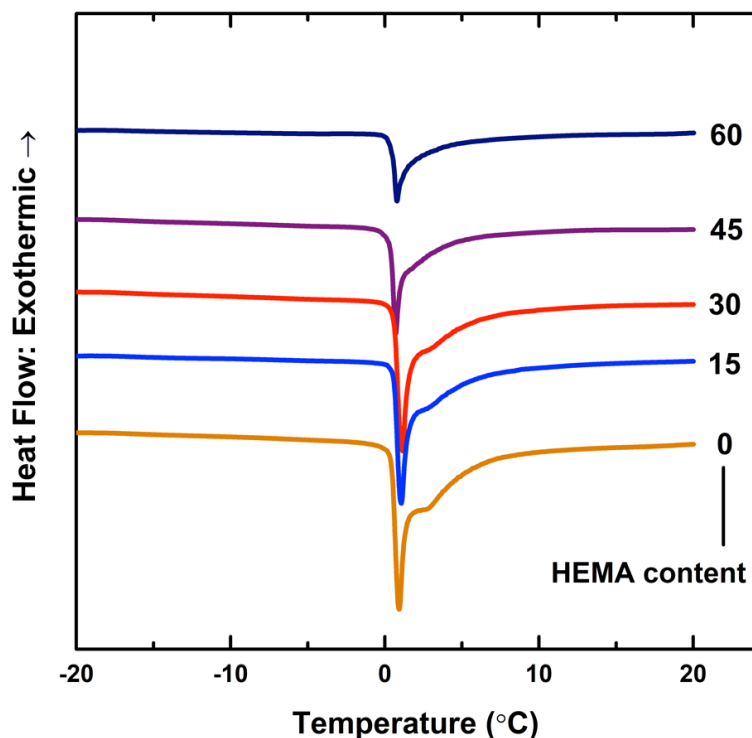


**Figure 6.4.** Differential scanning calorimetry (DSC) thermograms for the hydrated GMA:HEMA:GMAOH materials. The HEMA co-monomer composition of the pre-polymerization solution used to prepare each co-polymer is reported for each data set.

**Table 6.3.** The distribution of freezable and non-freezable water in the HEMA:GMA:GMAOH materials was calculated using water uptake (Table 6.1) and DSC data. The sum of  $w_f$  and  $w_{nf}$  is equivalent to the total water uptake of the material. The co-polymer composition is reported as in Figure 2.4.

HEMA:GMA:GMAOH Composition (by mass)	$W_f$ (%)	$W_{nf}$ (%)
<b>0:60:40</b>	2.3	21.2
<b>15:55:30</b>	1.9	22.3
<b>30:50:20</b>	1.8	21.7
<b>45:45:10</b>	1.2	22.3
<b>60:40:0</b>	0.9	22.4

State of water analysis suggests that materials with more HEMA had less freezable water than the materials containing more GMAOH. As such, the more distributed hydroxyl group configuration in the HEMA-rich materials may promote stronger water-polymer interactions. These interactions could reduce the likelihood of forming water clusters that contain freezable (or bulk-like) water; such clusters may be more favorable in the vicinal diol-rich materials that contain more GMAOH compared to HEMA. Formation of such bulk-like water clusters may reduce transport selectivity, so engineering materials to have more distributed functional groups throughout the polymer matrix may favor transport selectivity, which is critical for desalination applications.<sup>15, 43</sup>

The decrease in the HEMA:GMA:GMAOH apparent salt diffusion coefficient with increasing HEMA content (Figure 6.2B) may be the result of less freezable water (i.e., bulk-like water) clustering around the hydroxyl groups in the HEMA-rich materials. To illustrate this point, we calculated the freezable (i.e., bulk-like) water content per equivalent of hydroxyl group in the co-polymers, and increasing the HEMA content of the pre-polymerization solution from 0 to 60% by mass caused the amount of freezable water, in the co-polymer film, per equivalent of hydroxyl group to decrease by more than a factor of 2 (See Appendix E for additional details). This result suggests that freezable water content may be suppressed by preparing polymers with more

distributed hydrophilic functional groups. Such a situation could also result in more tortuous transport pathways,<sup>1,44</sup> which could impact salt diffusivity properties.

Additionally, the state of water results are consistent with the dielectric permittivity analysis (Figure 6.3) as they provide quantitative insight into the lower static permittivity of higher HEMA content materials. A more evenly distributed hydroxyl group configuration may allow water to interact with the polymer backbone to a greater extent, and this situation could reduce freezable water content compared to the situation where hydroxyl groups are situated closer together (i.e., the GMAOH-rich materials). In other polymers, freezable water content and relative permittivity properties appear to be related,<sup>1</sup> so the simultaneous reduction in freezable water content and relative permittivity observed in these materials, as HEMA content increases, is consistent with previously observed phenomena.

This study focused on salt transport properties, but water transport properties are also important for desalination applications. The water permeability, like salt permeability, can be described using the solution-diffusion model (i.e., water permeability is taken as the product of the water sorption coefficient and an apparent water diffusion coefficient).<sup>20, 45</sup> The slowing of water molecule motions, suggested by the dielectric permittivity data and state of water analysis presented here, cause a decrease in the apparent water diffusion coefficient reported in a separate study.<sup>15</sup> Importantly, however, the water sorption coefficient (unlike the salt sorption coefficient) remains constant as the HEMA content of the co-polymer increases. Therefore, the salt permeability decreases to a greater extent than the water permeability. As such, the water/salt selectivity, which is coupled to salt rejection and important for desalination applications, increases as the co-polymer composition shifts from the vicinal diol-rich material to the HEMA-rich co-polymer with more evenly distributed hydroxyl groups.<sup>15</sup>

### 6.3. Conclusions

The molecular configuration of hydroxyl groups in a series of equivalent water content methacrylate-based HEMA:GMA:GMAOH co-polymers influences salt transport properties. Shifting from a vicinal diol-rich hydroxyl group configuration (GMAOH-rich co-polymer) to a configuration where only a single hydroxyl group is present on the co-polymer side chain (HEMA-rich co-polymer) leads to a reduction in salt sorption and permeability coefficients, which is favorable for desalination membrane applications. The observed reduction in salt sorption as the HEMA content of the co-polymer increases is consistent with a simultaneous reduction in the relative permittivity (or dielectric constant) and the freezable water content of the hydrated co-polymer. A reduction in the apparent salt diffusion coefficient as the HEMA content of the co-polymer increases is also consistent with a hydrogen bonding environment where water molecules interact to a greater extent with the polymer backbone, and both of these conditions are consistent with the observed reduction in relative permittivity and freezable water content as the HEMA content of the co-polymer increased. These results suggest that salt transport properties can be engineered by exercising molecular control over functional group position in hydrated polymers. The results suggest that a more distributed functional group configuration may facilitate low rates of salt transport, which could be a viable strategy for preparing water/salt selective polymers for desalination membrane applications.

### 6.4. References

1. Chang, K.; Luo, H.; Geise, G. M., Water content, relative permittivity, and ion sorption properties of polymers for membrane desalination. *Journal of Membrane Science* **2019**, *574*, 24-32.

2. Yaroshchuk, A. E., Dielectric exclusion of ions from membranes. *Advances in Colloid and Interface Science* **2000**, *85* (2), 193-230.
3. Yaroshchuk, A. E., Non-steric mechanisms of nanofiltration: Superposition of Donnan and dielectric exclusion. *Separation and Purification Technology* **2001**, *22-23*, 143-158.
4. Zhang, H.; Geise, G. M., Modeling the water permeability and water/salt selectivity tradeoff in polymer membranes. *Journal of Membrane Science* **2016**, *520*, 790-800.
5. Chang, K.; Xue, T.; Geise, G. M., Increasing salt size selectivity in low water content polymers via polymer backbone dynamics. *Journal of Membrane Science* **2018**, *552*, 43-50.
6. Chang, K.; Korovich, A.; Xue, T.; Morris, W. A.; Madsen, L. A.; Geise, G. M., Influence of rubbery versus glassy backbone dynamics on multiscale transport in polymer membranes. *Macromolecules* **2018**, *51* (22), 9222-9233.
7. Luo, H.; Aboki, J.; Ji, Y.; Guo, R.; Geise, G. M., Water and salt transport properties of triptycene-containing sulfonated polysulfone materials for desalination membrane applications. *ACS Applied Materials & Interfaces* **2018**, *10* (4), 4102-4112.
8. Geise, G. M.; Lee, H.-S.; Miller, D. J.; Freeman, B. D.; McGrath, J. E.; Paul, D. R., Water purification by membranes: The role of polymer science. *Journal of Polymer Science Part B: Polymer Physics* **2010**, *48* (15), 1685-1718.
9. Geise, G. M.; Paul, D. R.; Freeman, B. D., Fundamental water and salt transport properties of polymeric materials. *Progress in Polymer Science* **2014**, *39* (1), 1-42.
10. Kamcev, J.; Freeman, B. D., Charged polymer membranes for environmental/energy applications. *Annual Review of Chemical and Biomolecular Engineering* **2016**, *7* (1), 111-133.
11. Hickner, M. A., Ion-containing polymers: New energy & clean water. *Materials Today* **2010**, *13* (5), 34-41.

12. Mackie, J. S.; Meares, P., The diffusion of electrolytes in a cation-exchange resin membrane I. Theoretical. *Proceedings of the Royal Society of London. Series A. Mathematical and Physical Sciences* **1955**, 232 (1191), 498-509.
13. Yasuda, H.; Lamaze, C. E.; Ikenberry, L. D., Permeability of solutes through hydrated polymer membranes. Part I. Diffusion of sodium chloride. *Die Makromolekulare Chemie* **1968**, 118 (1), 19-35.
14. Yasuda, H.; Lamaze, C. E.; Peterlin, A., Diffusive and hydraulic permeabilities of water in water-swollen polymer membranes. *Journal of Polymer Science Part A-2: Polymer Physics* **1971**, 9 (6), 1117-1131.
15. Luo, H.; Chang, K.; Bahati, K.; Geise, G. M., Engineering selective desalination membranes via molecular control of polymer functional groups. *Environmental Science & Technology Letters* **2019**.
16. Tan, J.; Liu, D.; Bai, Y.; Huang, C.; Li, X.; He, J.; Xu, Q.; Zhang, X.; Zhang, L., An insight into aqueous photoinitiated polymerization-induced self-assembly (photo-PISA) for the preparation of diblock copolymer nano-objects. *Polymer Chemistry* **2017**, 8 (8), 1315-1327.
17. Lama, R. F.; Lu, B. C. Y., Excess thermodynamic properties of aqueous alcohol solutions. *Journal of Chemical & Engineering Data* **1965**, 10 (3), 216-219.
18. Batov, D. V.; Zaichikov, A. M.; Slyusar, V. P.; Korolev, V. P., Enthalpies of mixing and state of components in aqueous-organic mixtures with nets of hydrogen bonds. *Russian Journal of General Chemistry* **2001**, 71 (8), 1208-1214.
19. Bevington, P. R.; Robinson, D. K., Chapter 4: Propagation of Errors. In *Data reduction and error analysis for the physical sciences*, McGraw Hill: New York, 2003; pp 56-65.
20. Wijmans, J. G.; Baker, R. W., The solution-diffusion model: A review. *Journal of Membrane Science* **1995**, 107 (1), 1-21.
21. Xie, W.; Ju, H.; Geise, G. M.; Freeman, B. D.; Mardel, J. I.; Hill, A. J.; McGrath, J. E., Effect of free volume on water and salt transport properties in directly copolymerized

disulfonated poly(arylene ether sulfone) random copolymers. *Macromolecules* **2011**, *44* (11), 4428-4438.

22. Paddison, S. J.; Reagor, D. W.; Zawodzinski Jr, T. A., High frequency dielectric studies of hydrated Nafion®. *Journal of Electroanalytical Chemistry* **1998**, *459* (1), 91-97.

23. Lu, Z.; Lanagan, M.; Manias, E.; Macdonald, D. D., Two-port transmission line technique for dielectric property characterization of polymer electrolyte membranes. *The Journal of Physical Chemistry B* **2009**, *113* (41), 13551-13559.

24. Paddison, S.; Bender, G.; Zawodzinski Jr, T. A., The microwave region of the dielectric spectrum of hydrated Nafion® and other sulfonated membranes. *Journal of New Materials for Electrochemical Systems* **2000**, *3*, 293-302.

25. Lu, Z.; Polizos, G.; Macdonald, D. D.; Manias, E., State of water in perfluorosulfonic ionomer (Nafion® 117) proton exchange membranes. *Journal of The Electrochemical Society* **2008**, *155* (2), B163-B171.

26. Lu, Z.; Manias, E.; Macdonald, D. D.; Lanagan, M., Dielectric relaxation in dimethyl sulfoxide/water mixtures studied by microwave dielectric relaxation spectroscopy. *The Journal of Physical Chemistry A* **2009**, *113* (44), 12207-12214.

27. Smith, G.; Duffy, A. P.; Shen, J.; Olliff, C. J., Dielectric relaxation spectroscopy and some applications in the pharmaceutical sciences. *Journal of Pharmaceutical Sciences* **1995**, *84* (9), 1029-1044.

28. Glueckauf, E., On the mechanism of osmotic desalting with porous membranes. *Proceedings of the First International Symposium on Water Desalination* **1967**, 143-150.

29. Anderson, J. E.; Pusch, W., The membrane/water partition coefficients of ions: Electrostatic calculations of dielectric heterogeneity. *Berichte der Bunsengesellschaft für physikalische Chemie* **1976**, *80* (9), 846-849.

30. Freger, V.; Bason, S., Characterization of ion transport in thin films using electrochemical impedance spectroscopy: I. Principles and theory. *Journal of Membrane Science* **2007**, *302* (1), 1-9.
31. Kamcev, J.; Galizia, M.; Benedetti, F. M.; Jang, E.-S.; Paul, D. R.; Freeman, B. D.; Manning, G. S., Partitioning of mobile ions between ion exchange polymers and aqueous salt solutions: Importance of counter-ion condensation. *Physical Chemistry Chemical Physics* **2016**, *18* (8), 6021-6031.
32. Kamcev, J.; Paul, D. R.; Manning, G. S.; Freeman, B. D., Predicting salt permeability coefficients in highly swollen, highly charged ion exchange membranes. *ACS Applied Materials & Interfaces* **2017**, *9* (4), 4044-4056.
33. Lu, Z., State of water in perfluorosulfonic acid membranes studied by microwave dielectric relaxation spectroscopy. **2006**, *Ph.D. Thesis, Department of Materials Science and Engineering, The Pennsylvania State University, University Park, Pennsylvania.*
34. Tran, T.; Lin, C.; Chaurasia, S.; Lin, H., Elucidating the relationship between states of water and ion transport properties in hydrated polymers. *Journal of Membrane Science* **2019**, *574*, 299-308.
35. Paddison, S. J., Proton conduction mechanisms at low degrees of hydration in sulfonic acid-based polymer electrolyte membranes. *Annual Review of Materials Research* **2003**, *33* (1), 289-319.
36. Mauritz, K. A.; Moore, R. B., State of understanding of Nafion®. *Chemical Reviews* **2004**, *104* (10), 4535-4586.
37. Kreuer, K.-D.; Paddison, S. J.; Spohr, E.; Schuster, M., Transport in proton conductors for fuel-cell applications: Simulations, elementary reactions, and phenomenology. *Chemical Reviews* **2004**, *104* (10), 4637-4678.
38. Elliott, J. A.; Paddison, S. J., Modelling of morphology and proton transport in PFSA membranes. *Physical Chemistry Chemical Physics* **2007**, *9* (21), 2602-2618.

39. Quinn, F. X.; Kampff, E.; Smyth, G.; McBrierty, V. J., Water in hydrogels. 1. A study of water in poly(N-vinyl-2-pyrrolidone/methyl methacrylate) copolymer. *Macromolecules* **1988**, *21* (11), 3191-3198.
40. Hodge, R. M.; Bastow, T. J.; Edward, G. H.; Simon, G. P.; Hill, A. J., Free volume and the mechanism of plasticization in water-swollen poly(vinyl alcohol). *Macromolecules* **1996**, *29* (25), 8137-8143.
41. Yoshida, H.; Miura, Y., Behavior of water in perfluorinated ionomer membranes containing various monovalent cations. *Journal of Membrane Science* **1992**, *68* (1), 1-10.
42. Shinyashiki, N.; Shimomura, M.; Ushiyama, T.; Miyagawa, T.; Yagihara, S., Dynamics of water in partially crystallized polymer/water mixtures studied by dielectric spectroscopy. *The Journal of Physical Chemistry B* **2007**, *111* (34), 10079-10087.
43. Werber, J. R.; Deshmukh, A.; Elimelech, M., The critical need for increased selectivity, not increased water permeability, for desalination membranes. *Environmental Science & Technology Letters* **2016**, *3* (4), 112-120.
44. Kreuer, K. D., On the development of proton conducting polymer membranes for hydrogen and methanol fuel cells. *Journal of Membrane Science* **2001**, *185* (1), 29-39.
45. Paul, D. R., Reformulation of the solution-diffusion theory of reverse osmosis. *Journal of Membrane Science* **2004**, *241* (2), 371-386.

## Chapter 7: Engineering Selective Desalination Membranes via Molecular Control of Polymer Functional Groups<sup>\*\*\*\*\*</sup>

### 7.1. Introduction

The ability to precisely place functional groups along a polymer backbone, with a high degree of molecular control over functional group position, is becoming increasingly viable.<sup>1,2</sup> This structural control, facilitated by advances in synthesis capabilities, could be important for engineering advanced desalination membranes. Little is known, however, about how functional group placement within a polymer influences water/salt selectivity.

We report the desalination (i.e., water/salt) selectivity properties of a series of model materials where the distribution of hydroxyl functional groups along the polymer backbone was varied from a clustered to a more uniform configuration. Importantly, this series of materials was prepared such that the membrane water content did not change as the distribution of the hydroxyl groups changed. Membrane water content has a significant influence on water/salt selectivity properties,<sup>3,4</sup> so the ability to vary the distribution of functional groups within the material without perturbing the water content enabled us to ascribe the observed results to changes in the functional group configuration.

Shifting the functional group configuration to space the hydroxyl groups out more evenly (compared to the more clustered configuration) resulted in increased water/salt permeability selectivity, which is directly related to desalination-critical salt rejection.<sup>5</sup> This increase in selectivity was largely driven by sorption, or thermodynamic, effects. The results suggest that an

---

<sup>\*\*\*\*\*</sup> This section has been adapted with permission from: Luo, H.; Chang, K.; Bahati, K.; Geise, G. M., Engineering selective desalination membranes via molecular control of polymer functional groups. *Environmental Science & Technology Letters* **2019**, 6 (8), 462-466.

even distribution of hydrophilic chemical functionality in polymers may lead to more selective membranes to address global demand for desalinated water.

## 7.2. Results and Discussion

Each composition of HEMA:GMA:GMAOH had equivalent water content ([Table 6.1](#)). Water content affects the transport (and, thus, desalination) selectivity of hydrated polymers, and increases in water content often correlate with decreases in selectivity.<sup>3, 4</sup> Therefore, preparing materials with equivalent water content is critical for decoupling the influence of functional group configuration on water/salt transport selectivity from the influence of changing water content on water/salt transport selectivity.

The equivalent water content of this series of HEMA:GMA:GMAOH co-polymers likely results from subtle changes in the extent of cross-linking and hydroxyl group content across the series of co-polymers. These changes were estimated to be reasonably small, as discussed in [Section F.1](#). Ultimately, maintaining equivalent water content in the series of materials was prioritized due to the strong influence of water content on the water and salt transport properties of hydrated polymers.<sup>3, 4</sup>

We compared the HEMA:GMA:GMAOH transport properties to those of cross-linked poly(ethylene glycol) diacrylate (PEG) hydrogels, as these materials also preferentially transport water over salt via a solution-diffusion mechanism.<sup>6</sup> The water content of these hydrogels can be manipulated by changing the ethylene glycol chain length or by adding a diluent to the pre-polymerization mixture.<sup>6</sup> Thus, the PEG materials illustrate how transport properties change with water content to contrast the situation in equivalent water content HEMA:GMA:GMAOH.

The water/salt transport selectivity is defined as the ratio of water to salt permeability,  $P_w/P_s$ , sorption  $K_w/K_s$ , or diffusion,  $D_w/D_s$ , coefficients, and the three selectivity values are related via the solution-diffusion model:<sup>3</sup>

$$P_w/P_s = (K_w/K_s) \times (D_w/D_s) \quad (7.1)$$

This water/salt permeability selectivity can be directly related to salt rejection, which is a critical characteristic of effective desalination membranes.<sup>5</sup> The salt rejection,  $\mathbf{R}$ , is defined as the salt concentration reduction from the bulk solution on the feed side of the membrane,  $C_{s,feed}$ , to the bulk solution on the permeate (or product) side of the membrane normalized by  $C_{s,feed}$  and depends on the water/salt permeability selectivity:

$$\mathbf{R} = \frac{C_{s,feed} - C_{s,permeate}}{C_{s,feed}} = \frac{\frac{P_w}{P_s} \frac{V_w}{RT} (\Delta p - \Delta \pi)}{1 + \frac{P_w}{P_s} \frac{V_w}{RT} (\Delta p - \Delta \pi)} \quad (7.2)$$

where  $V_w$  is the molar volume of water,  $\Delta p$  is the hydraulic pressure difference across the membrane,  $\Delta \pi$  is the osmotic pressure difference across the membrane,  $R$  is the ideal gas constant, and  $T$  is the absolute temperature.<sup>3</sup>

Water/salt permeability selectivity depends on a combination of both water/salt sorption and diffusivity selectivity properties (Equation 7.1). Functional group configuration significantly influenced the water/salt sorption selectivity of HEMA:GMA:GMAOH (Figure 7.1A). A distributed hydroxyl group configuration (HEMA-rich co-polymer) led to higher sorption selectivity compared to a vicinal-diol rich configuration (GMAOH-rich co-polymer), and this result can be attributed to more effective exclusion of salt from the HEMA-rich co-polymer compared to the GMAOH-rich co-polymer.

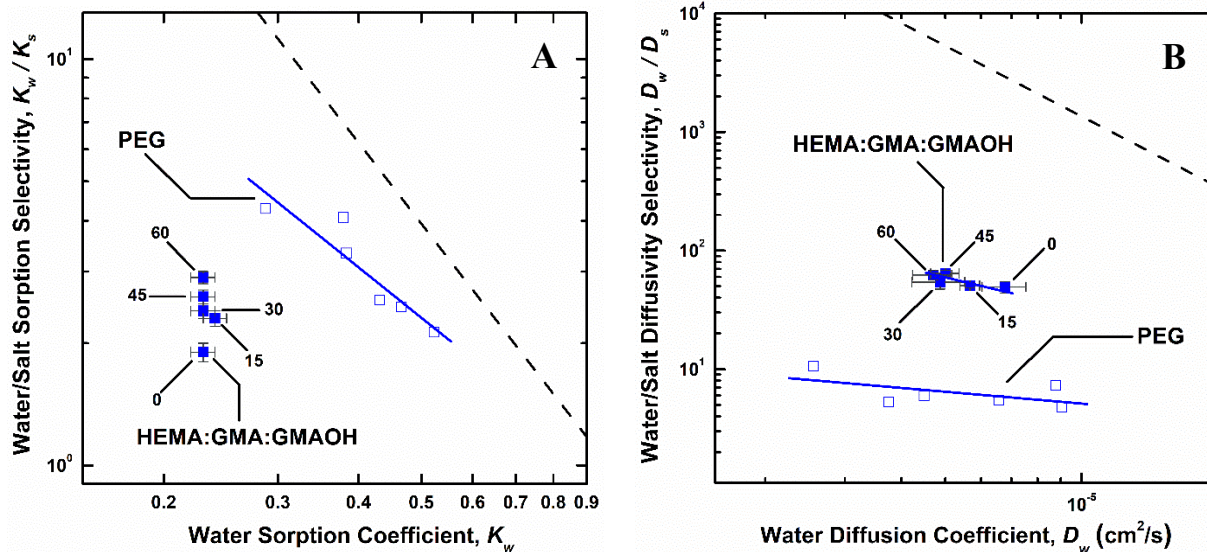


**Figure 7.1.** Water/salt sorption selectivity (A) and water/salt diffusivity selectivity (B) as a function of water sorption coefficient and apparent water diffusion coefficient, respectively, for HEMA:GMA:GMAOH (■) and PEG (□)<sup>6</sup> materials. For HEMA:GMA:GMAOH, the HEMA co-monomer composition of the pre-polymerization solution used to prepare the co-polymer is reported for each data point. The dashed lines represent reported empirical sorption (left) and diffusivity (right) trade-off frontiers for desalination membrane materials,<sup>7,8</sup> and the solid lines are least-squares fits to the data.

Comparing HEMA:GMA:GMAOH water/salt sorption selectivity with that of poly(ethylene glycol) diacrylate (PEG) hydrogels, we observed that the HEMA:GMA:GMAOH data points move vertically upwards as HEMA content increases in a manner different from the PEG materials (Figure 7.1A). The PEG result is expected if water content primarily drives sorption selectivity properties.<sup>6</sup> The HEMA:GMA:GMAOH result suggests that polymer chemistry, not changing water content, is responsible for the change in sorption selectivity of HEMA:GMA:GMAOH. Thus, preparing polymers with a distributed functional group configuration may be a viable strategy to increase the water/salt sorption selectivity.

The HEMA:GMA:GMAOH materials are approximately an order of magnitude more water/salt diffusion selective compared to the PEG materials (Figure 7.1B). This result may be due to the glassy nature of hydrated HEMA:GMA:GMAOH compared to the rubbery nature of PEG

(see [Section F.1.3](#)).<sup>9</sup> More rigid (glassy) polymer backbones are often more diffusion selective compared to more flexible (rubbery) polymer backbones.<sup>10-12</sup>

The apparent water diffusion coefficient decreases and the water/salt diffusivity selectivity increases as the co-polymer composition shifts toward a more HEMA rich (or distributed hydroxyl group configuration). This observed trend is similar to that observed for PEG. The water content of the PEG materials was varied systematically, and the explanation for the observed relationship between water/salt diffusivity selectivity and water diffusion coefficient is that reduction in the free volume of the polymer (as water content decreases) causes a general reduction in diffusion that influences the larger hydrated ions to a greater extent than water.<sup>6</sup> In HEMA:GMA:GMAOH, the change in co-monomer composition (and thus, distribution of hydroxyl groups) results in a situation where water diffusion slows as HEMA content increases. This reduction in water diffusivity is accompanied by an increase in water/salt diffusion selectivity that is similar in proportion to that of PEG. Therefore, changes in water diffusivity, due to compositional changes in the HEMA:GMA:GMAOH materials, may influence water/salt diffusivity selectivity in a manner similar to that in the free volume-based explanation where water diffusion depends strongly on free volume.<sup>3,4</sup>

Water/salt diffusivity selectivity is affected to a lesser extent, compared to water/salt sorption selectivity, by changing the HEMA content of the pre-polymerization solution. The water/salt diffusivity selectivity increases by 26% over the range of HEMA compositions considered. The water/salt sorption selectivity, by comparison, increases by 53% over the range of HEMA compositions considered. Importantly, the 53% increase in sorption selectivity comes without a change in the water sorption coefficient, which as discussed subsequently, means that,

as co-polymer composition changes, the water permeability will not change because of sorption effects.

The decrease in the apparent water diffusivity as the co-polymer composition changes at constant water content could be considered unexpected, as diffusivity in hydrated polymers is often a strong function of water content.<sup>3, 4, 13, 14</sup> Dielectric permittivity properties, however, provide insight into the observed water diffusivity. As further discussed in [Section F.3](#), the dielectric loss spectra can be interpreted in terms of time constants, which describe the dipole relaxation dynamics of different modes of water motion, and the dielectric strengths of those relaxations, which describe the relative amount of water in the material that is participating in each relaxation mode.<sup>15</sup>

Dielectric spectroscopy suggests three populations of dipolar water motion: highly restricted motion that relaxes on an order 0.1 ns timescale, less restricted motion that relaxes with a time constant of approximately 45 ps, and non-restricted (i.e., bulk water) motion that relaxes with a time constant of 8.8 ps (see [Appendix F](#) for additional discussion). In general, the dielectric strength associated with each mode of motion decreases as HEMA content increases ([Table F.2](#)), though the reduction is more pronounced for the non-restricted relaxation mode compared to the other two modes. This decrease in the dielectric strength associated with all three relaxation modes, coupled with the statistically equivalent water content of the materials, suggests that increasing HEMA content promotes water-polymer interactions that relax at frequencies lower than that probed in our experiments.

An example of such interactions would be water that is very tightly associated with the hydroxyl groups. Such (effectively immobile) water will not be detected by dielectric spectroscopy in the frequency range considered here.<sup>16</sup> As such, the dielectric strength data suggests that

distributing the hydroxyl groups in the polymer causes more water to tightly associate with hydroxyl groups compared to the situation in the vicinal diol-rich materials.

This molecular picture is consistent with a steric explanation suggesting that water molecules may be able to hydrate the hydroxyl group on a HEMA side chain to a greater extent compared to the more sterically hindered GMAOH side chain. This explanation is also consistent with estimates of the enthalpy of hydration for the hydroxyl groups on the side chains (see [Section F.4](#)). Ultimately, this reduction in water motion within the polymer appears to have a similar effect on both water and salt diffusion as reducing the water content of the polymer (as supported by the similar slopes of the data in [Figure 7.1B](#)).

Primarily due to the strong increase in water/salt sorption selectivity at constant water content, the HEMA:GMA:GMAOH water/salt permeability selectivity increases as the HEMA content of the pre-polymerization solution used to prepare the materials increases ([Figure 7.2](#)). A distributed hydroxyl group configuration (HEMA-rich) is more selective for water over salt transport compared to the vicinal-diol rich configuration (GMAOH-rich). The overall selectivity of the HEMA:GMA:GMAOH series of materials is greater than that of the PEG materials due to the previously discussed differences in the diffusivity selectivity properties.

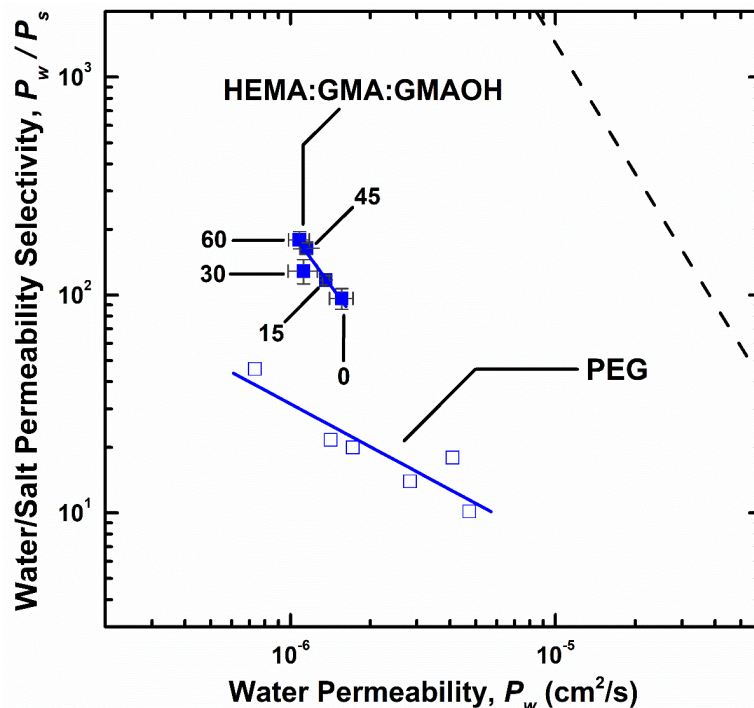


**Figure 7.2.** Water/salt permeability selectivity as a function of diffusive water permeability for HEMA:GMA:GMAOH (■) and PEG (□)<sup>6</sup> materials. For HEMA:GMA:GMAOH, the HEMA co-monomer composition of the pre-polymerization solution used to prepare the co-polymer is reported for each data point. The dashed line represents a reported empirical permeability trade-off frontier for desalination membrane materials,<sup>7,8</sup> and the solid lines are least-squares fits to the data.

The PEG materials exhibit a typical tradeoff relationship whereby water/salt selectivity tends to decrease as materials become more permeable to water. This tradeoff is often observed in cases where the water content of a series of materials is varied systematically.<sup>8</sup> In these cases, the higher water content polymers tend to have higher water permeability and lower water/salt selectivity compared to the lower water content polymers.

The HEMA:GMA:GMAOH materials suffer less of a reduction in the diffusive water permeability as water/salt selectivity increases compared to the PEG materials (i.e., the slope of the HEMA:GMA:GMAOH dashed line is steeper than that of the PEG dashed line in Figure 7.2). This result stems from the equivalent water content nature of the HEMA:GMA:GMAOH series of

materials and the fact that both water/salt sorption and diffusivity selectivity increase with increasing content of HEMA in the pre-polymerization solution.

### 7.3. Conclusions

Chemical modification of a series of water content equivalent co-polymers, from a vicinal diol-rich to a distributed hydroxyl group-rich configuration, increased water/salt permeability selectivity with a smaller water permeability penalty compared to that often observed in hydrated polymers. These results, obtained using a model series of co-polymers, suggest that controlling the spatial arrangement of functional groups in hydrated membrane materials may be important for engineering highly selective polymers for desalination applications. The results on these model materials represent a step toward establishing general water and salt transport structure-property relationships for membrane materials including polymers that are more chemically similar to commercial desalination membranes than those materials considered here. The results suggest that distributed hydrophilic functional groups may lead to increased selectivity and may represent a strategy for improving water/salt selectivity of advanced membrane materials to address global water shortages.

### 7.4. References

1. Solleder, S. C.; Zengel, D.; Wetzel, K. S.; Meier, M. A. R., A scalable and high-yield strategy for the synthesis of sequence-defined macromolecules. *Angewandte Chemie International Edition* **2016**, *55* (3), 1204-1207.
2. Lutz, J.-F., Defining the field of sequence-controlled polymers. *Macromolecular Rapid Communications* **2017**, *38* (24), 1700582.
3. Geise, G. M.; Paul, D. R.; Freeman, B. D., Fundamental water and salt transport properties of polymeric materials. *Progress in Polymer Science* **2014**, *39* (1), 1-42.

4. Yasuda, H.; Lamaze, C. E.; Ikenberry, L. D., Permeability of solutes through hydrated polymer membranes. Part I. Diffusion of sodium chloride. *Die Makromolekulare Chemie* **1968**, *118* (1), 19-35.
5. Baker, R. W., *Membrane Technology and Applications*. 3rd ed.; Wiley: New York, 2012.
6. Ju, H.; Sagle, A. C.; Freeman, B. D.; Mardel, J. I.; Hill, A. J., Characterization of sodium chloride and water transport in crosslinked poly(ethylene oxide) hydrogels. *Journal of Membrane Science* **2010**, *358* (1), 131-141.
7. Zhang, H.; Geise, G. M., Modeling the water permeability and water/salt selectivity tradeoff in polymer membranes. *Journal of Membrane Science* **2016**, *520*, 790-800.
8. Geise, G. M.; Park, H. B.; Sagle, A. C.; Freeman, B. D.; McGrath, J. E., Water permeability and water/salt selectivity tradeoff in polymers for desalination. *Journal of Membrane Science* **2011**, *369* (1), 130-138.
9. Ju, H.; McCloskey, B. D.; Sagle, A. C.; Kusuma, V. A.; Freeman, B. D., Preparation and characterization of crosslinked poly(ethylene glycol) diacrylate hydrogels as fouling-resistant membrane coating materials. *Journal of Membrane Science* **2009**, *330* (1), 180-188.
10. Chang, K.; Xue, T.; Geise, G. M., Increasing salt size selectivity in low water content polymers via polymer backbone dynamics. *Journal of Membrane Science* **2018**, *552*, 43-50.
11. Chang, K.; Korovich, A.; Xue, T.; Morris, W. A.; Madsen, L. A.; Geise, G. M., Influence of rubbery versus glassy backbone dynamics on multiscale transport in polymer membranes. *Macromolecules* **2018**, *51* (22), 9222-9233.
12. Paul, D. R.; Yampol'skii, Y. P., *Polymeric gas separation membranes*. CRC Press: Boca Raton, 1994.
13. Yasuda, H.; Ikenberry, L.; Lamaze, C., Permeability of solutes through hydrated polymer membranes. Part II. Permeability of water soluble organic solutes. *Die Makromolekulare Chemie* **1969**, *125* (1), 108-118.

14. Mackie, J. S.; Meares, P., The diffusion of electrolytes in a cation-exchange resin membrane I. Theoretical. *Proceedings of the Royal Society of London. Series A. Mathematical and Physical Sciences* **1955**, 232 (1191), 498-509.
15. Lu, Z.; Polizos, G.; Macdonald, D. D.; Manias, E., State of water in perfluorosulfonic ionomer (Nafion® 117) proton exchange membranes. *Journal of The Electrochemical Society* **2008**, 155 (2), B163-B171.
16. Smith, G.; Duffy, A. P.; Shen, J.; Olliff, C. J., Dielectric relaxation spectroscopy and some applications in the pharmaceutical sciences. *Journal of Pharmaceutical Sciences* **1995**, 84 (9), 1029-1044.

## **Chapter 8: Influence of Salt Concentration on Hydrated Polymer Relative Permittivity and State of Water Properties**

### **8.1. Introduction**

Dielectric permittivity and state of water properties inform insight into molecular interactions between water and the polymer backbone in hydrated polymers.<sup>1-4</sup> For example, relative permittivity properties and freezable water (i.e., bulk-like, or weakly bound water) content generally increase as polymer water content increases.<sup>1</sup> This result stems from greater interaction between water and the other water molecules in high water content polymers compared to the situation in low water content polymers.<sup>1</sup> Other studies suggest that, at equivalent water content, a distributed functional group configuration can suppress the relative permittivity and freezable water content of hydrated polymers and can promote interactions between water and the polymer backbone.<sup>2, 3</sup> These results suggest that polymer chemistry, not water content alone, affects molecular interactions between water and the polymer backbone that will further influence the dielectric permittivity and state of water properties of hydrated polymers.

Some structure–property relationships between polymer chemistry and dielectric permittivity properties in hydrated polymers are beginning to form, the functional relationship between dielectric permittivity properties and the salt concentration of solutions used to equilibrate the polymers remains elusive. This is resulting from studies focused on investigating the influence of polymer chemistry and water content on dielectric permittivity properties of pure water equilibrated polymers.<sup>1-3</sup> In bulk aqueous salt solution, dielectric permittivity properties decrease as salt concentration increases,<sup>5</sup> but it is still unclear how salt concentration of the equilibration solution can influence the molecular interactions between the ions, water, and polymer backbone and, thus, affecting the dielectric permittivity properties of hydrated polymers.

In this study, we report the influence of salt concentration on the relative permittivity, state of water, and sorption properties in a cross-linked glycidyl and glycerol methacrylate-based co-polymer. The exposure of the co-polymer to increasing salt concentration drove the de-swelling and the increasing ion sorption of the material, which is a result that is different from the electrostatic theory and Maxwell Garnett equation predictions. This result suggests competition between ions and water for interactions with the polymer backbone. Such ion–water competition was observed to be more apparent in low water content polymer, where its relative permittivity and bulk-like water content increased as salt concentration increased. At equivalent water content, the static permittivity of the co-polymer was higher when it was exposed to salt solutions as opposed to pure water. This unique observation suggests that the influence of salt concentration on hydrated polymer dielectric permittivity properties is fundamentally different from its influence on aqueous salt solutions. The information obtained from this study can be used to understand the fundamental factors that drive the sorption properties in hydrated polymers.

## **8.2. Results and Discussion**

One of the main goals of this study was to understand how the salt concentration of an aqueous solution equilibrated with a polymer influences relative permittivity and state of water properties of the hydrated polymer. To accomplish this goal, we measured the water uptake, water/salt sorption coefficients, and relative permittivity of pure water and aqueous NaCl solution equilibrated XL-pGMA-z samples. We also performed FT-IR measurements to characterize the state of water in these materials. The results importantly inform how the presence of sorbed salt may affect molecular interactions between the ions, water, and polymer backbone and the relative permittivity and state of water properties of the polymer.

### 8.2.1. Water Uptake

We varied the water content of XL-pGMA-z via acid hydrolysis in a manner consistent with previous work.<sup>1</sup> The control of polymer water content is important to enable meaningful comparison of sorption and dielectric permittivity properties between XL-pGMA-z and between XL-pGMA-z and other uncharged polymers. For all samples, water content decreased as external NaCl concentration increased (Figure 8.1). This result suggests, consistent with observations made on many hydrated polymers, that osmotic de-swelling in XL-pGMA occurs in these materials.<sup>6-8</sup> We also observed similar dry polymer density for all samples, which suggests that the hydrolysis procedure did not significantly affect polymer chain packing (Table G.1).

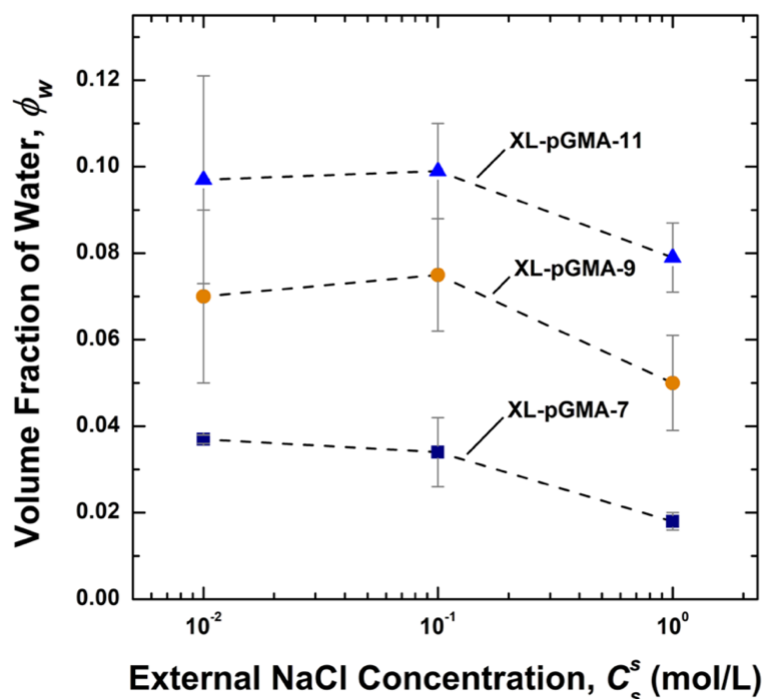


**Figure 8.1.** Volume fraction of water as a function of external NaCl concentration for XL-pGMA-z, where z represents the hydrolysis time in hours, ranging from 7 to 11 hours. The dashed lines are included to guide the eye. All measurements were made at  $22\text{ }^\circ\text{C} \pm 1\text{ }^\circ\text{C}$ , and the uncertainty was taken as one standard deviation from the mean of three measurements.

### 8.2.2. Salt Sorption Properties

The salt sorption properties of hydrated XL-pGMA-z were characterized to investigate the relationship between salt sorption coefficient and external salt concentration. For all samples, we observed that the salt sorption coefficient increased slightly as sample water content and external NaCl concentration increased (Figure 8.2). This result suggests that salt sorption properties of XL-pGMA-z depend on external NaCl concentration. This result is different from observations made on some uncharged polymers, where the salt sorption coefficient was found to be independent of the external salt concentration.<sup>6, 9</sup> The increase in the salt sorption coefficient as water content increased in XL-pGMA-z, on the other hand, is consistent with the observations made on many hydrated polymers.<sup>6, 10, 11</sup>

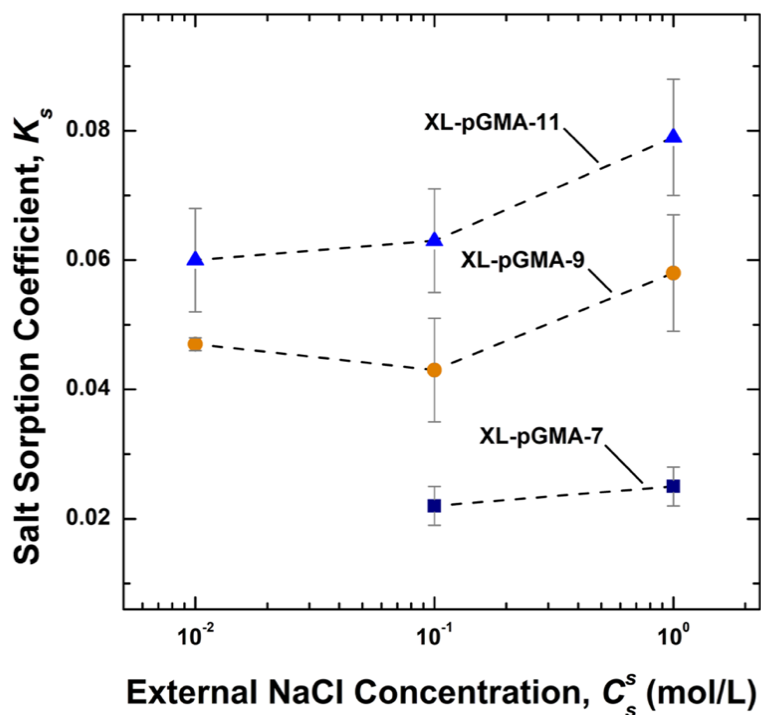


**Figure 8.2.** Salt sorption coefficient as a function of external NaCl concentration for XL-pGMA-z. Salt sorption in XL-pGMA-7 equilibrated with 0.01 mol/L NaCl solution was too low to measure reliably. The dashed lines are included to guide the eye. All measurements were made at  $22 \pm 1$  °C, and the uncertainty was taken as one standard deviation from the mean of three measurements.

In the simplest case (i.e., dilute salt solutions), salt sorption in hydrated polymers may be affected primarily by long range electrostatic forces.<sup>4, 10, 12-14</sup> To describe the influence of these forces on salt sorption, a hydrated polymer could be considered as a homogeneous dielectric medium, and the free energy change associated with movement of an ion from the external solution into the polymer could be taken as the solvation energy barrier,  $\Delta W_s$ , which can be described using the Born model (Equation 5.6). The salt sorption coefficient can subsequently be related to the solvation energy barrier as shown previously (Equation 5.5).<sup>1, 10</sup> While the Born model has known limitations resulting from the dielectric continuum assumption and the representation of the ion size,<sup>12, 14-16</sup> the model can provide qualitative insight into how polymer- and solution-related factors affect ion exclusion in hydrated polymers.<sup>4</sup>

Based on the Born model, one critical factor that affects the extent of ion exclusion in hydrated polymers is the static relative permittivity (i.e., dielectric constant) of the hydrated polymer. This static permittivity, however, is affected by the water content of the polymer (water sorption tends to increase the relative permittivity of the polymer-water mixture).<sup>1, 4</sup> The increase in the static dielectric constant with increasing water content has been described, based on data for some perfluorosulfonic acid polymers, using a linear relationship.<sup>10, 17</sup> While potentially reasonable in the absence of more specific data or guidance from models,<sup>10, 17</sup> the specific chemistry of the polymer can influence the relationship between the relative permittivity and the polymer water content.<sup>1</sup>

The variation of the static dielectric constant of a heterogeneous material can be modeled in terms of the static dielectric constants of the pure components that make up the heterogeneous material. The Maxwell Garnett model, for example, assumes that dilute spherical particles are

dispersed in a continuous polymer phase, and the static dielectric constant of the heterogeneous material, or the hydrated membrane polymer,  $\epsilon_{s,m}$ , can be determined as:<sup>18-21</sup>

$$\frac{\epsilon_{s,m} - \epsilon_{s,p}}{\epsilon_{s,m} + 2\epsilon_{s,p}} = \phi_w \frac{\epsilon_{s,w} - \epsilon_{s,p}}{\epsilon_{s,w} + 2\epsilon_{s,p}} \quad (8.1)$$

where  $\epsilon_{s,p}$  is the static dielectric constant of the dry polymer (i.e., continuous phase) and  $\epsilon_{s,w}$  is the static dielectric constant of water (i.e., dispersed phase). In this case, the Maxwell Garnett equation can be used, with the polymer as the continuous phase and water as the dispersed phase, to describe how the static permittivity of the hydrated polymer varies with the volume fraction of sorbed water. The Maxwell Garnett model describes the functional relationship between the static dielectric constant and the volume fraction of sorbed water in XL-pGMA-z (Figure 8.3). This observation suggests that the Maxwell Garnett equation may be useful for describing the variation in the static permittivity of uncharged network polymers with water content. At high water content (i.e.,  $\phi_w > 0.5$ ), we used the Maxwell Garnett equation with the polymer as the disperse phase and water as the continuous phase to predict the static dielectric constant of the hydrated polymers (Figure 8.3). This approach is to address the limitation of the model that was initially set-up for dilute spherical particles (i.e., water) dispersed in a continuous phase (i.e., polymer).

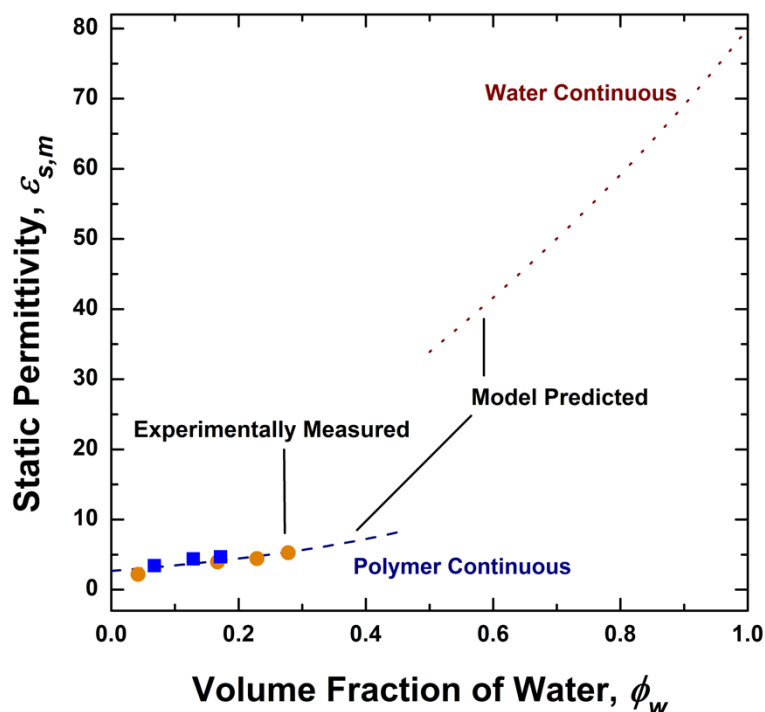


**Figure 8.3.** Experimentally measured (■) and reported<sup>1</sup> static permittivity (●) properties, as a function of the volume fraction of sorbed water, of XL-pGMA-z materials (squares) equilibrated in pure water. The dashed and dotted lines represent the prediction made using the Maxwell Garnett equation, the dashed line treats the dry polymer and the sorbed water as the continuous and the dispersed phase, respectively, for  $\phi_w < 0.45$ , whereas the dotted line treats the dry polymer and the sorbed water as the dispersed and the continuous phase, respectively, for  $\phi_w > 0.5$ .<sup>21</sup>

The Maxwell Garnett model description of the static dielectric constant of the hydrated polymer can be combined with the Born model and the definition of the salt sorption coefficient to develop an expression to describe the functional relationship between the salt sorption coefficient and the volume fraction of water in XL-pGMA-z. This step is done by combining [Equations 5.5](#), [5.6](#), and [8.1](#). The model predicts that the salt sorption coefficient increases as the volume fraction of water increases ([Figure 8.4](#)), which is consistent with results for many hydrated polymers.

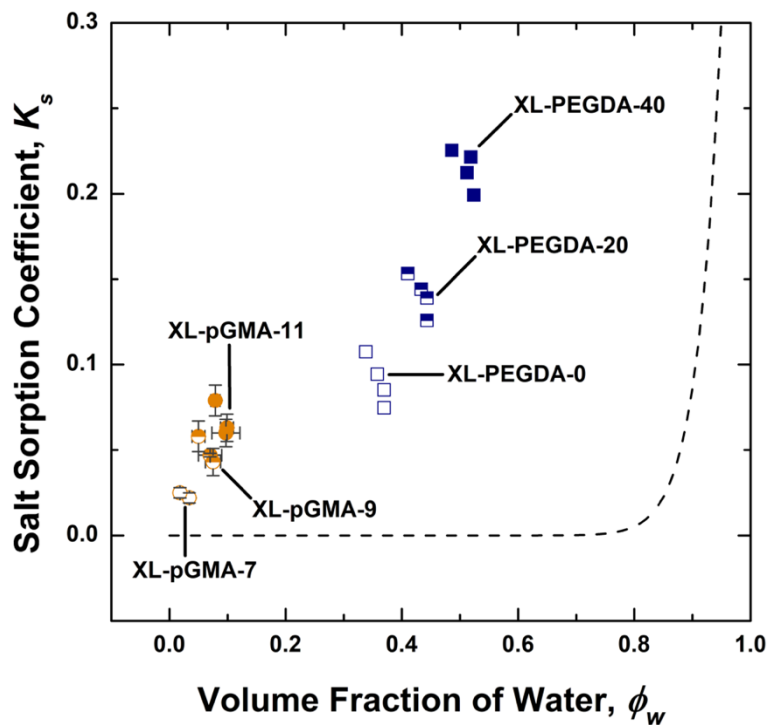


**Figure 8.4.** Salt sorption coefficient as a function of volume fraction of water for XL-pGMA-z (circles) and XL-PEGDA-w (squares)<sup>22</sup> materials. The value of w represents the percentage (by mass) of DI water added to the pre-polymerization mixture of XL-PEGDA.<sup>22</sup> The XL-pGMA-z materials were equilibrated with external salt solutions of 0.01, 0.1, and 1.0 mol/L NaCl, and the XL-PEGDA-w samples were equilibrated with external salt solutions of 0.01, 0.03, 0.1, 0.3, and 1.0 mol/L NaCl. For both materials, the value of the salt sorption coefficient increased as the external salt concentration increased (i.e., the lowest datum point for each material corresponds to the lowest external salt solution concentration (i.e. 0.01 mol/L NaCl), and the highest datum point for each material corresponds to the highest external salt solution concentration (i.e., 1.0 mol/L NaCl). The dashed line describes the variation of the salt sorption coefficient with the volume fraction of water in a situation where long-range electrostatic forces dominate ion sorption thermodynamics and the functional relationship between the static dielectric constant of the hydrated polymer and the volume fraction of water sorbed in the polymer is described by the Maxwell Garnett model.

When XL-pGMA-z is exposed to aqueous salt solutions of increasing concentration, the water content of the material decreases due to osmotic de-swelling (Figure 8.1). This decrease in water content is expected to result in a reduction in the static permittivity of the hydrated polymer and a corresponding decrease in the salt sorption coefficient according to the combined Maxwell Garnett and Born model approach to describing the salt sorption coefficient (i.e., Equations 5.5, 5.6, and 8.1). Interestingly, increases in the external salt concentration correspond to increases in the salt sorption coefficient (Figure 8.2) in these polymers, and this behavior is different from what

would be expected based on changes in water content alone (Figure 8.4). This observation is consistent with data reported for a cross-linked poly(ethylene glycol) diacrylate (XL-PEGDA) material,<sup>22</sup> which is shown for comparison in Figure 8.4. This result suggests that interactions between ions and the polymer backbone may influence the salt sorption coefficient in a manner that opposes changes that would be anticipated due to changes in water content.

Polymers that contain ether oxygen functionality (such as that in the XL-pGMA-z cross-linker and XL-PEGDA) are known to interact preferentially with alkali cations,<sup>23</sup> and specific interactions between sodium ions and these ether oxygen groups could explain the increase in the salt sorption coefficient with increasing external salt concentration (Figure 8.2). These ion-polymer interactions, not captured by the electrostatic-based theory, may influence the functional relationship between salt and water sorption properties in hydrated XL-pGMA-z. To explore these interactions further, we used microwave dielectric spectroscopy to characterize the dielectric permittivity properties of hydrated XL-pGMA-z that had been exposed to aqueous salt solutions.

### 8.2.3. Relative Permittivity

Microwave dielectric relaxation spectroscopy measurements provide insight into water molecule dynamics and the static dielectric constant of hydrated polymers.<sup>1</sup> The static dielectric constant of hydrated polymers generally increases, to varying extents, as the water content of the polymer increases.<sup>1,4,17,24-26</sup> The higher water content XL-pGMA-9 and -11 materials were found to be consistent with this correlation in that the relative permittivity increased as water content increased (Figures 8.5B and 8.5C). The greater values of the relative permittivity at low frequency observed for XL-pGMA-11 (spanning 4.2 to 4.8) compared to that for XL-pGMA-9 (spanning 3.9 to 4.5) are consistent with the greater water content of XL-pGMA-11 compared to XL-pGMA-9. Correspondingly, as the salt concentration in the external solution increased, the polymer water

content decreased due to osmotic de-swelling (Figure 8.1), and the relative permittivity decreased (Figures 8.5B and 8.5C). This result suggests that osmotic de-swelling drives the water content and dielectric permittivity properties of hydrated XL-pGMA-9 and -11.

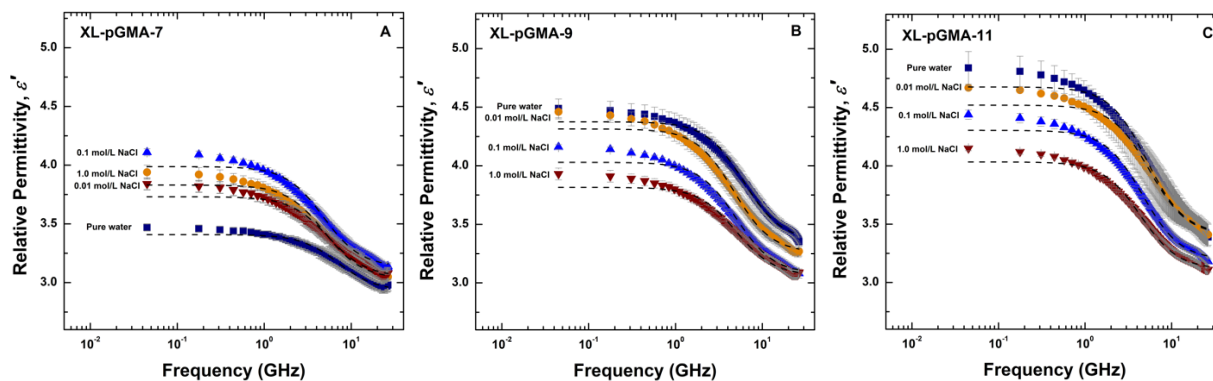


**Figure 8.5.** Frequency-dependent relative permittivity of hydrated XL-pGMA-7 (A), -9 (B), and -11 (C). Labeled on each curve is the external solution used to equilibrate the samples. Data for XL-pGMA-z are shown with the single Debye relaxation fit as dashed curves. All measurements were made at  $22\text{ }^{\circ}\text{C} \pm 1\text{ }^{\circ}\text{C}$ , and the uncertainty was taken as the standard deviation from the mean of three measurements.

The relative permittivity data of XL-pGMA-7, however, were different compared to that of XL-pGMA-9 and -11. We observed that the relative permittivity of XL-pGMA-7 initially increased when external NaCl concentration increased from pure water to 0.1 mol/L. Then, the relative permittivity of XL-pGMA-7 decreased as the external NaCl concentration increased from 0.1 to 1.0 mol/L (Figure 8.5A). This result suggests that osmotic de-swelling, observed in XL-pGMA-9 and -11, is not the only factor driving the dielectric permittivity properties in hydrated XL-pGMA-7.

The decrease in relative permittivity as external NaCl concentration increased from 0.1 to 1.0 mol/L, observed in XL-pGMA-7, may be a result of osmotic de-swelling. This observation is consistent with the result observed in XL-pGMA-9 and -11. The initial increase in relative permittivity of XL-pGMA-7 as external NaCl concentration increased, however, may be a result of increased extent of water-water interactions caused by ion-polymer interactions that liberate the

water molecules from interacting with the polymer backbone in the material. The ion-polymer interactions drove the high salt sorption coefficient in XL-pGMA-z (Figure 8.4).

To explore the XL-pGMA-7 result further, it is useful to consider a potential physical picture inside the low water content XL-pGMA-7 material (Figure 8.6). There is simply not enough sorbed water in XL-pGMA-7 to fully hydrate all of the ions and hydrophilic polymer backbone moieties in the material.<sup>8</sup> As a result, partially hydrated, or dehydrated, ions may compete with water molecules for hydrogen bonding sites on the polymer backbone (e.g., ether oxygen moieties) of the material (Figure 8.6). This competition between ions and water for interactions with the polymer backbone could, in turn, promote water-water interactions that could facilitate water dynamics and potentially increase relative permittivity properties in XL-pGMA-7. Such competition may also occur in XL-pGMA-9 and -11, but it may be less significant due to the relatively higher water content in XL-pGMA-9 and -11 compared to XL-pGMA-7.

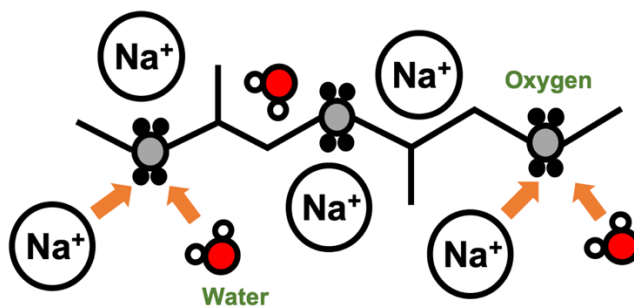


**Figure 8.6.** Illustration of possible sodium ion-water competition in the XL-pGMA-7 material.

Ultimately, the results suggest that relative permittivity (i.e., static dielectric constant) properties of hydrated polymers are sensitive to the presence of ions in hydrated polymers. To further investigate competition between ions and water for interactions with the XL-pGMA-z backbone, we used FTIR spectroscopy to gain quantitative insight into the different hydrogen-

bonding environments that water molecules experience in XL-pGMA-z.<sup>27, 28</sup> These data are discussed subsequently.

#### 8.2.4. State of Water

The previous section described a physical picture where competition between ions and water for interactions with the polymer backbone may liberate water from hydrating the polymer backbone in XL-pGMA-z (Figure 8.6). As such, the subsequent analysis is focused on the bulk-like water content of the materials in an effort to probe this liberated water based on FT-IR spectra. Representative FT-IR spectra for each of the XL-pGMA-z samples (Figure G.1) and the data for the intermediate and strongly-bound water content of XL-pGMA-z exposed to aqueous salt solutions are included in the Appendix G.

The bulk-like water content in XL-pGMA-9 and -11 decreased as the external NaCl concentration increased (Figure 8.7). In fact, the contents of all three water states decreased as the external NaCl concentration increased (Table G.2). This result is consistent with the overall water content (Figure 8.1) and suggests that osmotic de-swelling generally suppresses the amount of sorbed water in these materials.

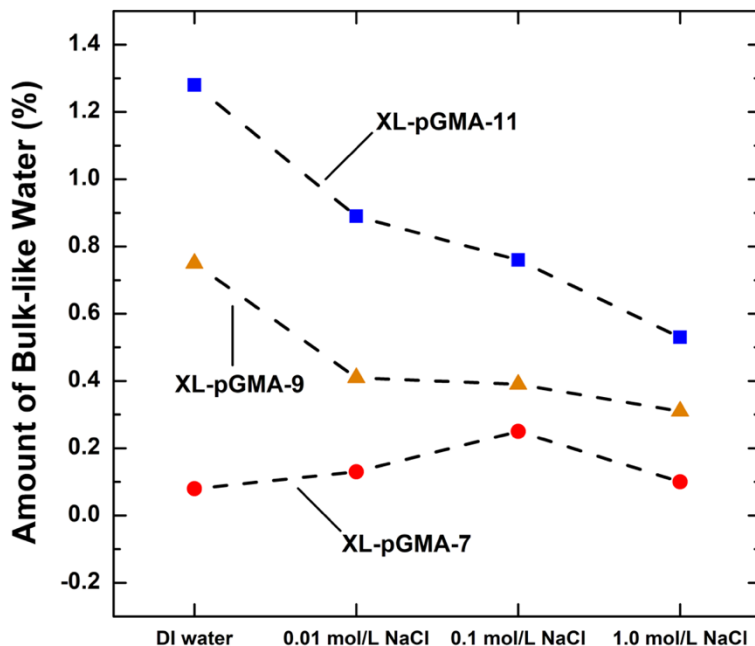


**Figure 8.7.** Bulk-like water content of XL-pGMA-z measured using samples that were equilibrated in DI water or 0.01, 0.1, and 1.0 mol/L aqueous NaCl solutions. The dashed curves were drawn to guide the eye. The bulk-like water content represents a percentage of the total sorbed water mass in XL-pGMA-z.

In XL-pGMA-7, the bulk-like water content initially increased as external NaCl concentration increased from 0 (pure water) to 0.1 mol/L. This observation may result from the liberation of polymer backbone-hydrating water by sorbed ions in the polymer. Then, the bulk-like water content decreased as the external NaCl concentration increased from 0.1 to 1.0 mol/L. This result suggests, consistent with the relative permittivity result (Figure 8.5), that liberation of polymer backbone-hydrating water due to competition between ions and water molecules may be responsible for the initial increase of the bulk-like water content and relative permittivity properties of XL-pGMA-7, but osmotic de-swelling may become more significant at higher salt concentrations and may then suppress the bulk-like water content and relative permittivity properties of XL-pGMA-7.

The functional relationship between the XL-pGMA-z bulk-like water content and external salt solution (Figure 8.7) are qualitatively similar to that of static permittivity and external salt solution (Figure G.2). These results support the physical picture that competition between ions and water for interactions with the polymer backbone may be important for understanding how salt concentration affects relative permittivity and state of water properties in hydrated XL-pGMA-z. Ion-water competition for hydrogen bonding, observed exclusively in XL-pGMA-7, may be a result of the competition being more significant in some polymer (i.e., XL-pGMA-7) than in others (i.e., XL-pGMA-9 and -11) where osmotic de-swelling may be a more important factor to drive polymer properties. Further, ion-water competition in XL-pGMA-z suggests the presence of additional ion-polymer interactions in the material, and the increased salt sorption coefficient as volume fraction of water decreased observation made on the material supports this statement (Figure 8.4).

#### **8.2.5. Static Permittivity**

To further understand the influence of external salt concentration, or the presence of sorbed ions, on the dielectric permittivity properties of XL-pGMA-z, it is useful to consider the static dielectric constant (or static permittivity). As expected, based on the Maxwell Garnett model, the static permittivity of the materials, exposed to each external solution, increases as the water content of the material increases (Figure 8.8). Interestingly, exposing the polymer to an aqueous salt solution causes a general increase in the static permittivity of the material at a specific water content.

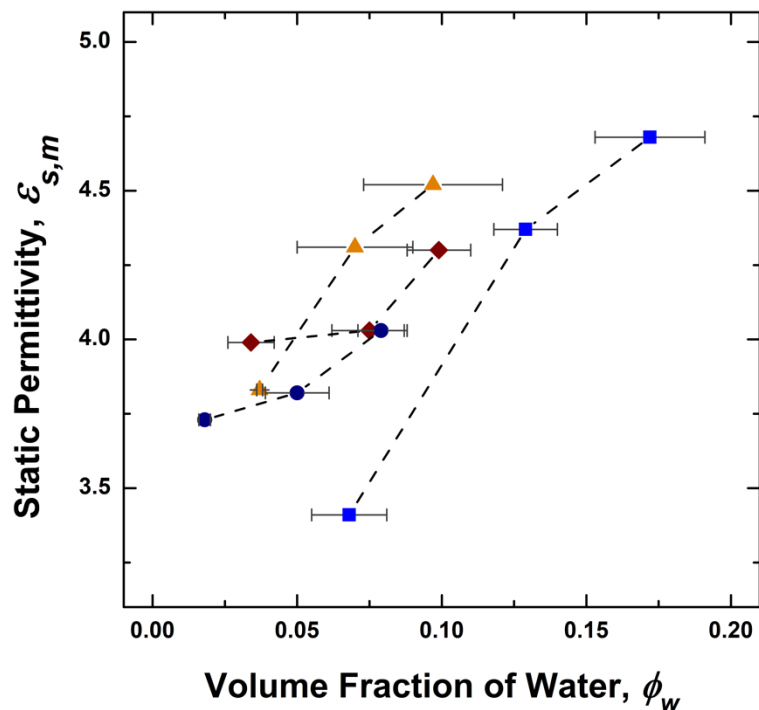


**Figure 8.8.** Static permittivity of XL-pGMA-z as a function of the volume fraction of water sorbed by the polymer. Samples were equilibrated in either pure water (■), 0.01 mol/L NaCl (▲), 0.1 mol/L NaCl (◆), or 1.0 mol/L NaCl (●). Each data set represented in the figure contains a data point for XL-pGMA-7, -9, and -11, and in all cases, the volume fraction of water increases as the z value of XL-pGMA-z increases. The dashed lines are included to guide the eye.

To understand the influence of exposure to salt on the relative permittivity properties of hydrated XL-pGMA-z, it is important to compare the data points at equivalent volume fractions of water because water content critically affects sorption properties.<sup>6</sup> At equivalent water content, the salt solution equilibrated samples universally had higher static permittivity values compared to the samples that were equilibrated with pure water (Figure 8.8). This result suggests that the simple presence of sorbed ions in the polymer tends to facilitate sorbed water motions within the material. Additionally, increases in the external NaCl concentration did not dramatically change the functional relationship between water content and dielectric permittivity properties (Figure 8.8). This result suggests that the presence of sorbed ions may be more important for affecting

dielectric permittivity properties than the concentration of sorbed ions (at least over the ranges of concentration considered here).

Interestingly, the dielectric constant (static permittivity) of bulk aqueous salt solution decreases as salt concentration increases (Figure G.3).<sup>5</sup> Therefore, the observation that the static permittivity of XL-pGMA-z increased upon equilibration with a salt solution is unexpected, as the equilibration process results in ion sorption. This unique observation suggests that the influence of sorbed ions (and, thus, external salt concentration) on hydrated polymer dielectric permittivity and state of water properties may be fundamentally different from what is observed in bulk solutions.

### **8.3. Conclusions**

The Maxwell Garnett equation, useful for describing the variation of static permittivity of a heterogeneous material, describes the functional relationship between static permittivity and volume fraction of water in hydrated XL-pGMA-z. The salt sorption properties of hydrated XL-pGMA-z depend on external salt concentration in a manner different from that observed in other hydrated materials. This observation may result from competition between ions and water for interactions with the polymer backbone. Microwave dielectric relaxation spectroscopy and state of water analysis suggested that the relative permittivity and bulk-like water content of hydrated XL-pGMA-z largely decrease as external salt concentration increases as a result of osmotic deswelling. An increase, as the external NaCl concentration increased from 0 (pure water) to 0.1 mol/L, in relative permittivity and bulk-like water content, however, was observed in low water content XL-pGMA-7. This observation is consistent with a physical picture where sorbed ions may compete with water molecules for interactions with the polymer backbone and may liberate water molecules that would hydrate the polymer backbone in the absence of the sorbed ions.

While the presence of sorbed salt does not dramatically change the functional relationship between the dielectric permittivity and water content properties of XL-pGMA-z, it does increase the relative permittivity of the materials, at a given water content, compared to materials that contain no sorbed ions. This result is fundamentally different from the decrease in the static permittivity of bulk aqueous solution that is observed as salt concentration increases. This information is critical to help understand the factors that influence the sorption properties in hydrated polymer.

#### **8.4. References**

1. Chang, K.; Luo, H.; Geise, G. M., Water content, relative permittivity, and ion sorption properties of polymers for membrane desalination. *Journal of Membrane Science* **2019**, *574*, 24-32.
2. Luo, H.; Chang, K.; Bahati, K.; Geise, G. M., Functional group configuration influences salt transport in desalination membrane materials. *Journal of Membrane Science* **2019**, *590*, 117295.
3. Luo, H.; Chang, K.; Bahati, K.; Geise, G. M., Engineering selective desalination membranes via molecular control of polymer functional groups. *Environmental Science & Technology Letters* **2019**, *6* (8), 462-466.
4. Chang, K.; Geise, G. M., Dielectric permittivity properties of hydrated polymers: Measurement and connection to ion transport properties. *Industrial & Engineering Chemistry Research* **2020**, *59* (12), 5205-5217.
5. Hasted, J. B.; Ritson, D. M.; Collie, C. H., Dielectric properties of aqueous ionic solutions. Parts I and II. *The Journal of Chemical Physics* **1948**, *16* (1), 1-21.
6. Geise, G. M.; Paul, D. R.; Freeman, B. D., Fundamental water and salt transport properties of polymeric materials. *Progress in Polymer Science* **2014**, *39* (1), 1-42.

7. Khare, A. R.; Peppas, N., Swelling/deswelling of anionic copolymer gels. *Biomaterials* **1995**, *16*, 559-567.
8. Chang, K.; Korovich, A.; Xue, T.; Morris, W. A.; Madsen, L. A.; Geise, G. M., Influence of rubbery versus glassy backbone dynamics on multiscale transport in polymer membranes. *Macromolecules* **2018**, *51* (22), 9222-9233.
9. Lonsdale, H. K.; Merten, U.; Riley, R. L., Transport properties of cellulose acetate osmotic membranes. *Journal of Applied Polymer Science* **1965**, *9* (4), 1341-1362.
10. Zhang, H.; Geise, G. M., Modeling the water permeability and water/salt selectivity tradeoff in polymer membranes. *Journal of Membrane Science* **2016**, *520*, 790-800.
11. Yasuda, H.; Lamaze, C. E.; Ikenberry, L. D., Permeability of solutes through hydrated polymer membranes. Part I. Diffusion of sodium chloride. *Die Makromolekulare Chemie* **1968**, *118* (1), 19-35.
12. Yaroshchuk, A. E., Dielectric exclusion of ions from membranes. *Advances in Colloid and Interface Science* **2000**, *85* (2), 193-230.
13. Glueckauf, E., On the mechanism of osmotic desalting with porous membranes. *Proceedings of the First International Symposium on Water Desalination* **1967**, 143-150.
14. Heyde, M. E.; Peters, C. R.; Anderson, J. E., Factors influencing reverse osmosis rejection of inorganic solutes from aqueous solution. *Journal of Colloid and Interface Science* **1975**, *50* (3), 467-487.
15. Duignan, T. T.; Parsons, D. F.; Ninham, B. W., A continuum solvent model of the multipolar dispersion solvation energy. *The Journal of Physical Chemistry B* **2013**, *117* (32), 9412-9420.
16. Duignan, T. T.; Parsons, D. F.; Ninham, B. W., A continuum solvent model of the partial molar volumes and entropies of ionic solvation. *The Journal of Physical Chemistry B* **2014**, *118* (11), 3122-3132.

17. Paddison, S. J.; Reagor, D. W.; Zawodzinski Jr, T. A., High frequency dielectric studies of hydrated Nafion®. *Journal of Electroanalytical Chemistry* **1998**, 459 (1), 91-97.
18. Wagner, K. W., Erklärung der dielektrischen Nachwirkungsvorgänge auf Grund Maxwellscher Vorstellungen. *Archiv für Elektrotechnik* **1914**, 2 (9), 371-387.
19. Wiener, O. H., *Die Theorie des Mischkörpers für das Feld der stationären Strömung*. Teubner: 1912.
20. Rayleigh, L., LVI. On the influence of obstacles arranged in rectangular order upon the properties of a medium. *The London, Edinburgh, and Dublin Philosophical Magazine and Journal of Science* **1892**, 34 (211), 481-502.
21. Lou, J.; Hatton, T. A.; Laibinis, P. E., Effective dielectric properties of solvent mixtures at microwave frequencies. *The Journal of Physical Chemistry A* **1997**, 101 (29), 5262-5268.
22. Jang, E.-S.; Kamcev, J.; Kobayashi, K.; Yan, N.; Sujanani, R.; Dilenschneider, T. J.; Park, H. B.; Paul, D. R.; Freeman, B. D., Influence of water content on alkali metal chloride transport in cross-linked Poly(ethylene glycol) Diacrylate.1. Ion sorption. *Polymer* **2019**, 178, 121554.
23. Ji, Y.; Luo, H.; Geise, G. M., Specific co-ion sorption and diffusion properties influence membrane permselectivity. *Journal of Membrane Science* **2018**, 563, 492-504.
24. Paddison, S.; Bender, G.; Zawodzinski Jr, T. A., The microwave region of the dielectric spectrum of hydrated Nafion® and other sulfonated membranes. *Journal of New Materials for Electrochemical Systems* **2000**, 3, 293-302.
25. Lu, Z.; Polizos, G.; Macdonald, D. D.; Manias, E., State of water in perfluorosulfonic ionomer (Nafion® 117) proton exchange membranes. *Journal of The Electrochemical Society* **2008**, 155 (2), B163-B171.
26. Lu, Z.; Lanagan, M.; Manias, E.; Macdonald, D. D., Two-port transmission line technique for dielectric property characterization of polymer electrolyte membranes. *The Journal of Physical Chemistry B* **2009**, 113 (41), 13551-13559.

27. Black, S. B.; Chang, Y.; Bae, C.; Hickner, M. A., FTIR characterization of water-polymer interactions in superacid polymers. *The Journal of Physical Chemistry B* **2013**, *117* (50), 16266-16274.
28. Smedley, S. B.; Chang, Y.; Bae, C.; Hickner, M. A., Measuring water hydrogen bonding distributions in proton exchange membranes using linear Fourier Transform Infrared Spectroscopy. *Solid State Ionics* **2015**, *275*, 66-70.

## **Chapter 9: Functional Group Modification Influences Relative Permittivity and Transport Properties in Sulfonated Polysulfone Desalination Materials**

### **9.1. Introduction**

The use of chemically stable polymer membrane materials could address the oxidative degradation challenges facing current state-of-the-art polyamide membranes used for desalination applications.<sup>1-5</sup> Among the membrane materials available, hydrocarbon polymers are of great interest because of their excellent chemical stability, but hydrocarbon polymers are often too hydrophobic to function effectively as water treatment membranes.<sup>2,3,5,6</sup> To address this challenge, hydrocarbon polymers can be modified to increase hydrophilicity, and sulfonation is a commonly applied approach.<sup>3-5, 7-13</sup> While increased hydrophilicity may make sulfonated polymers water permeable enough to be promising for desalination applications, most of these materials have not yet achieved water/salt selectivity properties comparable to that of commercially available polyamide desalination membranes.<sup>3,4, 14</sup>

One approach to improve the desalination performance of sulfonated polymers may be to incorporate distributed hydrophilic chemical functional groups in the polymer matrix. This strategy is based on previous results suggesting that a distributed functional group configurations in an uncharged polymer matrix can lead to increases in water/salt permeability selectivity, which is favorable for desalination applications.<sup>15, 16</sup> This observed increase in permeability selectivity was ascribed to a reduction in the relative permittivity (and thus, salt sorption coefficient) properties that occurred as the hydroxyl functional group configuration shifted from one rich in vicinal diol groups to a configuration where most side chains contained only a single hydroxyl group.<sup>15, 16</sup> Questions still remain, however, as to whether this result, observed in uncharged polymers (where salt sorption properties follow a simple partitioning mechanism<sup>17-20</sup>), can be

realized in charged polymers where salt sorption properties are often described via Donnan exclusion theory.<sup>3,21,22</sup>

In this study, we report the addition of methoxy functional groups to a sulfonated polysulfone polymer to determine whether this chemical modification can be used to increase water/salt selectivity via the sorption based mechanism recently reported.<sup>15, 16</sup> We report the influence of methoxy group addition on dry density, relative permittivity, and water and ion transport properties. Adding methoxy groups to the polymer backbone simultaneously increased water permeability and decreased salt permeability properties, and these changes in properties are both favorable for desalination application. Different from the uncharged polymers considered previously, relative permittivity and salt sorption results suggest that addition of methoxy groups to sulfonated polysulfone may not affect salt sorption properties in a manner more significant than Donnan exclusion. Additionally, the Donnan-Manning model did not quantitatively describe the salt sorption properties of these sulfonated polysulfone polymers perhaps due to a combination of low water content and a heterogeneous distribution of fixed charge groups. The changes in water and salt permeability upon the addition of methoxy groups to sulfonated polysulfone are discussed qualitatively within the framework of fractional free volume and/or the distribution of free volume element size. This study suggests that the addition of hydrophilic functional groups to a charged polysulfone more strongly influences the diffusion properties of the materials as opposed to the sorption selectivity properties, and this observation may be important for informing efforts to engineer charged polymers for desalination applications.

## 9.2. Results and Discussion

### 9.2.1. Water and Salt Permeability

The methoxy groups on the MHQ:BP backbone appear to affect transport properties in a manner that favors higher water permeability (Figure 9.1A) and lower salt permeability (Figure 9.1B) compared to the HQ:BP materials. Importantly, the observation holds when the materials are compared at equivalent water content, as water content is known to influence (sometimes dramatically) permeability properties.<sup>3, 16, 23, 24</sup> This result suggests that the use of MHQ versus HQ may directly influence transport properties independent of changes in polymer water content.

Addition of bulky functional groups (e.g., triptycene<sup>6, 25-28</sup> or Bisphenol A<sup>29-31</sup>) to sulfonated polysulfones can disrupt polymer chain packing. If polymer density decreases, as a result of this disruption in chain packing, the corresponding increase in fractional free volume can lead to increases in water permeability.<sup>6, 31</sup> The observations reported in Figure 9.1A appear to be consistent with this physical picture because the water permeability of the MHQ:BP materials is greater than that of the HQ:BP materials that do not contain methoxy groups along the polymer backbone.

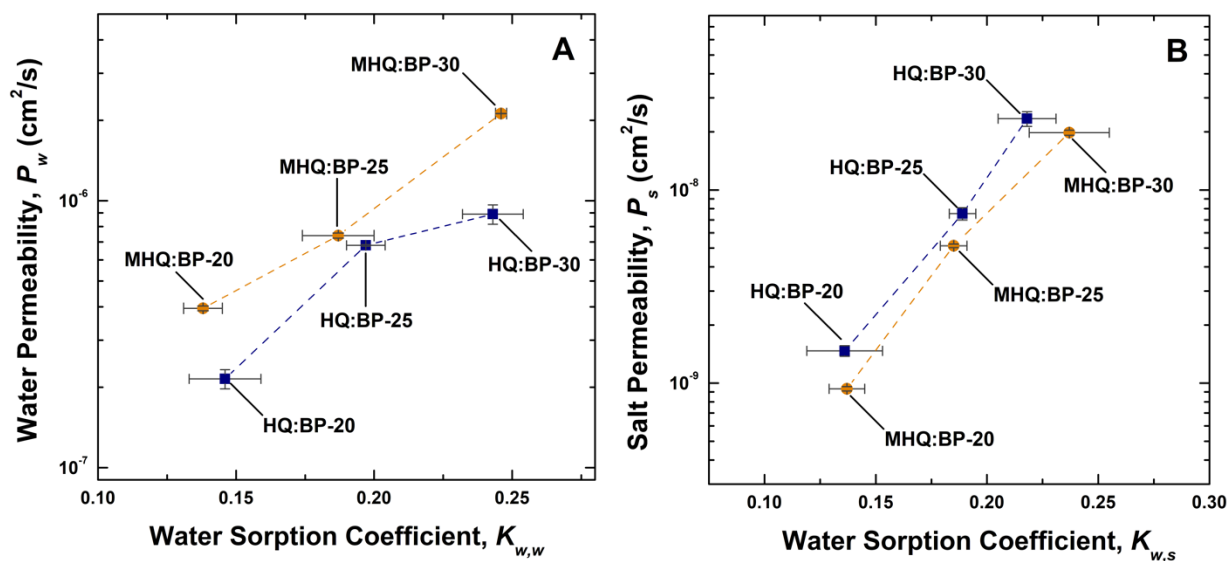


**Figure 9.1.** Water (A) and salt (B) permeability as a function of water content for the HQ:BP and MHQ:BP materials. The dashed lines are included to guide the eye. All measurements were made at  $22 \pm 1$  °C, and the uncertainty was taken as one standard deviation from the mean of three measurements.

The dry density values of the HQ:BP and MHQ:BP materials, however, are inconsistent with this physical picture. The methoxy groups on the MHQ:BP materials drive an increase in polymer density relative to the HQ:BP materials at a given degree of sulfonation (Table 9.1). The observed increase in polymer density, upon addition of the methoxy groups, may be a result of enhanced hydrogen bonding interactions, which could enhance chain packing,<sup>32</sup> as opposed to disrupting chain packing as observed when non-polar bulky groups are added to sulfonated polysulfone.<sup>6, 31</sup> The greater density in the MHQ:BP materials compared to the HQ:BP materials suggests a lower fractional free volume in MHQ:BP compared to HQ:BP, and this situation is consistent with the observation that salt permeability is lower in the MHQ:BP materials than that in the HQ:BP materials (Figure 9.1B).

**Table 9.1.** Dry polymer density data for the HQ:BP and MHQ:BP materials. All measurements were made at  $22 \pm 1$  °C. The uncertainty was taken as the standard deviation from the mean of three measurements.

Polymer	Dry Density (g/cm <sup>3</sup> )
HQ:BP-20	$1.25 \pm 0.07$
HQ:BP-25	$1.30 \pm 0.02$
HQ:BP-30	$1.35 \pm 0.03$
MHQ:BP-20	$1.31 \pm 0.03$
MHQ:BP-25	$1.40 \pm 0.01$
MHQ:BP-30	$1.42 \pm 0.01$

Ultimately, this chain packing, polymer density and fractional free volume discussion fails to satisfactorily explain both the water and salt permeability properties of the two sets of materials considered (Figure 9.1). To investigate further the governing factors that underlie the water and salt permeability properties of the HQ:BP and MHQ:BP materials, we will consider the thermodynamic and kinetic contributors to the water and salt permeability. Using the solution diffusion model, the discussion below further analyzes the water and salt permeability properties in terms of sorption (thermodynamics) and diffusion (kinetics) coefficients.<sup>33, 34</sup>

### 9.2.2. Water and Salt Sorption

The HQ:BP and MHQ:BP materials were prepared to have comparable water content (Figure 9.2). Comparing materials at equivalent water content is critical for this study, as water and salt transport in polymers is strongly influenced by water content.<sup>15, 16, 23, 24, 35</sup> By preparing materials with comparable water content, differences in transport properties can be ascribed to the use of either MHQ or HQ in the sulfonated polysulfones. We observed that adding methoxy groups to the polymer backbone of sulfonated polysulfone did not significantly influence the hydrophilicity of the polymers.

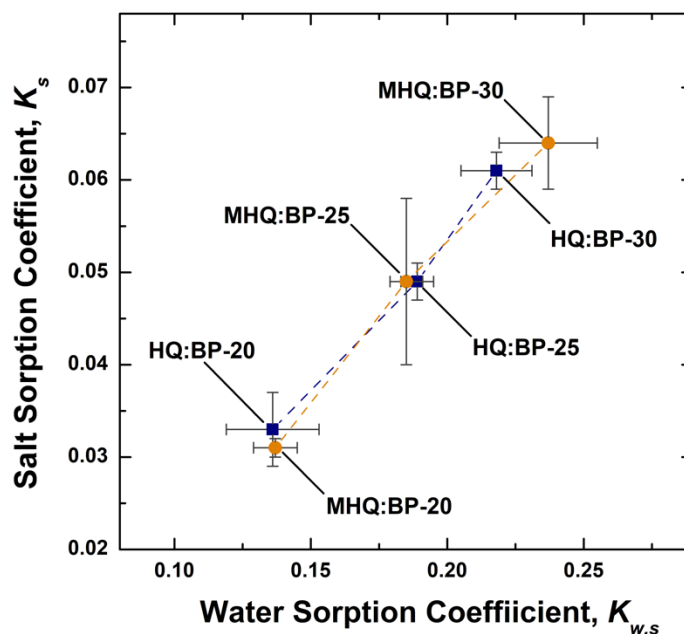


**Figure 9.2.** Salt (NaCl) sorption coefficient values as a function of water content for the HQ:BP and MHQ:BP materials. The dashed lines are included to guide the eye. All measurements were made at  $22 \text{ }^\circ\text{C} \pm 1 \text{ }^\circ\text{C}$ , and the uncertainty was taken as one standard deviation from the mean of three measurements.

We also observed statistically similar salt sorption coefficients for the water content equivalent HQ:BP and MHQ:BP materials (Figure 9.2). The results suggest that adding methoxy groups to sulfonated polysulfone affected neither water nor salt sorption properties significantly. This result was unexpected as previous studies observed a reduction in the salt sorption coefficient as hydrophilic polar functional groups were distributed more evenly throughout the uncharged polymer.<sup>15, 16</sup> It does importantly suggest a distinction, as those prior studies considered uncharged polymers.<sup>15, 16</sup> In this study, sulfonated polysulfone contains ionizable fixed charge groups that influence salt sorption properties in a manner very different from that of uncharged materials.<sup>2, 3,</sup>

14, 36

Donnan exclusion theory is used to describe the salt sorption properties of charged polymers, such as sulfonated polysulfone.<sup>2, 22, 37</sup> This approach is different from uncharged polymers where an electrostatic- (or dielectric-) based exclusion mechanism is used often to

describe salt sorption properties.<sup>3, 38, 39</sup> To further explore the salt sorption process in these sulfonated polysulfones from the perspective of both Donnan and electrostatic theories, we first characterized the hydrated polymer relative permittivity properties using the microwave dielectric relaxation spectroscopy (DRS) to investigate electrostatic contributions to ion sorption.<sup>15, 38, 39</sup>

The relative permittivity of MHQ:BP was lower than that of HQ:BP (Figure 9.3). Generally speaking, lower relative permittivity properties in hydrated polymers correlate with lower salt sorption coefficients (or higher ion exclusion).<sup>15, 38, 39</sup> In these materials, the salt sorption coefficients do not depend significantly on whether MHQ or HQ is used in the polymer (Figure 9.2), and thus, the relative permittivity properties do not correlate with the salt sorption coefficient properties in the manner typically observed.

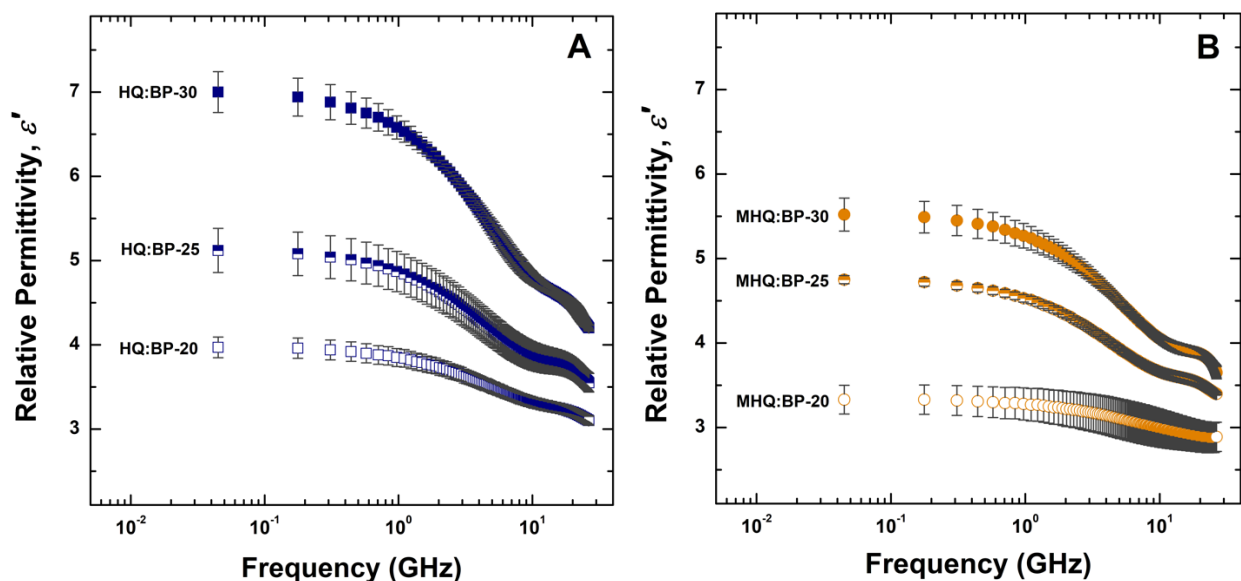


**Figure 9.3.** Frequency-dependent relative permittivity of the HQ:BP (A) and MHQ:BP (B) materials. All measurements were made at  $22\text{ }^{\circ}\text{C} \pm 1\text{ }^{\circ}\text{C}$ , and the uncertainty was taken as one standard deviation from the mean of three measurements.

Distributing methoxy functional groups throughout the sulfonated polysulfone matrix, however, drove a combination of low relative permittivity (Figure 9.3) and low salt permeability properties (Figure 9.1B) relative to the HQ-containing polysulfones. While this result is consistent with observations made on some uncharged materials,<sup>15, 16</sup> the reduction in salt permeability properties in uncharged materials can be attributed to a sorption based mechanism compared to the situation in charged materials where the salt permeability effect may stem from changes in diffusion properties (perhaps via changes in the fractional free volume and/or the distribution of free volume element size). For example, the reduction in relative permittivity along with the observed increase in polymer density, upon adding methoxy groups to the polymer, could suggest a simultaneous reduction in polymer fractional free volume and shift of the free volume element size distribution toward smaller sizes because the observed reduction in the relative permittivity (in the microwave frequency range) suggests that fewer water molecule dipoles are able to relax in the methoxy group containing materials.<sup>15, 38, 39</sup> Smaller free volume element sizes distributed more evenly throughout the methoxy group-containing material could lead to a decrease in the ability of water molecule dipoles to relax while simultaneously facilitating additional water transport pathways that could be sufficiently small to restrict transport of larger hydrated ions.

The observation that the relative permittivity (Figure 9.3) properties decrease upon addition of methoxy groups to sulfonated polysulfone while the sorption (Figure 9.2) properties do not change suggests that Donnan exclusion may dominate the salt sorption properties in these HQ:BP and MHQ:BP materials. The addition of methoxy groups to sulfonated polysulfone may reduce water molecule dipole relaxations due to the addition of more hydrogen bond acceptors in the material, but the resulting change in relative permittivity properties does not appear to influence salt sorption properties in the manner observed in charged polymers. The relative permittivity

properties of hydrated polymers can influence, however, salt sorption in a manner described by Donnan-Manning theory.<sup>2, 22</sup> As such, the connection between relative permittivity and salt sorption properties will be discussed subsequently within the framework of Donnan-Manning theory.

### 9.2.3. Donnan-Manning Counter-ion Condensation Theory

Donnan theory describes the salt sorption process in charged polymers and results from the combination of the thermodynamic equilibrium and electroneutrality criteria:<sup>2, 22, 37</sup>

$$K_s^m = \left[ \frac{1}{4} \left( \frac{C_A^{m,w}}{C_s^s} \right)^2 + \left( \frac{\gamma_{\pm}^s}{\gamma_{\pm}^m} \right)^2 \right]^{\frac{1}{2}} - \frac{1}{2} \left( \frac{C_A^{m,w}}{C_s^s} \right) \quad (9.1)$$

where  $C_A^{m,w}$  is the membrane fixed charge group concentration (normalized to the volume of sorbed water),  $C_s^s$  is the salt concentration in the external solution,  $\gamma_{\pm}^s$  is the mean ionic activity coefficient in the solution phase, and  $\gamma_{\pm}^m$  is the mean ionic activity coefficient in the membrane phase. The value of  $\gamma_{\pm}^m$  can be calculated using Manning's counter-ion condensation theory, which treats polymer chains as infinite line charges with charged groups evenly distributed along the polymer chain.<sup>37, 40, 41</sup> The Manning parameter,  $\xi$ , describes the linear charge density of the polymer chain as:<sup>37, 40, 41</sup>

$$\xi = \frac{\lambda_B}{b} = \frac{e^2}{4\pi\epsilon_0\epsilon_m k_B T b} \quad (9.2)$$

where  $\lambda_B$  is the Bjerrum length,  $e$  is the elementary charge,  $\epsilon_0$  is the permittivity of free space,  $\epsilon_m$  is the membrane phase static permittivity (or static dielectric constant),  $k_B$  is Boltzmann's constant,  $T$  is the absolute temperature, and  $b$  is the distance between fixed charge groups on the polymer chain.

A critical value of  $\xi = 1$ , defined for monovalent electrolytes, is applicable to our study.<sup>40</sup> When the Manning parameter is greater than unity, counter-ions condense on the polymer fixed charge groups to reduce  $\xi$  to unity, and the remaining uncondensed counter-ions are treated thermodynamically, using the Debye-Hückel approximation, as:<sup>40, 41</sup>

$$\gamma_{\pm}^m = \left[ \left( \frac{X/\xi + 1}{X + 1} \right) \exp \left( -\frac{X}{X + 2\xi} \right) \right]^{\frac{1}{2}} \quad (9.3)$$

where  $X = C_A^{m,w}/C_s^m$ . When the Manning parameter is less than unity, counter-ion condensation does not occur, and  $\gamma_{\pm}^m$  is calculated, using the Debye-Hückel approximation, as:<sup>40</sup>

$$\ln \gamma_{\pm}^m = -\frac{\xi X}{2(X + 2)} \quad (9.4)$$

The membrane fixed charge group concentration,  $C_A^{m,w}$ , for the HQ:BP and MHQ:BP materials was calculated from the theoretical ion exchange capacity (IEC) (Table H.2) and measured water uptake,  $w_u$ , data (Table H.1) as:

$$C_A^{m,w} = (IEC \times \rho_w)/w_u \quad (9.5)$$

where  $\rho_w$  is the density of water. The salt concentration in the external solution,  $C_s^s$ , was 1.0 mol/L, so the mean ionic activity coefficient in the solution phase,  $\gamma_{\pm}^s$ , was calculated to be 0.656 using the Pitzer model.<sup>42</sup> The distances between fixed charge groups on the HQ:BP and MHQ:BP polymer chains,  $b$ , were calculated based on the polymer structure information of the materials on ChemDraw (Table H.2).

The Manning parameter was calculated using Equation 9.2, and the mean ionic activity coefficient in the membrane phase,  $\gamma_{\pm}^m$ , was calculated subsequently using Equation 9.3. The

calculated values of  $\xi$  and  $\gamma_{\pm}^m$  (Table H.2, 1.3 to 2.0 and 0.4 to 0.5, respectively) for the HQ:BP and MHQ:BP materials were similar to the values calculated for a commercial cation exchange membrane (1.83 and 0.30, respectively, for CR61)<sup>41</sup>. The similar  $\xi$  and  $\gamma_{\pm}^m$  values of HQ- and MHQ-containing sulfonated polysulfones and CR61 is reasonable given that all materials were equilibrated with aqueous NaCl solution of the same concentration range (0.01 to 1.0 mol/L).

The HQ:BP and MHQ:BP salt sorption coefficients calculated using the Donnan-Manning model differed by roughly an order of magnitude from values measured experimentally. This result was surprising given that the Donnan-Manning model has been shown to describe satisfactorily salt sorption in other charged polymers,<sup>41, 43</sup> and because the values calculated for  $\xi$  and  $\gamma_{\pm}^m$  were similar to those values determined for materials where the salt sorption properties were well described by the Donnan-Manning model. The discrepancy observed between the measured and modeled salt sorption coefficients in these HQ:BP and MHQ:BP materials may be due to their low water content and the heterogeneous distribution of fixed charge groups inherent to the molecular structure of these polymers (Figure 2.5). As a result, the Donnan-Manning model may not work well for low water content sulfonated polysulfones that have heterogeneous distributions of charged groups.

**Table 9.2.** Salt sorption coefficients experimentally measured at  $22 \pm 1$  °C and predicted using the Donnan-Manning model (Equation 9.1). The uncertainty was taken as one standard deviation from the mean of three measurements.

Polymer	$K_s$ (Predicted)	$K_s$ (Measured)
HQ:BP-20	0.30	$0.033 \pm 0.004$
HQ:BP-25	0.32	$0.049 \pm 0.002$
HQ:BP-30	0.27	$0.061 \pm 0.002$
MHQ:BP-20	0.32	$0.031 \pm 0.001$
MHQ:BP-25	0.31	$0.049 \pm 0.009$
MHQ:BP-30	0.34	$0.064 \pm 0.005$

#### 9.2.4. Water and Salt Diffusion

Consistent with the permeability results (Figure 9.1), we observed higher water diffusivity and lower salt diffusivity in MHQ:BP compared to HQ:BP materials (Figure 9.4). The salt diffusivity results, however, were obtained from a typical diffusion cell experiment that was driven by a salt concentration gradient, and the experiment measures the bulk (or coupled) salt diffusion coefficients that contain contributions from both counter-ions and co-ions.<sup>44-46</sup> To understand if interactions between the counter-ions (i.e., cations) and the polymer<sup>41, 43, 46</sup> influenced the coupled salt diffusion properties differently depending on whether methoxy groups were present in the sulfonated polymers or not, individual ion diffusion coefficients ( $D_c^m$  for the co-ion (anion) and  $D_g^m$  for counter-ion (cation), respectively) were determined using the Nernst Planck equation for both concentration gradient driven,<sup>46-48</sup> Equation 9.6, and electric field driven,<sup>22, 46, 48</sup> Equation 9.7, ion transport:

$$D_s^m = \frac{D_g^m D_c^m (z_g^2 C_g^{m,p} + z_c^2 C_c^{m,p})}{z_g^2 D_g^m C_g^{m,p} + z_c^2 D_c^m C_c^{m,p}} \quad (9.6)$$

$$\kappa = \frac{F^2}{RT} (z_g^2 D_g^m C_g^m + z_c^2 D_c^m C_c^m) \quad (9.7)$$

where  $D_s^m$  is the bulk salt diffusion coefficients in a membrane determined from a typical diffusion cell experiments,  $z_g$  and  $z_c$  are the counter-ion and co-ion valences, respectively,  $C_g^{m,p}$  and  $C_c^{m,p}$  are the membrane phase counter-ion and co-ion concentrations (normalized to the volume of swollen polymer in the membrane), respectively,  $F$  is Faraday's constant,  $R$  is the ideal gas constant, and  $T$  is the absolute temperature.

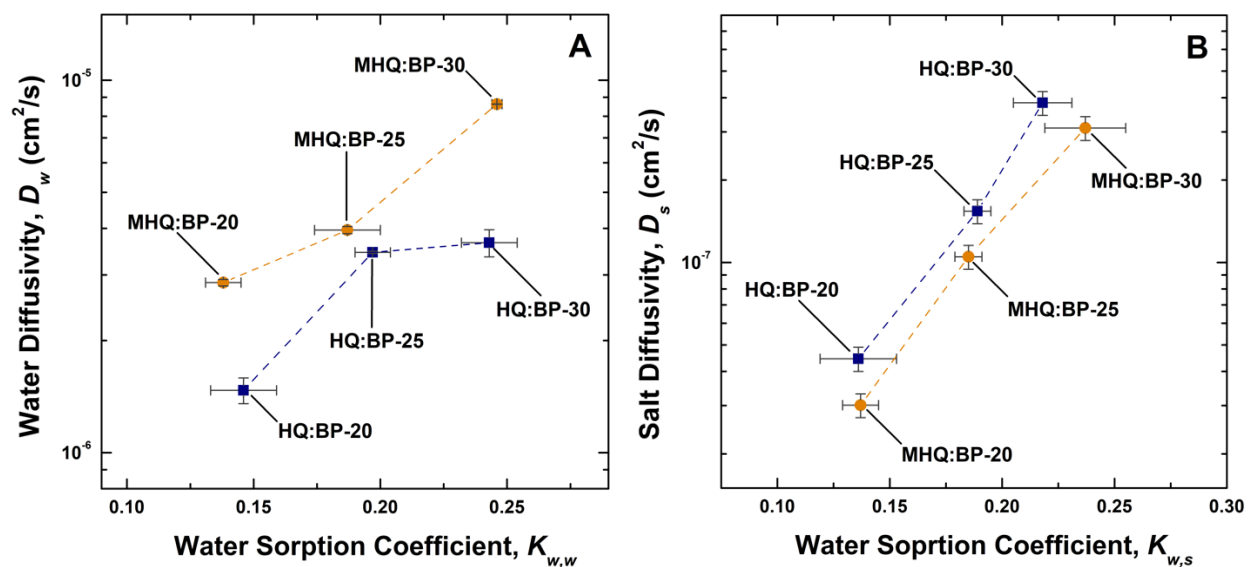


**Figure 9.4.** Water (A) and salt (B) diffusivity as a function of water content for HQ:BP and MHQ:BP. The dashed lines are included to guide the eye. All measurements were made at  $22 \text{ }^\circ\text{C} \pm 1 \text{ }^\circ\text{C}$ , and the uncertainty was taken as one standard deviation from the mean of three measurements.

We observed lower co-ion diffusivity in MHQ:BP than that in HQ:BP and statistically indistinguishable counter-ion diffusivity in these materials (Table 9.3). These results suggest that the bulk salt diffusion in these materials was driven by co-ions, which is consistent with the observations made on most charged materials.<sup>3,37</sup> The lower co-ion diffusivity in MHQ:BP than that in HQ:BP is an observation that is consistent with the salt permeability result (Figure 9.1B),

which stems from a situation where an increase in polymer density leads to decreased fractional free volume and impeded salt transport in the MHQ:BP materials when methoxy groups were added to sulfonated polysulfone.

**Table 9.3.** Diffusivity and conductivity data for HQ:BP and MHQ:BP. Samples were equilibrated with 1.0 mol/L NaCl solution prior to measurements. All measurements were made at  $22 \pm 1$  °C, and the uncertainty was taken as the standard deviation from the mean of three measurements. Co-ion and counter-ion diffusivity values were calculated by solving Equations 9.6 and 9.7 simultaneously.

Polymer	Salt Diffusivity, $D_s^m$ ( $\times 10^{-7}$ cm <sup>2</sup> /s)	Conductivity, $\kappa$ [mS/cm]	Co-ion Diffusivity, $D_c^m$ ( $\times 10^{-7}$ cm <sup>2</sup> /s)	Counter-ion Diffusivity, $D_g^m$ ( $\times 10^{-7}$ cm <sup>2</sup> /s)
<b>HQ:BP-20</b>	$0.46 \pm 0.06$	$0.50 \pm 0.01$	$0.43 \pm 0.06$	$1.51 \pm 0.21$
<b>HQ:BP-25</b>	$1.54 \pm 0.13$	$1.72 \pm 0.08$	$1.49 \pm 0.13$	$4.25 \pm 0.37$
<b>HQ:BP-30</b>	$3.83 \pm 0.36$	$2.80 \pm 0.24$	$3.75 \pm 0.36$	$6.18 \pm 0.59$
<b>MHQ:BP-20</b>	$0.30 \pm 0.01$	$0.49 \pm 0.01$	$0.29 \pm 0.01$	$1.35 \pm 0.05$
<b>MHQ:BP-25</b>	$1.05 \pm 0.19$	$1.48 \pm 0.01$	$1.02 \pm 0.19$	$3.30 \pm 0.61$
<b>MHQ:BP-30</b>	$3.10 \pm 0.26$	$3.66 \pm 0.08$	$3.01 \pm 0.26$	$7.45 \pm 0.64$

The higher water diffusivity in MHQ:BP compared to that in the HQ:BP materials (Figure 9.4A) may be a result of a morphological change in the distribution of hydrophilic and hydrophobic nano-domains in the polymer matrix. The polarity of the methoxy group oxygen atoms may interact favorably with the polar sulfonate groups in a manner that shifts the distribution of free volume toward a smaller nominal free volume element size. This shift toward lower average free volume element sizes could facilitate additional transport pathways for water while still restricting transport of larger hydrated ions. This physical picture is generally consistent with the observed simultaneous increases in water diffusivity and permeability (Figures 9.1A and 9.4A) and decreases in salt diffusivity and permeability (Figures 9.1B and 9.4B) when methoxy groups are added to the polymer and the dry polymer density increases. While explicit characterization of this molecular scale detail is outside of the scope of this study, the results suggest that changes, in

nanophase separation and/or the distribution of free volume within the polymer, upon incorporation of methoxy groups in sulfonated polysulfone may lead to increased rates of water transport and suppressed rates of salt transport.

### **9.3. Conclusions**

The addition of methoxy functional groups to sulfonated polysulfone, a promising membrane material for desalination applications, improved the water/salt permeability selectivity (i.e., the ratio of water permeability to salt permeability) and water permeability of the polymers. This increase was largely driven by diffusion factors, which was different from the results of studies focused on uncharged polymers. Water content, dry density, and transport property results suggest that polymer density and fractional free volume effects may drive lower salt diffusivity while a shift in the distribution of free volume element sizes toward smaller sizes may facilitate the observed increase in water diffusivity in MHQ:BP compared to that in HQ:BP. Donnan exclusion appears to be more important for determining salt sorption properties than relative permittivity in these charged polymers, and changes in co-ion diffusion coefficients, upon addition of methoxy groups, were responsible for the observed changes in salt diffusion properties. Furthermore, salt sorption in these sulfonated polysulfones was not quantitatively described by the Donnan-Manning model, which has been previously shown to describe satisfactorily the salt sorption properties of other charged polymers. This result may be due to the low water content and/or the heterogeneous distribution of fixed charge groups in these sulfonated polysulfones. The results reported here provide further guidance to inform the engineering of desalination materials with favorable performance.

#### 9.4. References

1. Cohen, Y.; Semiat, R.; Rahardianto, A., A perspective on reverse osmosis water desalination: Quest for sustainability. *AIChE Journal* **2017**, *63* (6), 1771-1784.
2. Geise, G. M.; Lee, H.-S.; Miller, D. J.; Freeman, B. D.; McGrath, J. E.; Paul, D. R., Water purification by membranes: The role of polymer science. *Journal of Polymer Science Part B: Polymer Physics* **2010**, *48* (15), 1685-1718.
3. Geise, G. M.; Paul, D. R.; Freeman, B. D., Fundamental water and salt transport properties of polymeric materials. *Progress in Polymer Science* **2014**, *39* (1), 1-42.
4. Park, H. B.; Freeman, B. D.; Zhang, Z.-B.; Sankir, M.; McGrath, J. E., Highly chlorine-tolerant polymers for desalination. *Angewandte Chemie International Edition* **2008**, *47* (32), 6019-6024.
5. Allegrezza, A. E.; Parekh, B. S.; Parise, P. L.; Swiniarski, E. J.; White, J. L., Chlorine resistant polysulfone reverse osmosis modules. *Desalination* **1987**, *64*, 285-304.
6. Luo, H.; Aboki, J.; Ji, Y.; Guo, R.; Geise, G. M., Water and salt transport properties of triptycene-containing sulfonated polysulfone materials for desalination membrane applications. *ACS Applied Materials & Interfaces* **2018**, *10* (4), 4102-4112.
7. Geise, G. M.; Freeman, B. D.; Paul, D. R., Characterization of a sulfonated pentablock copolymer for desalination applications. *Polymer* **2010**, *51* (24), 5815-5822.
8. Kimura, S. G., Reverse osmosis performance of sulfonated poly(2,6-dimethylphenylene ether) ion exchange membranes. *Industrial & Engineering Chemistry Product Research and Development* **1971**, *10* (3), 335-339.
9. Kim, Y.-J.; Lee, K.-S.; Jeong, M.-H.; Lee, J.-S., Highly chlorine-resistant end-group crosslinked sulfonated-fluorinated poly(arylene ether) for reverse osmosis membrane. *Journal of Membrane Science* **2011**, *378* (1), 512-519.

10. Zhang, Y.; Zhao, C.; Yan, H.; Pan, G.; Guo, M.; Na, H.; Liu, Y., Highly chlorine-resistant multilayer reverse osmosis membranes based on sulfonated poly(arylene ether sulfone) and poly(vinyl alcohol). *Desalination* **2014**, *336*, 58-63.
11. Glater, J.; Hong, S.-k.; Elimelech, M., The search for a chlorine-resistant reverse osmosis membrane. *Desalination* **1994**, *95* (3), 325-345.
12. Paul, M.; Park, H. B.; Freeman, B. D.; Roy, A.; McGrath, J. E.; Riffle, J. S., Synthesis and crosslinking of partially disulfonated poly(arylene ether sulfone) random copolymers as candidates for chlorine resistant reverse osmosis membranes. *Polymer* **2008**, *49* (9), 2243-2252.
13. Xie, W.; Geise, G. M.; Freeman, B. D.; Lee, H.-S.; Byun, G.; McGrath, J. E., Polyamide interfacial composite membranes prepared from m-phenylene diamine, trimesoyl chloride and a new disulfonated diamine. *Journal of Membrane Science* **2012**, *403-404*, 152-161.
14. Kamcev, J.; Freeman, B. D., Charged polymer membranes for environmental/energy applications. *Annual Review of Chemical and Biomolecular Engineering* **2016**, *7* (1), 111-133.
15. Luo, H.; Chang, K.; Bahati, K.; Geise, G. M., Functional group configuration influences salt transport in desalination membrane materials. *Journal of Membrane Science* **2019**, *590*, 117295.
16. Luo, H.; Chang, K.; Bahati, K.; Geise, G. M., Engineering selective desalination membranes via molecular control of polymer functional groups. *Environmental Science & Technology Letters* **2019**, *6* (8), 462-466.
17. Lonsdale, H. K.; Merten, U.; Riley, R. L., Transport properties of cellulose acetate osmotic membranes. *Journal of Applied Polymer Science* **1965**, *9* (4), 1341-1362.
18. Yasuda, H.; Lamaze, C. E., Improved membranes for reverse osmosis, Research and development progress report, United States Department of the Interior: Washington, D.C., 1969, p. 473.
19. Jang, E.-S.; Kamcev, J.; Kobayashi, K.; Yan, N.; Sujanani, R.; Dilenschneider, T. J.; Park, H. B.; Paul, D. R.; Freeman, B. D., Influence of water content on alkali metal chloride

transport in cross-linked Poly(ethylene glycol) Diacrylate.1. Ion sorption. *Polymer* **2019**, *178*, 121554.

20. Zhang, H.; Geise, G. M., Modeling the water permeability and water/salt selectivity tradeoff in polymer membranes. *Journal of Membrane Science* **2016**, *520*, 790-800.

21. Geise, G. M.; Falcon, L. P.; Freeman, B. D.; Paul, D. R., Sodium chloride sorption in sulfonated polymers for membrane applications. *Journal of Membrane Science* **2012**, *423*, 195-208.

22. Helfferich, F. G., *Ion Exchange*. Dover Publications, McGraw-Hill: New York, 1995.

23. Yasuda, H.; Lamaze, C. E.; Ikenberry, L. D., Permeability of solutes through hydrated polymer membranes. Part I. Diffusion of sodium chloride. *Die Makromolekulare Chemie* **1968**, *118* (1), 19-35.

24. Chang, K.; Korovich, A.; Xue, T.; Morris, W. A.; Madsen, L. A.; Geise, G. M., Influence of rubbery versus glassy backbone dynamics on multiscale transport in polymer membranes. *Macromolecules* **2018**, *51* (22), 9222-9233.

25. Wiegand, J. R.; Smith, Z. P.; Liu, Q.; Patterson, C. T.; Freeman, B. D.; Guo, R., Synthesis and characterization of triptycene-based polyimides with tunable high fractional free volume for gas separation membranes. *Journal of Materials Chemistry A* **2014**, *2* (33), 13309-13320.

26. Luo, S.; Liu, J.; Lin, H.; Kazanowska, B. A.; Hunckler, M. D.; Roeder, R. K.; Guo, R., Preparation and gas transport properties of triptycene-containing polybenzoxazole (PBO)-based polymers derived from thermal rearrangement (TR) and thermal cyclodehydration (TC) processes. *Journal of Materials Chemistry A* **2016**, *4* (43), 17050-17062.

27. Weidman, J. R.; Luo, S.; Zhang, Q.; Guo, R., Structure manipulation in triptycene-based polyimides through main chain geometry variation and its effect on gas transport properties. *Industrial & Engineering Chemistry Research* **2017**, *56* (7), 1868-1879.

28. Luo, S.; Zhang, Q.; Bear, T. K.; Curtis, T. E.; Roeder, R. K.; Doherty, C. M.; Hill, A. J.; Guo, R., Triptycene-containing poly(benzoxazole-co-imide) membranes with enhanced mechanical strength for high-performance gas separation. *Journal of Membrane Science* **2018**, *551*, 305-314.
29. Harrison, W. L.; Wang, F.; Mecham, J. B.; Bhanu, V. A.; Hill, M.; Kim, Y. S.; McGrath, J. E., Influence of the bisphenol structure on the direct synthesis of sulfonated poly(arylene ether) copolymers. I. *Journal of Polymer Science Part A: Polymer Chemistry* **2003**, *41* (14), 2264-2276.
30. Ueda, M.; Toyota, H.; Ouchi, T.; Sugiyama, J.-I.; Yonetake, K.; Masuko, T.; Teramoto, T., Synthesis and characterization of aromatic poly(ether sulfone)s containing pendant sodium sulfonate groups. *Journal of Polymer Science Part A: Polymer Chemistry* **1993**, *31* (4), 853-858.
31. Cook, J., Fundamental water and ion transport characterization of sulfonated polysulfone desalination materials. **2014**, *Ph.D. Thesis, Department of Chemical Engineering, The University of Texas at Austin, Austin, Texas, 2014*.
32. Xie, W.; Ju, H.; Geise, G. M.; Freeman, B. D.; Mardel, J. I.; Hill, A. J.; McGrath, J. E., Effect of free volume on water and salt transport properties in directly copolymerized disulfonated poly(arylene ether sulfone) random copolymers. *Macromolecules* **2011**, *44* (11), 4428-4438.
33. Wijmans, J. G.; Baker, R. W., The solution-diffusion model: A review. *Journal of Membrane Science* **1995**, *107* (1), 1-21.
34. Paul, D. R., Reformulation of the solution-diffusion theory of reverse osmosis. *Journal of Membrane Science* **2004**, *241* (2), 371-386.
35. Chang, K.; Xue, T.; Geise, G. M., Increasing salt size selectivity in low water content polymers via polymer backbone dynamics. *Journal of Membrane Science* **2018**, *552*, 43-50.

36. Park, H. B.; Kamcev, J.; Robeson, L. M.; Elimelech, M.; Freeman, B. D., Maximizing the right stuff: The trade-off between membrane permeability and selectivity. *Science* **2017**, *356* (6343).
37. Ji, Y.; Luo, H.; Geise, G. M., Specific co-ion sorption and diffusion properties influence membrane permselectivity. *Journal of Membrane Science* **2018**, *563*, 492-504.
38. Chang, K.; Luo, H.; Geise, G. M., Water content, relative permittivity, and ion sorption properties of polymers for membrane desalination. *Journal of Membrane Science* **2019**, *574*, 24-32.
39. Chang, K.; Geise, G. M., Dielectric permittivity properties of hydrated polymers: Measurement and connection to ion transport properties. *Industrial & Engineering Chemistry Research* **2020**, *59* (12), 5205-5217.
40. Manning, G. S., Limiting laws and counterion condensation in polyelectrolyte solutions I. Colligative properties. *The Journal of Chemical Physics* **1969**, *51* (3), 924-933.
41. Kamcev, J.; Galizia, M.; Benedetti, F. M.; Jang, E.-S.; Paul, D. R.; Freeman, B. D.; Manning, G. S., Partitioning of mobile ions between ion exchange polymers and aqueous salt solutions: Importance of counter-ion condensation. *Physical Chemistry Chemical Physics* **2016**, *18* (8), 6021-6031.
42. Pitzer, K. S.; Peiper, J. C.; Busey, R. H., Thermodynamic properties of aqueous sodium chloride solutions. *Journal of Physical and Chemical Reference Data* **1984**, *13* (1), 1-102.
43. Kamcev, J.; Paul, D. R.; Freeman, B. D., Ion activity coefficients in ion exchange polymers: Applicability of Manning's counterion condensation theory. *Macromolecules* **2015**, *48* (21), 8011-8024.
44. Kamcev, J.; Paul, D. R.; Manning, G. S.; Freeman, B. D., Predicting salt permeability coefficients in highly swollen, highly charged ion exchange membranes. *ACS Applied Materials & Interfaces* **2017**, *9* (4), 4044-4056.

45. Xie, W.; Cook, J.; Park, H. B.; Freeman, B. D.; Lee, C. H.; McGrath, J. E., Fundamental salt and water transport properties in directly copolymerized disulfonated poly(arylene ether sulfone) random copolymers. *Polymer* **2011**, *52* (9), 2032-2043.
46. Kamcev, J.; Paul, D. R.; Manning, G. S.; Freeman, B. D., Ion diffusion coefficients in ion exchange membranes: Significance of counterion condensation. *Macromolecules* **2018**, *51* (15), 5519-5529.
47. Kamcev, J.; Paul, D. R.; Manning, G. S.; Freeman, B. D., Accounting for frame of reference and thermodynamic non-idealities when calculating salt diffusion coefficients in ion exchange membranes. *Journal of Membrane Science* **2017**, *537*, 396-406.
48. Luo, H.; Agata, W.-A. S.; Geise, G. M., Connecting the ion separation factor to the sorption and diffusion selectivity of ion exchange membranes. *Industrial & Engineering Chemistry Research* **2020**, *59* (32), 14189-14206.

## Chapter 10: Conclusions and Recommendations

### 10.1. Conclusions

Fundamental structure-property relationships between polymer chemistry and desalination properties were established throughout the chapters of this dissertation. In uncharged polymers, preparing materials that have a rigid polymer backbone and/or a distributed chemical functional group configurations are important strategies for achieving high water/salt permeability selectivity, and in charged polymers, adding methoxy functional groups to the polymer backbone was determined to enhance the selectivity and water permeability properties of the materials. Important for desalination applications, the structure-property guidance reported in this dissertation may help future efforts to engineer and design highly selective polymer membranes, and ultimately, these advanced membranes, with excellent chemical stability and favorable desalination performance, can be used for efficient and effective future desalination. The detailed conclusions of each studies are summarized in the following paragraphs.

Chapters 3 and 4 report that in low water content uncharged polymers, the polymers with rigid and glassy backbones have slower ion diffusion, and thus, higher water/ion permeability selectivity properties than that of the polymers with flexible and rubbery backbones. This observation can be attributed to sub-micrometer length scale morphological and dynamical differences in the polymers. Comparable to gas separation membranes, rigid backbone polymers exhibit higher salt size selectivity, among the three electrolytes studied, than that of flexible backbone polymers. These results suggest that preparing polymers with rigid backbones is one strategy to achieve high water/ion selective properties for efficient and effective membrane desalination.

Chapter 5 reports that, at equivalent water content, the functional relationship between relative permittivity and water content in uncharged model polymers was observed to differ when compared to that of a commercially available ion exchange (i.e., charged) membrane. This result suggests that chemical details, not water content alone, influence the relative permittivity properties of some hydrated polymers. Consistent with some previous studies, relative permittivity of the model polymers increased as polymer water content increased. This result suggests more extensive water molecule dipole relaxation, which is consistent with the increase in freezable water content observed, in the polymers that sorb higher amount of water than the polymers that sorb lower amount of water.

Further, qualitative agreement between experimentally measured and electrostatic theory predicted ion sorption coefficients was observed. This result suggests that the relative permittivity measurements captured part of the physics that describes the ion sorption process in these hydrated model polymers. As a result, relative permittivity measurements may provide critical insight into the fundamental structure-property relationships between polymer chemistry and ion sorption that can be important for the design of advanced desalination polymer membrane.

In Chapters 6 and 7, the results showed that a distributed hydroxyl group configuration leads to suppressed salt sorption, and thus, increasing water/salt permeability selectivity properties compared to that of a vicinal diol-rich (i.e., two hydroxyl group) configuration. This reduction in salt sorption in polymers that have distributed hydroxyl group configurations was consistent with a simultaneous reduction in relative permittivity and the freezable water content. These results suggest a hydrogen bonding environment where water molecules interact to a greater extent with the polymer backbone when the chemical functional groups are evenly distributed in the polymer matrix. Consistent with the electrostatic exclusion theory, polymers that exhibit low relative

permittivity polymers can often suppress ion sorption (or promote ion exclusion) that is favorable for desalination applications. As a result, preparing polymers with distributed functional group configurations may be a viable strategy to engineer highly selective desalination membranes.

The increase in ion sorption coefficients in an uncharged polymer as external salt concentration increased, which was observed in [Chapter 8](#), is different from the observations made on some hydrated polymers where the ion sorption properties do not depend on the external salt concentration. This result may stem from the competition between ions and water for interactions with the polymer backbone, and such competition was observed to be more apparent in low water content polymers based on the relative permittivity and state of water results. Further, the increase in relative permittivity as salt concentration increased, observed in the model polymers, is fundamentally different from the observations made on the aqueous salt solutions where the relative permittivity decreased as salt concentration increased.

In [Chapter 9](#), the results showed that adding methoxy functional groups to the backbone of sulfonated polysulfone increased water/salt permeability selectivity, which is a property that is favorable for desalination applications. Functional group incorporation (i.e., adding methoxy groups) increased the dry polymer density and may reduce the fractional free volume to drive a decrease in salt diffusivity, and this change in polymer density also may be coupled with a shift in the distribution of free volume elements toward smaller nominal sizes to drive an increase in water diffusivity, in these sulfonated polysulfones. Relative permittivity and ion sorption results suggest that Donnan exclusion (electrostatic interactions between ions and fixed charge groups) may dominate the ion sorption properties in these charged polymers, which is different from the observations made on uncharged polymers, which exhibit a simple partitioning mechanism. Further, the Donnan-Manning model, known to describe the ion sorption process in highly charged

and highly swollen polymers, did not quantitatively describe the low water content sulfonated polysulfones that have a heterogeneous distribution of fixed charge groups.

## 10.2. Significance

Chapters 3 and 4 report important information about the functional relationship of polymer backbone rigidity and transport and selectivity properties in low water content polymers. Since commercially available desalination membranes often sorb relatively low amounts of water,<sup>1-3</sup> water molecules in these materials are expected to interact with the polymer backbone more significantly compared to that in highly hydrated materials. The results of these studies critically inform that the interactions between water molecules and the polymer backbone can be controlled, via backbone rigidity modifications, to achieve low salt diffusion and high water/salt selectivity properties that are favorable for desalination applications. Future work should continue to focus on making membrane materials that have rigid polymer backbones for favorable desalination properties.

For the first time, microwave dielectric relaxation spectroscopy (DRS) was used in Chapter 5 to characterize the frequency-dependent relative permittivity properties of desalination polymer membranes. The thermodynamic view (i.e., electrostatic exclusion theory) informs the importance of membrane phase relative permittivity in governing the ion sorption process in the materials.<sup>4-11</sup> The ability to accurately and reliably measure hydrated polymer relative permittivity, using microwave DRS, provides critical insight into the molecular-level interactions between water molecules and the polymer backbone, which can be used to understand the ion sorption process in the materials. The structure-property relationship between relative permittivity and ion sorption properties is important information that can be used in future research effort to guide the design of highly sorption selective desalination membranes.

Most studies that have focused on studying the fundamental influence of polymer chemistry on transport and selectivity properties often have had to deal with the challenge of the simultaneous change in polymer water content (or hydrophilicity).<sup>12-15</sup> To address this challenge, in [Chapters 6 and 7](#), a series of water content equivalent polymers were prepared by changing the ratio of co-monomers incorporated into the polymer films. This unique polymer preparation approach enabled studies on the structure-property relationship between chemical functional group positioning in the polymer matrix and the polymer transport and selectivity properties. Using microwave DRS, thermal and transport characterization techniques, the results of these studies provide critical structure-property relationships that can guide the engineering of highly selective desalination membranes. Future research should focus on preparing more water content equivalent materials of different polymer chemistry to understand the structure-property relationships in these desalination membrane materials.

In [Chapter 8](#), the fundamental influence of salt concentration on hydrated polymer relative permittivity and state of water properties was investigated, which is important because [Chapters 5, 6, and 7](#), and other studies<sup>16,17</sup> often focused on investigating the structure-property relationships of pure water equilibrated polymers. Questions still remain on how the introduction of ions can influence the relative permittivity, state of water, and ion sorption properties of hydrated polymers. In this study, microwave DRS and FT-IR techniques were used that provide insight into the interactions between ions, water, and the polymer backbone in the hydrated polymers that were equilibrated in a single electrolyte. This information is critical to help understand the factors that influence the sorption properties in the materials, and continuous research effort is needed to explore the influence of other and/or mixed electrolyte systems on the sorption properties of these hydrated polymers.

In [Chapter 9](#), the fundamental structure-property relationships in charged polymers was investigated, which is an important contribution to the field as fundamental structure-property studies often focused on studying uncharged polymers as demonstrated in [Chapters 3, 4, 5, 6, 7, and 8](#). Important for desalination applications, we observed that adding chemical functional groups (i.e., methoxy groups) to the polymer backbone of sulfonated polysulfones can drive favorable desalination properties. The results of the study opened up opportunities of continuous research on fundamental structure-property relationships of charged polymers, as they are candidates of future generation desalination membranes that can potentially replace the current state-of-the-art polyamide-based membranes.

### **10.3. Recommendations for Future Work**

#### **10.3.1. The Role of Experimental Factors in Dielectric Permittivity Measurements**

In [Chapters 5, 6, 7, 8, and 9](#), we used microwave DRS as an important tool to measure the frequency-dependent relative permittivity of hydrated polymers. The results obtained from microwave DRS can inform insight into the molecular-level interactions between water molecules, ions, and the polymer backbone, which is critical information to help understand the sorption processes in these materials. In the previous studies, microwave DRS measurements were conducted under room temperature ( $22 \pm 1$  °C) with only a certain concentration range of aqueous NaCl solutions (i.e., 0.01 to 1.0 M) considered. Questions still remain about the influence of temperature, other ions (both monovalent and multivalent), and ion concentration on relative permittivity properties of hydrated polymers. Using the same methacrylate-based model polymer and the characterization techniques described in [Chapters 5 and 8](#), the outcomes of this study will provide important insight into molecular-level interactions between different types of ions, water, and the polymer backbone, under the influence of different temperatures (controlled by a

temperature chamber). This information can be further used to understand the ion sorption process in hydrated polymers, which will be critical to guide the design of advanced polymer membranes used for desalination applications.

### **10.3.2. Influence of Chemical Functional Groups on Water and Ion Transport and Selectivity Properties in Sulfonated Polysulfone**

In [Chapter 9](#), we demonstrated that chemical functional group (i.e., methoxy group) incorporation on the polymer backbone can lead to increased polymer dry density, reduced fractional free volume and shifted distribution of free volume, and thus, high transport selective properties in sulfonated polysulfone materials (charged polymers). Questions still remain about whether the incorporation of hydrophilic side chains (i.e., hydroxyl groups, which are more hydrophilic than methoxy groups) to the backbone of sulfonated polysulfone can further promote the dielectric exclusion mechanism, which is expected to enhance water/ion permeability selectivity properties. The understanding of the influence of chemical functional groups on transport and selectivity properties of sulfonated polysulfones is important, because they are chemically and mechanically stable polymer membrane materials that may become the next generation desalination membranes. Structure-property understanding can help achieving the goal of preparing these sulfonated polysulfones to exhibit transport properties that are comparable to commercially available polyamide-based desalination membranes, and thus, replacing them for more efficient and effective future generation desalination.

## **10.4. References**

1. Freger, V., Swelling and morphology of the skin layer of polyamide composite membranes: An atomic force microscopy study. *Environmental Science & Technology* **2004**, *38* (11), 3168-3175.

2. Lonsdale, H. K.; Merten, U.; Riley, R. L., Transport properties of cellulose acetate osmotic membranes. *Journal of Applied Polymer Science* **1965**, *9* (4), 1341-1362.
3. Chan, E. P.; Young, A. P.; Lee, J.-H.; Chung, J. Y.; Stafford, C. M., Swelling of ultrathin crosslinked polyamide water desalination membranes. *Journal of Polymer Science Part B: Polymer Physics* **2013**, *51* (6), 385-391.
4. Zhang, H.; Geise, G. M., Modeling the water permeability and water/salt selectivity tradeoff in polymer membranes. *Journal of Membrane Science* **2016**, *520*, 790-800.
5. Glueckauf, E., On the mechanism of osmotic desalting with porous membranes. *Proceedings of the First International Symposium on Water Desalination* **1967**, 143-150.
6. Anderson, J. E.; Pusch, W., The membrane/water partition coefficients of ions: Electrostatic calculations of dielectric heterogeneity. *Berichte der Bunsengesellschaft für physikalische Chemie* **1976**, *80* (9), 846-849.
7. Yaroshchuk, A. E., Dielectric exclusion of ions from membranes. *Advances in Colloid and Interface Science* **2000**, *85* (2), 193-230.
8. Yaroshchuk, A. E., Non-steric mechanisms of nanofiltration: Superposition of Donnan and dielectric exclusion. *Separation and Purification Technology* **2001**, *22-23*, 143-158.
9. Freger, V.; Bason, S., Characterization of ion transport in thin films using electrochemical impedance spectroscopy: I. Principles and theory. *Journal of Membrane Science* **2007**, *302* (1), 1-9.
10. Kamcev, J.; Galizia, M.; Benedetti, F. M.; Jang, E.-S.; Paul, D. R.; Freeman, B. D.; Manning, G. S., Partitioning of mobile ions between ion exchange polymers and aqueous salt solutions: Importance of counter-ion condensation. *Physical Chemistry Chemical Physics* **2016**, *18* (8), 6021-6031.
11. Kamcev, J.; Paul, D. R.; Manning, G. S.; Freeman, B. D., Predicting salt permeability coefficients in highly swollen, highly charged ion exchange membranes. *ACS Applied Materials & Interfaces* **2017**, *9* (4), 4044-4056.

12. Geise, G. M.; Lee, H.-S.; Miller, D. J.; Freeman, B. D.; McGrath, J. E.; Paul, D. R., Water purification by membranes: The role of polymer science. *Journal of Polymer Science Part B: Polymer Physics* **2010**, *48* (15), 1685-1718.
13. Geise, G. M.; Paul, D. R.; Freeman, B. D., Fundamental water and salt transport properties of polymeric materials. *Progress in Polymer Science* **2014**, *39* (1), 1-42.
14. Kamcev, J.; Freeman, B. D., Charged polymer membranes for environmental/energy applications. *Annual Review of Chemical and Biomolecular Engineering* **2016**, *7* (1), 111-133.
15. Hickner, M. A., Ion-containing polymers: New energy & clean water. *Materials Today* **2010**, *13* (5), 34-41.
16. Lu, Z.; Polizos, G.; Macdonald, D. D.; Manias, E., State of water in perfluorosulfonic ionomer (Nafion® 117) proton exchange membranes. *Journal of The Electrochemical Society* **2008**, *155* (2), B163-B171.
17. Paddison, S. J.; Reagor, D. W.; Zawodzinski Jr, T. A., High frequency dielectric studies of hydrated Nafion®. *Journal of Electroanalytical Chemistry* **1998**, *459* (1), 91-97.

## Appendix A: Nomenclature

**Table A.1.** Nomenclature.

$w_u$	Water uptake
$m_{wet}$	Sample wet mass
$m_{dry}$	Sample dry mass
$\phi_w^m$	Volume fraction of water
$\rho_w$	Water density
$\rho_p$	Polymer density
$m_{air}$	Sample mass in air
$m_{aux}$	Sample mass in auxiliary liquid
$\rho_{air}$	Air density
$\rho_{aux}$	Auxiliary liquid density
$K_w$	Water sorption coefficient
$C_w^m$	Water concentration in the polymer
$C_w$	Water concentration in the bulk external solution
$M_w$	Molecular weight of water
$V_w$	Partial molar volume of water in the polymer
$K_s$	Salt sorption coefficient ( $= K_s^m$ )
$C_s^m$	Salt concentration in the membrane
$C_s^s$	Salt concentration in the external solution
$C_d$	Final salt concentration of desorption solution
$V_d$	Desorption volume
$V_p$	Volume of the hydrated sample
$S_{11,12,21,or 22}$	S-parameters
$\omega$	Angular frequency
$c$	Speed of light in vacuum
$\mu^*$	Relative complex permeability
$\epsilon^*$	Relative complex permittivity
$d$	Length dimension that describes how much of the transmission line is filled with sample
$I$	Signal intensity at a given gradient strength
$I_0$	Signal intensity at zero gradient strength
$D_w$	Water diffusion coefficient
$\gamma$	Gyromagnetic ratio of the $^1\text{H}$ nucleus
$g$	Gradient strength
$\delta$	Effective rectangular gradient pulse length
$\Delta$	Diffusion encoding time
$b$	Stejskal-Tanner parameter
$R_{m+s}$	Area resistance of the membrane + solution
$V_c$	Voltage for conductivity measurements
$I_c$	Current for conductivity measurements
$\sigma_m$	Membrane conductivity

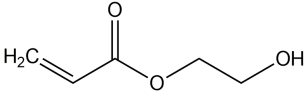
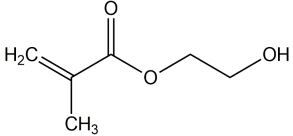
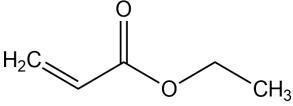
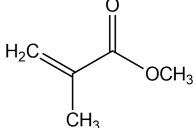
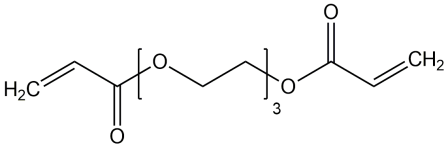
$R_m$	Area resistance of the membrane
$L$	Swollen membrane thickness
$M_t$	Mass of desorbed salt at time $t$
$M_\infty$	Mass of salt desorbed from the polymer at infinite time
$D_s$	The effective salt diffusion coefficient ( $= D_s^m$ )
$t$	Time
$V$	Volume of liquid in the donor and receiver chambers
$A$	Area available for transport
$C_R(t)$	Salt concentration in receiver chamber at time $t$
$C_D(0)$	Initial salt concentration in the donor chamber
$M_t$	Concentration of Desorption Solution at Time $t$
$M_\infty$	Concentration of Desorption Solution at Infinite Time
$P_s$	Salt permeability
$T_{gi}$	Glass transition temperature of component $i$
$\omega_i$	Mass fraction of component $i$
$D_s^s$	Average salt diffusivity in aqueous solution
$z_+$	Charge numbers of cations
$z_-$	Charge numbers of anions
$D_+$	Cation diffusion coefficients at infinite dilution in aqueous solution
$D_-$	Anion diffusion coefficients at infinite dilution in aqueous solution
$l_d$	Diffusion length
$\langle r^2 \rangle^{1/2}$	Root-mean-square distance that molecules travel during the NMR diffusometry experiment
$\mathfrak{S}$	Tortuosity
$\mathfrak{S}_{L-B}$	“Local-to-bulk” tortuosity
$\mathfrak{S}_{\mu-B}$	“Micron-to-bulk” tortuosity
$D_\infty$	Water diffusion coefficient at infinite diffusion time (or length)
$D_{loc}$	Water self-diffusion coefficient in bulk pure water
$D_0$	Water self-diffusion coefficient near the minimum measurable time of the NMR diffusometry experiments
$w_f$	Freezable water content
$w_{nf}$	Non-freezable water content
$m_f$	Mass of freezable water in the polymer
$\Delta H_{polymer}$	Enthalpy of melting in the polymer
$\Delta H_{m,H_2O}^\circ$	Enthalpy of melting for water
$\gamma_\pm^m$	Mean ionic activity coefficient in the membrane phase
$\gamma_+^m$	Cation activity coefficient in the membrane phase
$\gamma_-^m$	Anion activity coefficient in the membrane phase
$\gamma_\pm^s$	Mean ionic activity coefficient of the external solution
$C_+^m$	Counter-ion concentration in the membrane
$C_-^m$	Co-ion concentration in the membrane
$\Delta W_s$	Solvation energy barrier
$k_B$	Boltzmann’s constant
$T$	Absolute temperature

$z_s$	Ion charge number
$e$	Elementary charge
$\epsilon_0$	Permittivity of free space
$a_s$	Bare ion radius
$\epsilon_m$	Static relative permittivity (or dielectric constant) of the membrane
$\epsilon_{sol}$	Static relative permittivity (or dielectric constant) of the external solution
<b>R</b>	Salt rejection
$C_{s,feed}$	Salt concentration of the bulk solution on the feed side of the membrane
$C_{s,permeate}$	Salt concentration of the bulk solution on the permeate (or product) side of the membrane
$R$	Ideal gas constant
$\Delta p$	Hydraulic pressure difference across the membrane
$\Delta \pi$	Osmotic pressure difference across the membrane
$\epsilon_{s,m}$	Static dielectric constant of the heterogeneous material (or hydrated polymer membrane)
$\epsilon_{s,p}$	Static dielectric constant of the dry polymer
$\epsilon_{s,w}$	Static dielectric constant of water
$C_A^{m,w}$	Membrane fixed charge group concentration that is normalized to the volume of sorbed water ( $= C_A^m$ )
$\xi$	Dimensionless parameter
$\lambda_B$	Bjerrum length
$b$	Distance between fixed charge groups on the polymer chain
$IEC$	Ion exchange capacity
$D_g^m$	Counter-ion diffusivity
$D_c^m$	Co-ion diffusivity
$z_g$	Counter-ion valences
$z_c$	Co-ion valences
$C_g^{m,p}$	Counter-ion concentration
$C_c^{m,p}$	Co-ion concentration
$\kappa$	Salt conductivity
$F$	Faraday's constant
$K_{w,w}$	Water sorption coefficient measured using pure water
$K_{w,s}$	Water sorption coefficient measured using 1.0 mol/L NaCl

## Appendix B: Supporting Information for Chapter 3

### B.1. Chemical Structures of the Components Used to Prepare the Co-polymers

**Table B.1.** Chemical structures of the co-monomers and cross-linker used to prepare the HEMA-co-MMA and HEA-co-EA co-polymers. Pure water uptake data are included for polymers prepared from each component, and the homopolymer glass transition temperature is reported for polymers prepared from each component.

Component	Chemical Structure	Water Uptake <sup>a</sup> [g(water)/g(dry polymer)]	$T_g$ [°C]
HEA		1.60	-15 <sup>1,2</sup>
HEMA		0.60	55 <sup>3</sup>
EA		0.01	-24 <sup>3</sup>
MMA		0.01	106 <sup>3</sup>
PEGDA		0.05	-83 <sup>4</sup>

<sup>a</sup>The water uptake data for poly(HEA) and poly(HEMA) was measured using polymers of each component that were crosslinked with 3% PEGDA. The water uptake values of poly(EA), poly(MMA), and poly(PEGDA) were characterized using homopolymers prepared via UV-initiated free radical polymerization.

## B.2. Effective Salt Diffusion Coefficients (Experimentally Determined and Calculated)

**Table B.2.** Effective salt diffusion coefficients in the HEA-co-EA and HEMA-co-MMA materials,  $D_s$ , determined both experimentally and via the Mackie and Meares model.<sup>5</sup>

Material	Method	Effective Salt Diffusion Coefficient [ $\times 10^{-9}$ cm <sup>2</sup> /s]		
		LiCl	NaCl	KCl
HEA-co-EA	Experimental	3.3 ± 0.9	6.9 ± 2.2	18.6 ± 3.6
	Mackie and Meares	23.8	28.7	31.9
HEMA-co-MMA	Experimental	0.8 ± 0.1	2.7 ± 0.8	8.1 ± 1.2
	Mackie and Meares	22.6	34.1	41.2

## B.3. Comparison of Water Content and the Amount of Water Required to Hydrate Ions

To determine if sufficient water is sorbed by the HEA-co-EA and HEMA-co-MMA materials to fully hydrate the sorbed ions, information was needed about the water content of the polymers (Table 3.1 in Chapter 3), the salt sorption coefficients (Table 3.4 in Chapter 3), and the hydration numbers of the ions (Table B.3). The example calculation (below) determined the number of moles of water present in a given amount of polymer and the number of moles of water needed to hydrate the ions that are sorbed in the given amount of polymer. The final results are presented as a ratio of the moles of water available for hydration and the moles of water required to fully hydrate the sorbed ions.

**Table B.3.** Hydration numbers<sup>6</sup> for the ions considered.

Ion	Hydration Number
K <sup>+</sup>	2.6
Na <sup>+</sup>	3.5
Li <sup>+</sup>	5.2
Cl <sup>-</sup>	2.0

### Sample calculation for HEA-co-EA in equilibrium with 0.5 mol/L LiCl

The number of moles of water available in the polymer was calculated using the water sorption coefficient. With a  $K_w$  value of 0.080 (Table 3.1 in Chapter 3), 1 cm<sup>3</sup> (hydrated polymer) contained 0.080 g(water) or 4.4x10<sup>-3</sup> mol(water). The salt sorption coefficient was used to determine the moles of Li<sup>+</sup> and Cl<sup>-</sup> sorbed in the polymer at equilibrium with a 0.5 mol/L solution:

$$n_{LiCl} = n_{Li^+} = n_{Cl^-} = K_S \cdot 1cm^3(\text{hydrated polymer}) \cdot C_S^S \quad (\text{B.1})$$

With  $K_S = 0.022$  (Table 3.4) and  $C_S^S = 0.5$  mol/L, 1.1x10<sup>-5</sup> mol of Li<sup>+</sup> and Cl<sup>-</sup> sorbed into the polymer at equilibrium. The ion hydration numbers were used to determine the moles of water needed to hydrate the ions sorbed in the polymer, and using the data in Table B.3 gave a total of 7.9x10<sup>-5</sup> mol(water) needed to hydrate the Li<sup>+</sup> and Cl<sup>-</sup> in the polymer. Therefore, the 4.4x10<sup>-3</sup> mol(water) available in the polymer was divided by the 7.9x10<sup>-5</sup> mol(water) needed to hydrate the ions to determine that a factor of 56 more water molecules were available in the polymer compared to what was needed to hydrate the sorbed ions in the polymer. The ratios for the other electrolytes and the HEMA-co-MMA materials (calculated using the same approach described above) are presented in Table B.4.

**Table B.4.** Values of the number of moles of water available in the polymer divided by the number of moles of water required to fully hydrate the ions sorbed in the polymer.

Material	0.5 mol/L LiCl	0.5 mol/L NaCl	0.5 mol/L KCl
HEA-co-EA	56	102	169
HEMA-co-MMA	45	119	210

**Table B.5.** Free energy values for the hydration of monovalent ions at 25 °C.<sup>7</sup> The energies given on the per mole of water basis were calculated from the per mole of ion basis using the hydration numbers in Table B.3.

Ion	Free Energy of Hydration	
	[kcal/mol(ion)]	[kcal/mol(water)]
K <sup>+</sup>	-73.5	-28.3
Na <sup>+</sup>	-89.7	-25.6
Li <sup>+</sup>	-114.6	-22.0
Cl <sup>-</sup>	-84.2	-42.1

#### B.4. References

1. Technical Data Specialty Monomers. BASF: 2016.
2. Scientific Polymer Products, Poly(2-hydroxyethyl acrylate), Cat# 850. <https://scientificpolymer.com/shop/poly2-hydroxyethyl-acrylate-2/> (accessed September 13, 2017).
3. Mark, J. E., *Polymer Data Handbook*. Oxford University Press: 1999.
4. Oh, H. J.; Freeman, B. D.; McGrath, J. E.; Lee, C. H.; Paul, D. R., Thermal analysis of disulfonated poly(arylene ether sulfone) plasticized with poly(ethylene glycol) for membrane formation. *Polymer* **2014**, *55* (1), 235-247.
5. Mackie, J. S.; Meares, P., The diffusion of electrolytes in a cation-exchange resin membrane I. Theoretical. *Proceedings of the Royal Society of London. Series A. Mathematical and Physical Sciences* **1955**, *232* (1191), 498-509.
6. Marcus, Y., A simple empirical model describing the thermodynamics of hydration of ions of widely varying charges, sizes, and shapes. *Biophysical Chemistry* **1994**, *51* (2), 111-127.
7. Robinson, R. A.; Stokes, R. H., *Electrolyte Solutions*. 2nd ed.; Dover Publications: Mineola, NY, 2002.

## Appendix C: Supporting Information for Chapter 4

### C.1. Water Content Calculations

Calculations were made to determine the equivalents of water sorbed in the polymer per total equivalents of –OH and –O– moieties in the material. The calculations were performed using a basis of 1 g dry polymer, the theoretical mass composition/chemical structure of the material, and the measured gravimetric water uptake of the polymer (measured using 0.5 mol/L NaCl and reported in [Table 4.1](#) in [Chapter 4](#)). The mass of salt sorbed in the polymer (c.f., [Figure 4.1](#) in [Chapter 4](#)) was sufficiently less than 1 g to justify assuming that the contribution of sorbed salt mass to the calculation was negligible. The data are reported in [Table C.1](#) as equivalents of water per total equivalents of –OH and –O–.

**Table C.1.** Equivalents of sorbed water per total equivalents of –OH and –O– in the HEA-co-EA and HEMA-co-MMA co-polymers.

Co-polymer	Composition	$\frac{eq(water)}{eq(-OH \text{ and } -O-)}$
HEA-co-EA	30:70	1.5
	35:65	1.4
	40:60	1.6
HEMA-co-MMA	30:70	1.9
	35:65	1.8
	40:60	2.0

Additionally, we mentioned that (2.2 assumes the volumetric mixing of water and polymer is additive. However, in glassy polymers such as polyimides, this is not always the case.<sup>1</sup> Non-additive mixing will reduce the partial molar volume of water in the polymer matrix, which consequently will affect the water sorption coefficient described in [Equation 2.5](#). However in a

worst case where the partial molar volume of water is as low as  $6.6 \text{ cm}^3/\text{mol}$ , the effect on the water sorption coefficients for the glassy membranes is within the error of our measured values.

### C.2. Diffusion Length as a Function of Diffusion Time

The relationship between diffusion length and diffusion time in the NMR diffusometry measurements for the two co-polymers is shown as [Figure C.1](#).

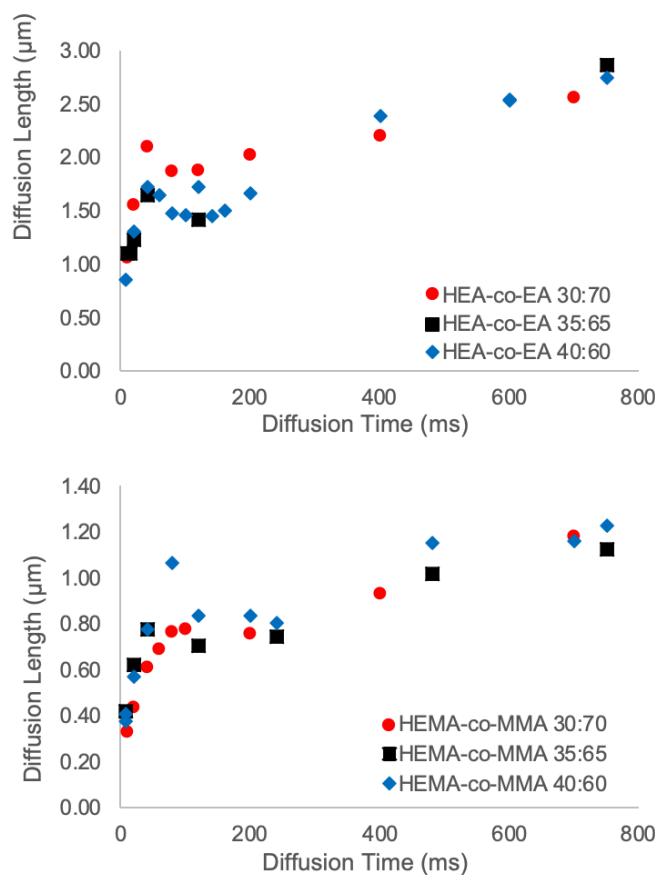


**Figure C.1.** Diffusion length as a function of the experimental diffusion time. At long diffusion times, we see a plateauing of the diffusion length due to restricted diffusion effects in both series of membranes.

### C.3. Mackie and Meares Model Calculations

The Mackie and Meares model<sup>2</sup> was used to calculate values of the local to bulk tortuosity (defined in [Equation 4.3](#) in [Chapter 4](#)). This model requires the volume fraction of water sorbed in the polymer, and the values of  $K_w$  measured using  $0.5 \text{ mol/L NaCl}$  ([Table 4.1](#) in [Chapter 4](#)) were

used for this purpose. The values of the local to bulk tortuosity, calculated using the Mackie and Meares model are reported in [Table C.2](#).

**Table C.2.** Local to bulk tortuosity values for the HEA-co-EA and HEMA-co-MMA materials calculated using the Mackie and Meares model ([Equation 4.5](#) in [Chapter 4](#)) and values of  $K_w$  measured using 0.5 mol/L NaCl ([Table 4.1](#) in [Chapter 4](#)).

Co-polymer	Composition	Local to Bulk Tortuosity, $\mathfrak{T}_{L-B}$
HEA-co-EA	30:70	292
	35:65	236
	40:60	159
HEMA-co-MMA	30:70	211
	35:65	190
	40:60	118

#### C.4. References

1. Dlubek, G.; Buchhold, R.; Hübner, C.; Nakladal, A., Water in Local Free Volumes of Polyimides: A Positron Lifetime Study. *Macromolecules* **1999**, *32* (7), 2348-2355.
2. Mackie, J. S.; Meares, P., The diffusion of electrolytes in a cation-exchange resin membrane I. Theoretical. *Proceedings of the Royal Society of London. Series A. Mathematical and Physical Sciences* **1955**, *232* (1191), 498-509.

## Appendix D: Supporting Information for Chapter 5

### D.1. Cross-linked Poly(glycidyl methacrylate) (XL-pGMA)

#### D.1.1. Polymer Synthesis

A representative synthesis of poly(glycidyl methacrylate) (pGMA) using initiators for continuous activator regeneration atom transfer radical polymerization (ICAR ATRP)<sup>1</sup> is described in this section. In an amber glass vial, 6.5 mg of copper bromide (CuBr<sub>2</sub>, 99%, Sigma-Aldrich) and 8.4 mg of tris(2-pyridylmethyl)amine (TPMA, 98%, Sigma-Aldrich) were dissolved in 2 mL anhydrous *N,N*-dimethylformamide (DMF, 99.8%, Sigma-Aldrich) to prepare the catalyst solution. In a separate amber glass vial, 18.6 mg of a reducing agent, 2,2'-azobis(2-methylpropionitrile) (AIBN, 98%, Sigma-Aldrich), was dissolved in 3 mL anhydrous DMF. The polymerization inhibitor, monomethyl hydroquinone (MEHQ), was removed from the as received glycidyl methacrylate (GMA, 97%, Sigma-Aldrich) by passing the monomer through an alumina column packed with commercially available inhibitor remover (Catalog Number 311332, Sigma-Aldrich) prior to the polymerization.

In a typical synthesis, 1 mL of catalyst solution, 1.5 mL of AIBN solution, 108.4  $\mu$ L of diethyl 2-bromo-2-methylmalonate (Et<sub>2</sub>BrMM, 98%, Sigma-Aldrich) initiator, 15 mL of GMA, and 12.5 mL anisole were charged into a 50 mL three-neck round bottom flask that was subsequently sealed using rubber caps. The flask was placed in an ice bath and purged with argon for 30 minutes, and high vacuum grease was used to prevent air infiltration. Then, the flask was transferred to an oil bath at 60 °C, and the polymerization was allowed to proceed for 6 hours. After the reaction, the solution was cooled to room temperature, diluted with 25 mL anhydrous acetone, and poured into 500 mL (i.e., 10 fold) methanol, which was vigorously stirred. The

precipitated crude polymer was recovered via filtration and was further purified by dissolving the polymer in acetone and subsequently precipitating the polymer in methanol. This precipitation process was conducted 3 times. The polymer was then dried under vacuum at 80 °C for 12 hours, and finally collected as a white powder (9.3 g, 57.4% yield).

### **D.1.2. Membrane Casting**

To obtain dense XL-pGMA films, 0.5 g of pGMA and 0.21 g of crosslinker poly(propylene glycol) bis(2-aminopropyl ether) ( $M_n \sim 2,000$  g/mol, Sigma-Aldrich) were dissolved in a mixed solvent composed of 10 mL dimethyl sulfoxide (DMSO,  $\geq 99.9\%$ , Macron Fine Chemicals) and 2 mL of *N*-methyl-2-pyrrolidone (NMP, laboratory grade, Fisher Chemical). The solution was stirred at room temperature for 1 hour, filtered using a 0.45  $\mu\text{m}$  PTFE syringe filter, poured into a flat PTFE evaporation dish, and this dish was transferred onto a leveled metal plate inside a convection oven at 75 °C. Solvent was initially removed and an amine-epoxide ring opening reaction (which cross-linked the polymer) was allowed to proceed at 75 °C in the oven for 2 days. The resulting polymer film was both flexible and transparent. The film was removed from the dish, dried under vacuum at 70 °C for another 24 hours to further remove solvent, and equilibrated in DI water prior to any further treatment and/or characterization.

### **D.1.3. Fourier-Transform Infrared Spectroscopy (FT-IR)**

The FT-IR spectra of pGMA and XL-pGMA-z are shown in [Figure D.1](#). The amine-epoxide ring opening (cross-linking) reaction was confirmed by the strong absorption band of the O-H stretching vibration mode at 3400  $\text{cm}^{-1}$  in all of the XL-pGMA-z samples.<sup>2,3</sup> All characteristic pGMA peaks were observed in the XL-pGMA-z spectra, indicating that the cross-linking reaction was confined to acid hydrolysis of the epoxide ring.

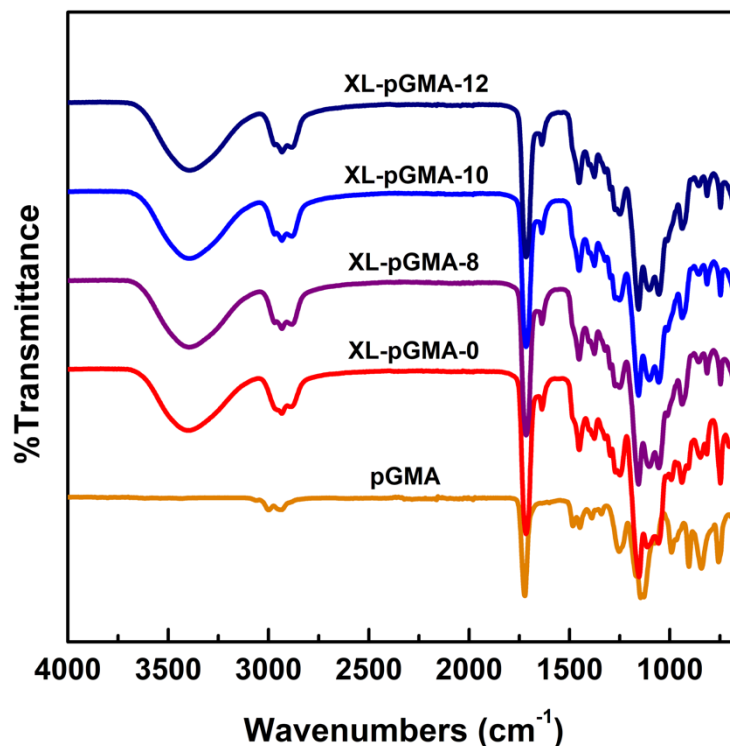


**Figure D.1.** FT-IR spectra of pGMA and XL-pGMA-z measured using film samples and an attenuated total reflectance (ATR) cell.

## D.2. Scattering Parameters (S-parameters)

The two-port transmission line method, described in the main text, generates four S-parameters. These parameters are identified by subscripts that correspond to the origin and destination of the electromagnetic radiation (Figure D.2). For example,  $S_{12}$  is a measure of electromagnetic radiation generated at Port 1 and transmitted to Port 2, and  $S_{11}$  is a measure of electromagnetic radiation generated at Port 1 and reflected back to Port 1.<sup>4</sup>

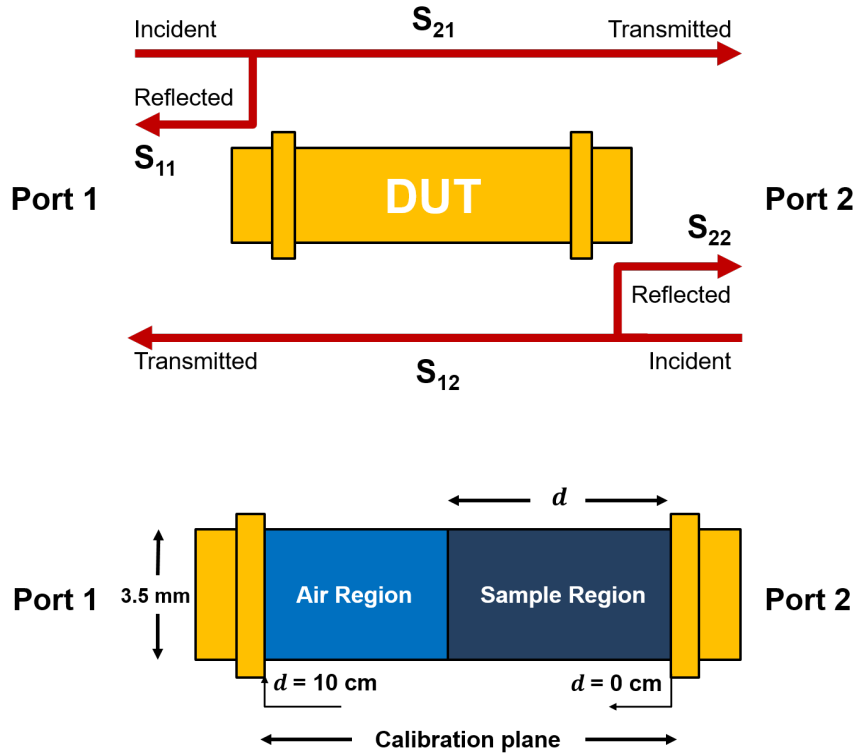


**Figure D.2.** Schematic of the four S-parameters in a two-port vector network analyzer measurement (Top).<sup>4</sup> DUT stands for device under test. The calibration plane (i.e., the region between the two coaxial cable ports) and both the air and sample regions in the DUT are illustrated (Bottom). The amount of sample loaded in the transmission line is represented by the length dimension,  $d$ .

### D.3. Microwave Dielectric Spectroscopy

#### D.3.1. Dielectric Permittivity Properties of Air and PTFE

Dielectric permittivity properties (i.e.,  $\epsilon'$  and  $\epsilon''$ ) were measured for air and PTFE (Figure D.3).

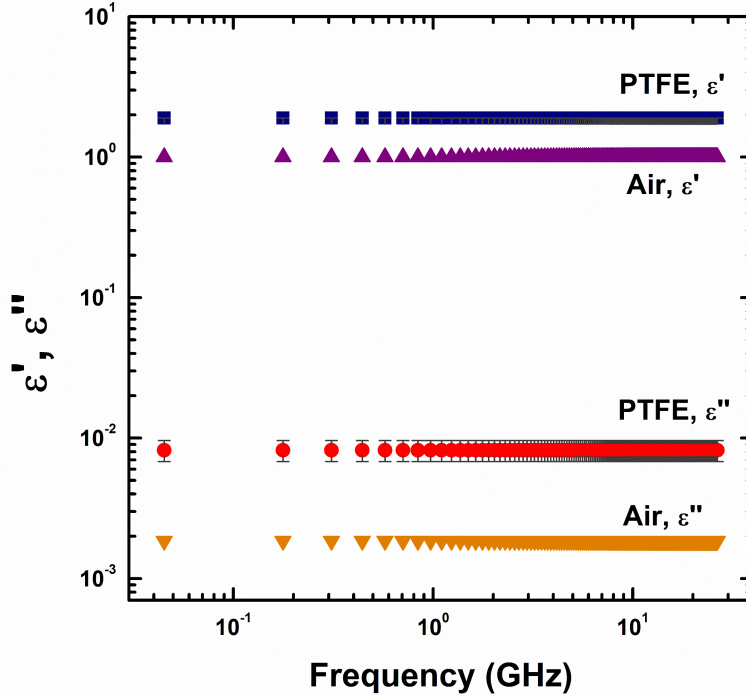


**Figure D.3.** Dielectric permittivity properties for air (i.e., an empty transmission line) and PTFE. Measurements were made at  $22 \pm 1$  °C, and the uncertainty for PTFE was taken as the standard deviation from the mean of three measurements.

### D.3.2. Dielectric Permittivity Properties of Water

The dielectric permittivity properties of DI water were measured (Figure D.4). Due to the high dielectric loss nature of water, different values of  $d$  (Figure D.2) were used in different frequency ranges to optimize the measurement.<sup>5</sup> Dielectric permittivity measurements were made using  $d = 5$  cm (45 MHz – 4 GHz), 2 cm (3 – 9 GHz), 0.5 cm (8 – 18 GHz), and 0.2 cm (17 – 26.5 GHz). The values of  $d$  were determined based on the amount of water pipetted into the transmission line and the geometry of the annular space in the transmission line.

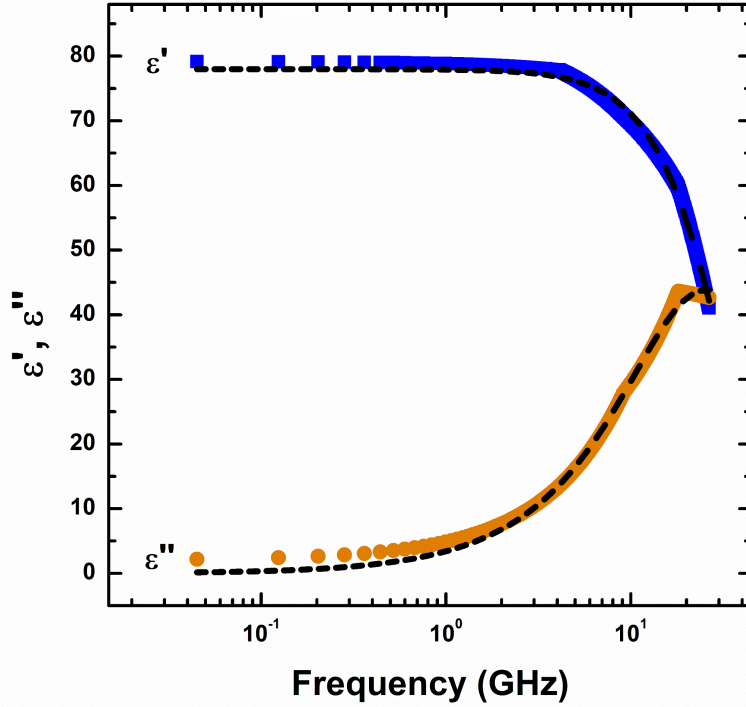


**Figure D.4.** Dielectric permittivity properties measured for DI water. Data were fit to a single Debye relaxation process (dashed curves). Measurements were made at  $22 \pm 1$  °C using different sample lengths (values of  $d$ ) to optimize the measurement over the entire frequency range.

Dielectric permittivity data for DI water (Figure D.4) were well represented by the Debye relaxation process with a single time constant:<sup>6-8</sup>

$$\varepsilon^* = \varepsilon_\infty + \frac{\varepsilon_s - \varepsilon_\infty}{1 + i\omega\tau} \quad (\text{D.1})$$

where  $\varepsilon^*$  is the relative complex permittivity,  $\varepsilon_\infty$  is the high frequency dielectric constant limit,  $\varepsilon_s$  (static permittivity) is the low frequency dielectric constant limit (often referred to as simply the dielectric constant),  $\omega (= 2\pi f, f$  is frequency) is the angular frequency of the applied field, and  $\tau (= 1/2\pi f_{max\ loss})$  is the relaxation time, which is the frequency at where the maximum dielectric loss occurs. The real part and imaginary parts of the relative complex permittivity can be expressed using the Debye dispersion formulae:

$$\varepsilon' = \varepsilon_{\infty} + \frac{\varepsilon_s - \varepsilon_{\infty}}{1 + (\omega\tau)^2} \quad (\text{D.2})$$

$$\varepsilon'' = \frac{(\varepsilon_s - \varepsilon_{\infty})\omega\tau}{1 + (\omega\tau)^2} \quad (\text{D.3})$$

#### D.4. References

1. Tsarevsky, N. V.; Jakubowski, W., Atom transfer radical polymerization of functional monomers employing Cu-based catalysts at low concentration: Polymerization of glycidyl methacrylate. *Journal of Polymer Science Part A: Polymer Chemistry* **2011**, *49* (4), 918-925.
2. Cheng, F.; Luo, H.; Hu, L.; Yu, B.; Luo, Z.; Fidalgo de Cortalezzi, M., Sludge carbonization and activation: From hazardous waste to functional materials for water treatment. *Journal of Environmental Chemical Engineering* **2016**, *4* (4, Part A), 4574-4586.
3. Zhang, Q.; Shi, C.-Y.; Qu, D.-H.; Long, Y.-T.; Feringa, B. L.; Tian, H., Exploring a naturally tailored small molecule for stretchable, self-healing, and adhesive supramolecular polymers. *Science Advances* **2018**, *4* (7), eaat8192.
4. Keysight Technologies, Understanding the Fundamental Principles of Vector Network Analysis, <http://literature.cdn.keysight.com/litweb/pdf/5965-7707E.pdf>, (accessed June 18th, 2018).
5. Lu, Z.; Lanagan, M.; Manias, E.; Macdonald, D. D., Two-port transmission line technique for dielectric property characterization of polymer electrolyte membranes. *The Journal of Physical Chemistry B* **2009**, *113* (41), 13551-13559.
6. Lu, Z.; Polizos, G.; Macdonald, D. D.; Manias, E., State of water in perfluorosulfonic ionomer (Nafion® 117) proton exchange membranes. *Journal of The Electrochemical Society* **2008**, *155* (2), B163-B171.
7. Debye, P., *Polar Molecules*. Dover: New York, 1929.

8. Smith, G.; Duffy, A. P.; Shen, J.; Olliff, C. J., Dielectric relaxation spectroscopy and some applications in the pharmaceutical sciences. *Journal of Pharmaceutical Sciences* **1995**, *84* (9), 1029-1044.

## Appendix E: Supporting Information for Chapter 6

### E.1. Fourier-Transform Infrared Spectroscopy (FT-IR)

The FT-IR spectra of the hydrated HEMA:GMA:GMAOH film samples are shown in Figure E.1. All peak intensities were normalized to the C–O peak (for ester and ether functional groups) located at approximately  $1160\text{ cm}^{-1}$ .<sup>1</sup> The location and intensity of most of the major peaks in the spectra are very similar, which is in good agreement with the structural similarity and equivalent water content nature of the materials.

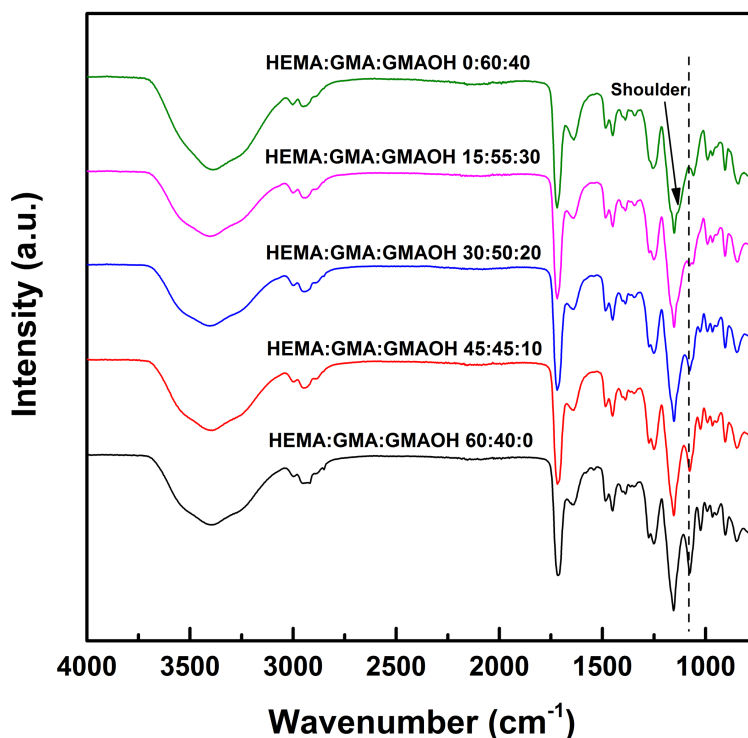


**Figure E.1.** FT-IR spectra of hydrated HEMA:GMA:GMAOH film samples measured using an attenuated total reflectance (ATR) cell. The composition of the pre-polymerization solution used to prepare each co-polymer is listed for each spectrum. The dashed line indicates the position of the primary alcohol stretching peak (approximately  $1070\text{ cm}^{-1}$ ) for the HEMA:GMA:GMAOH 60:40:0 material to illustrate the shift that occurs as GMAOH content increases. Additionally, the shoulder on the  $1160\text{ cm}^{-1}$  peak is identified.

The C–O stretching peak, attributed to primary alcohol functionality ( $-\text{CH}_2\text{CH}_2\text{OH}$ ) and located at approximately  $1070\text{ cm}^{-1}$ ,<sup>1</sup> shifts to a lower wavenumber as the GMAOH composition

of the pre-polymerization solution (used to prepare the co-polymers) increases. We attribute this peak shift to an increase in the vicinal diol content ( $-CHOHCH_2OH$ ) of the material that lowers the bond stretching energy for the primary alcohol moiety in GMAOH.<sup>1</sup> Furthermore, the presence of the secondary alcohol group in GMAOH ( $-CHOHCH_2OH$ ) could lead to multiple peaks in the range of 1150–1075  $cm^{-1}$  due to coupling, and these peaks could overlap with the aforementioned C-O peak at 1160  $cm^{-1}$  to yield the observed broad absorbance and a peak shoulder.<sup>1</sup> Hence, the FT-IR results support the qualitative increase in the GMAOH content of the co-polymer as the GMAOH content in the pre-polymerization solution increases.

## **E.2. Freezable Water Content Per Equivalent of Hydroxyl Group Functionality**

To further explore the formation of freezable (i.e., bulk-like) water in the co-polymers, we calculated the number of moles of freezable water sorbed in the co-polymer per equivalent of hydroxyl group functionality in the material (Table E.1). This quantity provides additional insight into the distribution of water within the co-polymer. The vicinal diol-rich materials (i.e., the low HEMA-content co-polymers) have more freezable water compared to the HEMA-rich co-polymers, and each hydroxyl group in the GMAOH-rich materials contributes more to the formation of freezable or bulk-like water. In other words, distributing the hydroxyl groups more evenly throughout the co-polymer (as in the HEMA-rich materials) results in a situation where each hydroxyl group creates less freezable water.

**Table E.1.** The freezable water content, non-freezable water content, and the number of moles of freezable water per equivalent of hydroxyl group in the hydrated HEMA:GMA:GMAOH co-polymers.

HEMA:GMA:GMAOH Composition (by mass)	$W_f$ (%)	$W_{nf}$ (%)	mol(freezable water) / eq(hydroxyl group)
<b>0:60:40</b>	2.3	21.2	0.26
<b>15:55:30</b>	1.9	22.3	0.22
<b>30:50:20</b>	1.8	21.7	0.21
<b>45:45:10</b>	1.2	22.3	0.14
<b>60:40:0</b>	0.9	22.4	0.11

A sample calculation is provided for the HEMA:GMA:GMAOH 15:55:30 co-polymer. First, a dry polymer mass ( $m_{dry}$ ) basis was taken to be 1 g(dry polymer). The number of moles of freezable water in 1 g(dry polymer),  $n_{fw}$ , was calculated as:

$$n_{fw} = \frac{m_{dry} \times W_f}{MW(water)} = \frac{1 \text{ g} \times 0.019}{18 \text{ g/mol}} = 0.00106 \text{ mol} \quad (\text{E.1})$$

where  $W_f$  is the mass of freezable water in the polymer per gram of dry polymer expressed as a decimal. The number of equivalents of hydroxyl functional groups in 1 g(dry polymer) was calculated using the theoretical composition of the co-polymer:

$$n_{OH} = m_{dry} \left( \frac{wt\%(GMAOH) \times 2}{MW(GMAOH)} + \frac{wt\%(HEMA)}{MW(HEMA)} \right) = 1 \text{ g} \left( \frac{30\% \times 2}{160 \text{ g/eq}} + \frac{15\%}{130 \text{ g/eq}} \right) \quad (\text{E.2})$$

$$= 0.0049 \text{ eq}$$

Therefore,  $n_{fw} / n_{OH} = 0.22$  mol(freezable water) per equivalent of hydroxyl group in the hydrated co-polymer.

### E.3. References

1. Socrates, G., *Infrared and raman characteristic group frequencies: Tables and charts*. 3rd ed.; John Wiley & Sons: West Sussex, England, 2004.

## Appendix F: Supporting Information for Chapter 7

### F.1. Additional Material Properties and Characterization

#### F.1.1. Chemical Structure and Composition

The chemical structure of the cross-linked HEMA:GMA:GMAOH co-polymer is shown as [Figure 2.3](#). The pre-polymerization solutions used to prepare the co-polymers for this study were prepared to contain a x:y:z, by mass, ratio of the HEMA:GMA:GMAOH co-monomers. While the sample nomenclature is based on this mass composition of the co-monomers in the pre-polymerization solution, the pre-polymerization solution co-monomer and cross-linker mole fractions are provided in [Figure F.1](#) along with the theoretical hydroxyl group content of the materials, which was calculated under the assumption that the compositions of the pre-polymerization solution and the resulting co-polymer are identical.

**Table F.1.** Pre-polymerization solution co-monomer and cross-linker mole fractions and the theoretical hydroxyl group content of the materials.

Co-Polymer Sample	Pre-Polymerization Solution Co-Monomer and Cross-Linker Mole Fractions				Hydroxyl Group Content (meq -OH/ g dry polymer)
	HEMA	GMA	GMAOH	PEGDMA	
<b>0:60:40</b>	0	0.612	0.362	0.026	4.5
<b>15:55:30</b>	0.163	0.547	0.265	0.026	4.5
<b>30:50:20</b>	0.318	0.485	0.172	0.025	4.4
<b>45:45:10</b>	0.465	0.426	0.084	0.024	4.3
<b>60:40:0</b>	0.606	0.370	0	0.024	4.2

The data in [Table F.1](#) suggest that the extent of cross-linking and the hydroxyl group content of the co-polymer decrease slightly (by 8% and 7%, respectively) across the range of materials considered. Extent of cross-linking is known to affect water and salt transport properties,<sup>1-4</sup> and the hydroxyl group content may influence transport properties as well. The compositions chosen for this study yielded co-polymers with equivalent water content (as

discussed in more detail in [Chapter 7](#)), and this result may be due to the simultaneous 8% reduction in cross-link density, which would be expected to cause an increase in water content,<sup>4</sup> and 7% decrease in hydroxyl group content, which would be expected to cause a decrease in water content (due to the reduction in the concentration of hydrophilic moieties in the material). It is possible that these factors may influence the water and salt transport properties of the materials considered in this study, but due to the significant influence of polymer water content on water and salt transport properties,<sup>5-7</sup> the water content was held constant in this study to minimize the influence of water content changes on water and salt transport properties.

### **F.1.2. Fourier-Transform Infrared (FT-IR) Spectroscopy**

The co-polymers were analyzed using Fourier-transform infrared (FT-IR) spectroscopy. The spectra ([Figure F.1](#)) are very similar for the five materials considered, which is expected given the structural similarity of the co-polymers. The peak located at approximately  $1050\text{ cm}^{-1}$  broadened as the content of GMAOH in the pre-polymerization solution increased, and peaks in this range of the spectrum can be attributed to the C–O stretch associated with the hydroxyl groups on the side chains.<sup>8</sup> The broadening of this peak is consistent with a shift toward a higher vicinal diol content of the co-polymer due to the presence of the second hydroxyl group on the GMAOH side chain.<sup>8</sup> Thus, these results suggest a qualitative increase in the co-polymer GMAOH content as the pre-polymerization solution GMAOH content increased.

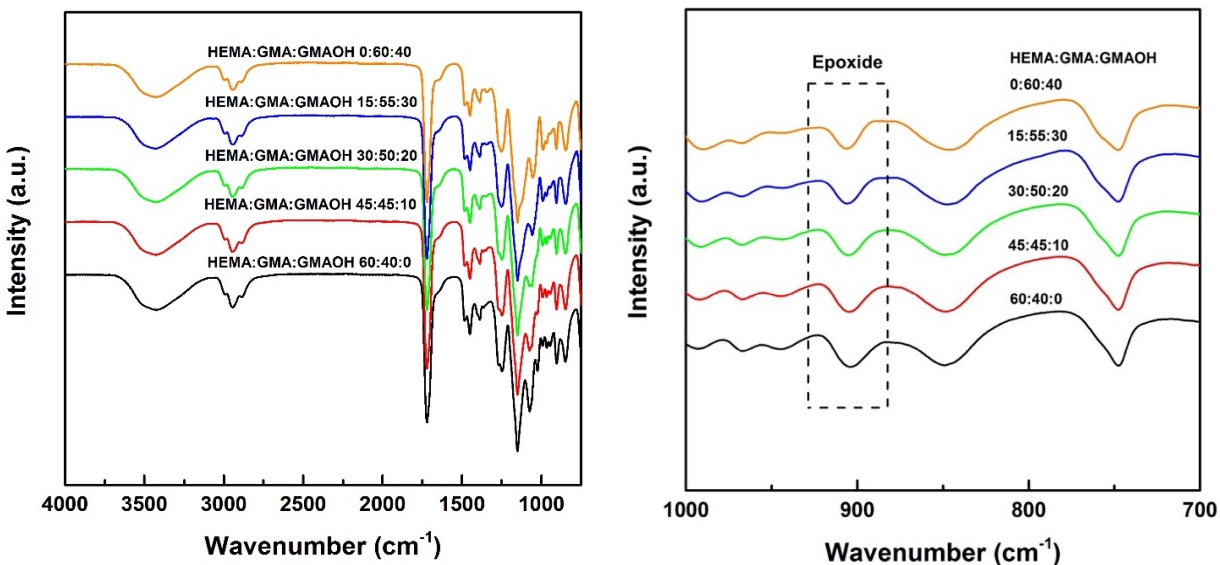


**Figure F.1.** Fourier-transform infrared (FT-IR) spectra for dry HEMA:GMA:GMAOH co-polymers. The spectra were obtained in attenuated total reflectance mode using co-polymers that had been dried under vacuum for 24 hours after an approximately 2 month long period where the films were soaked in DI water. The figure on the right highlights the 700 to 1000  $\text{cm}^{-1}$  region of the spectra shown on the left.

Additionally, the FT-IR data suggest that the potentially reactive epoxide on the GMA side chain may be uniformly stable across the series of materials considered. The peak slightly above 900  $\text{cm}^{-1}$  can be attributed to the epoxide on the GMA co-monomer.<sup>8</sup> This peak is similar for all of the materials. Furthermore, the FT-IR analysis was performed on co-polymers that had been soaked in DI water for approximately 2 months (before being dried in advance of the FT-IR measurement). As such, the FT-IR results suggest that the epoxide functionality in the co-polymers remains after 2 months of soaking in DI water.

### F.1.3. Thermal Properties

In [Chapter 7](#), the difference between the water/salt diffusivity selectivity properties of the HEMA:GMA:GMAOH and PEG materials is suggested to be due to the glassy nature of the HEMA:GMA:GMAOH co-polymers compared to the rubbery nature of the PEG materials. The glass transition temperatures of the materials can be used to further support this explanation. The

PEG materials reported in [Figures 7.1](#) and [7.2](#) in the main text<sup>9</sup> are cross-linked poly(ethylene glycol) diacrylate hydrogels, and these materials have reported glass transition temperatures that are all below 0 °C.<sup>10</sup> As a result, the PEG materials referenced in the main text were all rubbery polymers at the room temperature measurement conditions.

The glass transition temperatures of the hydrated HEMA:GMA:GMAOH materials can be estimated using the Fox equation.<sup>11,12</sup> While this approach is only a first approximation, it provides an estimate of the glass transition temperature of hydrated materials, such as HEMA:GMA:GMAOH, where the glass transition may be obscured by vaporization of some of the water sorbed in the polymer. Additionally, reasonable agreement between Fox equation calculated and measured glass transition temperatures has been reported for co-polymers containing HEMA.<sup>13</sup> The Fox equation suggests that the glass transition temperature of the hydrated HEMA:GMA:GMAOH co-polymers increases in the order of 108 °C, 113 °C, 116 °C, 121 °C, and 126 °C as the pre-polymerization solution HEMA composition increases from 0 to 60 % (by mass). As such, these materials can be assumed to be glassy materials at room temperature as the glass transition temperatures of the materials are expected to be well above room temperature. Because segmental dynamics are significantly slower in glassy polymers compared to rubbery polymers,<sup>14,15</sup> the segmental dynamics of the glassy HEMA:GMA:GMAOH co-polymers are likely much slower compared to the segmental dynamics in the rubbery PEG materials.

## **F.2. Hydrated Polymer Dielectric Property Characterization**

Dielectric permittivity properties were characterized from 0.45 to 20 GHz using a vector network analyzer (VNA) to study dipole relaxation dynamics of water sorbed in the materials. The measurement, described elsewhere,<sup>16</sup> was made on hydrated film samples that were wrapped

around the center conductor of a 3.5 mm diameter coaxial transmission line. To improve the resolution of the dielectric loss spectra,<sup>17</sup> the annular space of the 5 cm long transmission line was filled with either 1 cm (for frequencies between 0.45 and 4 GHz) or 0.5 cm (for frequencies between 1 and 20 GHz) of sample. The remaining space in the transmission line was filled with air, which was accounted for during data analysis. The data measured between 1 and 4 GHz for the two different sample lengths overlapped, as expected. The calibrated VNA measured S-parameters were then related to the complex dielectric permittivity.<sup>16, 18</sup>

### **F.3. Microwave Dielectric Spectroscopy**

We measured the microwave frequency dielectric loss spectra for the hydrated co-polymers to probe dipole relaxation dynamics of water sorbed in the materials. The dielectric loss spectra for the hydrated HEMA:GMA:GMAOH co-polymers have features similar to that of pure water.<sup>16, 17, 19</sup> This similarity is reasonable given that water dipoles relax in the microwave frequency range (as opposed to polymer segmental dynamics that relax at lower frequencies).<sup>20</sup>

As the HEMA content of the pre-polymerization solution used to prepare the co-polymer increased, the magnitude of the dielectric loss decreased, across the entire spectrum, but the shape of each spectrum remained similar (Figure F.2). This result suggests that, as the HEMA content of the pre-polymerization solution used to prepare the co-polymer increased, both energy dissipation and orientation polarizability for sorbed water molecules in the co-polymers decreased. This result may be due to a suppression of water motions caused by increased water interactions with the hydrophilic hydroxyl groups as the hydroxyl groups are more evenly distributed throughout the co-polymer.

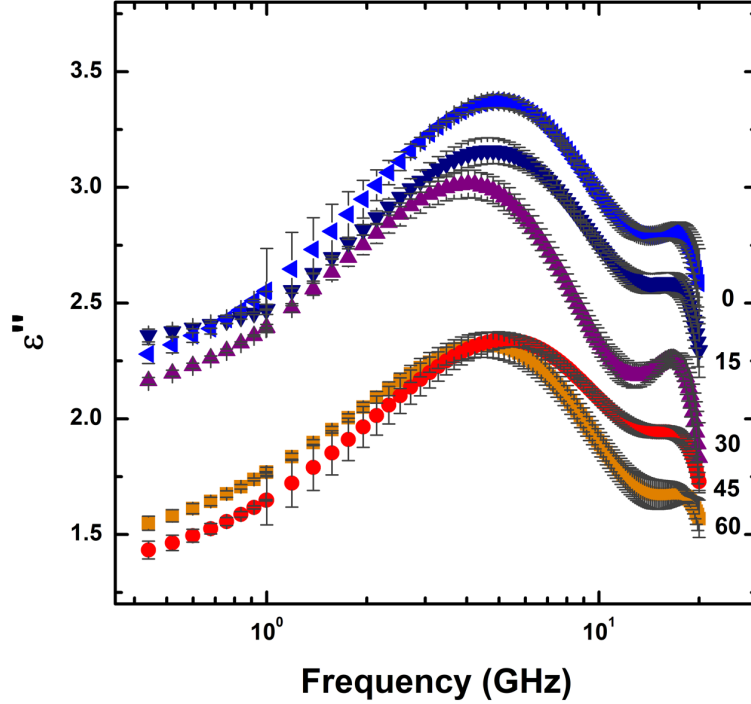


**Figure F.2.** Frequency-dependent dielectric loss spectra,  $\epsilon''$ , for the hydrated HEMA:GMA:GMAOH co-polymers. The spectra are labeled with the composition of the HEMA content of the pre-polymerization solution used to prepare the co-polymer. All measurements were made at  $22 \pm 1$  °C, and the uncertainty was taken as one standard deviation from the mean of three measurements.

To further analyze the water-polymer interactions in hydrated HEMA:GMA:GMAOH, we fit the dielectric loss data to a model containing three Debye relaxation processes that we attributed to three different water relaxation modes: highly restricted (HR) motion, less restricted (LR) motion, and non-restricted (NR) (i.e., bulk water) motion.<sup>21-23</sup> This approach is consistent with reports<sup>17, 21, 24</sup> suggesting that multiple Debye relaxation processes can be observed in hydrated polymers and that the necessary number of Debye relaxation processes depends on the polymer water content.<sup>17, 24</sup> The dielectric loss can be expressed as a summation over all relaxation processes,  $i$ , as:

$$\epsilon'' = \sum_i \frac{\Delta\epsilon_i \omega \tau_i}{1 + (\omega \tau_i)^2} \quad (\text{F.1})$$

We used a three relaxation model, so  $i$  represented the different relaxation modes (i.e., HR, LR, and NR). The dielectric strength,  $\Delta\varepsilon_i$ , is a measure of relative amount of water that contributes to a particular relaxation mode.<sup>17</sup> The frequency of the microwave radiation used in the measurement,  $f$ , was expressed as the angular frequency,  $\omega = 2\pi f$ , and the relaxation time constant of a particular relaxation mode,  $\tau_i$ , is related to the frequency where maximum dielectric loss occurs,  $f_{max}$ , as  $\tau_i = 1/2\pi f_{max}$ .

In the three Debye relaxation model, six parameters ( $\Delta\varepsilon_i$  and  $\tau_i$  for  $i = \text{HR, LR, and NR}$ ) are needed to describe the dielectric loss spectra (Figure F.2). Because the non-restricted relaxation mode was taken as that of bulk water, the value of  $\tau_{NR}$  was fixed at a measured value of 8.8 ps.<sup>16</sup> The remaining five parameters (Table F.2) were regressed, for each of the co-polymers, using Equation F.1 and a generalized reduced gradient, GRG, nonlinear method in Microsoft Excel. Regressions were performed separately on three spectra for each co-polymer, and the regressed parameters were averaged. The uncertainty in the regressed parameters was taken as one standard deviation from the average value.

**Table F.2.** Relaxation time constants and dielectric strengths determined by fitting the dielectric loss spectra (Figure F.2) to a three Debye relaxation process model (Equation F.1). The uncertainty was taken as one standard deviation from the mean of three parameters regressed from three distinct dielectric loss spectra.

Co-Polymer Sample	$\tau_{HR}$ (ps)	$\Delta\varepsilon_{HR}$	$\tau_{LR}$ (ps)	$\Delta\varepsilon_{LR}$	$\tau_{NR}^a$ (ps)	$\Delta\varepsilon_{NR}$
<b>0:60:40</b>	401 ± 78	3.3 ± 0.2	46 ± 2	4.6 ± 0.1	8.8	3.5 ± 0.1
<b>15:55:30</b>	433 ± 8	3.5 ± 0.1	46 ± 1	4.4 ± 0.2	8.8	3.1 ± 0.2
<b>30:50:20</b>	485 ± 80	3.1 ± 0.1	51 ± 4	4.5 ± 0.2	8.8	2.5 ± 0.1
<b>45:45:10</b>	379 ± 29	2.0 ± 0.1	42 ± 2	3.2 ± 0.2	8.8	2.3 ± 0.1
<b>60:40:0</b>	377 ± 13	2.2 ± 0.1	43 ± 2	3.5 ± 0.1	8.8	1.7 ± 0.1

<sup>a</sup>The time constant for the non-restricted (i.e. bulk water) relaxation mode was fixed at a measured value of 8.8 ps.<sup>16</sup>

The results of the regression (Table F.2) suggest that the relaxation time constants for the three relaxation modes span two orders of magnitude. Additionally, the dielectric strength (and,

thus, relative amount of water) associated with all three relaxation modes decreases as the HEMA content of the pre-polymerization solution used to prepare the materials increases. These results suggest that polymer chemistry influences the distribution of sorbed water across the different relaxation modes in water content equivalent materials. Preparing polymers with distributed hydrophilic groups (e.g., higher HEMA content in this study) may promote stronger water-polymer interactions.

#### **F.4. Hydration of Hydroxyl Groups in HEMA and GMAOH**

As discussed in the main text and in [Section F.3](#), the microwave dielectric spectroscopy data suggest that water may hydrate the hydroxyl group on the HEMA side chain to a greater extent compared to the hydroxyl groups on the GMAOH side chain. In addition to the steric explanation discussed in the main text, an enthalpy of mixing analysis can be considered. In lieu of enthalpy of mixing data for the water:HEMA and water:GMAOH systems, enthalpy of mixing data were considered for the water:ethanol<sup>25</sup> and water:1,2-propanediol<sup>26</sup> systems, as the side chains of the HEMA and GMAOH co-monomers contain ethanol and 1,2-propanediol moieties, respectively.

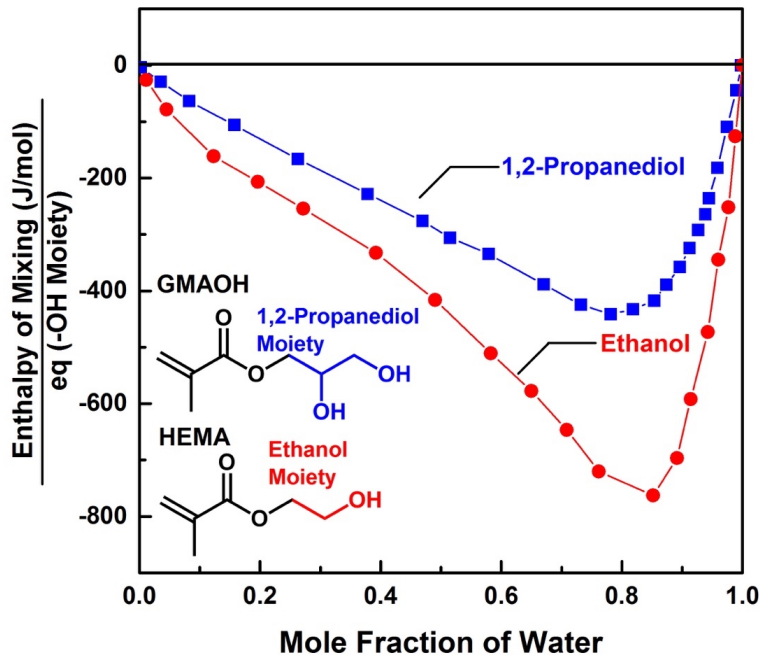


**Figure F.3.** Enthalpy of mixing data as a function of mole fraction of water for mixtures of water and either ethanol<sup>25</sup> or 1,2-propanediol<sup>26</sup> at 25 °C. Ethanol and 1,2-propanediol were chosen because of their similarity to the side chain moieties on the HEMA and GMAOH co-monomers. The enthalpy of mixing data were normalized by the equivalents of -OH moieties in the organic molecule (i.e., 1 eq(-OH) for ethanol and 2 eq(-OH) for 1,2-propanediol).

The enthalpy of mixing data in Figure F.3 are normalized by the equivalents of -OH moieties in the organic molecule (i.e., 1 eq(-OH) for ethanol and 2 eq(-OH) for 1,2-propanediol). On this per eq(-OH) basis, the enthalpy of mixing data for water and ethanol are more negative (i.e., more thermodynamically favored) compared to the situation for water and 1,2-propanediol over the entire range of composition. Thus, the enthalpy of mixing data for representative small molecules and water further support the microwave dielectric data by suggesting that water may interact more strongly with the hydroxyl group on the HEMA side chain compared to the hydroxyl groups on the GMAOH side chain.

## F.5. References

1. Paul, M.; Park, H. B.; Freeman, B. D.; Roy, A.; McGrath, J. E.; Riffle, J. S., Synthesis and crosslinking of partially disulfonated poly(arylene ether sulfone) random copolymers as candidates for chlorine resistant reverse osmosis membranes. *Polymer* **2008**, *49*, 2243-2252.
2. Song, Y.; Sun, P.; Henry, L. L.; Sun, B., Mechanisms of structure and performance controlled thin film composite membrane formation via interfacial polymerization process. *J. Membr. Sci.* **2005**, *251* (1), 67-79.
3. Petersen, R. J., Composite reverse osmosis and nanofiltration membranes. *J. Membr. Sci.* **1993**, *83*, 81-150.
4. Sundell, B. J.; Jang, E.-S.; Cook, J. R.; Freeman, B. D.; Riffle, J. S.; McGrath, J. E., Cross-linked disulfonated poly(arylene ether sulfone) telechelic oligomers. 2. Elevated transport performance with increasing hydrophilicity. *Industrial & Engineering Chemistry Research* **2016**, *55* (5), 1419-1426.
5. Geise, G. M.; Paul, D. R.; Freeman, B. D., Fundamental water and salt transport properties of polymeric materials. *Progress in Polymer Science* **2014**, *39* (1), 1-42.
6. Yasuda, H.; Lamaze, C. E.; Ikenberry, L. D., Permeability of solutes through hydrated polymer membranes Part I. Diffusion of sodium chloride. *Die Makromolekulare Chemie* **1968**, *118*, 19-35.
7. Meares, P., The mechanism of water transport in membranes. *Philosophical Transactions of the Royal Society of London B* **1977**, *278*, 113-150.
8. Socrates, G., *Infrared and raman characteristic group frequencies: Tables and charts*. 3rd ed.; John Wiley & Sons: Hoboken, NJ, 2004.
9. Ju, H.; Sagle, A. C.; Freeman, B. D.; Mardel, J. I.; Hill, A. J., Characterization of sodium chloride and water transport in poly(ethylene oxide) hydrogels. *J. Membr. Sci.* **2010**, *358*, 131-141.

10. Ju, H.; McCloskey, B. D.; Sagle, A. C.; Kusuma, V. A.; Freeman, B. D., Preparation and characterization of crosslinked poly(ethylene glycol) diacrylate hydrogels as fouling-resistant membrane coating materials. *Journal of Membrane Science* **2009**, *330* (1), 180-188.
11. Fox, T. G. J.; Flory, P. J., Second-order transition temperatures and related properties of polystyrene. I. Influence of molecular weight. *Journal of Applied Physics* **1950**, *21* (6), 581-591.
12. Hiemenz, P. C.; Lodge, T. P., *Polymer Chemistry*. 2nd ed.; CRC Press LLC: Boca Raton, Florida, 2007.
13. Chang, K.; Korovich, A.; Xue, T.; Morris, W. A.; Madsen, L. A.; Geise, G. M., Influence of rubbery versus glassy backbone dynamics on multiscale transport in polymer membranes. *Macromolecules* **2018**, *51* (22), 9222-9233.
14. Van Krevelen, D. W., *Properties of Polymers*. 3rd ed.; Elsevier: Amsterdam, 1997.
15. Hodge, I. M., Physical aging in polymer glasses. *Science* **1995**, *267*, 1945-1947.
16. Chang, K.; Luo, H.; Geise, G. M., Water content, relative permittivity, and ion sorption properties of polymers for membrane desalination. *Journal of Membrane Science* **2019**, *574*, 24-32.
17. Lu, Z.; Polizos, G.; Macdonald, D. D.; Manias, E., State of water in perfluorosulfonic ionomer (Nafion® 117) proton exchange membranes. *Journal of The Electrochemical Society* **2008**, *155* (2), B163-B171.
18. Bartley, P. G.; Begley, S. B., A new technique for the determination of the complex permittivity and permeability of materials. *2010 IEEE Instrumentation & Measurement Technology Conference Proceedings* **2010**, 54-57.
19. Ellison, W. J.; Lamkaouchi, K.; Moreau, J. M., Water: A dielectric reference. *Journal of Molecular Liquids* **1996**, *68* (2), 171-279.
20. Runt, J. P.; Fitzgerald, J. J., *Dielectric Spectroscopy of Polymeric Materials: Fundamentals and Applications*. American Chemical Society: Washington, DC, 1997.

21. Lu, Z., State of water in perfluorosulfonic acid membranes studied by microwave dielectric relaxation spectroscopy. **2006**, *Ph.D. Thesis, Department of Materials Science and Engineering, The Pennsylvania State University, University Park, Pennsylvania.*
22. Debye, P., *Polar Molecules*. Dover: New York, 1929.
23. Smith, G.; Duffy, A. P.; Shen, J.; Olliff, C. J., Dielectric relaxation spectroscopy and some applications in the pharmaceutical sciences. *Journal of Pharmaceutical Sciences* **1995**, *84* (9), 1029-1044.
24. Lu, Z.; Lanagan, M.; Manias, E.; Macdonald, D. D., Two-port transmission line technique for dielectric property characterization of polymer electrolyte membranes. *The Journal of Physical Chemistry B* **2009**, *113* (41), 13551-13559.
25. Lama, R. F.; Lu, B. C. Y., Excess thermodynamic properties of aqueous alcohol solutions. *J. Chem. Eng. Data* **1965**, *10* (3), 216-219.
26. Batov, D. V.; Zaichikov, A. M.; Slyusar, V. P.; Korolev, V. P., Enthalpies of mixing and state of components in aqueous-organic mixtures with nets of hydrogen bonds. *Russ. J. Gen. Chem.* **2001**, *71* (8), 1208-1214.

## Appendix G: Supporting Information for Chapter 8

**Table G.1.** Water uptake,  $w_u$ , water volume fraction,  $\phi_w$ , and dry polymer density data measured at  $22 \pm 1$  °C. Water uptake measurements were made on samples initially equilibrated with either DI water or an aqueous solution of 0.01, 0.1, or 1.0 mol/L NaCl. The uncertainty was taken as one standard deviation from the mean of three measurements. Hydrolysis time,  $z$ , refers to the length of time (in hours) that the XL-pGMA- $z$  samples were immersed in 0.5 mol/L H<sub>2</sub>SO<sub>4</sub> at 40 °C.

Polymer	Hydrolysis Time, $z$ (h)	Dry Density (g/cm <sup>3</sup> )	Measured using pure water		Measured using 0.01 mol/L NaCl		Measured using 0.1 mol/L NaCl		Measured using 1.0 mol/L NaCl	
			$w_u$	$\phi_w$	$w_u$	$\phi_w$	$w_u$	$\phi_w$	$w_u$	$\phi_w$
XL-pGMA- $z$	7	$1.19 \pm 0.02$	$0.061 \pm 0.012$	$0.068 \pm 0.013$	$0.033 \pm 0.001$	$0.037 \pm 0.001$	$0.030 \pm 0.007$	$0.034 \pm 0.008$	$0.015 \pm 0.002$	$0.018 \pm 0.002$
	9	$1.26 \pm 0.04$	$0.118 \pm 0.010$	$0.129 \pm 0.011$	$0.059 \pm 0.017$	$0.070 \pm 0.020$	$0.064 \pm 0.011$	$0.075 \pm 0.013$	$0.041 \pm 0.009$	$0.050 \pm 0.011$
	11	$1.23 \pm 0.03$	$0.168 \pm 0.018$	$0.172 \pm 0.019$	$0.087 \pm 0.021$	$0.097 \pm 0.024$	$0.089 \pm 0.009$	$0.099 \pm 0.011$	$0.070 \pm 0.007$	$0.079 \pm 0.008$

**Table G.2.** Amounts of strongly-bound, intermediate, and bulk-like water present in XL-pGMA- $z$  when equilibrated in DI water or 0.01, 0.1, or 1.0 mol/L aqueous NaCl solutions. The results were obtained by fitting the OD stretch of each FTIR spectrum of XL-pGMA- $z$  with three Gaussian curves. Each curve represents a different water state, and the area of each Gaussian curve was divided by the total area of the OD stretch. The three values for each material and condition sum to the overall volume fraction of sorbed water,  $\phi_w$ . Hydrolysis time,  $z$ , refers to the length of time (in hours) that the XL-pGMA- $z$  samples were immersed in 0.5 mol/L H<sub>2</sub>SO<sub>4</sub> at 40 °C.

Polymer	Hydrolysis Time, $z$ (h)	Measured using pure water			Measured using 0.01 mol/L NaCl			Measured using 0.1 mol/L NaCl			Measured using 1.0 mol/L NaCl		
		Strongly-bound water ( $\times 10^{-2}$ )	Inter-mediate water ( $\times 10^{-2}$ )	Bulk-like water ( $\times 10^{-2}$ )	Strongly-bound water ( $\times 10^{-2}$ )	Inter-mediate water ( $\times 10^{-2}$ )	Bulk-like water ( $\times 10^{-2}$ )	Strongly-bound water ( $\times 10^{-2}$ )	Inter-mediate water ( $\times 10^{-2}$ )	Bulk-like water ( $\times 10^{-2}$ )	Strongly-bound water ( $\times 10^{-2}$ )	Inter-mediate water ( $\times 10^{-2}$ )	Bulk-like water ( $\times 10^{-2}$ )
XL-pGMA- $z$	7	0.45	6.27	0.08	0.35	3.23	0.13	0.30	2.86	0.25	0.11	1.59	0.10
	9	0.82	11.33	0.75	0.58	6.00	0.41	0.68	6.43	0.39	0.30	4.39	0.31
	11	1.37	14.56	1.28	0.74	8.07	0.89	0.81	8.33	0.76	0.51	6.85	0.53

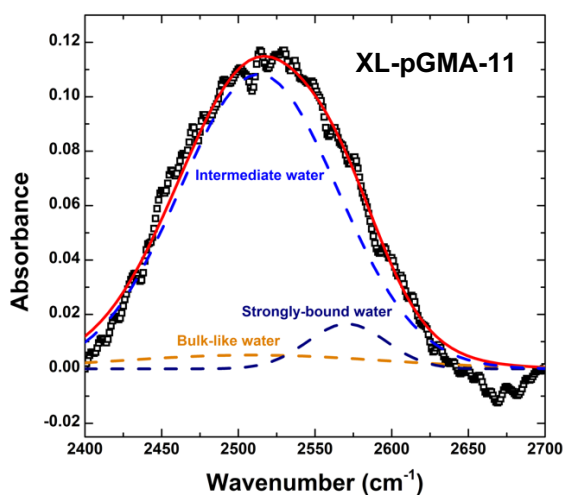
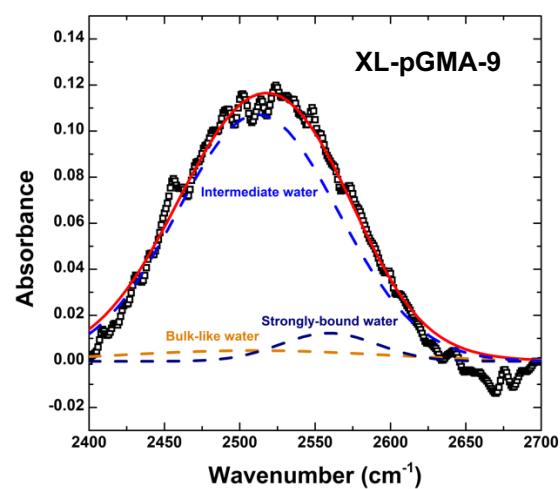
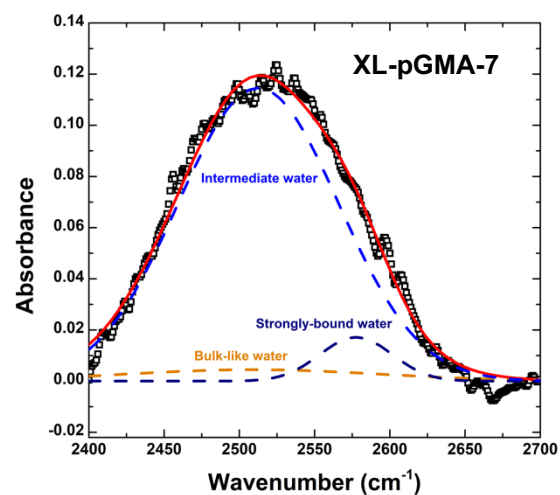


**Figure G.1.** Representative FT-IR spectra for XL-pGMA-7 (top), -9 (middle), and -11 (bottom) materials that were equilibrated in 1.0 mol/L NaCl. The three Gaussian peaks that represent the three water states (bulk-like water, intermediate water, and strongly-bound water) are labeled on the figures.

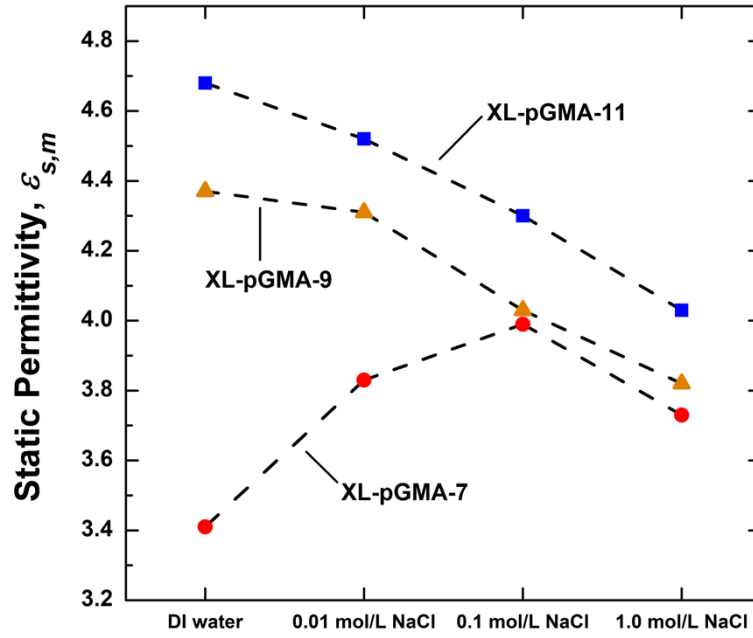


**Figure G.2.** Static permittivity of XL-pGMA-z measured using samples that were equilibrated in DI water or 0.01, 0.1, and 1.0 mol/L aqueous NaCl solutions. The dashed line is included to guide the eye.

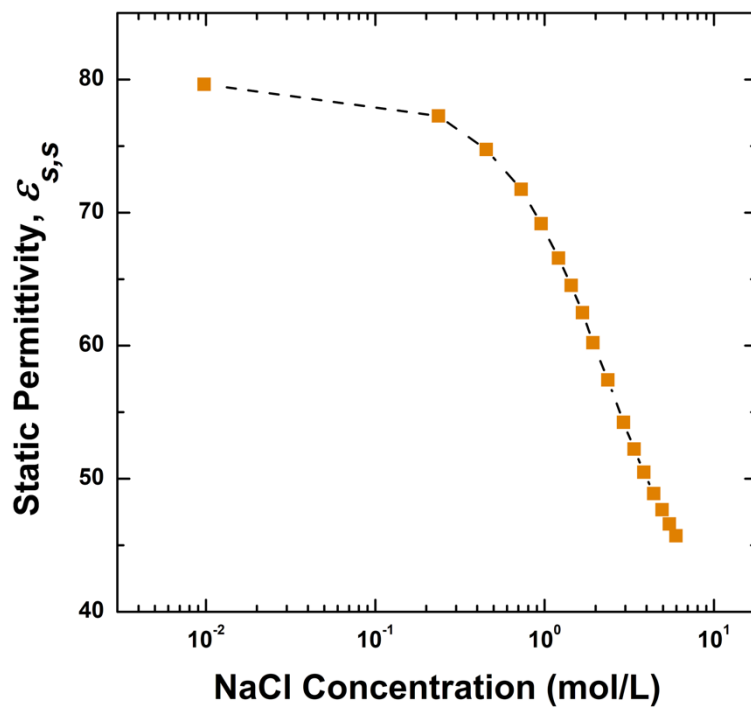


**Figure G.3.** Static permittivity as a function of NaCl concentration for bulk aqueous NaCl solution.<sup>1</sup> The dashed line is included to guide the eye.

### G.1. References

1. Hasted, J. B.; Ritson, D. M.; Collie, C. H., Dielectric properties of aqueous ionic solutions. Parts I and II. *The Journal of Chemical Physics* **1948**, *16* (1), 1-21.

## Appendix H: Supporting Information for Chapter 9

**Table H.1.** Water uptake and dry polymer density data for the HQ:BP and MHQ:BP materials. The volume fraction of water in the polymer (equivalent to the water sorption coefficient) was calculated from water uptake and dry density data using Equation 2.5. All measurements were made at  $22 \pm 1$  °C. The uncertainty was taken as the standard deviation from the mean of three measurements.

Polymer	Measured using Pure Water		Measured using 1.0 mol/L NaCl	
	Water Uptake [g(water)/g(dry polymer)]	$K_{w,w}$	Water Uptake [g(water)/g(dry polymer)]	$K_{w,s}$
HQ:BP-20	$0.137 \pm 0.010$	$0.146 \pm 0.013$	$0.127 \pm 0.015$	$0.136 \pm 0.017$
HQ:BP-25	$0.190 \pm 0.006$	$0.197 \pm 0.007$	$0.180 \pm 0.005$	$0.189 \pm 0.006$
HQ:BP-30	$0.237 \pm 0.009$	$0.243 \pm 0.011$	$0.206 \pm 0.011$	$0.218 \pm 0.013$
MHQ:BP-20	$0.122 \pm 0.006$	$0.138 \pm 0.007$	$0.121 \pm 0.012$	$0.137 \pm 0.008$
MHQ:BP-25	$0.165 \pm 0.012$	$0.187 \pm 0.013$	$0.163 \pm 0.005$	$0.185 \pm 0.006$
MHQ:BP-30	$0.230 \pm 0.001$	$0.246 \pm 0.002$	$0.219 \pm 0.016$	$0.237 \pm 0.018$

**Table H.2.** Properties of HQ:BP and MHQ:BP materials used to conduct the Donnan-Manning counter-ion condensation theory analysis described in Chapter 9.

Polymer	IEC [meq/g(dry polymer)]	$C_A^{m,w}$ [mol fixed charge groups/ L(water sorbed)]	$b$ (nm)	$\xi$	$\gamma_{\pm}^m$
HQ:BP-20	0.83	$6.04 \pm 0.01$	8.7	1.64	0.48
HQ:BP-25	1.01	$5.33 \pm 0.01$	6.9	1.60	0.49
HQ:BP-30	1.19	$5.02 \pm 0.01$	6.3	1.29	0.54
MHQ:BP-20	0.81	$6.61 \pm 0.01$	8.7	1.96	0.44
MHQ:BP-25	0.99	$5.99 \pm 0.01$	6.9	1.73	0.47
MHQ:BP-30	1.16	$5.05 \pm 0.01$	6.3	1.63	0.49

## **Vita**

Kevin Chang, son of Yuan-Da Chang and Shu-Hui Tang, was born in New York, USA in 1992 and grew up in his home town at Taipei, Taiwan. He graduated from the British International School Shanghai (Shanghai, China) in 2011, and then he moved to the UK to study at the University of Surrey (Guildford, Surrey, UK) and the University College London (UCL, London, UK). After earning a Bachelor of Engineering and a Master of Science degrees in Chemical Engineering (graduated with Second Class Honors, Upper Division in 2014) and Biochemical Engineering (graduated with Merit in 2015), respectively, Kevin began his Ph.D. studies in the Department of Chemical Engineering at the University of Virginia (Charlottesville, Virginia, USA) under the supervision of Professor Geoffrey M. Geise. Upon completion of his Ph.D. in December 2020, Kevin will join the Department of Downstream Process Development at GlaxoSmithKline (King of Prussia, Pennsylvania, USA) as an Investigator to begin his professional career at the biopharmaceutical industry.

Permanent address: No. 12, Section 1, Minsheng East Road, Zhongshan District, Taipei, Taiwan 10491

This dissertation was typed by the author – Kevin Chang.